The Molecular Basis of Motion Detection in *Drosophila Melanogaster*

Renée Marie Vieira

München 2024

The Molecular Basis of Motion Detection in *Drosophila Melanogaster*

Renée Marie Vieira

Dissertation
an der Fakultät für Biologie
der Ludwig–Maximilians–Universität
München

vorgelegt von
Renée Marie Vieira
aus Georgetown, Guyana

München, den 25. September 2024

Erstgutachter: Prof. Dr. Alexander Borst

Zweitgutachter: Prof. Dr. John Parsch

Tag der mündlichen Prüfung: 3. Februar 2025

Eigenständigkeitserklärung

Hiermit versichere ich an Eides statt, dass die vorliegende Dissertation mit dem Titel

The Molecular Basis of Motion Detection in *Drosophila Melanogaster*

von mir selbstständig verfasst wurde und dass keine anderen als die angegebenen Quellen und Hilfsmittel benutzt wurden. Die Stellen der Arbeit, die anderen Werken dem Wortlaut oder dem Sinne nach entnommen sind, wurden in jedem Fall unter Angabe der Quellen (einschließlich des World Wide Web und anderer elektronischer Text- und Datensammlungen) kenntlich gemacht. Weiterhin wurden alle Teile der Arbeit, die mit Hilfe von Werkzeugen der künstlichen Intelligenz de novo generiert wurden, durch Fußnote/Anmerkung an den entsprechenden Stellen kenntlich gemacht und die verwendeten Werkzeuge der künstlichen Intelligenz gelistet. Die genutzten Prompts befinden sich im Anhang. Diese Erklärung gilt für alle in der Arbeit enthaltenen Texte, Graphiken, Zeichnungen, Kartenskizzen und bildliche Darstellungen.

Munich, 03.04.2025

(Ort / Datum)

Renee Vieira _____ _____

(Vor und Nachname in Druckbuchstaben) (Unterschrift)

Affidavit

Herewith I certify under oath that I wrote the accompanying Dissertation myself.

Title: The Molecular Basis of Motion Detection in *Drosophila Melanogaster*

In the thesis no other sources and aids have been used than those indicated. The passages of the thesis that are taken in wording or meaning from other sources have been marked with an indication of the sources (including the World Wide Web and other electronic text and data collections). Furthermore, all parts of the thesis that were de novo generated with the help of artificial intelligence tools were identified by footnotes/annotations at the appropriate places and the artificial intelligence tools used were listed. The prompts used were listed in the appendix. This statement applies to all text, graphics, drawings, sketch maps, and pictorial representations contained in the Work.

Munich, 03.04.2025

(Location/date)

Renee Vieira _____ _____

(First and last name in block letters) (Signature)

Erklärung
Declaration

Hiermit erkläre ich, *
Hereby I declare

☒ dass die Dissertation nicht ganz oder in wesentlichen Teilen einer anderen Prüfungskommission vorgelegt worden ist.
that this work, complete or in parts, has not yet been submitted to another examination institution

☒ dass ich mich anderweitig einer Doktorprüfung ohne Erfolg **nicht** unterzogen habe.
*that I did **not** undergo another doctoral examination without success*

☒ dass ich mich mit Erfolg der Doktorprüfung im Hauptfach
that I successfully completed a doctoral examination in the main subject

und in den Nebenfächern
and in the minor subjects

bei der Fakultät für
at the faculty of Biology

der
at Ludwig–Maximilians–Universität München
(Hochschule/*University*)

unterzogen habe.

☒ dass ich ohne Erfolg versucht habe, eine Dissertation einzureichen oder mich der Doktorprüfung zu unterziehen.
that I submitted a thesis or did undergo a doctoral examination without success

Munich, 03.04.2025
Ort, Datum/*place, date*

Renee Vieira
Unterschrift/*signature*

*) Nichtzutreffendes streichen/
delete where not applicable

Contents

List of Figures

Abbreviations

2A	Self-cleaving peptide sequence
3'UTR	3' Untranslated Region
5'UTR	5' Untranslated Region
ACh	Acetylcholine
AMPA	Alpha-Amino-3-Hydroxy-5-Methyl-4-Isoxazolepropionic Acid (receptor)
BACs	Bacterial Artificial Chromosomes
BDSC	Bloomington Drosophila Stock Center
BL	Barlow-Levick (model)
Ca_v	Voltage-gated Calcium Channels
Cas9	CRISPR-associated protein 9
ChAT	Choline Acetyltransferase
ChR2	Channelrhodopsin-2
cDNA	Complementary DNA
C	Centrifugal neurons
CNS	Central Nervous System
cpGFP	Circularly Permutated Green Fluorescent Protein
CRIMIC	CRISPR-Mediated Integration Cassette
CRISPR	Clustered Regularly Interspaced Short Palindromic Repeats
CT	Complex Tangential neurons
DA	Dopamine
DDC	DOPA Decarboxylase
DOPA	3,4-Dihydroxyphenylalanine
EM	Electron Microscopy
FRT	FLP Recombination Target
FLP	Flippase
GAL4	Galactose-responsive Transcription Factor
GABA	Gamma-Aminobutyric Acid
GCaMP	GFP, calmodulinm M13, myosin light chain kinase peptide fusion protein
GECIs	Genetically Encoded Calcium Indicators
GFP	Green Fluorescent Protein

GEVIs	Genetically Encoded Voltage Indicators
GPCRs	G-protein Coupled Receptors
GRASP	GFP Reconstitution Across Synaptic Partners
GtACR1	Guillardia theta Anion Channelrhodopsin 1
HCN	Hyperpolarisation-activated Cyclic Nucleotide-gated channels
HDC	Histidine Decarboxylase
HR	Hassenstein-Reichardt (model)
hs-FLP	Heat Shock Flippase
IHC	Immunohistochemistry
Inx	Innexin (invertebrate gap junction proteins)
K_v	Voltage-gated Potassium Channels
L	Lamina monopolar neurons
LexA	A bacterial transcription factor used in binary expression systems
LexAop	LexA Operator (binding site for LexA)
LPi	Lobula Plate Intrinsic neurons
LPTCs	Lobula Plate Tangential Cells
mAChR	Muscarinic Acetylcholine Receptor
Mi	Medulla intrinsic neurons
MiMIC	Minos-Mediated Integration Cassette
mGluR	Metabotropic Glutamate Receptor
nAChR	Nicotinic Acetylcholine Receptor
Na_v	Voltage-gated Sodium Channels
ND	Null Direction
NMDA	N-Methyl-D-Aspartate (receptor)
PCR	Polymerase Chain Reaction
PD	Preferred Direction
RFP	Red Fluorescent Protein
RNA	Ribonucleic Acid
RNAi	RNA interference
RMCE	Recombination-Mediated Cassette Exchange
STaR	Synaptic Tagging with Recombination
T	Bushy T neurons
Tm	Transmedullary neurons
TRH	Tryptophan Hydroxylase
TTX	Tetrodotoxin
UAS	Upstream Activation Sequence
VAChT	Vesicular Acetylcholine Transporter
VGAT	Vesicular GABA Transporter
VS	Vertical System

Summary

Visual perception is a fundamental mechanism through which sighted animals perceive their environment. For *Drosophila*, it is essential for performing life-sustaining behaviours such as foraging, mating, and avoiding threats. The motion vision pathway relies on a series of well-characterised neural processes that begin in the compound eyes and extend through various layers of the visual system, encased in what is known as the optic lobe. The main components of this pathway have been extensively studied over the years; the neurons and their synaptic connections have all been mapped through reconstructions with electron microscopy, and their response properties have been characterised in great detail. However, the molecular mechanism underpinning direction selectivity has remained unknown until recently. Neurotransmitter receptors and ion channels are fundamental to the biophysical properties of neurons, influencing both the nature of responses mediated by receptors and the dynamics governed by voltage-gated ion channels. Similarly, electrical synapses contribute to fast, often synchronised communication between neurons, yet their full range of roles and expression patterns remain largely unexplored. My thesis aims to advance our understanding of these essential subcellular components within the motion detection pathway in the fly's optic lobe.

Understanding the localisation and types of neurotransmitter receptors and ion channels within neurons is essential for decoding neural computation. However, the precise subcellular distribution of these proteins within neurons of the *Drosophila* visual system had yet to be characterised. In Manuscript 1, we developed two techniques: the flippase-dependent expression of GFP-tagged receptor subunits in individual neurons and FlpTag, a tool for the conditional labelling of endogenous proteins. Utilising these methods, we examined the subcellular distribution of GluClα, Rdl, Dα7 receptors, and para and Ih ion channels within motion-sensing T4/T5 neurons. Our findings revealed a strictly segregated distribution of these proteins, with a sequential spatial arrangement of glutamate, acetylcholine, and GABA receptors along the dendrite that correlates with previously reported synaptic distributions from electron microscopy reconstructions. Additionally, we discovered that the ion channels Ih and para are distinctly distributed within the

neuronal compartments, with Ih predominantly localised to the dendrites and para primarily found in the axonal fibres.

Electrical synapses, which are found in almost all organisms with a nervous system, allow direct electrical communication between neurons. However, the full extent of their expression and contribution to brain function is not well understood in many species, including *Drosophila*. Of particular importance is the role these synapses play in visual processing and neuronal stability. In Manuscript 2, an anatomical study using light microscopy and immunohistochemistry was conducted to map the distribution of innexin proteins, which form gap junctions—the core components of electrical synapses—in the central nervous system of *Drosophila*. We found that while some innexins localise to glial cells, others, such as shakB, are predominantly expressed in neurons.

Focusing on shakB in VS/HS visual projection neurons, we discovered its importance for maintaining intrinsic neuronal stability. Loss of shakB in VS/HS neurons resulted in spontaneous, cell-autonomous oscillations of voltage and calcium, revealing a critical role for electrical synapses in the intrinsic stability of these neurons. Additionally, loss of shakB in upstream visual circuits had differential effects on the ON and OFF visual motion pathways but did not affect the computation of direction selectivity. This suggests that while shakB is important for processing motion, it does not directly affect the ability of neurons to determine the direction of movement.

This thesis highlights the critical roles of both chemical and electrical synaptic components in the neural circuitry of *Drosophila*. The precise subcellular distribution of neurotransmitter receptors and ion channels deepened our knowledge of the biophysical mechanisms underlying motion vision, while electrical synapses, particularly those formed by shakB innexins, are essential for neuronal stability and nuanced visual motion processing. These findings advance our understanding of how different synaptic mechanisms collaborate to maintain and regulate complex neural processes such as motion vision.

Chapter 1

Introduction

1.1 History of Fruit Fly Research

For most, the fruit fly *Drosophila melanogaster* is no more than a house pest. So, how did this seemingly insignificant insect become the research powerhouse it is today? The first recorded entry of *Drosophila* into the laboratory dates back to the early 1900s when Charles Woodworth, an entomologist at Harvard, recommended its use in research. Woodworth's colleague, William Castle, followed this suggestion and employed *Drosophila* in his studies on inbreeding, marking the beginning of the fly's lustrous scientific career (Castle et al., 1906). However, the major breakthrough for *Drosophila* came from Thomas Hunt Morgan's laboratory at Bryn Mawr. Nettie Stevens, a talented cytologist, brought *Drosophila* into Morgan's lab to study the chromosomal basis of sex determination (Stevens, 1908). Her work laid the foundation for Morgan's revolutionary research, which ultimately proved the chromosomal theory of inheritance. Morgan's discovery that the white gene resides on the X chromosome was a landmark achievement, earning him the Nobel Prize in Physiology or Medicine in 1933 (Morgan & Cattell, 1912). The momentum generated by Morgan's discoveries carried *Drosophila* to the forefront of genetic research. Hermann J. Muller, a key figure in the fly's scientific ascent, was awarded the Nobel Prize in 1946 for discovering that X-ray irradiation could induce mutations. Muller's work was crucial in developing balancer chromosomes, which maintain deleterious mutations within a population by suppressing recombination during meiosis. In subsequent decades, *Drosophila* remained central to groundbreaking research. In 1995, the Nobel Prize in Physiology or Medicine was awarded to Edward B. Lewis, Christiane Nüsslein-Volhard, and Eric Wieschaus for their pioneering work on embryogenesis. They identified numerous genes involved in various aspects of *Drosophila* development, including segmentation,

which were later found essential for mammalian development. The use of *Drosophila* in cancer research also proved pivotal, as many tumour suppressor genes were initially identified on the fly before their human homologues were detected and linked to oncogenesis (Gateff, 1978; Moreno et al., 2002; Mirzoyan et al., 2019). In 2017, Jeffrey C. Hall, Michael Rosbash, and Michael W. Young were awarded the Nobel Prize in Physiology or Medicine for their discovery of the molecular mechanisms controlling circadian rhythm in *Drosophila*. The *Drosophila* genome project, completed in 2000, further cemented the fly's status as a premier model organism. Comparisons between the *Drosophila* and human genomes revealed significant homologies, with nearly 75% of human disease-related genes having functional orthologues in *Drosophila* (Adams et al., 2000; Myers et al., 2000; Yamamoto et al., 2014). This genetic similarity confirmed *Drosophila* as an invaluable model for studying human diseases. Thus, *Drosophila melanogaster* consistently remains at the forefront of modern biology, serving as a pioneering model in which critical genetic discoveries, gene engineering advancements, and novel biological insights are often first achieved. These breakthroughs in *Drosophila* are frequently foundational, paving the way for broader applications in other organisms. The fly's remarkable versatility as a model organism is no accident but rather a result of its unique attributes and the work of visionary scientists who recognised its potential.

1.2 Neuroscience Methods in *Drosophila*

The exquisite stereotypy of the fruit fly brain makes it an invaluable model for circuit neuroscience. The fly brain, comprising approximately 100,000 neurons, is far less complex than the 70 million neurons in the mouse brain or the 86 billion in the human brain (Scheffer et al., 2020). This relative simplicity, in combination with the ability of the fly to perform quite complex behaviours such as olfaction, vision, and learning, makes it an ideal organism for studying how neural circuits integrate sensory inputs and transform them into behavioural outputs. The neuronal anatomy has been characterised in great detail down to the level of the individual neurons, their axonal and dendritic processes, and their synaptic connections. Types of neurons are distinguished by their morphology, functional response properties, and molecular expression profiles. These identifiable neuronal types exhibit remarkable stereotypy, appearing consistently with similar numbers and properties across many individual flies. That consistency in connectivity and functional signalling makes the fly quintessential for circuit computation, in which specific neuronal transformations are preserved across individuals. Hence,

Drosophila is an excellent model for dissecting neural circuits and understanding the cell types and subcellular organisation involved in specific behaviours or sensory processes, such as motion vision.

1.2.1 Targeting Genetically Defined Cell Types

The ability to target genetically defined cell types is arguably one of the most powerful tools in *Drosophila* genetics, significantly advancing the field of circuit neuroscience. Targeting genetically defined cell types is crucial for dissecting neural circuits and linking specific neuronal populations to distinct anatomy, behaviours, and functions. The first binary system developed by Brand & Perrimon (1993) allows researchers to express genes in a cell-type-specific manner by using the transcription factor galactose-responsive transcription factor (Gal4), which binds to the upstream activation sequence (UAS) to control gene expression in targeted neurons. Transcriptional activators, like Gal4 or LexA, are driven by cell-type-specific promoters known as driver lines. These activators bind to responder elements, UAS or LexAop, upstream of the gene of interest, triggering its expression. However, the system is not foolproof, as unintended expression in non-target cells can occur (Manseau et al., 1997; Ito et al., 2003). To enhance specificity, split-GAL4 lines were developed, where the DNA-binding and activation domains of Gal4 are separated into different lines. Only neurons expressing both domains result in the expression of Gal4, thus enhancing targeting specificity (Pfeiffer et al., 2008, 2010; Jenett et al., 2012). More than ten thousand driver lines are currently available. Generally, these lines are developed by randomly inserting transcription factor sequences into endogenous genomic sites, known as the gene trap method (Gohl et al., 2011). Other driver lines are developed by cloning distinct putative enhancer fragments upstream of a transcription factor sequence (Pfeiffer et al., 2008, 2010; Jenett et al., 2012; Kvon et al., 2014). To further modulate Gal4 expression, a recombinase-based approach such as the Flipase/Flipase Recognition Target (Flp/FRT) system can be implemented. Flp recombinase can be paired with a heat shock promoter, which enables temporal control and adjustable expression levels by varying heat shock duration and intensity. This enables precise spatial and temporal control of gene expression, further expanding the ability to manipulate specific neuronal populations (Nern et al., 2015).

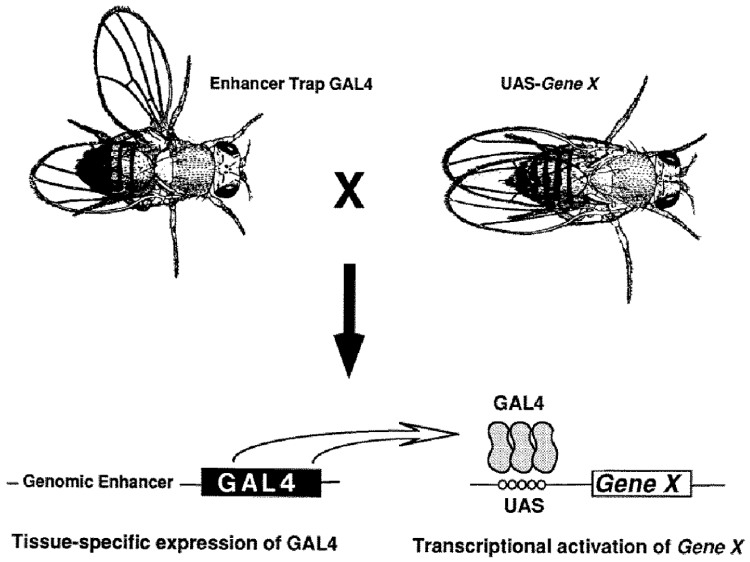

Figure 1.1: In *Drosophila*, targeted gene expression is achieved through the GAL4/UAS system. To generate transgenic lines that express GAL4 in various cell- or tissue-specific patterns, the GAL4 gene is randomly inserted into the genome, where different genomic enhancers drive its expression. A GAL4-dependent target gene can be constructed by positioning the gene of interest downstream of UAS (GAL4 binding sites). This target gene remains inactive in the absence of GAL4. To activate the target gene in specific cells or tissues, flies carrying the UAS-target gene (UAS-Gene X) are crossed with flies expressing GAL4 (Enhancer Trap GAL4). In the progeny of this cross, UAS-Gene X is activated in cells where GAL4 is expressed. Figure used with permission from Brand & Perrimon (1993).

1.2.2 Measuring Neuronal Activity

With the advent of the ability to consistently label specific cell types, researchers could now use various methods to record from specific populations of cells. In flies, brain activity is almost solely acquired through *in vivo* recordings. Electrophysiology, particularly whole-cell patch clamp techniques, directly measure electrical properties in neurons. This technique involves forming a tight seal with the cell membrane using a glass pipette, followed by suction to access the cell's interior, enabling the measurement of electrical currents and changes in membrane potential. Applying voltage or current through the pipette allows researchers to manipulate the membrane potential using a voltage-clamp, or to record changes in membrane potential in response to neuronal activity using a current-clamp (Marty, 1983). Electrophysiology is often referred to as the gold standard for studying neuronal electrical properties, as it directly measures ionic currents and membrane potentials (Hille, 1992; Wilson et al., 2004; Gruntman et al., 2018). However, electrophysiology can be challenging due to the small size and density of many fly

neurons, particularly those in the optic lobe. This has led to the development of alternative methods to indirectly study neuronal activity.

Genetically encoded calcium indicators (GECIs), such as the widely used GCaMP sensors, were designed by fusing the calcium-binding protein calmodulin to a circularly permutated green fluorescent protein (cpGFP) (Nakai et al., 2001). When calcium binds to calmodulin, GCaMP undergoes a conformational change, causing cpGFP to emit fluorescence in response to excitation light. These GECIs have been continuously refined since the early 2000s, with improved sensitivity, signal-to-noise ratio, and dynamic range (Chen et al., 2013; Dana et al., 2019). Despite its slower temporal resolution compared to electrophysiology, calcium imaging excels in spatial resolution, enabling the study of activity across multiple neurons simultaneously (Gruntman & Turner, 2013). Another way to infer neuronal activity is by using voltage imaging, which employs genetically encoded voltage indicators (GEVIs) such as ArcLight that provide a direct readout of membrane potential changes in the cells where it is expressed (Jin et al., 2012). Unlike calcium indicators, which detect secondary ionic changes, GEVIs respond to the primary electrical signals generated by neuronal activity, offering a more immediate and accurate depiction of neuronal dynamics. GEVIs function by undergoing conformational changes or shifts in fluorescence properties in response to voltage changes across the cell membrane. This enables real-time visualisation of the electrical activity of neurons with high temporal resolution. These indicators have several advantages, allowing researchers to monitor the fast, transient voltage changes associated with action potentials and synaptic potentials, providing insights into the precise timing and coordination of neuronal activity within circuits. Despite its advantages, voltage imaging also presents certain limitations. The relatively low signal-to-noise ratio of some GEVIs can make it challenging to detect small voltage changes, and the dynamic range of these indicators may not capture the full spectrum of neuronal activity (Yang & St-Pierre, 2016).

1.2.3 Manipulating Neuronal Activity

Manipulating neuronal activity is vital for understanding the connections between neural circuits and behaviour in *Drosophila*. An effective way to silence a group of neurons in *Drosophila* is to utilise a tissue-specific driver line to express effectors that disrupt synaptic transmission. Two of the most commonly used tools are Tetanus toxin light chain (TNT) and shibire^{ts} (Sweeney et al., 1995; Kitamoto, 2001). TNT silences neurons by cleaving synaptobrevin, a key protein involved in neurotransmitter release, thereby permanently blocking synaptic communication

(Sweeney et al., 1995). However, prolonged release of TNT can cause vesicle trafficking deficits and significantly alter cell health (Hiesinger et al., 1999). The temperature-sensitive properties of shibire^{ts} allow for precise temporal control. Shibire encodes dynamin, a GTPase essential for synaptic vesicle recycling. Shifting to a high restrictive temperature blocks vesicle recycling, thereby disrupting synaptic transmission. Neuronal activity can also be silenced by modifying neuronal excitability. Kir2.1 is an inward rectifying potassium channel that hyperpolarises neurons, reducing their excitability and preventing them from firing action potentials, offering a more controlled and reversible method of silencing neurons (Baines et al., 2001).

Another approach to manipulating neurons is to modulate their activity using optogenetic tools. This technique is based on the genetic expression of light-sensitive ion channels in the cell membrane, enabling the activation and inhibition of neurons in response to light. Channelrhodopsin-2 (ChR2) is one of the most widely used optogenetic channels that activate neurons when exposed to blue light (470 nm), effectively triggering action potentials and neuronal firing (Nagel et al., 2003). Another channel is CsChrimson, a red-shifted channelrhodopsin variant activated by red light (630 nm), which is particularly useful in experiments requiring deeper tissue penetration or where blue light might interfere with other processes (Klapoetke et al., 2014). For inhibiting neurons, channels like GtACR1/GtACR2 offer precise control. These light-gated anion channels are activated by blue-green light (470 nm) and lead to the hyperpolarisation of the neuron and inhibition of action potentials by allowing chloride ions to flow into the cell (Mauss et al., 2017). These tools provide a versatile way to study neural circuits and behaviour in *Drosophila* by enabling both the activation and inhibition of specific neurons.

Gene knockdown and knockout techniques, such as RNA interference (RNAi) and CRISPR/Cas9-mediated knockout, are used to manipulate neuronal activity at the molecular level. The most prominent method for conditional knockdown is RNA interference (RNAi), which degrades mRNA, thereby preventing the translation of target proteins. In *Drosophila*, RNAi can be expressed in a cell-type-specific manner using transgenic binary expression systems, allowing researchers to selectively inactivate almost any gene in the genome (Dietzl et al., 2007; Ni et al., 2009). This approach has been widely used to investigate the role of different receptors, such as $GABA_A$, $GABA_B$, and GluClα, in sensory processing (Root et al., 2008; Freifeld et al., 2013; Liu & Wilson, 2013). Despite its utility, RNAi-mediated knockdown is rarely complete and can be influenced by the specific driver line used, leading to variability in the extent of gene silencing. Additionally, RNAi can have off-target effects, impacting multiple genes and complicating the

interpretation of results (Fedorov et al., 2006; Perkins et al., 2015). While RNAi remains a valuable tool for dissecting neuronal signalling, the development of more precise methods, such as CRISPR/Cas9-mediated knockout, has expanded the toolkit for conditional loss-of-function studies in *Drosophila* (Port et al., 2014, 2020; Heidenreich & Zhang, 2016). CRISPR/Cas9 can create complete gene knockouts through DNA double-strand breaks, leading to permanent loss of gene function (Housden et al., 2017). Furthermore, CRISPR/Cas9 enables a wide range of genetic manipulations resulting in loss of function, such as gene knockouts, point mutations, and the introduction of a conditional stop cassette.

1.2.4 Mapping Neural Anatomy

Understanding the anatomical structure of neural circuits is crucial for linking neuronal activity to behaviour in *Drosophila*. Electron microscopy (EM) and connectomics are the primary techniques used for this purpose. EM provides high-resolution images of neuronal structures to visualise synaptic connections and the detailed morphology of neurons (Mauss et al., 2017). Connectomics, which involves the comprehensive mapping of neural connections using advanced EM techniques, has been instrumental in generating detailed maps of the *Drosophila* brain. This approach reveals the complex wiring of neural circuits and how different neurons are interconnected. This is essential for understanding how specific neural circuits contribute to sensory processing, motor control, and other behaviours in the fly (Nern et al., 2015). In recent years, volumetric electron microscopy of the *Drosophila* optic lobe has provided crucial insights into the intricate organisation and connectivity of neural circuits, revealing both the detailed synaptic architecture and the complex interactions between different neuron types involved in motion detection (Takemura et al., 2017; Shinomiya et al., 2019).

A recent advancement in the field is the release of a hemibrain connectome for Drosophila (Scheffer et al., 2020). This was achieved after extensive human proofreading efforts equivalent to 50 person-years to create a first draft of the hemibrain connectome. Though this represented a significant breakthrough, its scalability is limited by the labor-intensive human proofreading process and the fact that only a portion of the fly brain is represented. To address these limitations, FlyWire, an open online community platform, was introduced for proofreading the full connectome of the adult fly brain (FAFB) (Zheng et al., 2018; Dorkenwald et al., 2022). Utilizing a novel data structure, the ChunkedGraph, FlyWire efficiently represents neurons as connected components and enables collaborative proofreading, which significantly speeds up the proofreading process.

1.3 Neuronal Signalling Elements

The electrical properties of neurons and their ability to process information are governed by various transmembrane channels, each with a specific function. Neurotransmitter receptors, including ligand-gated ion channels and GPCRs, respond to neurotransmitters to initiate and modulate synaptic signals. Voltage-gated ion channels open in response to changes in the membrane potential, allowing specific ions to flow across the cell membrane. This ion flow leads to the depolarisation and repolarisation of the neuronal membrane, thereby transmitting electrical signals along neurons and across synapses. Gap junctions facilitate direct electrical communication between neurons, allowing for rapid and synchronous responses. The precise and dynamic regulation of these channels allows *Drosophila* neurons to maintain and alter membrane potentials, thereby supporting the complex behaviours and sensory processing necessary for the fly's interaction with its environment.

1.3.1 Neurotransmitters and Receptors

In both simple and complex organisms, neurotransmitters play a vital role as the brain's chemical messengers, transmitting signals across synapses to facilitate communication between neurons. This intricate system of chemical messengers ensures that different regions of the brain can coordinate activities and respond to stimuli, with specific neurotransmitters eliciting distinct responses depending on the receptors they interact with. *Drosophila* has several neurotransmitters analogous to those present in mammals, including gamma-aminobutyric acid (GABA), glutamate, acetylcholine, dopamine, serotonin, and histamine (Martin & Krantz, 2014). Additionally, *Drosophila* synthesises two distinct neurotransmitters, tyramine and octopamine, which bear structural resemblance to mammalian noradrenaline and adrenaline (Martin & Krantz, 2014). In *Drosophila*, acetylcholine functions predominantly as an excitatory neurotransmitter, whereas GABA serves an inhibitory role, mirroring the neurotransmitter functions observed in vertebrates (Lee et al., 2003; Su & O'Dowd, 2003). In contrast to the mammalian system, glutamate in *Drosophila* can act as either an excitatory or inhibitory neurotransmitter, with the latter effect mediated through a glutamate-gated chloride channel (Liu & Wilson, 2013; Mauss et al., 2014).

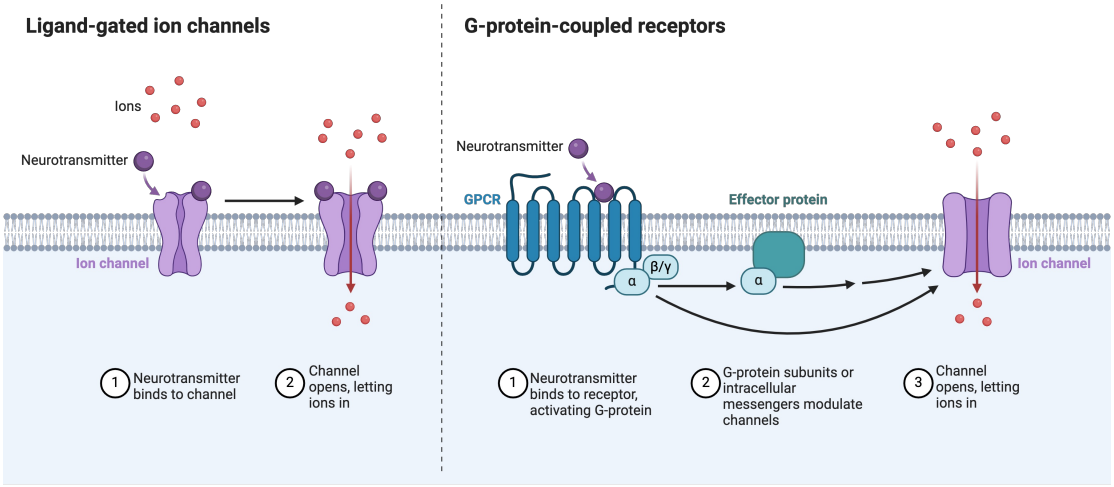

Figure 1.2: On the left, the ligand-gated ion channel mechanism is depicted, where a neurotransmitter binds directly to the ion channel, causing it to open and allow ions to flow into the cell. On the right, the GPCR mechanism is shown, where the neurotransmitter binds to the receptor, activating a G-protein. The activated G-protein then interacts with an effector protein, which leads to the opening of an ion channel, allowing ions to flow in.

Neurons are specialised cells designed to receive, process, and transmit information. Information within neurons is represented electrically, while communication between neurons is chemical, involving neurotransmitters. Upon release, neurotransmitters diffuse across synapses and bind to postsynaptic receptors, which can either be ligand-gated channels or G protein-coupled receptors (GPCRs) (Purves et al., 2001). Ligand-gated channels open a central pore to permit ion passage, directly converting chemical signals to electrical ones. GPCRs, on the other hand, activate intracellular signalling cascades through trimeric G proteins (Kandel, 2013). Although neurotransmitters are often identified as excitatory or inhibitory, they do not possess such qualities intrinsically; their effects depend on the types of receptors they bind to on the postsynaptic neuron and the ion conductances that these receptors activate (Bear et al., 2020). For instance, when the neurotransmitter glutamate binds to its ionotropic receptors, such as AMPA or NMDA receptors, it typically causes depolarisation by allowing positively charged ions like sodium (Na^+) and calcium (Ca^{2+}) to enter the postsynaptic neuron, generating an excitatory response. Conversely, when the neurotransmitter GABA binds to $GABA_A$ receptors, it usually results in hyperpolarisation by allowing chloride (Cl^-) ions to enter the postsynaptic neuron, producing an inhibitory response. Similarly, GABA can bind to $GABA_B$ receptors, leading to the opening of potassium (K^+) channels and further hyperpolarisation. This balance between excitatory and

inhibitory responses is crucial for the proper functioning of neural circuits, enabling neurons to integrate and transmit information efficiently across the nervous system.

Acetylcholine

Acetylcholine (ACh) is the most prevalent excitatory neurotransmitter and neuromodulator in the nervous system of *Drosophila* (Lee & O'Dowd, 1999; Gu & O'Dowd, 2006; Su & O'Dowd, 2003; Eckstein et al., 2024). The synthesis of ACh is catalysed by the enzyme choline acetyltransferase (ChAT), which converts choline and acetyl-CoA into acetylcholine. ChAT is widely used as a marker for identifying cholinergic neurons. Another essential component in cholinergic synaptic transmission is the vesicular acetylcholine transporter (VAChT), responsible for packaging ACh into synaptic vesicles for release into the synapse. VAChT also serves as a key marker for cholinergic neurons. Reductions in VAChT protein levels or activity can lead to impaired locomotion, while complete loss of VAChT function is lethal (White et al., 2020).

Similar to mammals, acetylcholine in *Drosophila* interacts with two types of receptors: ionotropic nicotinic acetylcholine receptors (nAChRs) and muscarinic acetylcholine receptors (mAChRs), the latter being GPCRs. Both types of receptors are activated by acetylcholine, with nAChRs responding to nicotine and mAChRs to muscarine. Of the two receptor types, nAChRs are the most studied and are similar to their counterparts in mammals. These ionotropic receptors are ligand-gated cation channels that allow the influx of sodium (Na^+) and potassium (K^+), and to a lesser extent, calcium (Ca^{2+}), leading to rapid depolarisation of the postsynaptic neuron. nAChRs are pentameric structures belonging to the large family of Cys-loop receptors. Each subunit contains an N-terminal extracellular domain with a characteristic Cys-loop, four transmembrane regions, and a large intracellular loop. The ACh-binding site is located in the N-terminal domain. Subunits with a pair of adjacent cysteine residues in the extracellular ligand-binding domain are designated as α subunits, while those without are β subunits. At least two α subunits are necessary for receptor function, with different subunit compositions influencing the receptor's properties. Among these, Dα7 is the most studied nAChR subunit, forming homomeric pentameric receptors with excitatory effects. Dα7 is particularly important in the giant fibre system, where it mediates jump escape behaviour in flies (Fayyazuddin et al., 2006). Additionally, Dα7 is localised to the dendrites of lobula plate tangential cells (LPTCs) in the visual system, receiving cholinergic input from T4/T5 neurons involved in motion detection (Raghu et al., 2009; Mauss et al., 2014). While Dα5, Dα6, and Dα7 subunits can form functional

heteromers in vitro (Lansdell & Millar, 2004; Lansdell et al., 2012), their in vivo formation and function is yet understood.

As with most GPCRs, insect mAChRs are characterised by a single seven transmembrane α-helix, with an N-terminal extracellular domain and a C-terminal intracellular domain. Unlike ionotropic receptors, mAChRs do not directly open ion channels but instead trigger signalling pathways inside the cell that lead to slower and often prolonged cellular responses. There are three known mAChR subtypes in *Drosophila*: mAChR-A, mAChR-B, and mAChR-C. Traditionally, mAChR-A was believed to cause excitatory effects by increasing intracellular Ca^{2+} levels (Millar et al., 1995). However, recent studies have shown that mAChR-A can also have inhibitory effects on Kenyon cells in the olfactory system, where it plays a role in synaptic plasticity related to odor-associated learning by acting on the dendrites of these cells (Bielopolski et al., 2019). mAChR-B, in contrast, reduces Ca^{2+} levels in the neuron, leading to inhibitory effects. This receptor is particularly important for creating the sign inversion necessary for establishing the OFF channel in the larval *Drosophila* visual pathway (Qin et al., 2019). In comparison, little is known about the functional roles and distribution of mAChR-C (Xia et al., 2016). Together, these mAChRs regulate various cholinergic signalling pathways in *Drosophila*, playing significant roles in both physiological and behavioural processes.

GABA

Gamma-aminobutyric acid (GABA) is the primary inhibitory neurotransmitter in the nervous system of *Drosophila*, playing a crucial role in modulating neural activity and maintaining the balance between excitation and inhibition (Waddell et al., 2011; Lee et al., 2003). GABA is synthesised from glutamate by the enzyme glutamic acid decarboxylase (GAD), which is highly expressed in the central nervous system (CNS) and is commonly used as a marker to detect GABAergic neurons (Jackson et al., 1990). GABA is packed and stored in synaptic vesicles via the vesicular GABA transporter (VGAT), which can be used as a marker for GABAergic neuron terminals (Enell et al., 2007; Fei et al., 2010). In VGAT mutants, GABA release is decreased, leading to impaired object tracking in flies, but not affecting the optomotor response, indicating distinct roles of GABAergic signalling in the visual system of *Drosophila* (Fei et al., 2010).

In flies, GABA acts on two main types of receptors: ionotropic $GABA_A$ receptors and metabotropic $GABA_B$ receptors. Ionotropic $GABA_A$ receptors are ligand-gated chloride channels that mediate fast synaptic inhibition by allowing the influx of chloride ions (Cl^-) into the postsynaptic neuron, leading to hyperpolarisation and

reduced neuronal excitability (Liu et al., 2007). These receptors are pentameric structures, with each subunit containing an extracellular ligand-binding domain, four transmembrane regions, and a large intracellular loop. The *Drosophila* genome encodes three $GABA_A$ receptor subunits: Rdl, Lcch3, and Grd. Rdl, the best-studied subunit, is highly expressed in the antennal lobes and mushroom body, where it negatively regulates associative olfactory memory (Liu et al., 2007) and is crucial for creating ON selectivity in the visual pathway (Molina-Obando et al., 2019). While Rdl can form homomers, Lcch3 and Rdl can also form functioning heteromers when co-expressed in cell culture (Zhang et al., 1995). However, in vivo, Lcch3 and Grd have been shown to form heteromeric cation channels, potentially leading to excitatory currents, though their exact role in vivo remains unclear (Gisselmann et al., 2004; Davis et al., 2020).

Metabotropic $GABA_B$ receptors, on the other hand, are GPCRs that mediate slower, prolonged inhibitory effects through second messenger systems. These receptors are characterised by their seven transmembrane domains, extracellular ligand-binding sites, and intracellular loops that interact with G proteins to modulate intracellular signalling pathways (Enell et al., 2007). In *Drosophila*, three $GABA_B$ receptor subunits have been identified: GABA-B-R1, GABA-B-R2, and GABA-B-R3. GABA-B-R1 and GABA-B-R2 are often co-expressed in similar regions, such as the antennal lobe, visual system, mushroom body, and ellipsoid body, where they are involved in presynaptic inhibition and regulation of olfactory information (Olsen & Wilson, 2008; Deng et al., 2019). GABA-B-R3, however, is differentially expressed, notably absent from the mushroom body but present in the ellipsoid body (Mezler et al., 2001). $GABA_B$ receptors play critical roles in various behaviours, including sleep drive and responses to alcohol (Ki & Lim, 2019; Ranson et al., 2020). Moreover, $GABA_B$ receptors contribute to subtractive gain control in the antennal lobe by mediating inhibition in projection neurons (Suzuki et al., 2020).

Glutamate

Glutamate, which has been studied for almost 50 years, is the major excitatory neurotransmitter in the mammalian CNS and *Drosophila* neuromuscular junctions (NMJs) (Jan & Jan, 1976). Since glutamate is the most abundant amino acid in the brain and is present in every cell, it is challenging to define glutamatergic neurons based on a unique biosynthetic enzyme. Instead, the vesicular glutamate transporter (VGlut), which is responsible for the transport of glutamate into synaptic vesicles, is used as a marker for glutamatergic neurons, as it is unique to

glutamatergic synapses (Daniels et al., 2004). Several glutamatergic neurons have been described throughout the *Drosophila* brain, with several studies demonstrating the excitatory action of glutamate (Das et al., 2011; Wu et al., 2007).

Glutamate acts on two main classes of receptors: ionotropic glutamate receptors (iGluRs) and metabotropic glutamate receptors (mGluRs). Both receptors are activated by glutamate and its analogues, such as NMDA and non-NMDA for ionotropic receptors and quisqualate for metabotropic receptors. Of the two receptor types, iGluRs are more well-studied and are similar to their mammalian counterparts. These receptors form tetramers and are part of the larger family of ligand-gated ion channels (Sobolevsky, 2015). Each subunit has an extracellular ligand-binding domain, three transmembrane regions, and a pore-forming loop. The glutamate-binding site is in the extracellular domain. iGluRs in *Drosophila* are divided into NMDA and non-NMDA types. In total, 15 putative ionotropic glutamate receptor subunits are thought to exist, although their exact functions may not be fully confirmed. NMDA receptors, including Nmdar-1 and Nmdar-2, are unique in that they require both ligand binding and membrane depolarisation to allow calcium (Ca^{2+}) and sodium (Na^{+}) ions to flow in. These receptors are involved in synaptic plasticity and memory formation, as well as sleep behaviour and olfactory learning and memory (Baez et al., 2018). Non-NMDA receptors, such as GluRIIA, GluRIIB, and GluRIIC, are located at the neuromuscular junction and play a key role in muscle control. Recently, it has been demonstrated that glutamate can serve a dual function, acting as an inhibitory neurotransmitter when it binds to the GluClα receptor (Liu & Wilson, 2013). This inhibitory effect plays a crucial role in regulating olfactory processing in the antennal lobe, ensuring proper sensory modulation. Additionally, the GluClα receptor is essential for motion opponency in the visual system, allowing flies to detect and process motion effectively (Mauss et al., 2015).

In *Drosophila*, mGluRs, which are slower-acting receptors, exert their effects indirectly by modulating presynaptic excitability and synaptic architecture, contributing to synaptic plasticity (Bogdanik et al., 2004). Structurally, mGluRs consist of a single seven-transmembrane α-helix with an N-terminal extracellular domain and a C-terminal intracellular domain like all other GPCRs described so far (Lee et al., 2000). The glutamate-binding site is located in the extracellular region formed by the transmembrane domains, while the intracellular loops and C-terminal tail interact with G proteins to mediate signalling (Kunishima et al., 2000). Upon glutamate binding, mGluRs activate a membrane-bound G-protein that triggers a second messenger system, leading to changes in gene expression and

protein synthesis, resulting in longer-lasting cellular responses. There is only one mGluR subtypes in *Drosophila*: mGluR-A (Mitri et al., 2004; Hanlon & Andrew, 2015; Brody & Cravchik, 2000). It is involved in modulating clock neurons, demonstrating the diverse roles glutamate plays in *Drosophila* neurobiology (Hamasaka et al., 2007).

1.3.2 Monoamines

One way circuit-wide changes in neuronal excitability can be achieved is through neuromodulation, where biogenic amines and other neuromodulators diffuse through the brain and influence general brain activity. Monoamines are a class of neuromodulators involved in fine-tuning neuronal excitability and direct synaptic transmission. Their neurotransmitters contain one amino group connected to an aromatic ring by a carbon-carbon chain. This class of neuromodulators includes dopamine, serotonin, norepinephrine and its invertebrate analogue octopamine, histamine, and trace amines such as tyramine. The most abundant monoamines in the *Drosophila* nervous system are dopamine, octopamine, and serotonin, each of which will be discussed in detail below, along with histamine, which is particularly relevant to the visual system in *Drosophila*.

Dopamine

Dopamine (DA) in *Drosophila* plays a crucial role in modulating a wide range of behaviours, much like it does in mammals. The adult *Drosophila* brain contains approximately 128-130 dopaminergic neurons, organised into clusters that innervate various brain regions and mediate behaviours such as locomotion, odour response, appetite regulation, circadian rhythms, and learning and memory (Kasture et al., 2018; Nitz et al., 2002; Schwaerzel et al., 2003; Riemensperger et al., 2011; Alekseyenko et al., 2013; Waddell, 2013; Yamagata et al., 2015; Berry et al., 2015; Aso et al., 2014). Two prominent sites of dopaminergic innervation are the mushroom body and the central complex. The mushroom body is essential for olfactory learning and memory (Aso et al., 2014), while the central complex is involved in motor activity and sleep regulation (Nitz et al., 2002; Berry et al., 2015).

Dopamine exerts its effects through several GPCRs in *Drosophila*. These include two D1-like receptors, Dop1R1 and Dop1R2, which activate adenylyl cyclase and increase cyclic adenosine monophosphate (cAMP) levels, leading to excitatory postsynaptic currents (Hearn et al., 2002). In contrast, the D2-like receptor,

Dop2R, inhibits adenylyl cyclase, resulting in neuronal inhibition (Hearn et al., 2002). Additionally, *Drosophila* possesses a non-canonical dopamine/ecdysteroid receptor, DopEcR, which binds both dopamine and the arthropod ecdysteroids ecdysone and 20-hydroxyecdysone (20E). DopEcR is implicated in the regulation of courtship memory within the mushroom body circuits, where it integrates signals from dopamine and ecdysteroids to influence memory formation and retention (Ishimoto et al., 2013).

Serotonin

The serotonergic system in *Drosophila* has not been as extensively studied as the dopaminergic system, but it is known to be involved in regulating key pathways such as insulin signalling, organismal growth, locomotion, aggression, sleep, and reproductive function (Kaplan et al., 2008; Neckameyer et al., 2007; Dierick & Greenspan, 2007; Johnson et al., 2009; Alekseyenko et al., 2010; Yuan et al., 2005; Nichols, 2007). This system is composed of approximately 80 serotonergic neurons distributed across various clusters throughout the fly brain. Serotonin is synthesised in a two-step process where the enzyme tryptophan hydroxylase (TRH) catalyses the conversion of the amino acid tryptophan into 5-hydroxytryptophan, which is then decarboxylated by 3,4-dihydroxyphenylalanine (DOPA) decarboxylase (DDC) to produce serotonin (Livingstone & Tempel, 1983; Neckameyer & White, 1992; Hirsh & Davidson, 1981).

In *Drosophila*, there are five known serotonin receptors: 5-HT1A, 5-HT1B, 5-HT2, 5-HT7, and 5-HT2B, which share sequence and functional homology with their mammalian counterparts (Yuan et al., 2005; Nichols, 2007). These receptors are expressed throughout the fly brain and play significant roles in various neural processes. For instance, studies have shown that the receptor d5-HT1A promotes sleep, with mutations in this receptor leading to reduced and fragmented sleep patterns (Yuan et al., 2006).

Octopamine

Octopamine, a biogenic amine extensively studied in invertebrates, functions as a neurotransmitter, neuromodulator, and neurohormone in various physiological processes in *Drosophila* and other insects (David & Coulon, 1985; Evans & Robb, 1993; Bicker & Menzel, 1989). While octopamine is considered a trace amine in mammals, in insects, including *Drosophila*, octopamine and tyramine are primary neurotransmitters, playing roles analogous to noradrenaline in vertebrates.

In *Drosophila*, octopamine receptors are classified into three groups based on structural and signalling similarities to vertebrate adrenergic receptors. These include α-adrenergic-like receptors (OctαR), β-adrenergic-like receptors (OctβR), and octopamine/tyramine receptors (Oct-TyrR) (Evans & Maqueira, 2005). The α-adrenergic-like receptors, such as the newly characterised DmOctα2R, are more closely related to vertebrate α-adrenergic receptors and are involved in various physiological responses (Balfanz et al., 2005; Maqueira et al., 2005). The β-adrenergic-like receptors, encoded by genes such as DmOctβ1R, DmOctβ2R, and DmOctβ3R, increase intracellular cAMP levels upon activation, mediating excitatory responses. In contrast, the Oct-TyrR receptors can be stimulated by both octopamine and tyramine and typically reduce cAMP levels, contributing to the fine-tuning of cellular signalling (Balfanz et al., 2005).

Histamine

Histamine in *Drosophila* serves as a critical neurotransmitter involved in several key physiological functions, primarily photoreception and mechanosensitivity (Hardie, 1989; Buchner et al., 1993). Histamine is synthesised from the amino acid L-histidine by the enzyme histidine decarboxylase (HDC), making HDC a reliable marker for identifying histamine-producing neurons in both the central nervous system and peripheral nervous system. Two genes, *ora transientless* (*ort*) and *Histamine-gated chloride channel subunit 1* (*HisCl1*), encode histamine receptors in *Drosophila* (Gisselmann et al., 2002; Zheng et al., 2002; Gengs et al., 2002). Both receptors function as histamine-gated chloride channels, leading to cell hyperpolarisation.

1.3.3 Voltage-gated Ion Channels

Voltage-gated ion channels are multimeric proteins embedded within the cell membrane of excitable cells that open and close in response to changes in the electrical voltage across the membrane. The gating of these channels is triggered by changes in membrane potential, permitting the selective permeation of cations such as sodium (Na^+), potassium (K^+), and calcium (Ca^{2+}). These channels are classified based on the specific ions they conduct, leading to three main categories: voltage-gated sodium, voltage-gated potassium, and voltage-gated calcium channels. Similar to humans, *Drosophila* ion channels are composed of multiple homologous domains, each typically consisting of six transmembrane segments, S1 to S6. The S4 segment in each domain acts as the voltage sensor, detecting changes in membrane potential, which triggers a conformational change, allowing the central pore to either open or close.

Voltage-gated Na^+

Voltage-gated sodium (Na_V) channels are essential for initiating and propagating action potentials in excitable cells. Activated by membrane depolarisation, these channels allow a rapid influx of sodium ions. This influx further depolarises the membrane, creating a positive feedback loop that allows even more sodium (Na^+) to enter, which is critical for the upstroke of the action potential. Shortly after opening, the channels quickly inactivate, halting sodium (Na^+) entry. This sharp change in voltage is necessary for the action potential to propagate along the neuron. The genome of *Drosophila* has only two genes predicted to encode Na_V proteins: *paralytic* (*para*) and *Na channel protein 60E* (*NaCP60E*) (Suzuki et al., 1971; Okamoto et al., 1987; Tseng-Crank et al., 1991; Hong & Ganetzky, 1994). *para* is the putative Na_V channel, as *NaCP60E* null animals are viable with no loss of inward sodium currents detected in neurons using patch clamp (Germeraad et al., 1992; Anholt et al., 1996; Kulkarni et al., 2002). In contrast, *para* null animals die as first instar larvae with no detectable inward sodium current in neurons using patch clamp (Loughney et al., 1989; Hong & Ganetzky, 1994). Despite having just one functional Na_V gene when compared to nine in mammals, a similar degree of channel protein diversity could be achieved via alternative splicing (Huang et al., 2017). *para* has 60 predicted isoforms, some of which have different developmental expression patterns (Lin et al., 2009, 2012).

Voltage-gated Ca^+

Voltage-gated calcium (Ca_V) channels play a multifaceted role in various physiological processes, including neurotransmitter release, muscle contraction, and the regulation of gene expression. Activated by membrane depolarisation, these channels allow a rapid influx of calcium ions. This influx further depolarises the membrane and triggers calcium-dependent signalling pathways, which are crucial for synaptic transmission and other cellular functions. In *Drosophila*, the *cacophony* (*cac*) gene encodes the primary α1 subunit of voltage-gated calcium channels (Smith et al., 1996; Littleton & Ganetzky, 2000). However, several other Ca_V channels exist, including two other pore-forming channels, Ca-α1T and Ca-α1D, as well as several accessory subunits, namely Ca-β, Ca-Ma2d, CG16868, and *stol*. Mutations in *cac* lead to defects in synaptic transmission, courtship behaviour, and visual physiology (Kawasaki et al., 2002; Wheeler et al., 1990).

Voltage-gated K^+

Voltage-gated potassium (K_V) channels play a crucial role in the repolarisation phase of action potentials. These channels facilitate the efflux of potassium (K^+), which counterbalances the influx of sodium (Na^+), thereby restoring the membrane potential to its resting state. This potassium (K^+) outflow is vital for terminating the action potential and ensuring proper timing and frequency of neuronal firing. Nine genes encode K_V channel proteins in *Drosophila*, including *Shaker* (*Sh*), *Shab*, *Shaw*, and *Shal* (Butler et al., 1989; Covarrubias et al., 1991; Tsunoda & Salkoff, 1995). Notably, the *Drosophila* mutant *Sh*, which exhibits leg shaking under ether anaesthesia, has defects in a fast and transient K^+ current in muscles and neurons, leading to impaired action potential repolarisation (Kaplan & Trout, 1969; Tanouye et al., 1981; Wu et al., 1983).

1.3.4 Gap Junctions

Gap junctions are among the most common forms of intercellular communication in multicellular animals. They are composed of membrane-spanning proteins that form a channel permeable to ions and small molecules, connecting the cytoplasm of adjacent cells. Interestingly, two distinct gene families carry out this highly conserved function. In vertebrates, gap junctions are made from a large family of proteins called connexins (Cx), while invertebrate gap junctions are composed of innexins (Inxs). Despite having no significant amino acid sequence similarity, Cxs and Inxs are strikingly similar in structure (Miller & Pereda, 2017). They are four-pass transmembrane proteins with two extracellular loops, one cytoplasmic loop, and intracellular N- and C-termini.

In *Drosophila*, the eight distinct innexin genes that encode the proteins forming gap junctions are *inx1*, *inx2*, *inx3*, *inx4*, *inx5*, *inx6*, *ogre* (also known as *inx7*), and shakB (also known as *inx8*) (Alexopoulos et al., 2004). In addition to their role in forming electrical synapses between neurons, innexins are vital for various biological processes, including embryonic development, stem cell division, blood-brain barrier formation, and spermatogenesis (Bohrmann & Zimmermann, 2008; Spéder & Brand, 2014; Zhang et al., 2018; Smendziuk et al., 2015).

1.4 Protein Tagging, A Light Bulb Moment

Unravelling the precise localisation of proteins within their cellular environment is a cornerstone of modern life sciences, offering invaluable insights into cellular function and molecular mechanisms. The field of protein visualisation was first revolutionised by the advent of immunohistochemistry (IHC) in the early 20th century, providing scientists with the ability to detect and localise specific proteins within fixed tissue sections. However, this method was limited to static images of fixed samples. The next significant leap came in the 1990s with the discovery and application of the Green Fluorescent Protein (GFP), which revolutionised the visualisation of proteins. The groundbreaking work by Chalfie et al. (1994) demonstrated the use of GFP, initially derived from the jellyfish *Aequorea victoria*, as a marker for gene expression in living organisms. This discovery, along with subsequent enhancements and derivatives of GFP, allowed scientists to visualise and study proteins in living cells and organisms (Matz et al., 1999; Cinelli et al., 2000; Chudakov et al., 2010; Shemetov et al., 2017; Nienhaus & Nienhaus, 2022). Over the years, protein tagging has evolved into two main approaches: transgenically tagged proteins, where tagged versions of proteins are introduced into cells using vectors, and endogenous protein tagging, which involves tagging proteins at their native genomic loci. These methods can be applied at varying levels of specificity, from whole tissue labelling, which involves tagging proteins throughout an entire tissue (constitutive labelling), to cell type-specific labelling (conditional labelling), targeting specific cell populations, and even down to single-cell labelling, which allows for the study of individual cells within complex tissue. To achieve a particular level of specificity, it is essential to carefully consider the choice of protein tagging method. Below, we will introduce each of these methods for visualising proteins, with a particular focus on transmembrane proteins, as it applies to the context of this thesis.

1.4.1 Immunohistochemistry

Immunohistochemistry originated in the early 20th century as researchers sought methods to visualise and study the distribution of specific proteins within tissue sections. The pioneering concept of using antibodies to detect proteins in tissues was introduced by Coons et al. (1941). He developed a method to conjugate antibodies with fluorescent dyes, which permitted the visualisation of pneumococcal antigens within infected tissue samples under a fluorescence microscope (Coons et al., 1941). This research laid the foundation for modern IHC techniques. Since then, significant advancements in IHC include the development of monoclonal antibodies, enzyme

labels, and multiplexing capabilities (Köhler & Milstein, 1975; Nakane & Pierce, 1967). Despite these advancements, IHC still faces challenges such as non-specific binding, reliance on the quality of antibodies, and difficulties in quantification. Another major limitation of IHC is that it only permits the labelling of static or fixed tissues without the ability to achieve cell-type specificity.

With respect to scalability, generating new, specific antibodies is labour-intensive and often does not produce high-quality antibodies suitable for various applications. Less than 5% of all *Drosophila* proteins can be detected by readily available antibodies (Nagarkar-Jaiswal, DeLuca, et al., 2015), thus hampering large-scale analysis of protein localisation, stability, and dynamics. Nonetheless, IHC has been a pivotal tool in examining the spatial distribution and protein interactions of key neuronal transmembrane proteins. A polyclonal antibody against the GABA receptor Rdl revealed the protein's high expression in specific regions of the *Drosophila* CNS, such as the optic lobes and antennal lobes (Aronstein & Ffrench-Constant, 1995). Additionally, antibodies against the potassium channel Shaker have shown its expression in specific regions of the *Drosophila* CNS and helped reveal its role in regulating sleep through interaction with the SLEEPLESS protein (Wu et al., 2010).

1.4.2 Transgenic Protein Tags

The primary prerequisite for tagging a gene is the ability to insert foreign DNA into the fly genome. The introduction of methods to stably incorporate foreign DNA, coupled with the use of GFP as a reporter, initiated the protein tagging revolution in genetic research. Pioneering work by Spradling & Rubin (1982) on P-element mediated transformation provided a robust technique for integrating transgenes into the *Drosophila* genome, allowing for stable genetic modifications. In 1994, the incorporation of GFP into *Drosophila* further advanced the field. The use of GFP as a reporter gene allowed researchers to observe gene expression and protein localisation in real-time within living tissues, without the need for staining in fixed tissue preparations. This combination of stable DNA integration and stain-free labelling transformed the ability to study proteins in vivo.

Fluorescently tagged proteins can be expressed from a transgenic DNA construct either under their endogenous control by including upstream and downstream genomic segments or under exogenous control using the UAS/GAL4 system. The UAS/GAL4 system can be used to express proteins in specific tissues and cells of interest, enabling the precise control of the spatial and temporal expression of tagged proteins. As the name suggests, there are two parts to this system: GAL4,

which drives the expression in a spatially restricted pattern using a tissue-specific promoter, and UAS, which is the upstream activating sequence that the GAL4 protein binds to, initiating transcription of the downstream gene in tissues that express GAL4. GAL4 lines are created by either inserting the GAL4 coding sequence randomly into the genome using transposons, thus trapping the enhancer or by directly fusing it to a promoter sequence before integrating it into the fly genome. The second component, UAS, is placed upstream of the cDNA of the protein of interest. In the past, cDNA for a protein of interest was generated by PCR and cloned into a plasmid via cloning sites. However, with the rise of affordable gene synthesis, it is now common to synthesise the cDNA of interest. A single GAL4 transgene can drive the expression of multiple UAS constructs, enabling the simultaneous expression of a transmembrane protein and the labelling of the specific cell in which it is expressed, for example by using UAS-myr-tdTomato to label the cell membrane. Various laboratories have deposited independently generated fly lines for over 300 genes to the Bloomington *Drosophila* Stock Center (BDSC), each expressing a different single protein isoform fused with a fluorescent protein under UAS control. One such neurotransmitter receptor line generated was for the nicotinic acetylcholine receptor, Dα7. The UAS-Dα7-GFP line was used to investigate the subcellular distribution of Dα7 in two sets of LPTCs by using two different GAL4 lines, GAL4-DB331 (Joesch et al., 2008) and GAL4-3A (Scott et al., 2002), to target specific VS and HS cells in *Drosophila* (Raghu et al., 2009).

In addition to the independent generation of UAS transgene lines, the FlyORF consortium has initiated a centralised, large-scale effort to create transgenic lines for over 4,000 UAS-cDNA constructs, which are C-terminally tagged with HA, a small epitope derived from the human influenza haemagglutinin protein (Bischof et al., 2013). This collection primarily consists of regulatory genes, encompassing nearly all transcription factors and single-exon genes. However, this collection notably excludes many transmembrane proteins, particularly neurotransmitter receptors, ion channels, and gap junctions, which are core components of neuronal transduction and the focus of this dissertation.

The main strength of expressing a tagged protein using the UAS/GAL4 system is the ability to control expression at all levels of specificity. Multiple GAL4 lines exist that are controlled by ubiquitously expressed neuronal promoters, such as *Elav*, *nSyb*, and *Appl*, enabling widespread pan-neuronal expression of UAS constructs (Koushika et al., 1996; Weaver et al., 2020). Additionally, extensive libraries of thousands of GAL4 lines allow for targeted expression in specific cell types (Jenett et al., 2012; Li et al., 2014; Manning et al., 2012; Kvon et al., 2014). Furthermore, this system can be regulated with GAL80, a GAL4-specific

repressor, and its temperature-sensitive variant GAL80^{ts}, allowing for finer tuning and the capability to generate single-cell specificity (Lee & O'Dowd, 1999; McGuire et al., 2004).

While the GAL4/UAS system provides spatial and temporal control, it may not accurately reflect the natural expression patterns of the endogenous gene, potentially altering protein localisation and quantity. To overcome these limitations, genomic transgenes, including the gene's genomic sequence plus 5' and 3' UTRs, can be incorporated into large circular DNAs like fosmids or bacterial artificial chromosomes (BACs). These large DNA constructs, which include enhancers in the flanking sequence, can be 20-30 kb or larger and cannot be cloned using traditional methods. To generate these large tagged proteins, recombineering in *E. coli* is used, followed by ϕC31-mediated site-directed transgenesis to facilitate their transformation into flies. Using this method, a library of over 800 C-terminal tagged genomic protein lines was generated. The FlyFos library has an average genomic insert size of 36kb, and proteins are labelled with a multi-epitope tag (Sarov et al., 2016). In this collection, 207 lines were analysed, but none covered neuronal transmembrane proteins. The main caveat of this method is that what is gained from endogenous expression is lost in specificity. Since these large genomic transgenes incorporate native enhancers and promoters to reflect their endogenous expression patterns, they do not allow for altering the cell types in which they are expressed.

1.4.3 Endogenous Protein Tags

Tagging proteins at their endogenous gene loci ideally replicates the natural expression levels and localisation patterns. Historically, the first endogenously tagged proteins were created using gene trap collections with transposable elements (TEs). These collections were generated using TEs, which somewhat randomly insert artificial exons containing a tag into protein-coding regions of genes. This method relied on TEs like P-elements and PiggyBacs, and several hundred protein trap lines were created this way. However, these efforts were labour-intensive and required screening millions of animals. This was because P-elements exhibited a strong insertion bias towards promoters, while PiggyBacs were more challenging to mobilise (Häcker et al., 2003). To overcome these limitations, the Minos-mediated integration cassette (MiMIC) approach was developed (Venken et al., 2011). Minos transposons integrate almost randomly within the genome, showing a subtle preference for introns, making them more suitable for protein trapping. MiMIC includes a mutator cassette with splice acceptors and stop codons, which can be replaced with

practically any construct, particularly various protein tags, through recombination-mediated cassette exchange (RMCE) using ϕC31 integrase (Bateman et al., 2006; Venken et al., 2011). The MiMIC collection has generated approximately 18,000 insertions, with 7,500 deposited in the Bloomington *Drosophila* Stock Center, covering 2,854 coding introns of 1,862 genes (Nagarkar-Jaiswal, et al., 2015).

However, like the other TEs, the primary drawback of Minos is that it inserts itself randomly. This randomness necessitates extensive screening to identify useful insertions and does not guarantee that the integration results in an expressed protein tag, thus failing to provide information on protein localisation or dynamics. With the advent and ease of using CRISPR/Cas9 for targeted genome editing, these drawbacks can be mitigated by allowing precise insertion of MiMIC and MiMIC-like Swappable Insertion Cassette (SIC) at specific genomic locations (Lee et al., 2018; Kanca et al., 2019). The *Drosophila* Genome Disruption Project has shifted from generating untargeted MiMIC insertions to targeted CRIMIC insertions using CRISPR/Cas9-mediated genome editing, aiming to insert CRIMIC (for CRISPR-mediated integration cassette) into 2,500 genes that encode human gene homologues not yet targeted by MiMIC. In combination, the MiMIC and CRIMIC collections will target more than 4,000 genes, representing about one-third of all *Drosophila* protein-coding genes (Lee et al., 2018; Kanca et al., 2019). In addition to these efforts, further studies have employed similar strategies to target specific gene loci, such as neurotransmitter receptor genes, building on the advancements in targeted genetic insertions. A study used CRISPR/Cas9-mediated genome editing to insert a T2A-Gal4 gene trap cassette into the endogenous locus at the C-terminus of 75 neurotransmitter receptor genes (Kondo et al., 2020). Similar to the MiMIC and CRIMIC collections, the original cassette can be swapped with a reporter such as Venus, a variant of yellow fluorescent protein, to visualise neurotransmitter receptor localisation. Direct loci modification for tagging proteins offers precise recapitulation of protein expression levels by integrating tags directly at the endogenous locus. This approach is also highly expandable and versatile, permitting the replacement of cassettes with various tags or functional modules using RMCE. However, a limitation shared with traditional genomic transgenes is that proteins tagged via endogenous locus modification are expressed ubiquitously in all cells, thus lacking cell-type specificity.

The ideal protein labelling strategy would ensure both endogenous expression and cell-type specificity, providing accurate protein expression and localisation within the context of specific cell types. To date, only a few techniques have achieved this. The first of these strategies developed was Synaptic Tagging with Recombi-

nation (STaR), a method for cell-type-specific labelling of synapses (Chen et al., 2014). In this study, the genomic regions of *brp* and *ort* genes were modified to include an FRT-Stop-FRT cassette along with a tag and a 2A sequence. This modification enabled the conditional labelling of the presynaptic protein BRP and the postsynaptic histamine receptor ort with small epitope tags V5 or OLLAS in specific cell types. These modified genetic sequences were introduced into the fly genome using B ACs. The study found that the number and distribution of BRP puncta labelled using STaR were consistent with T-bars identified by EM studies, validating the accuracy of this method. Using a similar method, an inducible FRT-STOP-FRT-VAChT::HA allele, which conditionally tags the vesicular acetylcholine transporter (VAChT), was generated (Pankova & Borst, 2017). Using this line, VAChT was identified in the axons of Mi1 and Tm3 neurons, indicating that these neurons provide cholinergic input to the T4 neurons (Pankova & Borst, 2017). Recently, the STaR method has been expanded and improved to generate conditional single-cell labelling (Sanfilippo et al., 2024). To generate tagged alleles, the endogenous genomic loci encoding neurotransmitter receptor subunits were modified by directed knock-in of DNA sequences encoding a STOP cassette and epitope tags using CRISPR/Cas9-mediated genome editing. To label the cell of interest, a plasmid containing UAS followed by a membrane marker such as myr-RFP and a noncanonical recombinase KDR was used. Expression of a cell-specific Gal4 would label the cell of interest by activating KDR recombinase, which would remove the stop cassette in only the cell type of interest, thus labelling the protein as well. This method was applied to 11 neurotransmitter receptor subunits from the cys-loop superfamily. GFP Reconstitution Across Synaptic Partners (GRASP) is another method that has been modified to generate endogenous cell-type-specific labelling (Luo et al., 2020). As the name suggests, GFP is split into two parts, only becoming activated and fluorescent upon reconstitution (Feinberg et al., 2008). The protein of interest is tagged with a GFP11 fragment in the endogenous gene loci. The other GFP fragment, GFP1-10, is expressed in a conditional manner using the UAS/GAL4 system and Flp recombinase to remove a STOP cassette in the particular cell type of interest. This method visualised insulin receptors (InR) in *Drosophila's* developing Dm8 neurons, revealing their dynamic regulation during dendritic development.

1.5 Motion Vision Pathway in *Drosophila*

1.5.1 General Anatomy of the Fly Eye

One of the most striking features of fruit flies is their large compound eyes, each built from approximately 750 ommatidia (Ready et al., 1976). Within a single ommatidium, eight different photoreceptors (R1-R8) reside. The outer photoreceptors, R1–R6, form a ring surrounding the inner two photoreceptors, R7 and R8, which are positioned one above the other (Dietrich, 1909; Wolken et al., 1957; Braitenberg, 1966, 1967). Photoreceptors R1-R6 contain a green-sensitive rhodopsin as a photopigment and are the main input to the fly visual system (Harris et al., 1976; O'Tousa et al., 1985). The mutant form of the rhodopsin Rh1 (encoded by the gene *ninaE*) exhibits motion blindness and cannot elicit an optomotor response (Heisenberg & Buchner, 1977; Yamaguchi et al., 2008; Zhu et al., 2009). The inner photoreceptors R7 and R8, which are mainly responsible for colour vision, have specific photopigments that are sensitive to different wavelengths of light depending on the subtypes they reside in. R7 photoreceptors express either Rh3 (UV-sensitive) in pale R7 cells or Rh4 (UV-sensitive) in yellow R7 cells. Similarly, R8 photoreceptors express Rh5 (blue-sensitive) in pale R8 cells or Rh6 (green-sensitive) in yellow R8 cells (Papatsenko et al., 1997; Wardill et al., 2012). Each photoreceptor has a receptive field with a diameter of about 5° at half-maximum sensitivity and an interommatidial angle of 5° (Götz, 1964). Each ommatidium covers a distinct part of the visual field with minimal overlap, resulting in a pixelated, low-resolution view of the world. Despite the low spatial resolution of individual photoreceptors, the compound eye's design enables nearly complete panoramic vision without the need for eye movement, ideally suiting the detection of motion and wide-field coverage over fine detail.

1.5.2 Motion Vision Circuit

The fly devotes around half of its brain to processing visual information. The optic lobe, which receives visual input from the compound eye, is divided retinotopically into four main neuropil layers: lamina, medulla, lobule, and lobule plate (Fischbach & Dittrich, 1989; Bausenwein et al., 1992; Takemura et al., 2008; Morante & Desplan, 2008). Within these neuropils, approximately 100 different cell types can be found within each column. Over a hundred years ago, the first anatomical representation of the optic lobe at the cellular level was created using the Golgi staining method (Fischbach & Dittrich, 1989; Ramón y Cajal et al., 1915; Strausfeld, 1971). Recently, this catalogue was extended by large electron microscopy datasets

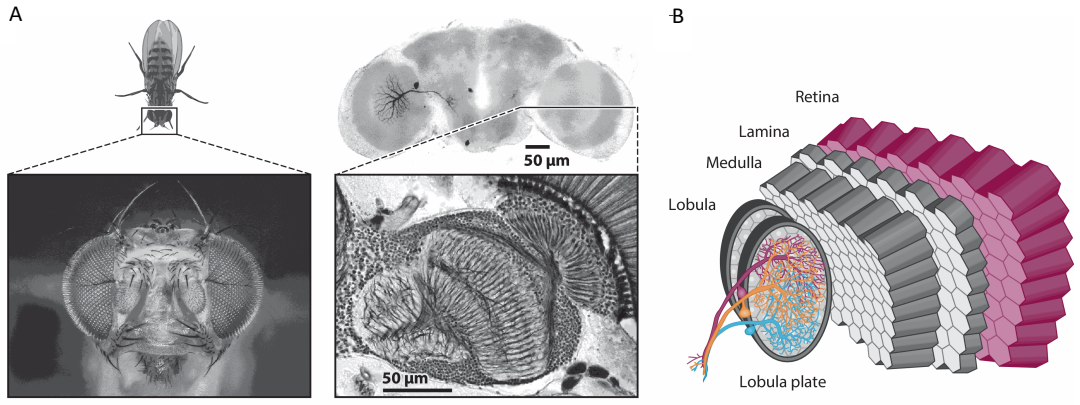

Figure 1.3: **A**: Micrograph showing the *Drosophila* head, with a facet eye visible on each side (left). The top image presents a frontal cross-section of the *Drosophila* brain, highlighting a single lobula plate tangential cell stained following patch-clamp recording. The bottom image illustrates a horizontal cross-section of the optic lobe, stained using Bodian's method, revealing the columnar organisation (right). **B**: Diagram of the optic lobe, displaying the retina and its four distinct neuropils: lamina, medulla, lobula, and lobula plate. Figure used with permission from Borst & Groschner (2023).

from the Janelia Research Campus (Takemura et al., 2013; Takemura et al., 2017; Shinomiya et al., 2019).

Within the optic lobe, the outer photoreceptors R1-R6 are the first cells in the motion vision circuit to receive sensory cues in the form of light. Photoreceptors convert the light energy into electrical signals through the phototransduction pathway, which leads to cell depolarisation (Juusola & Hardie, 2001). This triggers the release of histamine, resulting in the hyperpolarisation of large monopolar cells, L1-L5, which reside in the lamina, the first optic neuropil (Gisselmann et al., 2002; Hardie, 1989; Meinertzhagen & O'Neil, 1991). At this point, luminance signals from the photoreceptors are split into two divergent pathways: the ON and OFF pathways, which act in parallel to each other. The ON pathway processes luminance increments, while the OFF pathway processes luminance decrements (Joesch et al., 2010). The ON pathway signals downstream via glutamatergic L1 neurons as the prominent input, in addition to cholinergic L3 and L5 neurons. The signal inversion in L1 neurons from hyperpolarisation to depolarisation in postsynaptic neurons is facilitated by the inhibitory glutamate receptor GluClα and involves multiple synaptic steps. The OFF pathway signals via cholinergic

L2-L4 neurons, with L2 being the major input (Meier et al., 2014; Takemura et al., 2011).

In the subsequent neuropil, the medulla, axons of laminar cells traverse the first optic chiasm and synapse with various medulla intrinsic (Mi) and transmedullary (Tm) neurons in layers 1-5 of the outer medulla. Mi neurons connect the different layers of the medulla, whereas the Tm neurons, as their name implies, connect specific medulla regions to layers of the lobula and lobula plate. Additionally, centrifugal (C) neurons make connections between the medulla and lamina. The complex cell 1 (CT1) primarily forms connections in the medulla and the lobula. Specifically, the dendritic arbors of CT1 extensively innervate the M10 layer of the medulla and the Lo1 layer of the lobula. L1 neurons provide input to several neurons in the ON pathway, namely, Mi1, Tm3, and C3, while L5 primarily provides input to Mi4. L3 synapses onto the glutamatergic neuron Mi9 in the medulla. In addition to CT1, the medulla neurons synapse onto the dendrites of columnar T4 cells, whose dendrites are located in the M10 layer of the medulla (Ammer et al., 2015; Takemura et al., 2017). In contrast, OFF pathway neurons L2-L4 provide input to Tm1, Tm2, Tm4, and Tm9, which synapse onto the dendrites of T5 cells, whose dendritic arbors are located in the Lo1 region of the lobula (Meier et al., 2014; Serbe et al., 2016; Shinomiya et al., 2014).

T4 and T5 neurons are the first cells in the visual pathway where the direction of motion is explicitly represented, as none of their presynaptic cells are direction-selective (Fisher et al., 2015; Maisak et al., 2013; Serbe et al., 2016). Each T4/T5 dendrite collects information from approximately eight columns, with each subtype responding to one of the four cardinal directions, and their axons terminating in one of the four specific layers of the lobula plate (Fisher et al., 2015; Maisak et al., 2013). Blocking synaptic transmission from T4 and T5 neurons results in a complete loss of the fly's optomotor response, indicating their crucial role in motion detection (Bahl et al., 2013; Schnell et al., 2010). T4 neurons, associated with the ON pathway, respond to light increments and reside in layer 10 of the medulla, while T5 neurons, associated with the OFF pathway, respond to light decrements and reside in layer 1 of the lobula. These neurons provide cholinergic input to lobula plate tangential cells (LPTCs), and blocking their synaptic output leads to unresponsive LPTCs and diminished behavioural responses to visual motion stimuli (Mauss et al., 2014; Shinomiya et al., 2014; Schnell et al., 2012; Bahl et al., 2013; Schilling & Borst, 2015).

Lobula plate tangential cells are a class of motion-sensitive neurons in the fly visual system, first described in the blowfly (Dvorak et al., 1975). These neurons are key integrators of visual motion information, receiving input from

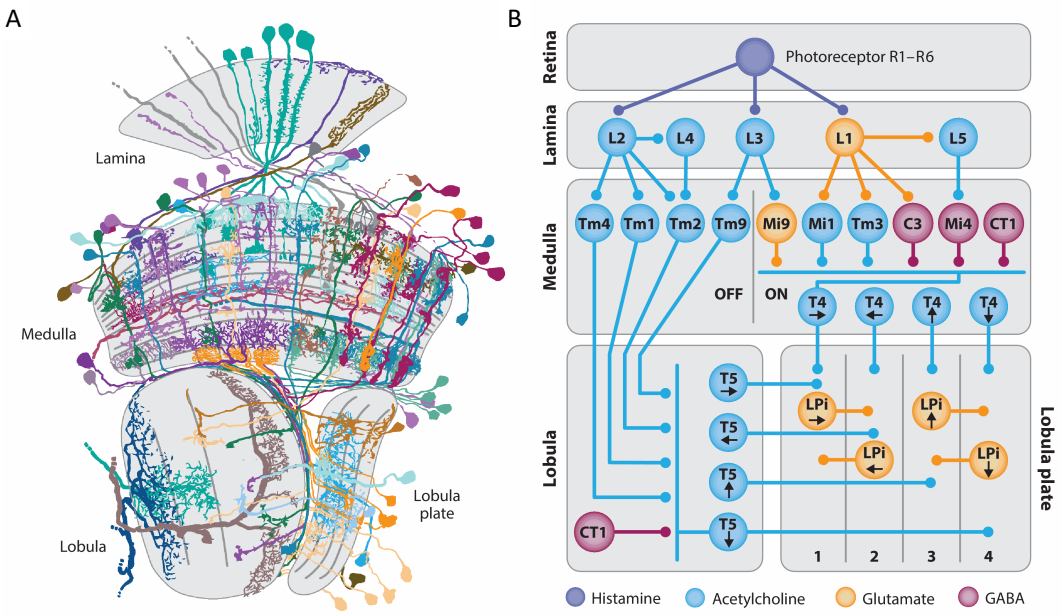

Figure 1.4: A: Illustration depicting various cell types present in the *Drosophila* optic lobe. **B:** Simplified schematic of the motion vision circuit. Photoreceptors connect to lamina (L) cells, which divide signals into ON and OFF pathways. Transmedullary (Tm), medulla intrinsic (Mi), centrifugal (C), and complex tangential (CT) cells relay these temporally filtered signals to the dendrites of T4 cells in the medulla and T5 cells in the lobula. The axons of different T4 and T5 cell types project to one of the four layers of the lobula plate, where they synapse onto lobula plate intrinsic (LPi) and lobula plate tangential cells, not shown in this diagram for simplicity. Figure used with permission from Borst & Groschner (2023).

T4 and T5 neurons, which are responsible for encoding local motion signals. LPTCs are characterised by their direction-selective and motion-opponent responses, depolarising to stimuli in their preferred direction and hyperpolarising to stimuli in their null direction (Joesch et al., 2010; Schnell et al., 2012). They are divided into two main types based on their response to motion: horizontal system (HS) cells and vertical system (VS) cells. HS cells, which arborise in layers 1 and 2 of the lobula plate, are tuned to horizontal motion, whereas VS cells, which arborise in layers 3 and 4, are tuned to vertical motion (Borst & Egelhaaf, 1989; Haag & Borst, 2004). These cells span hundreds of columns in the lobula plate and integrate ON and OFF signals from T4 and T5 neurons, enabling them to cover large visual fields (Bishop & Keehn, 1966; Hausen, 1976; Joesch et al., 2008). The motion-opponent characteristic of LPTCs is enhanced by the input from lobula plate-intrinsic (LPi) neurons, which provide inhibitory signals via glutamate and the glutamate-gated chloride channel GluClα. This interaction increases the selectivity of LPTCs to flow fields during flight by providing null direction inhibition (Mauss et al., 2015). LPTCs project wide-field motion information to higher processing centres

in the central brain, including neck motor neurons and descending neurons, playing a crucial role in visual feedback for self-motion and flight stability (Krapp & Hengstenberg, 1996; Buschbeck & Strausfeld, 1997; Haag & Borst, 2002; Wertz et al., 2008; Kim et al., 2014; Suver et al., 2016). The synaptic transmission from T4 and T5 neurons to LPTCs is essential for generating the fly's optomotor response, a reflex that stabilises flight by adjusting to visual motion cues (Schnell et al., 2012; Maisak et al., 2013).

1.5.3 Computational Models

The Hassenstein-Reichardt (HR) and Barlow-Levick (BL) detector models are foundational to our understanding of direction selectivity (Hassenstein & Reichardt, 1956; Barlow & Levick, 1965). They elucidate how neural circuits process motion by integrating spatially and temporally offset signals from adjacent photoreceptors. These models highlight the roles of signal delay, multiplicative enhancement, and inhibitory suppression, providing a framework for understanding how motion direction is encoded at the neuronal level. The HR model, developed in the 1950s, uses a delay-and-compare mechanism where signals from two adjacent photoreceptors are temporally delayed and then multiplicatively combined, enhancing responses to motion in the preferred direction (Hassenstein & Reichardt, 1956). In contrast, the BL model, proposed in the 1960s, employs inhibitory mechanisms to suppress responses to motion in the null direction. This suppression occurs when signals from adjacent photoreceptors arrive simultaneously at the neuron, activating an inhibitory response that blocks the excitatory signal (Barlow & Levick, 1965). This mechanism ensures that the neuron only responds to motion in the preferred direction, enhancing direction selectivity by effectively "vetoing" signals that would indicate motion in the opposite, or null, direction. Recent research suggests that the computation of direction selectivity in T4/T5 neurons utilises a combination of both the Hassenstein-Reichardt (HR) and Barlow-Levick (BL) models (Haag et al., 2016, 2017; Leong et al., 2016; Arenz et al., 2017). The hybrid detector model HR-BL integrates preferred-direction enhancement, as proposed by the HR model, with null-direction suppression, as suggested by the BL model. This combination allows T4/T5 neurons to achieve high directional tuning by enhancing signals in the preferred direction and suppressing those in the null direction (Arenz et al., 2017; Haag et al., 2016; Leong et al., 2016).

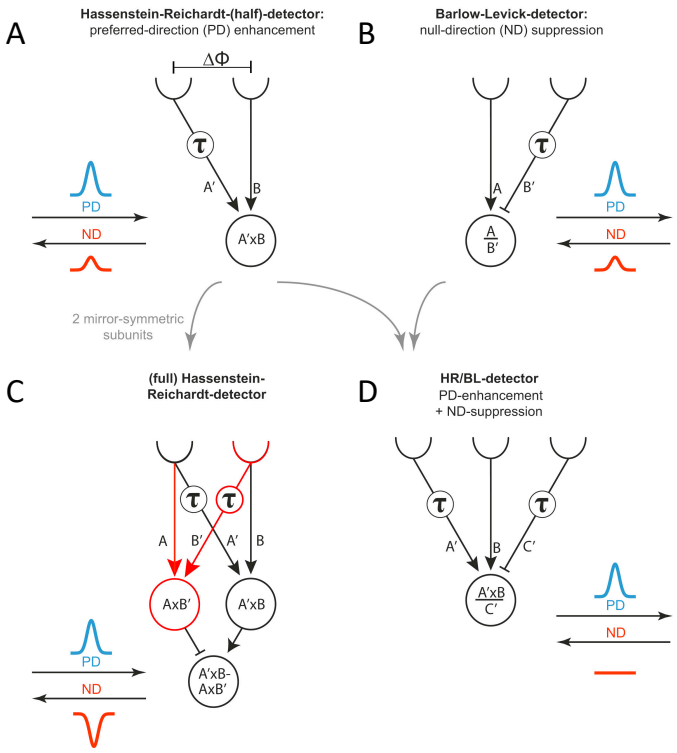

Figure 1.5: **(A)** In the Hassenstein-Reichardt (HR) model, shown here with a half-detector, a delay (t) is applied to the first of two arms, which are activated by motion in the preferred direction (PD). This causes the signals from adjacent photoreceptors, separated by a visual angle (Df), to coincide. **(B)** The Barlow-Levick (BL) detector places the delay on the opposite arm, introducing a non-linearity that suppresses responses to motion in the null direction (ND). **(C)** In a complete HR correlator, two mirror-symmetric subunits are combined, leading to an opponent detector that depolarises in the PD and hyperpolarises in the ND. **(D)** A combination of the HR and BL models, based on the response of T4 neurons to motion stimuli, integrates PD enhancement and ND suppression along the PD axis. Figure used with permission from Arenz et al. (2017).

At the cellular level, this hybrid detector model, HR-BL, achieves direction selectivity in T4/T5 neurons by integrating various synaptic inputs. T4 neurons of the ON pathway receive a combination of glutamatergic, GABAergic, and cholinergic inputs that enable precise motion detection (Shinomiya et al., 2019). Glutamatergic inputs from Mi9 enhance responses to stimuli in the preferred direction, while GABAergic inputs from Mi4, C3, and CT1 on the proximal side suppress responses to the null direction. Cholinergic inputs from Mi1 and Tm3 in the central region of the dendrite serve as the primary sources of excitatory signals (Shinomiya et al., 2019). T5 neurons, responsible for detecting motion in the OFF pathway, receive a

complex array of inputs that enable precise detection of light decrements (Joesch et al., 2010). These neurons receive inhibitory GABAergic inputs from CT1 and TmY15, which are crucial for suppressing responses to motion in the null direction. Additionally, T5 neurons receive excitatory cholinergic inputs from several sources, including Tm1, Tm2, Tm4, and Tm9, distributed across the central and distal dendritic areas (Shinomiya et al., 2019). This combination of inhibitory and excitatory signals ensures that T5 neurons can accurately differentiate between motion in the preferred direction and the null direction. The HR-BL model effectively captures the complex integration of excitatory and inhibitory inputs, reflecting the high degree of direction selectivity observed in T4/T5 neurons.

1.6 Thesis Overview and Objectives

The intricate roles of neurotransmitter receptors, ion channels, and electrical synapses in shaping neuronal function are fundamental to our understanding of neural circuits. However, most previous studies have focused on dissecting the motion vision circuit at the cellular level, as described in the previous chapter. Tools to visualise the expression and distribution of neurotransmitter receptors and ion channels were lacking.

To close this research gap in Manuscript 1, we created tools to label neurotransmitter receptors and voltage-gated ion channels in a cell-type-specific manner, focusing on the motion-sensing T4/T5 neurons. In particular, we developed FlpTag, a novel genetic tool for cell-type-specific and endogenous protein labelling. This tool is designed to be versatile and flexible, making it relatively easy to apply to label other proteins in *Drosophila*. Our findings revealed that the glutamate receptor GluClα, the GABA receptor Rdl, and the acetylcholine receptor Dα7 are unevenly distributed along the dendrites of T4/T5 neurons. Additionally, we mapped the locations of the voltage-gated ion channels *para* and *Ih* within these neurons.

In Manuscript 2, we focused on electrical synapses formed by innexin gap junction proteins, which permit direct communication between adjacent cells throughout the nervous system. However, the full extent of their role in neural circuits, especially in visual processing, had not been thoroughly explored. The specific types of gap junctions expressed in the fly brain and their exact locations were largely unknown. To address this gap, we developed a comprehensive map of innexin expression throughout the central nervous system using immunohistochemistry. The study found that different innexin proteins are distributed across various

regions of the nervous system, with some localised to glial cells and others primarily in neurons. Notably, shakB was identified as the most widely expressed neuronal innexin and was crucial for maintaining stability in VS/HS neurons, preventing spontaneous voltage and calcium oscillations.

Chapter 2

Publications

2.1 Manuscript 1: Conditional protein tagging methods reveal highly specific subcellular distribution of ion channels in motion- sensing neurons

Sandra Fendl*, **Renee Marie Vieira*** and Alexander Borst

* equal contribution

Author contributions: S.F. conceived and designed the study; imaged all data shown and processed confocal images; wrote the manuscript and prepared the figures with the help of R.M.V. and A.B; R.M.V. conceived and designed the study; analyzed and quantified all imaged data; developed and created the UAS-lines and the FlpTag-construct and stocks with the help of S.F; A.B., Conceptualization, Resources, Supervision, Project administration, Writing - review and editing.

Renee Marie Vieira

Sandra Fendl

Alexander Borst

eLife

TOOLS AND RESOURCES

Conditional protein tagging methods reveal highly specific subcellular distribution of ion channels in motion-sensing neurons

Sandra Fendl[1,2†]*, Renee Marie Vieira[1†], Alexander Borst[1,2]

[1]Max Planck Institute of Neurobiology, Martinsried, Germany; [2]Graduate School of Systemic Neurosciences, LMU Munich, Martinsried, Germany

Abstract Neurotransmitter receptors and ion channels shape the biophysical properties of neurons, from the sign of the response mediated by neurotransmitter receptors to the dynamics shaped by voltage-gated ion channels. Therefore, knowing the localizations and types of receptors and channels present in neurons is fundamental to our understanding of neural computation. Here, we developed two approaches to visualize the subcellular localization of specific proteins in *Drosophila*: The flippase-dependent expression of GFP-tagged receptor subunits in single neurons and 'FlpTag', a versatile new tool for the conditional labelling of endogenous proteins. Using these methods, we investigated the subcellular distribution of the receptors GluClα, Rdl, and Dα7 and the ion channels para and Ih in motion-sensing T4/T5 neurons of the *Drosophila* visual system. We discovered a strictly segregated subcellular distribution of these proteins and a sequential spatial arrangement of glutamate, acetylcholine, and GABA receptors along the dendrite that matched the previously reported EM-reconstructed synapse distributions.

***For correspondence:** sfendl@neuro.mpg.de

[†]These authors contributed equally to this work

Competing interest: See page 21

Funding: See page 22

Received: 10 September 2020
Accepted: 14 October 2020
Published: 20 October 2020

Reviewing editor: Claude Desplan, New York University, United States

Introduction

How neural circuits implement certain computations in order to process sensory information is a central question in systems neuroscience. In the visual system of *Drosophila*, much progress has been made in this direction: numerous studies examined the response properties of different cell-types in the fly brain and electron microscopy studies revealed the neuronal wiring between them. However, one element crucial to our understanding is still missing; these are the neurotransmitter receptors used by cells at the postsynaptic site. This knowledge is essential since neurotransmitters and corresponding receptors define the sign and the time-course of a connection, that is whether a synapse is inhibitory or excitatory and whether the signal transduction is fast or slow. The same neurotransmitter can act on different receptors with widely differing effects for the postsynaptic neuron. Glutamate for instance is mainly excitatory, however, in invertebrates it can also have inhibitory effects when it acts on a glutamate-gated chloride channel, known as GluClα (***Cully et al., 1996***; ***Liu and Wilson, 2013***; ***Mauss et al., 2015***). Recently, it has also been shown that acetylcholine, usually excitatory, might also be inhibitory in *Drosophila*, if it binds to the muscarinic mAChR-A receptor (***Bielopolski et al., 2019***). Hence, knowledge inferring the type of transmitter receptor at a synapse is essential for our understanding of the way neural circuits process information.

Moreover, voltage-gated ion channels shape synaptic transmission and the integration of synaptic inputs by defining the membrane properties of every neural cell type. The voltage-gated calcium channel cacophony, for instance, mediates influx of calcium ions that drives synaptic vesicle fusion at presynaptic sites (***Kawasaki et al., 2004***; ***Fisher et al., 2017***). Voltage-gated sodium channels like paralytic (para) are important for the cell's excitability and the generation of sodium-dependent

action potentials. The voltage-gated channel Ih influences the integration and kinetics of excitatory postsynaptic potentials (**Magee, 1999**; **Littleton and Ganetzky, 2000**; **George et al., 2009**). However, only little is known about how these channels are distributed in neurons and how this shapes the neural response properties.

One of the most extensively studied neural circuits in *Drosophila* is the motion vision pathway in the optic lobe and the underlying computation for direction-selectivity. The optic lobe comprises four neuropils: lamina, medulla, lobula, and lobula plate (**Figure 1A**). As in the vertebrate retina, the fly optic lobe processes information in parallel ON and OFF pathways (**Joesch et al., 2010**; **Borst and Helmstaedter, 2015**). Along the visual processing chain, T4/T5 neurons are the first neurons that respond to visual motion in a direction selective way (**Maisak et al., 2013**; **Behnia et al., 2014**; **Fisher et al., 2015a**; **Arenz et al., 2017**; **Strother et al., 2017**). T4 dendrites reside in layer 10 of the medulla and compute the direction of moving bright edges (ON-pathway). T5 dendrites arborize in layer 1 of the lobula and compute the direction of moving dark edges (OFF-pathway) (**Maisak et al., 2013**). The four subtypes of T4/T5 neurons (a, b, c, d), project axon terminals to one of the four layers in the lobula plate, each responding only to movement in one of the four cardinal directions, their preferred direction (**Maisak et al., 2013**).

How do T4/T5 neurons become direction-selective? Both T4 and T5 dendrites span around eight columns collecting signals from several presynaptic input neurons, each of which samples information from visual space in a retinotopic manner (**Haag et al., 2016**; **Shinomiya et al., 2019**). The functional response properties of the presynaptic partners of T4/T5 have been described in great detail (**Behnia et al., 2014**; **Ammer et al., 2015**; **Fisher et al., 2015a**; **Fisher et al., 2015b**; **Serbe et al., 2016**; **Arenz et al., 2017**; **Strother et al., 2017**; **Strother et al., 2018**; **Drews et al., 2020**) along with their neurotransmitter phenotypes (**Takemura et al., 2017**; **Richter et al., 2018**; **Shinomiya et al., 2019**; **Davis et al., 2020**). T4 dendrites receive glutamatergic, GABAergic and cholinergic input, whereas T5 dendrites receive GABAergic and cholinergic input only. These input synapses are arranged in a specific spatial order along T4/T5 dendrites (s. **Figure 1C and D**; for overview **Takemura et al., 2017**; **Shinomiya et al., 2019**).

Which receptors receive this repertoire of different neurotransmitters at the level of T4/T5 dendrites? Recently, several RNA-sequencing studies described the gene expression pattern of nearly all cell-types in the optic lobe of the fruit fly including T4/T5 neurons (**Pankova and Borst, 2016**; **Konstantinides et al., 2018**; **Davis et al., 2020**; **Hörmann et al., 2020**). T4/T5 neurons were found to express numerous receptor subunits of different transmitter classes and voltage-gated ion channels at various expression strengths. However, RNA-sequencing studies do not unambiguously answer the above question for two reasons: mRNA and protein levels are regulated in complex ways via post-transcriptional, translational, and protein degradation mechanisms making it difficult to assign protein levels to RNA levels (**Vogel and Marcotte, 2012**). Secondly, standard RNA-sequencing techniques cannot provide spatial information about receptor localizations, hence, they are not sufficient to conclude which transmitter receptors receive which input signal. Both shortcomings could in principle be overcome by antibody staining since immunohistochemical techniques detect neurotransmitter receptors at the protein level and preserve spatial information. However, high-quality antibodies are not available for every protein of interest and may have variable affinity due to epitope recognition (**Fritschy, 2008**). Furthermore, labeling ion channels via antibodies and ascribing expression of a given channel to a cell-type in dense neuronal tissue remains challenging. The disadvantages of the above techniques highlight the need for new strategies for labeling neurotransmitter receptors in cell types of interest.

In this study, we employed existing and generated new genetic methods to label and visualize ion channels in *Drosophila*. For endogenous, cell-type-specific labeling of proteins, we developed a generalizable method called FlpTag which expresses a GFP-tag conditionally. Using these tools, we explored the subcellular distribution of the glutamate receptor subunit GluClα, the acetylcholine receptor subunit Dα7, and the GABA receptor subunit Rdl in motion-sensing T4/T5 neurons. We found these receptor subunits to be differentially localized between dendrites and axon terminals. Along the dendrites of individual T4/T5 cells, the receptor subunits GluClα, Rdl, and Dα7 reveal a distinct distribution profile that can be assigned to specific input neurons forming synapses in this area. Furthermore, we demonstrated the generalizability of the FlpTag approach by generating lines for the metabotropic GABA receptor subunit Gaba-b-r1 and the voltage-gated ion channels para

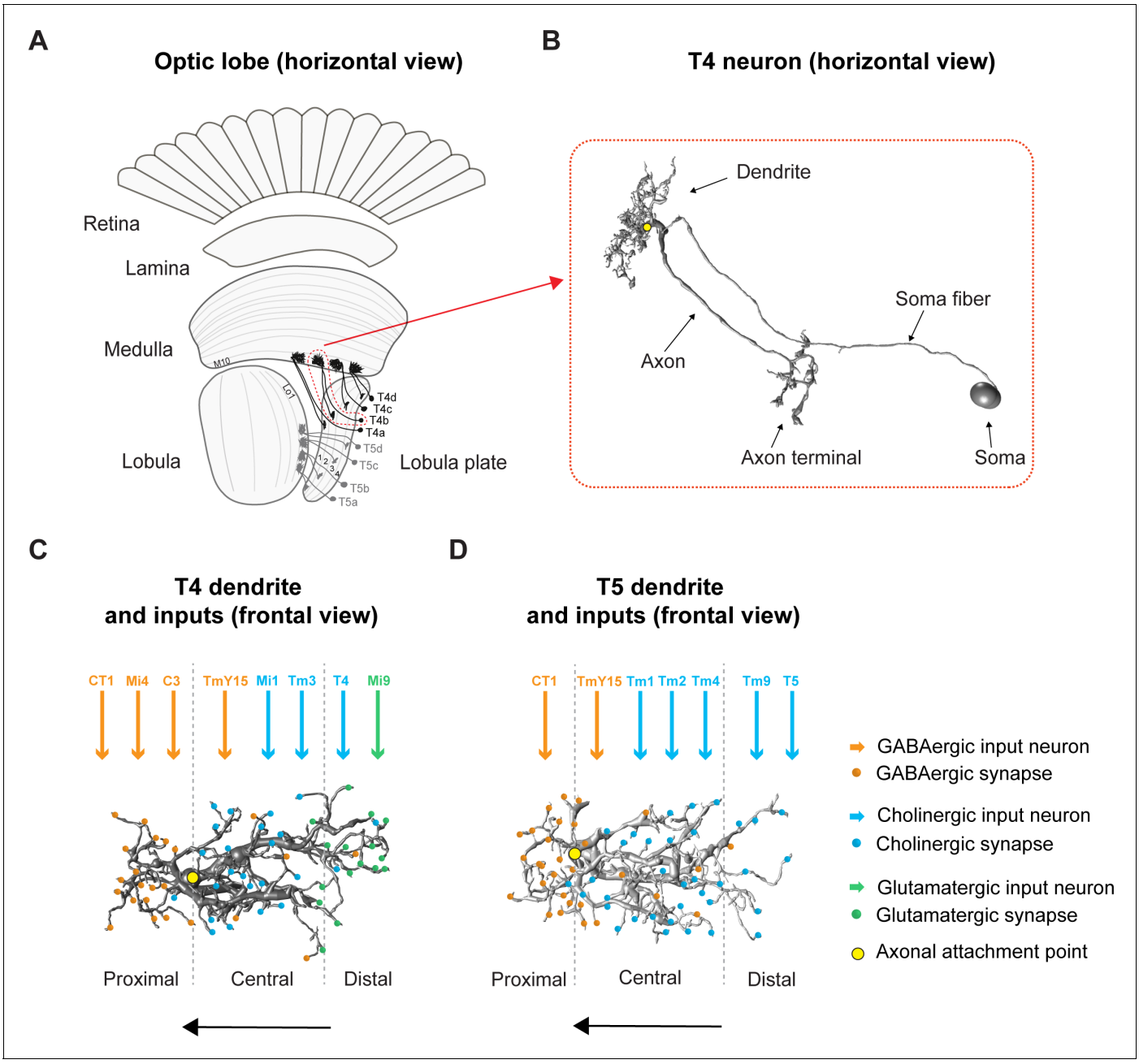

Figure 1. Overview of the fly optic lobe and anatomy of T4/T5 neurons with their presynaptic partners and distribution of input synapses. (**A**) Horizontal view of optic lobe with retina, lamina, medulla, lobula, and lobula plate. T4 dendrites (darker gray) reside in layer 10 of the medulla, T5 dendrites (lighter gray) in layer 1 of the lobula. T4/T5 axon terminals of all subtypes (**a, b, c, d**) project to the lobula plate in four layers. (**B**) Close-up, horizontal view of EM-reconstructed single T4 neuron with dendrite, axon, axon terminal, soma fiber and soma (image extracted from Seven medulla column connectome dataset, https://emdata.janelia.org/#/repo/medulla7column, #3b548, Janelia Research Campus). (**C**) Scheme of individual T4 dendrite and distribution of input synapses (frontal view). The dendrite depicted here is oriented pointing to the right side against its preferred direction from right to left (indicated by arrow). Input on proximal base of T4 dendrite: GABAergic CT1, Mi4 and C3. In the central area: GABAergic TmY15 and cholinergic Mi1 and Tm3. On the distal tips T4 receive input from cholinergic T4 from the same subtype and glutamatergic Mi9. Yellow circle labels first branching point of the dendritic arbor. Reproduced from ***Figure 4***, ***Shinomiya et al., 2019***, eLife, published under the Creative Commons Attribution 4.0 International Public License (CC BY 4.0; https://creativecommons.org/licenses/by/4.0/). (**D**) Scheme of individual T5 dendrite and distribution of input synapses (frontal view). The dendrite depicted here is oriented pointing to the right side against its preferred direction from right to left (indicated by arrow). The T5 dendrite receives GABAergic input from CT1 on the proximal base and from TmY15 in the central area. Cholinergic synapses are formed with Tm1, Tm2, and Tm4 in the central area and with Tm9 and T5 from the same subtype on the distal dendritic tips. Yellow circle labels first branching

Figure 1 continued on next page

Figure 1 continued

point of the dendritic arbor. Reproduced from ***Figure 4***, ***Shinomiya et al., 2019***, eLife, published under the Creative Commons Attribution 4.0 International Public License (CC BY 4.0; https://creativecommons.org/licenses/by/4.0/).

and Ih. The strategies described here can be applied to other cells as well as other proteins to reveal the full inventory and spatial distribution of the various ion channels within individual neurons.

Results

Subcellular localization of the inhibitory glutamate receptor GluClα in T4/T5 neurons

As suggested by the connectome (***Takemura et al., 2017***; ***Shinomiya et al., 2019***) and antibody staining against the vesicular glutamate transporter VGluT (***Richter et al., 2018***), T4 cells receive input on their dendrites from the glutamatergic medulla neuron Mi9. Since a multitude of glutamate receptors exist, both excitatory and inhibitory, we explored which glutamate receptor forms the synapse between the glutamatergic Mi9 input and T4 dendrites.

According to a RNA-sequencing study, GluClα is the most highly expressed glutamate receptor in T4 neurons (***Davis et al., 2020***). To investigate the distribution of this glutamate receptor in T4 and T5 neurons, we developed a transgenic fly line that allowed us to express a GFP-tagged GluClα in a cell-type specific way. We created a *UAS-GluClα::GFP* line bearing the cDNA of GluClα with a GFP-insertion (***Supplementary file 1***). This construct can be combined with any *Gal4*-line to study the receptor's expression and its subcellular localization. We combined the *UAS-GluClα::GFP* line with a membrane-bound *UAS-myr::tdTomato* and expressed both constructs under the control of a T4/T5-specific *Gal4*-driver line. We found GluClα in T4 dendrites of the medulla, where it is distributed in discrete puncta (***Figure 2A***; horizontal section, first two panels). A top view of the medulla of these flies reveals that these puncta are arranged in circular clusters, each corresponding to one column (***Figure 2A***, right panel). Since Mi9 is the only glutamatergic presynaptic partner of T4 cells in the medulla (***Takemura et al., 2017***; ***Richter et al., 2018***; ***Shinomiya et al., 2019***), this columnar arrangement likely reflects the columnar array of Mi9 cell inputs. Conversely, T5 dendrites are completely devoid of GluClα signal (***Figure 2A***, first two panels). This result is in agreement with T5 dendrites not receiving glutamatergic input (***Richter et al., 2018***). In addition to the medulla layer 10, GFP signal of GluClα::GFP is also visible in the axon terminals of T4/T5 in the lobula plate (***Figure 2A***, first two panels). However, both T4 and T5 cells send their axons into the lobula plate, therefore, this staining cannot be assigned to one of the cell types specifically. To differentiate between the two cell types, we used two different driver lines, one specific for either T4 or T5 cells. We confirmed the presence of GluClα in the dendritic layer of T4 cells (***Figure 2B***) and the lack thereof in the dendritic layer of T5 cells (***Figure 2C***). Interestingly, with these specific driver lines, both T4 and T5 neurons express the glutamate receptor in their axon terminals in the lobula plate (***Figure 2B*** and ***Figure 2C***). The presence of GluClα in the axon terminals of T5 neurons explains the high GluClα-mRNA levels in T5 (***Davis et al., 2020***) even though T5 dendrites are missing a glutamatergic presynaptic partner (***Takemura et al., 2017***; ***Richter et al., 2018***; ***Shinomiya et al., 2019***).

One caveat associated with overexpression-lines is a potential mis-localization of proteins. To control for this effect, we used a pan-neuronal *Gal4-line* to express the *UAS-GluClα::GFP* construct and compared this expression pattern to an existing MiMIC protein trap line with GFP insertion (MiMIC GFSTF) in the endogenous locus of GluClα (Mi02890) (***Nagarkar-Jaiswal et al., 2015a***). We observed broad expression of GluClα throughout all neuropils of the optic lobe in both genotypes (***Figure 2—figure supplement 1A and B***). We quantified the mean fluorescence intensity of manually drawn ROIs around the medulla and found both values to be similar for the pan-neuronal *UAS-GluClα::GFP* and the MiMIC line (***Figure 2—figure supplement 1D***). Furthermore, we expressed the *UAS-GluClα::GFP* line with a driver line for T1, a cell-type which lacks GluClα mRNA (***Davis et al., 2020***). Our *UAS*-line confirmed this result as we could not detect significant levels of GluClα::GFP protein in T1 (***Figure 2—figure supplement 1E***). Hence, overexpression of GFP-tagged GluClα, introduced as a transgene, leads to a subcellular localization pattern that seems to be identical to the endogenous GluClα protein.

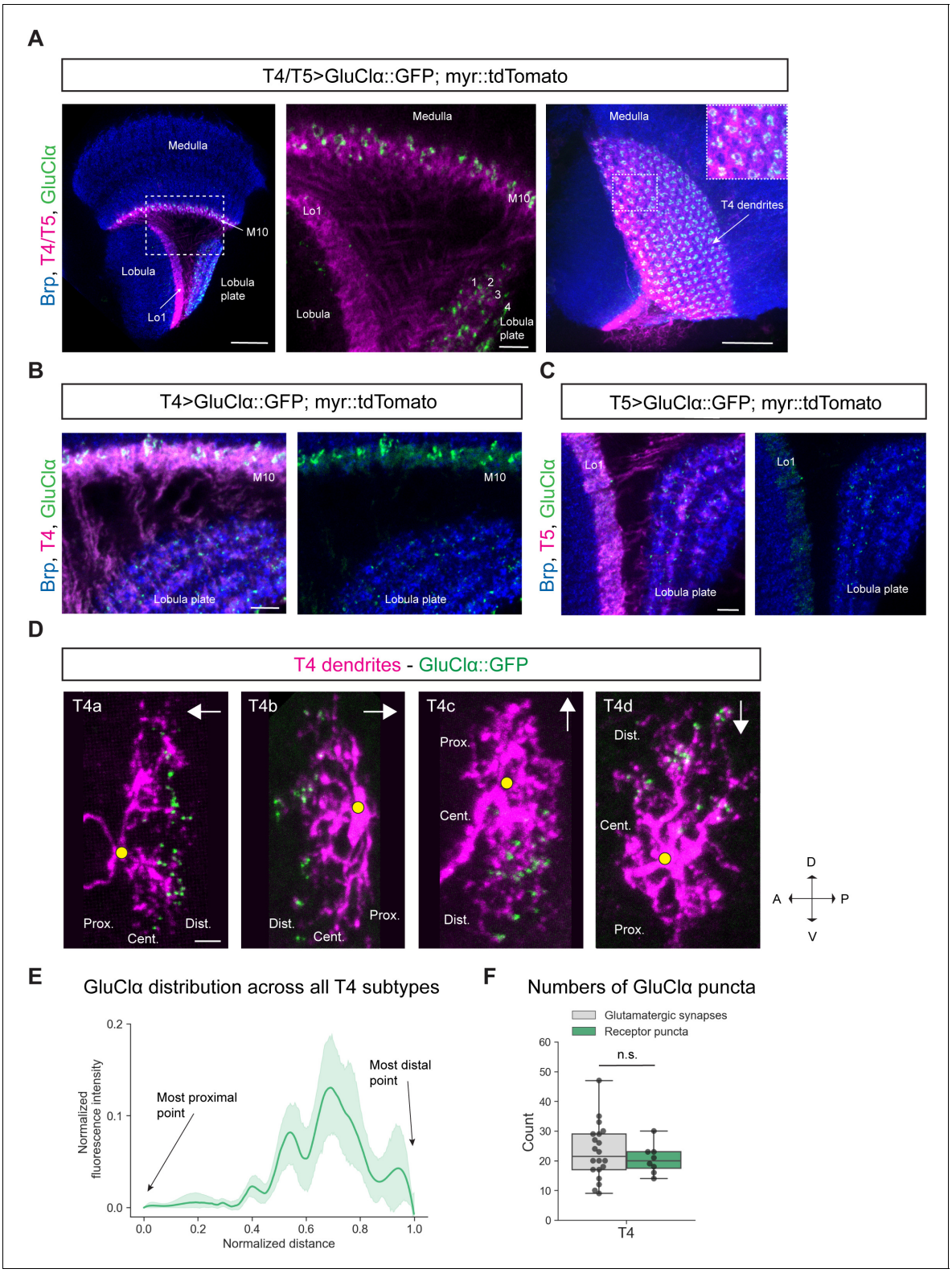

Figure 2. Subcellular localization of the inhibitory glutamate receptor GluClα in T4/T5 neurons. (**A**) Optic lobe with T4/T5 neurons labeled with myr::tdTomato and GluClα::GFP. Left panel: horizontal view on the optic lobe overview (scale bar: 20 µm). Central panel: close-up of medulla layer M10, lobula layer Lo1 and lobula plate layers 1–4 (scale bar: 5 µm). Right panel: Frontal view on medulla layer M10 with T4 dendrites (scale bar: 20 µm); inset: close-up of columnar GluClα::GFP structure in layer 10 of the medulla. (**B**) Close-up of T4 dendrites in layer 10 of the medulla and axon terminals in

Figure 2 continued on next page

Figure 2 continued

lobula plate labeled with myr::tdTomato and GluClα::GFP (scale bar: 5 μm). (**C**) Close-up of T5 dendrites in layer 1 of the lobula and axon terminals in lobula plate labeled with myr::tdTomato and GluClα::GFP (scale bar: 5 μm). (**D**) Individual T4 dendrites labeled with tdTomtato and GluClα::GFP; subtypes a-d pointing in their natural orientation in visual space coordinates (A = anterior, p=posterior, D = dorsal, V = ventral). White arrows indicate preferred directions for every subtype and the dendrites' proximal (Prox.), central (Cent.) and distal (Dist.) areas are labeled (scale bar: 2 μm). Yellow circle labels first branching point of the dendrite. (**E**) Quantification of GluClα distribution over the whole dendritic length (normalized distance) averaged across several T4 dendrites from all subtypes (n = 8). All dendrites were aligned pointing to the right with the most proximal point at 0.0 and the most distal point at 1.0. (**F**) Quantification of GluClα puncta averaged across several T4 dendrites from all subtypes (mean ± SD = 20.5, 4.98 [n = 8]) (same cells used in E) compared to number of glutamatergic input synapses from Mi9 (mean ± SD = 23.0, 9.34 [n = 20]) (EM numbers: personal communication, K. Shinomiya, May 2020). n.s., not significant p>0.05 (p=0.37, t-test).

The online version of this article includes the following source data and figure supplement(s) for figure 2:

Source data 1. Table with numbers of GluClα puncta quantified for T4 dendrites.

Figure supplement 1. Pan-neuronal GluClα levels and distribution in the optic lobe are comparable for MiMIC GFSTF, FlpTag and *UAS*-line.

Given that Mi9 is the only glutamatergic input neuron to T4 dendrites and GluClα is the corresponding glutamate receptor, we hypothesized that GluClα should localize on the individual T4 dendrite exclusively where Mi9 makes glutamatergic synapses with the latter. Therefore, we wanted to visualize the distribution of GluClα at the single-cell level along individual T4 dendrites. The dendrites of each T4/T5 subtype are oriented pointing against their preferred direction (***Takemura et al., 2017***; ***Shinomiya et al., 2019***). With respect to the point of axonal attachment to the dendrite, T4/T5 dendrites can be divided into a proximal, central and distal region (summarized in ***Figure 1B–D***). Electron microscopy studies have shown that Mi9 forms synaptic contacts with T4 on the distal tips of its dendrite (***Figure 1C***; ***Takemura et al., 2017***; ***Shinomiya et al., 2019***). Since T4/T5 dendrites are strongly intermingled in their respective layers, it is not possible to resolve receptor localizations at the single-cell level by labeling the whole population. We used a flippase-based mosaic approach (***Gordon and Scott, 2009***) to sparsely label single T4/T5 neurons with tdTomato together with the *UAS-GluClα::GFP* construct. By using a *FRT-Gal80-FRT* with an hs-FLP, both *UAS-myr::tdTomato* and *UAS-GluClα::GFP* expression are dependent on the same stochastic FLP-event. A heat-shock-activated flippase removes the FRT-flanked *Gal4-repressor Gal80*, which disinhibits Gal4, promoting transcription of both *UAS*-reporters simultaneously resulting in expression of membrane-bound tdTomato and GFP-tagged GluClα in only a few cells of interest. In individual T4 dendrites, we observed that GluClα was predominantly localized to the distal tips, which holds true for all four T4 subtypes (***Figure 2D***). We quantified the intensity distribution of the GluClα::GFP-signal over dendritic distance in individual T4 dendrites. To combine and average this distribution for all four subtypes, we rotated dendrites from each subtype such that the proximal side was on the left side of the image and the distal tips were pointing to the right. Averaged intensities across all subtypes confirmed our observations on individual cells, showing that GluClα is indeed localized toward the distal dendritic tips of T4 dendrites (***Figure 2E***). In addition, we quantified the numbers of GluClα puncta for all subtypes and compared them to the synapse numbers of glutamatergic Mi9 inputs onto T4 determined by the previous EM study (***Shinomiya et al., 2019***). The number of GluClα-puncta per T4 cell dendrite (mean: 20.5 puncta) matches closely the number of glutamatergic input synapses made by Mi9 onto one T4 cell (mean: 23 synaptic contacts; personal communication, K. Shinomiya, May 2020) (***Figure 2F***). This suggests that every GluClα-punctum resolved by confocal microscopy in individually labeled T4 dendrites represents one postsynaptic GluClα receptor cluster corresponding to one Mi9-T4 synapse.

In summary, GluClα localizes to the dendrites of T4 cells and to the axon terminals of both T4 and T5 cells. At the single-cell level, GluClα is distributed toward the distal tips of the dendrites in all T4 subtypes. Strikingly, the number of GluClα puncta closely matches the number of input synapses provided by Mi9, the only glutamatergic input neuron to T4 dendrites.

Rdl localizes to T4/T5 dendritic compartments receiving GABAergic input

Having identified glutamatergic synapses, we employed similar methods to visualize GABAergic synapses in T4/T5 neurons. T4 dendrites receive input from several GABAergic cell-types in the medulla: on the proximal base of the dendrite, these are the columnar cells Mi4, C3; the multicolumnar

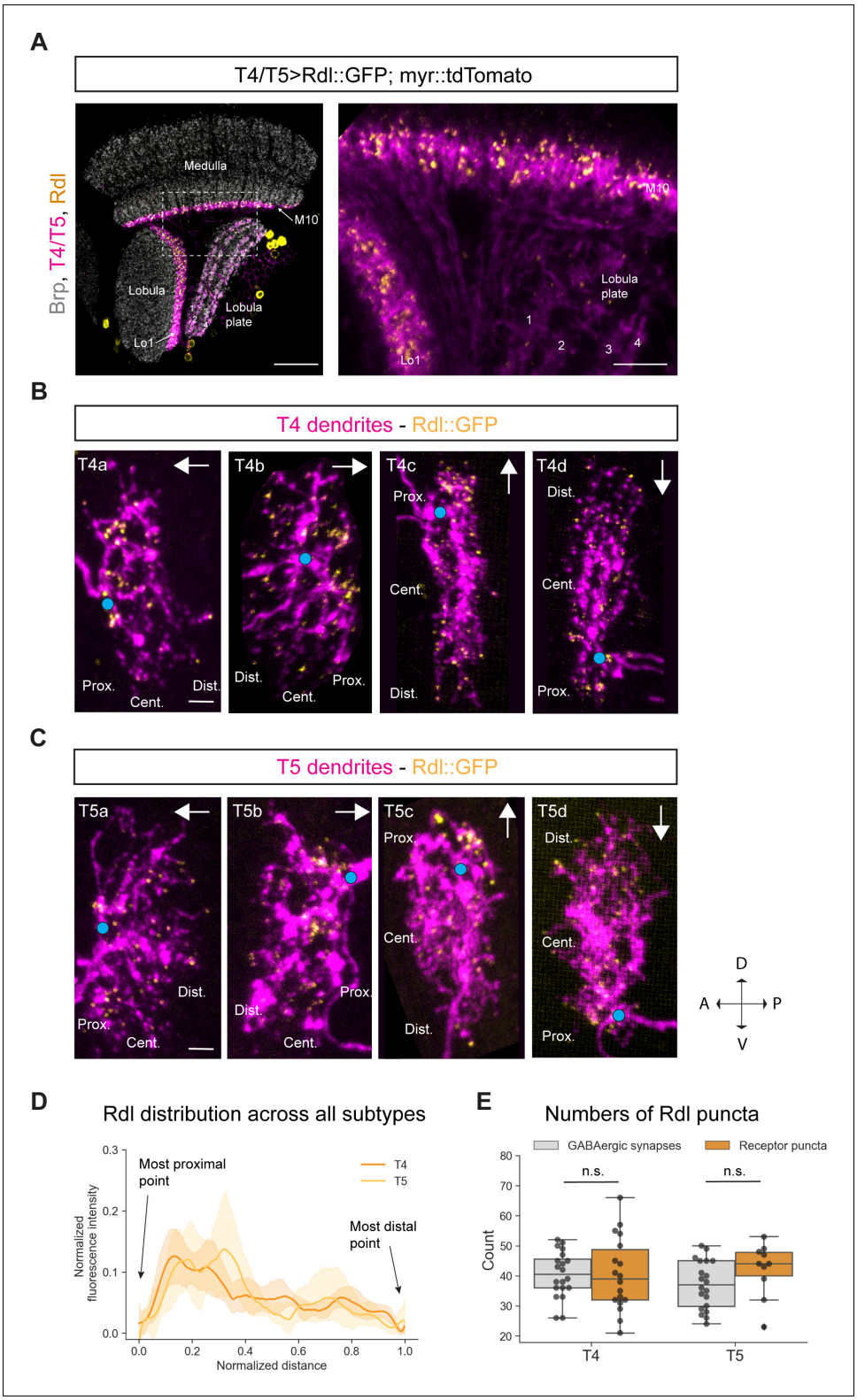

Figure 3. Subcellular localization of the GABA receptor Rdl in T4/T5 neurons. (**A**) Optic lobe with T4/T5 neurons labeled with myr::tdTomato and Rdl::GFP. Left panel: horizontal view on the optic lobe overview (scale bar: 20 µm). Right panel: close-up of medulla layer M10, lobula layer Lo1 and lobula plate layers 1–4 (scale bar: 5 µm). (**B**) Individual T4 dendrites labeled with tdTomtato and Rdl::GFP; subtypes a-d pointing in their natural orientation in visual space coordinates (A = anterior, p=posterior, D = dorsal, V = ventral). White arrows indicate preferred directions for every subtype and the

Figure 3 continued on next page

Figure 3 continued

dendrites' proximal (Prox.), central (Cent.) and distal (Dist.) areas are labeled (scale bar: 2 µm). Blue circle labels first branching point of the dendrite. (**C**) Individual T5 dendrites labeled with tdTomtato and Rdl::GFP; subtypes a-d pointing in their natural orientation in visual space coordinates (A = anterior, p=posterior, D = dorsal, V = ventral). White arrows indicate preferred directions for every subtype and the dendrites' proximal (Prox.), central (Cent.) and distal (Dist.) areas are labeled (scale bar: 2 µm). Blue circle labels first branching point of the dendrite. (**D**) Quantification of Rdl distribution over the whole dendritic length (normalized distance) averaged across several T4 (n = 18) and T5 dendrites (n = 10) from all subtypes. All dendrites were aligned pointing to the right with the most proximal point at 0.0 and the most distal point at 1.0. (**E**) Quantification of Rdl puncta averaged across several T4 (mean ± SD = 40.4, 12.17 [n = 18]) and T5 dendrites (mean ± SD = 42.2, 8.88 [n = 10]) (same cells used in D) from all subtypes compared to number of GABAergic input synapses from T4 (mean ± SD = 40.5, 7.67 [n = 20]) and T5 (mean ± SD = 37.0, 8.05 [n = 20]) (EM numbers: personal communication, K. Shinomiya, May 2020). n.s., not significant p>0.05 (p=0.99 and p=0.13 respectively, t-test).
The online version of this article includes the following source data and figure supplement(s) for figure 3:

Source data 1. Table with numbers of Rdl puncta quantified for T4/T5 dendrites.
Figure supplement 1. Rdl is not detectable in the lamina neuron L1.

amacrine cell CT1 in the middle and distal part of the dendrite as well as TmY15 (***Figure 1C***). In contrast, T5 dendrites receive GABAergic input from only two cell-types: CT1 on the proximal base and TmY15 again throughout the central and distal area of the dendrite (***Figure 1D***). In total, T4 and T5 dendrites receive roughly the same number of GABAergic input synapses (***Takemura et al., 2017***; ***Shinomiya et al., 2019***). Three ionotropic GABA receptor subunits are described in the *Drosophila* genome: Rdl, Lcch3, and Grd (***Liu et al., 2007***). We focused on the GABA receptor subunit Rdl, since RNA-sequencing studies had identified Rdl as the most highly expressed ionotropic GABA receptor subunit in T4 and T5 neurons (***Pankova and Borst, 2016***; ***Davis et al., 2020***). Five Rdl subunits can form a homomeric chloride channel which leads to hyperpolarization upon GABA-binding, thus representing a receptor (***Ffrench-Constant et al., 1993***). Previous studies had created and used a UAS-Rdl::HA line to investigate the distribution of this GABA receptor subunit in *Drosophila* motoneurons and LPTCs (***Sánchez-Soriano et al., 2005***; ***Raghu et al., 2007***; ***Kuehn and Duch, 2013***). In our hands, the anti-HA staining of this line was too weak for conclusive results (data not shown), hence, we created a *UAS-Rdl::GFP* line, consisting of the coding sequence of Rdl and a GFP-tag (***Supplementary file 2***). Combining this line with a T4/T5 specific *Gal4*-line and a membrane-bound tdTomato revealed Rdl expression in both T4/T5 dendrites, but not in the axon terminals (***Figure 3A***). Taken together, both T4 and T5 neurons receive GABAergic inhibition via Rdl receptors on their dendrites.

In a control experiment, we tested for potential overexpression artifacts of the *UAS-Rdl::GFP* line. According to RNA-sequencing, Rdl is not expressed in the lamina monopolar neuron L1 (***Davis et al., 2020***). When we overexpressed *UAS-Rdl::GFP* by means of a *L1-Gal4* driver line, Rdl signal is not detectable in L1 dendrites (***Figure 3—figure supplement 1***). The Rdl::GFP protein was only visible in the cell bodies, presumably due to impaired protein translocation. This suggests that overexpressed Rdl only localizes to endogenous GABA synapses that are composed of the Rdl subunit. Hence, this line can be used to study the subcellular localization of Rdl in any given cell of interest.

Next, we looked at the distribution of the GABA receptor Rdl on individual T4 and T5 dendrites. Using the sparse labeling technique described above, we examined the Rdl::GFP distribution in individual T4/T5 dendrites. We found Rdl on the proximal base and in the central area of both T4 and T5 dendrites across all four subtypes (***Figure 3B*** and ***Figure 3C***). On the proximal base most of the Rdl-signal was arranged in strong discrete clusters, whereas sparse puncta localized to the central area and toward the distal tips. The strong Rdl-signal on the proximal base of the dendrite likely corresponds to the high number of GABAergic inputs provided by the following inputs: CT1, Mi4 and C3 for T4 (32.2 synapses) and CT1 for T5 (30.3 synapses) (personal communication, K. Shinomiya, May 2020). The sparsely distributed Rdl-puncta in the center and tips likely correspond to TmY15 inputs for both T4 and T5 dendrites. This distribution is recapitulated in the intensity quantification across all T4/T5 subtypes, with high Rdl intensity on the proximal side and lower signal in the central and distal area (***Figure 3D***). We quantified the numbers of Rdl receptor clusters in T4 and T5 dendrites and compared them to the sum of all GABAergic input synapses (Mi4, C3, CT1, TmY15 for T4 and CT1, TmY15 for T5) to T4/T5 mapped by EM studies. We found similar numbers of roughly 40 receptor clusters for both T4 and T5 which match the sum of all GABAergic input synapses to T4

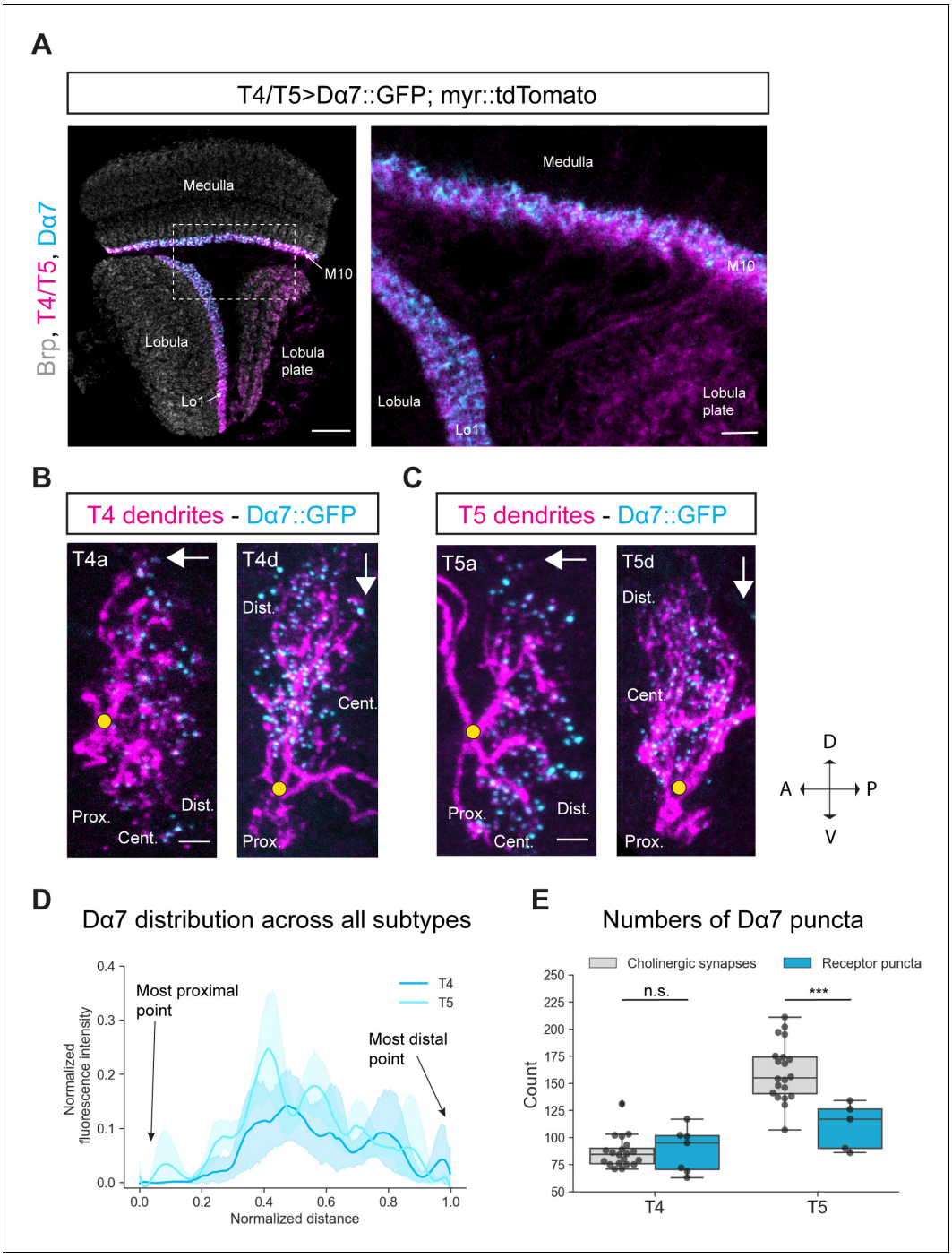

Figure 4. Subcellular localization of the ACh receptor subunit Dα7 in T4/T5 neurons. (**A**) Optic lobe with T4/T5 neurons labeled with myr::tdTomato and Dα7::GFP. Left panel: horizontal view on the optic lobe overview (scale bar: 20 µm). Right panel: close-up of medulla layer M10, lobula layer Lo1 and lobula plate layers 1–4 (scale bar: 5 µm). (**B**) Individual T4 dendrites labeled with tdTomtato and Dα7::GFP; subtypes a and d pointing in their natural orientation in visual space coordinates (A = anterior, p=posterior, D = dorsal, V = ventral). White arrows indicate preferred directions for every subtype and the dendrites' proximal (Prox.), central (Cent.) and distal (Dist.) areas are labeled (scale bar: 2 µm). Yellow circle labels first branching point of the dendrite. (**C**) Individual T5 dendrites labeled with tdTomtato and Dα7::GFP; subtypes a and d pointing in their natural orientation in visual space coordinates (A = anterior, p=posterior, D = dorsal, V = ventral). White arrows indicate preferred directions for every subtype and the dendrites' proximal (Prox.), central (Cent.) and distal (Dist.) areas are labeled (scale bar: 2 µm). Yellow circle labels first branching point of the dendrite. (**D**) Quantification of Dα7 distribution over the whole dendritic length (normalized distance) averaged across several T4 (n = 6) and T5 dendrites (n = 5) from all subtypes. All dendrites were aligned pointing to the right with the most proximal point at 0.0 and the most distal point at 1.0. (**E**) Quantification

Figure 4 continued on next page

Figure 4 continued

of Dα7 puncta averaged across several T4 (mean ± SD = 92.67, 18.67 [n = 6]) and T5 dendrites (mean ± SD = 110.6, 21.53 [n = 5]) (same cells like in D) from all subtypes compared to number of cholinergic input synapses for T4 (mean ± SD = 86.45, 14.37 [n = 20]) and T5 (mean ± SD = 160.50, 26.93 [n = 20]) (EM numbers: personal communication, K. Shinomiya, May 2020). n.s., not significant, p>0.05; ***p<0.001 (p=0.46 and p=2.1e-4 respectively, t-test).

The online version of this article includes the following source data and figure supplement(s) for figure 4:

Source data 1. Table with numbers of Dα7 puncta quantified for T4/T5 dendrites.

Figure supplement 1. Pan-neuronal Dα7 levels and distribution in the optic lobe as seen with *UAS-Dα7::GFP* line, Dα7 antibody staining and *Dα7-Trojan-Gal4* line.

(mean: 40.45) and T5 (mean: 37) (***Figure 3E***) (EM numbers: personal communication, K. Shinomiya, May 2020). Taken together, Rdl receptor subunits localize to the proximal base, and to a lesser extent, in the central area of the dendritic arbor of T4 and T5 neurons, reflecting their GABAergic inputs revealed by EM (***Shinomiya et al., 2019***).

Dα7 localizes to T4/T5 dendritic compartments receiving cholinergic input

According to connectome data, T4 dendrites receive most of their input synapses from cholinergic Mi1 and Tm3 cells at the center of their dendrite (***Takemura et al., 2017***; ***Shinomiya et al., 2019***). Furthermore, T4 neurons of the same subtype form synapses with each other at the distal tips of their dendrites (***Figure 1C***). As T4 neurons are cholinergic (***Mauss et al., 2014***; ***Davis et al., 2020***), these T4-T4 synapses are thought to be cholinergic as well. With the exception of GABAergic CT1, T5 dendrites receive cholinergic input from Tm1, Tm2, and Tm4 in the central area of the dendrite. Tm9 and T5 provide cholinergic input mainly towards the distal tips of the dendrite (***Figure 1D***; ***Takemura et al., 2017***; ***Shinomiya et al., 2019***). T5 dendrites receive almost twice as many cholinergic inputs as T4; 160 and 87 synapses, respectively (***Shinomiya et al., 2019***). We used an existing GFP-tagged *UAS-Dα7::GFP* line to explore the subcellular distribution of these cholinergic synapses (***Raghu et al., 2009***). Dα7 is one of 10 different nicotinic ACh receptor subunits (Dα1-Dα7 and Dß1-Dß3) found in the *Drosophila* genome. All these subunits can form heteromeric receptors consisting of two or three subunits. In addition, Dα5, Dα6, and Dα7 can also form homomeric ACh receptors (***Lansdell and Millar, 2004***; ***Lansdell et al., 2012***). According to RNA-sequencing data, both T4 and T5 neurons express almost every ACh receptor subunit, except for Dα6 and Dß3 (***Davis et al., 2020***). Expression of *UAS-Dα7::GFP* with a *T4/T5-Gal4* line, revealed the distribution of Dα7 to both T4 and T5 dendrites while their axon terminals remained devoid (***Figure 4A***).

As previously conducted, we tested for potential overexpression artifacts of the *UAS-Dα7::GFP* line. We expressed Dα7::GFP in all neurons and compared the expression pattern to two controls: first, an antibody staining against Dα7, and second, a MiMIC Trojan-*Gal4* (TG4) line for Dα7 combined with *UAS-Dα7::GFP* (***Figure 4—figure supplement 1A–C***; ***Fayyazuddin et al., 2006***; ***Diao et al., 2015***; ***Lee et al., 2018***). The Trojan-*Gal4* (TG4) line has a *Gal4* insertion in the Dα7 gene, which drives expression of *Gal4* only under endogenous transcriptional control of Dα7. Combining this line with the reporter lines *UAS-myr::tdTomato* and *UAS-Dα7::GFP* should label all Dα7-expressing cells with tdTomato, and only within those cells, the Dα7 receptor subunits with GFP. In the pan-neuronal overexpression of *UAS-Dα7::GFP*, the ACh receptor subunit is broadly expressed throughout all neuropils with specific strong Dα7 signal in medulla layer 10 where T4 dendrites reside and lobula layer 1 where T5 dendrites reside (***Figure 4—figure supplement 1A***). However, in both the antibody- and the TG4-experiment, there is only weak Dα7 signal in M10 and Lo1 detectable (***Figure 4—figure supplement 1B and C***). Thus, under UAS-driven overexpression, the levels of Dα7 are increased compared to endogenous Dα7 levels in M10 and Lo1.

To assess whether the subcellular distribution of Dα7 is qualitatively altered by overexpression, we characterized the distribution of Dα7 in a cell type that does not express this receptor subunit endogenously. Transcriptomic data revealed that Dα7 is not expressed in Mi1 (***Davis et al., 2020***). However, Mi1 receives cholinergic input from L3 and L5 and expresses several different ACh receptor subunits (***Takemura et al., 2017***; ***Shinomiya et al., 2019***; ***Davis et al., 2020***). We tested the *UAS-Dα7::GFP* line in Mi1 to explore the qualitative overexpression-effects of this line. When *UAS-*

Dα7::GFP was overexpressed in Mi1, Dα7 localized to layers 1 and 5 of the medulla, where the dendrites of Mi1 neurons arborize and receive cholinergic input from L3 and L5 (***Takemura et al., 2017***; ***Figure 4—figure supplement 1D***). This suggests that overexpressed Dα7::GFP localizes to cholinergic synapses and becomes part of an ACh-receptor, even if this subtype is not endogenously expressed in this neuron. If this scenario is true, the *UAS-Dα7::GFP* line does not report real endogenous subunit compositions with Dα7, but in general it can still be used as a marker for postsynaptic cholinergic sites.

To test this hypothesis, we performed sparse labeling of individual T4/T5 dendrites with the earlier described Gal80-hs-flippase method to explore the subcellular distribution of Dα7 along T4/T5 dendrites. Dα7 was distributed along the central area and distal tips of both T4 and T5 dendrites whereas the proximal base of the dendrite was completely devoid of Dα7 signal (***Figure 4B and C***). In the quantification, it becomes clear that for all subtypes the Dα7-intensity is strongest in the central area and slightly reduced toward the distal tips (***Figure 4D***). Taken together, these results demonstrate that with the *UAS-Dα7::GFP* line, Dα7 localizes to the areas where T4/T5 dendrites receive cholinergic input and not to the proximal base which receives only GABAergic synapses. We quantified the number of Dα7-puncta and compared it to the number of cholinergic synaptic contacts from T4/T5 inputs. For T4 dendrites the numbers of Dα7 puncta quantified (mean: 88.4) matched the numbers of cholinergic input synapses mapped by EM reconstruction (mean: 86.9; personal communication, K. Shinomiya, May 2020) (***Figure 4E***). This strongly suggests that Dα7 localizes only to cholinergic synapses. However, for T5 dendrites the Dα7 puncta exhibited 60 synapses less on average when compared to the mean of the summed cholinergic EM input synapse (***Figure 4E***). The levels of Dα7 along the dendrite are similar for T4 and T5 (***Figure 4D***), even though T5 receive more cholinergic inputs on their distal tips than T4 (***Shinomiya et al., 2019***). The main cholinergic input to T5 in the distal area is Tm9, which makes approximately 60 synapses with T5 dendrites. These 60 synapses could potentially be formed via different cholinergic receptors other than Dα7, for instance muscarinic ACh receptors (***Davis et al., 2020***).

In summary, the *UAS-Dα7::GFP* line cannot be used to define the exact composition of ACh receptor subunits of cholinergic synapses, but labels (nicotinic) ACh receptors in general. It, nevertheless, can be used as a marker for postsynaptic ACh receptors. Using this approach, we found that the central and distal areas of both T4 and T5 dendrites possess cholinergic receptors. The proximal base of the dendrites, as well as axon terminals are devoid of cholinergic input.

FlpTag - a new tool for cell-type-specific, endogenous protein labeling

Additionally, we sought to observe the spatial distribution of endogenous receptors using a cell-type specific approach. We designed FlpTag, a new conditional, endogenous protein labeling strategy inspired by recently published flippase-dependent methods (***Fisher et al., 2017***; ***Nagarkar-Jaiswal et al., 2017***; ***Williams et al., 2019***).

The FlpTag cassette is a protein trap cassette consisting of a central GFP tag placed between a splice acceptor (SA) and splice donor (SD), flanked by specific Frt sites forming a FLEX-switch for stable inversion (***Figure 5A***, upper panel) (***Schnütgen et al., 2003***; ***Xue et al., 2014***). The FlpTag cassette is integrated into an intronic coding region of interest by recombinase mediate cassette exchange (RMCE) in vivo. We used the existing intronic MiMIC gene trap with attP landing sites to facilitate ΦC31-dependent exchange of the MiMIC insertion with our FlpTag cassette, consisting of ΦC31 integrase attB sites on either end (***Venken et al., 2011***; ***Nagarkar-Jaiswal et al., 2015b***). After ΦC31-dependent knock-in, two independent lines can be isolated. One in which the GFP is in the 5′ to 3′ direction; the same orientation as the gene. In this configuration FlpTag acts as a protein trap, revealing the protein's expression pattern. In the alternate orientation the FlpTag cassette is in the 3′ to 5′ direction; oppositely oriented to the gene. For the FlpTag approach, we used the oppositely oriented line in which the coding intron with the FlpTag cassette is naturally cut out during mRNA splicing and no labeling takes place. Only upon UAS-Gal4 driven, cell-type-specific expression of the Flp recombinase, the cassette is flipped in the same orientation as the gene. Due to the presence of flanking SA and SD, the GFP cassette is then spliced into the mature mRNA which is translated, labeling the protein with GFP (***Figure 5A***, lower panel).

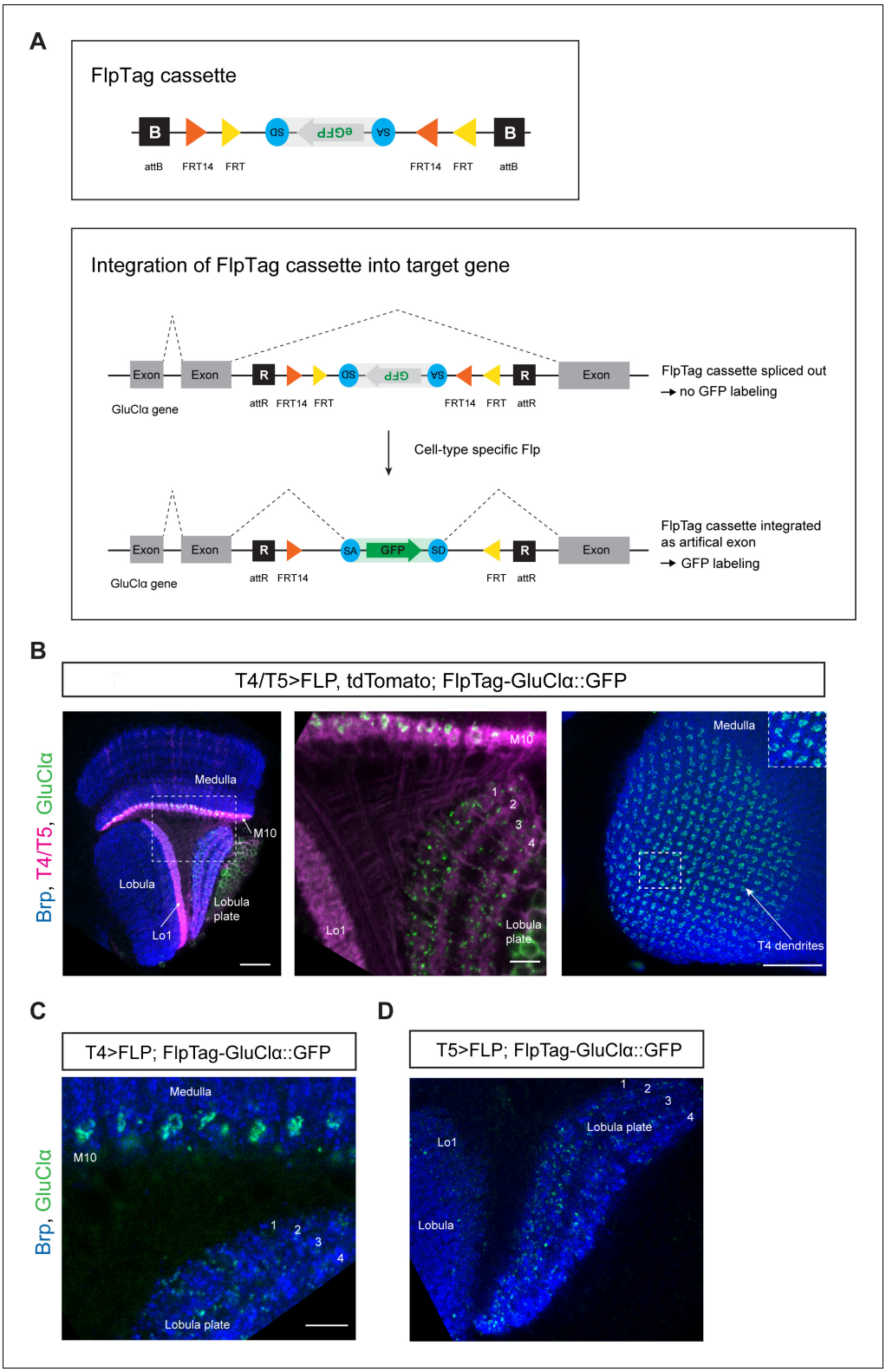

Figure 5. FlpTag, a new tool for cell-type-specific, endogenous labeling as shown with GluClα. (**A**) Scheme of FlpTag cassette (first panel) and integration of FlpTag cassette into target gene (second panel). The FlpTag cassette consists of attB-sites, specific FRT sites which form a FLEx-switch, a splice acceptor, GFP and a splice donor. After ΦC31-dependent integration of the FlpTag cassette into a coding intron of the GluClα target gene, two lines with opposite orientations of the cassette can be obtained. In the initial line with the cassette and GFP in opposite orientation with respect to the

Figure 5 continued on next page

Figure 5 continued

gene (shown here), the cassette is spliced out together with the intron and no GFP-labeling occurs. After cell-type-specific Flp expression, the FlpTag cassette is flipped, stably integrated as an artificial exon and GluClα is labeled with GFP. (**B**) Optic lobe with T4/T5 neurons labeled with myr::tdTomato and FlpTag-GluClα::GFP. Left panel: horizontal view on the optic lobe overview (scale bar: 20 μm). Central panel: close-up of medulla layer M10, lobula layer Lo1 and Lobula plate layers 1–4 (scale bar: 5 μm). Right panel: Frontal view on medulla layer M10 with T4 dendrites (scale bar: 20 μm); inset: close-up of columnar GluClα::GFP structure in layer 10 of the medulla. (**C**) Close-up of FlpTag-GluClα::GFP driven with a *T4-Gal4*-line; shown are layer 10 of the medulla where T4 dendrites reside and lobula plate layers 1–4 where T4 project their axon terminals to (scale bar: 5 μm). (**D**) Close-up of FlpTag-GluClα::GFP driven with a *T5-Gal4*-line; shown are layer 10 of the medulla where T4 dendrites reside and lobula plate layers 1–4 where T4 project their axon terminals to (scale bar: 5 μm).

FlpTag line for GluClα

In a first proof-of-principle experiment, we generated a FlpTag line for the glutamate receptor subunit GluClα. The FlpTag cassette was inserted in the MiMIC insertion site MI02890, in the coding intron between the last two exons of the GluClα gene. For comparison of the various GluClα-tagged lines, we examined the expression patterns generated by pan-neuronal FlpTag-GluClα::GFP, MiMIC GFSTS GluClα, and pan-neuronal *UAS-GluClα::GFP*. The expression patterns were similar for all three lines (***Figure 2—figure supplement 1***). We combined the GluClα-FlpTag line with *UAS-FLPD.1* and a T4/T5-specific driver-line. The distribution pattern of GluClα seen here is virtually identical to the *UAS-GluClα::GFP* genotype: GluClα is localized to T4 dendrites, the T5 dendrite area is devoid of GluClα signal, and T4/T5 axon terminals in the lobula plate co-localize with GluClα (***Figure 5B***, compare with ***Figure 2A***). Expression of flippase and FlpTag-GluClα in T4 neurons only further demonstrates the localization of the glutamate receptor to T4 dendrites and axon terminals, as seen before with the *UAS-GluClα::GFP* line (***Figure 5C***, compare with ***Figure 2B***). Specific expression of flippase and FlpTag-GluClα in T5 neurons revealed that the receptor localizes specifically to the axon terminals in all T5 subtypes, as visualized by the presence of GluClα puncta in all layers of the lobula plate (***Figure 5D***, compare with ***Figure 2C***).

Taken together, we generated a new *UAS*-line and developed a new tool for studying the localization of GluClα in a cell-type-specific manner. Both the *UAS-GluClα::GFP* line and the FlpTag-line led to similar results when compared to the pan-neuronal and T4/T5-specific experiments. These tools can be used interchangeably to study the subcellular localization of GluClα in any given cell of interest.

FlpTag lines for Gaba-b-r1, para and Ih

The FlpTag approach is generalizable and can be applied to any of the >2800 fly lines available with MiMIC attP insertions in coding introns (***Nagarkar-Jaiswal et al., 2015b***). To demonstrate the universal applicability of our FlpTag strategy, we set out to generate more FlpTag lines with the aforementioned approach of integrating the FlpTag cassette into existing MiMIC landing sites in coding introns. In keeping with our interest in neurotransmitter receptors we explored another GABA receptor subunit, the metabotropic channel Gaba-b-r1. Additionally, we examined other proteins that shape the biophysical response properties of neurons, such as the voltage-gated ion channels para and Ih.

The metabotropic GABA receptor subunit Gaba-b-r1 is the most highly expressed GABA receptor subunit in T4/T5 neurons after Rdl (***Pankova and Borst, 2016***; ***Davis et al., 2020***). Gaba-b-r1 is one out of three G-protein-coupled GABA receptor subunits described in *Drosophila* and has been shown to be involved in sleep and appetitive long-term memory (***Mezler et al., 2001***; ***Kim et al., 2017***; ***Pavlowsky et al., 2018***). We inserted the FlpTag cassette in the MiMIC site between the first and second exon (MI01930) of the Gaba-b-r1 locus via RMCE. Again, two lines with two different orientations of the FlpTag cassette were obtained. The line with the cassette in the same orientation as the gene was used to observe the pan-neuronal distribution of the endogenous GABA receptor subunit. Gaba-b-r1 is expressed throughout all neuropils with strongest signal in the outer distal layers of the medulla and the medial part of the lobula (***Figure 6A***). Upon cell-type specific, FLP-dependent inversion of the FlpTag cassette in T4/T5 neurons, we could not observe any Gaba-b-r1::GFP signal in T4/T5 dendrites or axons (***Figure 6B***). Although RNAseq studies detected Gaba-b-r1 mRNA in T4/T5 neurons (***Pankova and Borst, 2016***; ***Davis et al., 2020***), we could not confirm this result at the protein level.

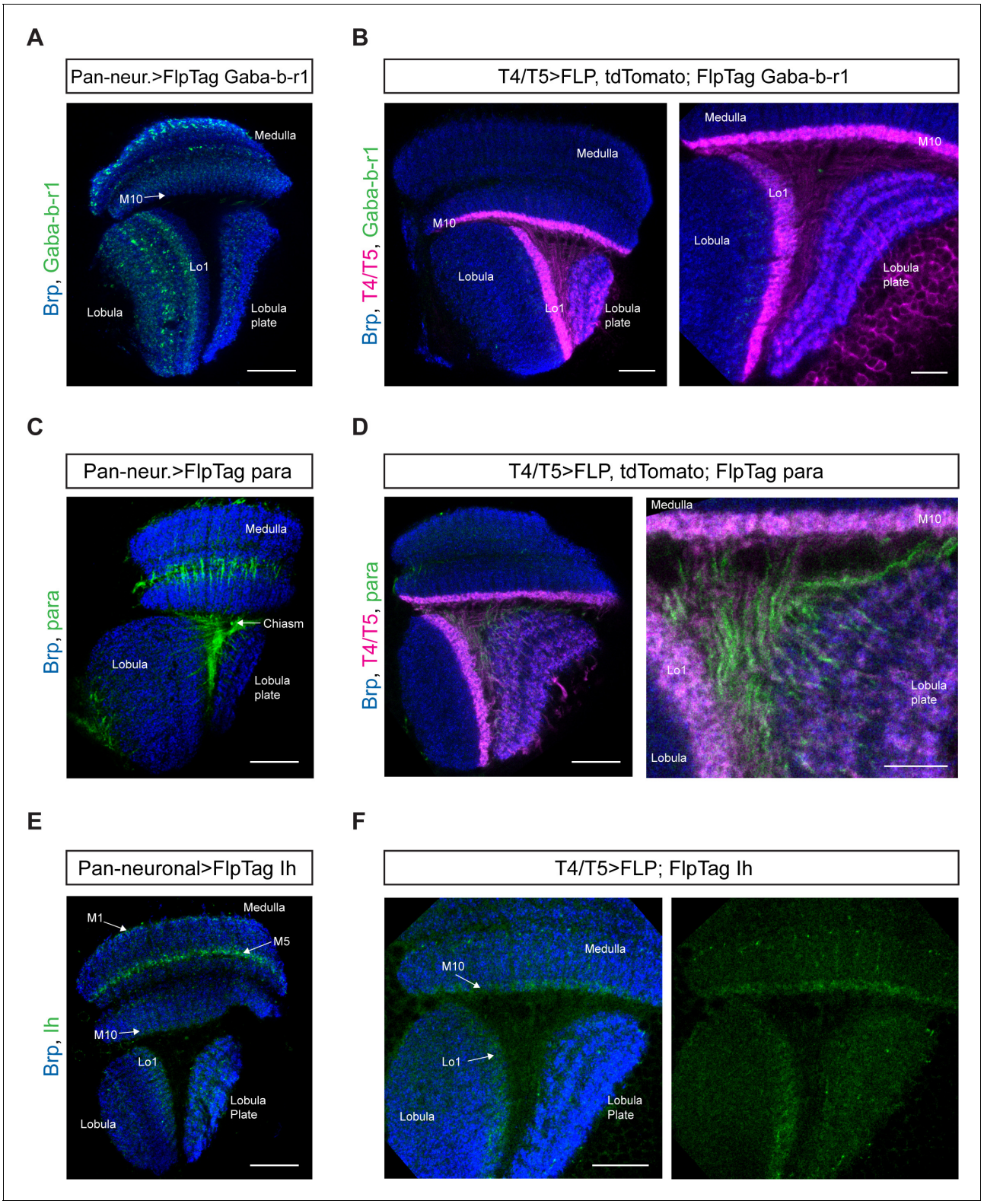

Figure 6. FlpTag lines for Gaba-b-r1, para and Ih. Optic lobes with pan-neuronal expression of FlpTag Gaba-b-r1 (**A**), FlpTag para (**C**), and FlpTag Ih (**E**). (**B**) Expression of FlpTag Gaba-b-r1 in T4/T5 neurons labeled with myr::tdTomato. Left panel: horizontal view on the optic lobe overview (scale bar: 20 µm). Right panel: close-up of medulla layer M10, lobula layer Lo1 and Lobula plate layers 1–4 (scale bar: 10 µm). (**D**) Expression of FlpTag para in T4/T5 neurons labeled with myr::tdTomato. Left panel: horizontal view on the optic lobe overview (scale bar: 20 µm). Right panel: close-up of medulla layer

Figure 6 continued on next page

Figure 6 continued

M10, lobula layer Lo1 and Lobula plate layers 1–4 (scale bar: 10 μm). (**F**) Expression of FlpTag Ih in T4/T5 neurons. Horizontal view on the optic lobe with medulla layer M10, lobula layer Lo1 and Lobula plate layers 1–4 (scale bar: 12 μm). Left panel: Background staining anti-brp in blue and. Right panel: Ih::GFP signal only.

Paralytic (para) is the only voltage-gated sodium channel described in *Drosophila* and highly expressed in T4/T5 neurons (***Pankova and Borst, 2016***). It is required for the generation of sodium-dependent action potentials. We created the FlpTag para line by inserting the FlpTag cassette into the MiMIC landing site between the first and second exon (MI08578), thereby covering all of its 60 isoforms. Surprisingly, the pan-neuronal expression pattern is rather sparse with some bundles labeled in the medulla across the serpentine layer and axonal fibers in the chiasm between medulla, lobula and lobula plate (***Figure 6C***). In the T4/T5 specific FlpTag genotype, para is strongly expressed in the axonal fibers connecting dendrites and axon terminals in T4/T5 neurons (***Figure 6D***).

Ih is a voltage-gated, hyperpolarization-activated ion channel which is highly expressed in T4/T5 neurons (***Chen and Wang, 2012***; ***Hu et al., 2015***; ***Pankova and Borst, 2016***). To generate the corresponding FlpTag line, the FlpTag cassette was inserted in the MiMIC site MI12136 housed by the coding intron between the first and second exons of the Ih gene locus. In the pan-neuronal FlpTag line, Ih is expressed most strongly in two layers of the distal medulla (M1 and M5), as well as in the lobula plate and in Lo1 of the lobula (***Figure 6E***). In the T4/T5-specific FlpTag genotype, Ih is localized to the T4 and T5 dendrite area in medulla layer 10 and lobula plate layer 1 (***Figure 6F***).

Taken together, we generated four working FlpTag lines which uncovered the differential subcellular distribution of the neurotransmitter receptor subunits GluClα and Gaba-b-r1 and the voltage-gated ion channels para and Ih. We demonstrated that the FlpTag approach is generalizable and can be expanded to many genes with MiMIC insertion sites.

Discussion

Neurotransmitter receptors are essential neuronal elements that define the sign and temporal dynamics of synaptic connections. For our understanding of complex neural circuits, it is indispensable to examine which transmitter receptor types are used by the participating neurons and to which compartment they localize. Here, we developed FlpTag, a generalizable method for endogenous, cell-type-specific labeling of proteins. Alongside several GFP-tagged UAS-lines, we used our newly developed FlpTag lines to explore the distribution of receptor subunits GluClα, Rdl, Dα7, Gaba-b-r1 and voltage-gated ion channels para and Ih in motion-sensing T4/T5 neurons of the visual system of *Drosophila*. We found that these ion channels are localized to either the dendrite, the axonal fiber or the axon terminal (summarized in ***Figure 7A and C***). Even at the level of individual dendrites, GluClα, Rdl and Dα7 were differentially distributed precisely matching the locations where T4 and T5 neurons sample signals from their glutamatergic, cholinergic, or GABAergic input neurons, respectively (summarized in ***Figure 7***).

Protein tagging methods: endogenous tags and UAS-lines

Working with *Drosophila* as model organism bears some unrivaled advantages when it comes to genetic tools. The MiMIC and FlyFos libraries, for instance, are large-scale approaches of enormous value for the fly community as they provide GFP-tagged protein lines for thousands of *Drosophila* genes including several neurotransmitter receptors and voltage-gated ion channels (***Venken et al., 2011***; ***Nagarkar-Jaiswal et al., 2015a***; ***Sarov et al., 2016***). Recently, Kondo et al. expanded these existing libraries with T2A-Gal4 insertions in 75 neurotransmitter receptor genes that can also be exchanged by the fluorescent protein tag Venus (***Kondo et al., 2020***). While all these approaches tag genes at their endogenous locus, none of them are conditional, for example they cannot be applied in a cell-type-specific manner. Hence, ascribing the expression of the pan-neuronally tagged proteins to cell-types of interest are challenging in dense neuronal tissue.

To overcome these difficulties, we used two conditional strategies for the investigation of membrane protein localizations in our cell types of interest, T4 and T5 neurons. First, we developed GFP-tagged *UAS*-lines for GluClα and Rdl and tested an existing *UAS-Dα7::GFP* line. As stated above,

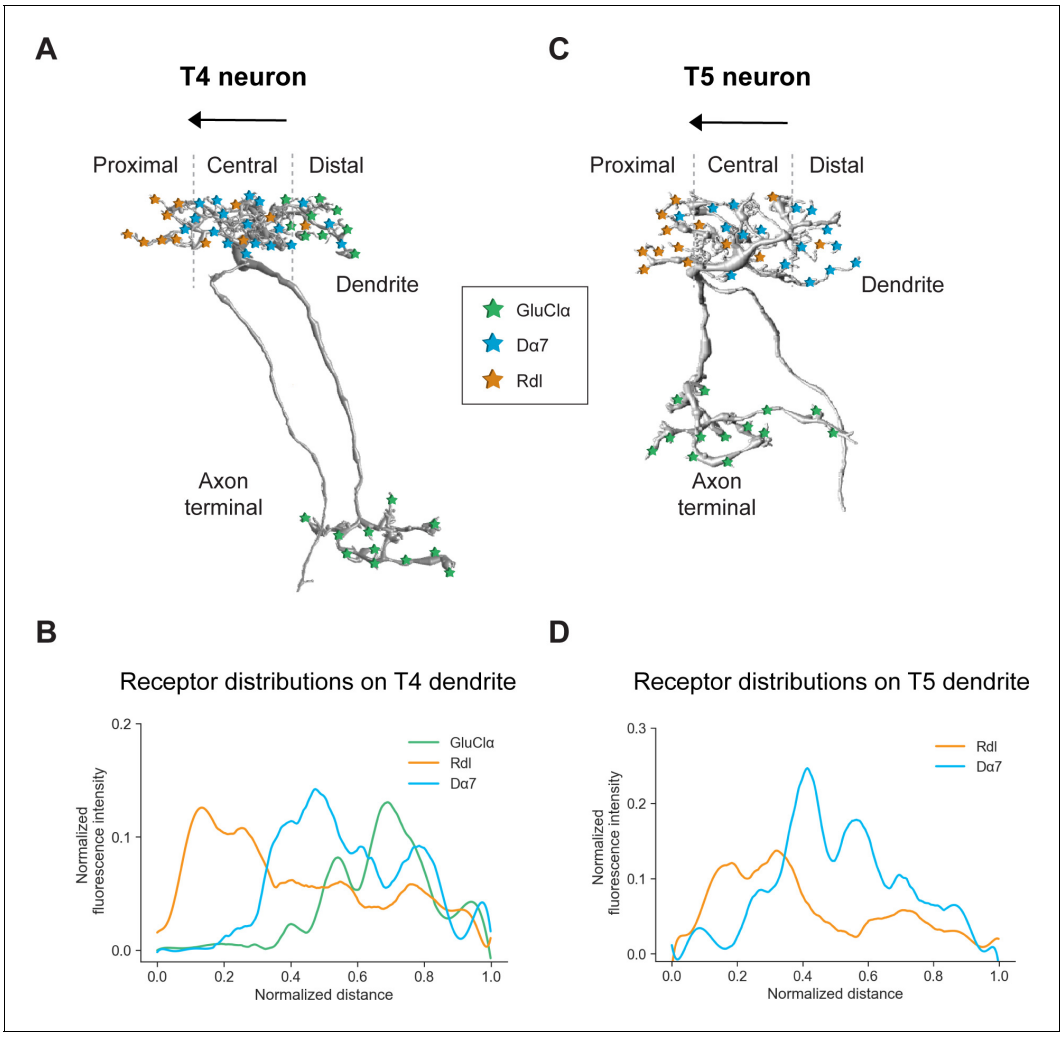

Figure 7. Summary of the receptor distributions of GluClα, Rdl and Dα7 in T4 and T5 neurons. (**A**) Scheme of EM-reconstructed T4 neuron with distribution of receptors on dendrite and axon terminal (image extracted from Seven medulla column connectome dataset, https://emdata.janelia.org/#/repo/medulla7column, #3b548, Janelia Research Campus). (**B**) Quantification of GluClα (green), Rdl (orange) and Dα7 (blue) distribution over the whole dendritic length (distance) averaged across several T4 from all subtypes (combined data from ***Figures 4D*** and ***5D***). All dendrites were aligned pointing to the right with the most proximal point at 0.0 and the most distal point at 1.0. (**C**) Scheme of EM-reconstructed T5 neuron with distribution of receptors on dendrite and axon terminal (image extracted from Seven medulla column connectome dataset, https://emdata.janelia.org/#/repo/medulla7column, #3b548, Janelia Research Campus). (**D**) Rdl (orange) and Dα7 (blue) distribution over the whole dendritic length (normalized distance) averaged across several T5 from all subtypes (combined data from ***Figures 3D*** and ***4D***). All dendrites were aligned pointing to the right with the most proximal point at 0.0 and the most distal point at 1.0.

aberrant localization of overexpressed proteins can occur, however, this is not always the case. Overexpression of *UAS-GluClα::GFP* shows a similar receptor localization pattern as both MiMIC and FlpTag endogenous lines (***Figure 2—figure supplement 1***), thus, validating the use of *UAS-GluClα::GFP* for studying receptor distribution. Additionally, previous studies reported that the *UAS-Dα7::GFP* line showed proper localization of the acetylcholine receptor to endogenous synapses when compared to antibody stainings or endogenous bruchpilot (Brp) puncta (***Kuehn and Duch, 2013***; ***Mosca and Luo, 2014***). Here, we confirmed this finding and further showed that Dα7::GFP presumably localizes only to cholinergic synapses. Overexpressing Dα7::GFP in a medulla neuron that is devoid of endogenous Dα7 demonstrated that Dα7::GFP localized to apparent cholinergic synapses. Hence, the *UAS-Dα7::GFP* line can be used to study the distribution of cholinergic synapses, but not the exact composition of cholinergic receptor subunits. A recent study showed that quantitatively the levels of the postsynaptic density protein PSD95 change when overexpressed, but qualitatively

the localization is not altered (**Willems et al., 2020**). Altogether, this suggests that tagged overexpression lines can be used for studying protein localizations, but they have to be controlled carefully and drawn conclusions might be different for every line.

The FlpTag method is generalizable and can be expanded to many genes

Ideally, a tool for protein tagging should be both endogenous and conditional. This can be achieved by introducing an FRT-flanked STOP cassette upstream of the gene of interest which was engineered with an epitope tag or fluorescent protein. Only upon cell-type specific expression of Flp, the tagged protein will be expressed in a cell-type specific manner. This genetic strategy was utilized by two independent studies to label the presynaptic protein Brp, the histamine channel ort and the vesicular acetylcholine transporter VAChT (**Chen et al., 2014**; **Pankova and Borst, 2017**). Recently, a new approach based on the split-GFP system was utilized for endogenous, conditional labeling of proteins in two independent studies (**Kondo et al., 2020**; **Luo et al., 2020**). However, all these aforementioned approaches are not readily generalizable and easily applicable to any gene of interest.

The FlpTag strategy presented here overcomes these caveats by allowing for endogenous, conditional tagging of proteins and by offering a generalizable toolbox for targeting many genes of interest. Similar to the conditional knock-out tools FlpStop and FlipFlop (**Fisher et al., 2017**; **Nagarkar-Jaiswal et al., 2017**), FlpTag utilizes a FLEx switch to conditionally control expression of a reporter gene, in our case GFP. Likewise, FlpTag also easily integrates using the readily available intronic MiMIC insertions. Here, we attempted to generate FlpTag lines for six genes, GluClα, Rdl, Dα7, Gaba-b-r1, para and Ih (overview of lines in **Table 1**). Four out of these six lines yielded conditional GFP-tagged protein lines (GluClα, Gaba-b-r1, para, Ih). We injected the FlpTag cassette in MI02620 for Rdl and MI12545 for Dα7, but could not observe any GFP expression across the brain (data not shown). The MiMiC insertion sites used for Rdl and Dα7 seem to be in a suboptimal location for tagging the protein.

Expansion of the FlpTag toolbox

As of now, there are MiMIC insertions in coding introns for more than 2800 genes available, which covers approximately 24% of neuronal genes (**Venken et al., 2011**; **Nagarkar-Jaiswal et al., 2015a**; **Fisher et al., 2017**). Additionally, the attP insertion sites generated in the study by Kondo et al. provide possible landing sites for the FlpTag cassette for 75 neurotransmitter receptor genes (**Kondo et al., 2020**). Transmembrane proteins such as neurotransmitter receptors form complex 3D structures making fluorescent tagging especially difficult. Neither the MiMIC insertion sites, nor the target sites of the Kondo study at the C-terminus of several transmitter receptor genes, ensure a working GFP-tagged protein line. For genes of interest lacking a suitable MiMIC insertion site we generated a homology directed repair (HDR) cassette which utilizes CRISPR/Cas9-mediated gene

Table 1. Overview of available MiMIC GFSTF and FlpTag lines for investigated genes.

	Gene	MiMIC insertion (coding intron)	MiMIC GFSTF existing	MiMIC GFSTF working	Chromosome	Phase	FlpTag working	Localization in T4/T5 neurons
1	GluClα	MI02890, MI14426	MI02890	Yes	III	2	Yes, MI02890	T4: dendrites + terminals; T5: terminals
2	Rdl	MI02620, MI02957	MI02620	No	III	0	No, MI02620	From UAS line: dendrites
3	Dα7	MI12545	This study (MI12545)	No	X	1	No	From UAS line: dendrites
4	Gaba-b-r1	MI01930, MI05755	MI01930	Yes	II	0	Yes, MI01930	No
5	para	MI08578	This study (MI08578)	Yes	X	0	Yes, MI08578	T4/T5 axonal fibers
6	Ih	MI03196, MI12136	This study (MI12136)	Yes	II	2	Yes, MI12136	T4/T5 dendrites

editing to integrate the FlpTag cassette in any desired gene locus (**Supplementary file 6–8**; **Gratz et al., 2014**; **Fisher et al., 2017**). The plasmid consists of the FlpTag cassette flanked by multiple cloning sites for the insertion of homology arms (HA). Through HDR the FlpTag cassette can be knocked-in into any desired locus. Taken together, the FlpTag cassette is a generalizable tool that can be integrated in any available attP-site in genes of interest (**Venken et al., 2011**; **Nagarkar-Jaiswal et al., 2015a**; **Kondo et al., 2020**) or inserted by CRISPR-HDR into genes lacking attP landing sites. This allows for the investigation of the endogenous spatial distributions of proteins, as well as the correct temporal dynamics of protein expression.

Further, the FlyFos project demonstrated that most fly lines with an extra copy of GFP-tagged protein-coding genes worked normally and GFP-tagged proteins could be imaged in living fly embryos and pupae (**Sarov et al., 2016**). In principle, live-imaging of the GFP-tagged lines we created could be performed during different developmental stages of the fruit fly. In general, the tools generated here can be used as specific postsynaptic markers, visualizing glutamatergic, GABAergic, and cholinergic synapses with standard confocal light microscopy. This extends the existing toolbox of *Drosophila* postsynaptic markers (**Sánchez-Soriano et al., 2005**; **Raghu et al., 2009**; **Andlauer et al., 2014**; **Chen et al., 2014**; **Petzoldt et al., 2014**; **Kondo et al., 2020**; **Luo et al., 2020**) for studying the localization and development of various types of synapses.

Functional relevance of transmitter receptors and voltage-gated channels for *Drosophila* motion-sensitive neurons

T4/T5 neurons combine spatiotemporal input from their presynaptic partners, leading to selective responses to one of the four cardinal directions. Numerous studies investigated the mechanisms underlying direction-selective responses in T4/T5 neurons, yet the computation is still not fully understood. At an algorithmic level, a three-arm detector model is sufficient to describe how direction-selective responses in T4/T5 neurons arise (**Arenz et al., 2017**; **Haag et al., 2017**). This model relies on the comparison of signals originating from three neighboring points in space via a delay-and-compare mechanism. The central arm provides fast excitation to the neuron. While one flanking arm amplifies the central signal for stimuli moving along the preferred direction, the other inhibits the central signal for stimuli moving along the null direction of the neuron. Exploring the neurotransmitter receptors and their distribution on T4/T5 dendrites allows us to define the sign as well as the temporal dynamics of some of the input synapses to T4/T5.

According to the algorithmic model, we expect an excitatory, amplifying input signal on the distal side of T4/T5 dendrites. Here, we found that T4 cells receive an inhibitory, glutamatergic input from Mi9 via GluClα, which, at first sight, seems to contradict our expectation. However, since Mi9 has an OFF-center receptive field (**Arenz et al., 2017**; **Richter et al., 2018**; **Drews et al., 2020**), this glutamatergic synapse will invert the polarity from Mi9-OFF to T4-ON. Theoretically, in darkness, Mi9 inhibits T4 via glutamate and GluClα, and this inhibition is released upon an ON-edge moving into its receptive field. The concomitant closure of chloride channels and subsequent increased input resistance in T4 cells results in an amplification of a subsequent excitatory input signal from Mi1 and Tm3. As shown by a recent modeling study, this biophysical mechanism can indeed account for preferred direction enhancement in T4 cells (**Borst, 2018**). Some studies failed to detect preferred direction enhancement in T4/T5 neurons and they proposed that the enhanced signal in PD seen in GCaMP recordings could be a result from a non-linear calcium-to-voltage transformation (**Gruntman et al., 2018**; **Gruntman et al., 2019**; **Wienecke et al., 2018**). If this was really the case, the role of Mi9 and GluClα must be reconsidered and future functional experiments will shed light onto this topic.

Nevertheless, Strother et al. showed that the RNAi- knock-down of GluClα in T4/T5 neurons leads to enhanced turning responses on the ball set-up for faster speeds of repeating ON and OFF edges (**Strother et al., 2017**). Although this observation cannot answer the question about preferred direction enhancement in T4 cells, it indicates that both T4 and T5 receive inhibitory input and that removal of such create enhanced turning responses at the behavioral level. In line with these observations, we also found the glutamate receptor GluClα in T4/T5 axon terminals. A possible functional role of these inhibitory receptors in the axon terminals could be a cross-inhibition of T4/T5 cells with opposite preferred directions via lobula plate intrinsic neurons (LPis). Glutamatergic LPi neurons are known to receive a cholinergic, excitatory signal from T4/T5 neurons within one layer and to inhibit lobula plate tangential cells, the downstream postsynaptic partners of T4/T5 neurons, via GluClα in

the adjacent oppositely tuned layer. This mechanism induces a motion opponent response in lobula plate tangential cells and increases their flow-field selectivity (**Mauss et al., 2015**). In addition, LPi neurons could also inhibit T4/T5 neurons presynaptically at their axon terminals via GluClα in order to further sharpen the flow-field selectivity of lobula plate tangential cells. Taken together, exploring the subcellular distribution of GluClα in T4/T5 neurons highlights its differential functional roles in different parts of these cell types.

Secondly, the Dα7 signal in the center of T4/T5 dendrites discovered here, corresponds to ionotropic, cholinergic input from Mi1 and Tm3 for T4, and Tm1, Tm2 and Tm4 for T5. These signals correspond to the central, fast, excitatory arm of the motion detector model. As T4 and T5 express a variety of different ACh receptor subunits (**Davis et al., 2020**), the exact subunit composition and underlying biophysics of every cholinergic synapse on T4/T5 dendrites still awaits further investigations.

Third, inhibition via GABA plays an essential role in creating direction-selective responses in both T4 and T5 neurons (**Fisher et al., 2015a**; **Arenz et al., 2017**; **Strother et al., 2017**; **Gruntman et al., 2018**) by providing null direction suppression. Computer simulations showed that direction selectivity decreases in T4/T5 motion detector models without this inhibitory input on the null side of the dendrite (**Arenz et al., 2017**; **Borst, 2018**; **Strother et al., 2017**). Here, we show that T4 and T5 neurons possess the inhibitory GABA receptor subunit Rdl mainly on the proximal base on the null side of their dendrites, providing the synaptic basis for null direction suppression. We did not detect the metabotropic GABA receptor subunit Gaba-b-r1 in T4/T5 neurons using the newly generated FlpTag Gaba-b-r1 line. Finally, all of the receptor subunits GluClα, Rdl and Dα7 investigated here are ionotropic, fast receptors, which presumably do not add a temporal delay at the synaptic level. In the detector model described above, the two outer arms provide a slow and sustained signal, and such properties are already intrinsic properties of these input neurons (**Arenz et al., 2017**; **Serbe et al., 2016**). However, we cannot exclude that slow, metabotropic receptor subunits for acetylcholine or GABA (e.g. Gaba-br2) which are also present in T4/T5 and could induce additional delays at the synaptic level (**Takemura et al., 2011**; **Davis et al., 2020**).

Furthermore, we investigated the subcellular distribution of the voltage-gated ion channels para and Ih in T4/T5 neurons. We found para, a voltage-gated sodium channel, to be distributed along the axonal fibers of both T4 and T5 neurons. As para is important for the generation of sodium-dependent action potentials, it will be interesting for future functional studies to investigate, if T4/T5 really fire action potentials and how this shapes their direction-selective response. Further, we detected Ih, a voltage-gated ion channel permeable for several types of ions, in T4/T5 dendrites using the FlpTag strategy. Ih channels are activated at negative potentials below −50 mV and as they are permeable to sodium and potassium ions, they can cause a depolarization of the cell after hyperpolarization (**Magee, 1999**; **Littleton and Ganetzky, 2000**; **George et al., 2009**). Loss-of-function studies will unravel the functional role of the Ih channel for direction-selective responses in T4/T5 neurons.

Outlook

Since the ability to combine synaptic inputs from different neurotransmitters at different spatial sites is common to all neurons, the approaches described here represent an important future perspective for other circuits. Our tools can be used to study the ion channels GluClα, Rdl, Dα7, Gaba-b-r1, para and Ih in any given *Drosophila* cell-type and circuit. Furthermore, the FlpTag tool box can be used to target many genes of interest and thereby foster molecular questions across fields.

The techniques described here can be transferred to other model organisms as well, to study the distribution of different transmitter receptors. For instance, in the mouse retina - similar to motion-sensing T4/T5 neurons in the fruit fly - so-called On-Off direction-selective ganglion cells receive asymmetric inhibitory GABAergic inputs from presynaptic starburst amacrine cells during null-direction motion. A previous study investigated the spatial distribution of GABA receptors of these direction-selective ganglion cells using super-resolution imaging and antibody staining (**Sigal et al., 2015**). Additionally, starburst amacrine cells also release ACh onto ganglion cells which contributes to the direction-selective responses of ganglion cells. Thus, mapping the distribution of ACh receptors on direction-selective ganglion cells will be the next important step to further investigate cholinergic transmission in this network (**Sethuramanujam et al., 2020**).

Overall, we demonstrated the importance of exploring the distributions of neurotransmitter receptors and ion channels for systems neuroscience. The distinct distributions in T4/T5 neurons discovered here and the resulting functional consequences expand our knowledge of the molecular basis of motion vision. Although powerful, recent RNAseq studies lacked information about spatial distributions of transmitter receptors which can change the whole logic of wiring patterns and underlying synaptic signs. Future studies can use this knowledge to target these receptors and directly probe their role in functional experiments or incorporate the gained insights into model simulations. However, this study is only highlighting some examples of important neural circuit components: expanding the approaches described here to other transmitter receptors and ion channels, as well as gap junction proteins will reveal the full inventory and the spatial distributions of these decisive determinants of neural function within an individual neuron.

Materials and methods

Fly strains

Flies were raised at 25˚C and 60% humidity on standard cornmeal agar medium at 12 hr light/dark cycle. The following driver lines were used: *R42F06-Gal4* to label T4/T5 neurons, *R57C10-Gal4* for addressing all neurons, *SS03734-splitGal4* to address L1, *R19F01-AD; R71D01-DBD* to address Mi1, *10–50* Gal4 to label T1, and *Dα7-TG4* (BL#77828). The *T4-splitGal4* line was generated by combining the hemidriver lines *VT16255-AD* (BL#75205) and *VT12314-DBD* (unpublished, T. Schilling); the *T5-splitGal4* line was generated by combining the hemidriver lines *VT13975-AD* and *R42F06-DBD* (unpublished, T. Schilling). The following *UAS*-reporter lines were used for labeling cell-types and drive flippase-expression: *UAS-myr::tdTomato* (BL#32222), and *UAS-FLP1.D* (BL#4539). For labeling individual T4/T5 neurons stochastically together with the receptor lines, we combined *UAS-myr::tdTomato; UAS-GluClα::GFP/UAS-Rdl::GFP/UAS-Dα7::GFP* with *hs-FLP; FRT-Gal80-FRT; R42F06-Gal4* and heat-shocked pupae (P1-P3) for 5–8 min at 37˚C in a water bath.

Generation of new genetic *UAS*-lines

The coding sequencing (CDS) of *GluClα* isoform K was acquired from flybase.org and along with the sequence of *GFP* flanked by 4xGGS linker was synthesized by Eurofins Genomics and inserted into pEX-A258 backbone between NotI and XbaI restriction sites. Using restriction digestion with NotI and XbaI the *GluClα* fragment was cloned into *pJFRC7-20XUAS-IVS-mCD8::GFP* (**Pfeiffer et al., 2010**) vector. Similarly, the CDS of *Rdl* isoform F was acquired from flybase.org and with the sequence of *GFP* flanked by 4xGGS linker was synthesized as three DNA fragments by Invitrogen GeneArt Gene Synthesis. Each fragment carried a complementary overlapping section of 25–35 bps on both ends. *pJFRC7-20XUAS-IVS-mCD8::GFP* (**Pfeiffer et al., 2010**) vector was digested with NotI and XbaI restriction enzymes and all three DNA fragments were inserted using NEBuilder HiFi DNA Assembly. Embryo injections were performed by BestGene Inc (Chino Hills, CA, USA).

For the generation of the FlpTag constructs, the pFlip-Flop-P0 plasmid (**Nagarkar-Jaiswal et al., 2017**) ordered from *Drosophila* Genomics Resource Center (NIH Grant 2P40OD010949) was digested with BsmFI and EcoRI leaving the plasmid backbone with FRT, FRT14 and attB sites. Six DNA fragments were synthesized by Invitrogen GeneArt Gene Synthesis. Three fragments contained a predicted splice donor site (one for each phase) and half of an inverted 4xGGS-GFP. The other three contained half of an inverted GFP-4xGGS followed by a slice acceptor (SA) site (one for each phase). All fragments had complementary overlapping sections of 25–35 bps which was used to insert phase-paired fragments into the digested pFlip-Flop plasmid using NEBuilder HiFi DNA Assembly. Embryo injections were performed by BestGene Inc (Chino Hills, CA, USA), including PCR-verifications and balancing.

S2 Schneider cell culture

We used *Drosophila* S2R+ Schneider cells in culture *Drosophila* Genomics Resource Center, stock #150 for testing the newly generated *UAS*-receptor::GFP constructs before embryo injections. S2R+ cells were cultured in Schneider's *Drosophila* medium (Thermo Fisher Scientific) supplemented with 10% fetal bovine serum (Thermo Fisher Scientific) and penicillin/streptomycin (Cytiva). *UAS*-constructs were tested by transfecting 250 ng of *UAS*-plasmid and 250 ng of *actin5C-Gal4* plasmid (gift

from T. Kornberg) in 24-well plates using the FuGENE HD Kit (Promega). Two days later, we checked for GFP-expression in transfected S2 cells with a fluorescence binocular microscope.

Immunohistochemistry

Fly brains were dissected in cold 0.3% PBST and fixed in 4% PFA in 0.3% PBST for 25 min at room temperature. Subsequently, brains were washed four to five times in 0.3% PBST and blocked in 10% normal goat serum (NGS) in 0.3% PBST for 1 hr at room temperature. Primary antibodies used were mouse anti-Bruchpilot Brp (nc82, Developmental Studies Hybridoma Bank, 1:20, RRID:AB_2314867), rabbit anti-dsRed (Takara Bio, 1:300, RRID:AB_10013483), and rat anti-Dα7 (gift from H. Bellen, 1:2000). Secondary antibodies used were: goat anti-mouse ATTO 647N (Rockland, 1:300, RRID:AB_2614870), goat anti-rabbit Alexa Fluor 568 (Thermo Fisher Scientific, 1:300, RRID:AB_10563601), and goat anti-rat Alexa Fluor 647 (Thermo Fisher Scientific, 1:300, RRID:AB_141778). GFP-labeled receptors were imaged natively without antibody staining. 5% NGS was added to all antibody solutions and both primary and secondary antibodies were incubated for at least 48 hr at 4˚C. Brains were mounted in Vectashield Antifade Mounting Medium (Vector Laboratories) and imaged on a Leica TCS SP8 confocal microscope equipped with 488-, 561-, and 633 nm lasers, using a 63X glycerol objective.

Quantifications of receptor distributions and number of puncta

For intensity quantification, confocal stacks were processed in ImageJ using maximum intensity projection. These images were then analyzed in python using the Skimage and Numpy packages. For each image, florescence was normalized to the maximum intensity within an image. Additionally, images were cropped to include the entire dendritic cross section and aligned pointing to the right with the most proximal point to the left and the most distal point to the right. These images were normalized to the maximum cropped image length.

For quantification of number of receptor puncta, confocal stacks were taken from the entire cross-section of the dendrite as above. Puncta were counted in ImageJ software using the 3D object counter plugin of Fiji (***Bolte and Cordelières, 2006***).

Statistical analysis

Statistical significance was tested with a Student t-test when comparing two groups. A p-value below 0.05 was considered significant. In the case of pan-neuronal quantification where multiple groups were compared, statistical significance was tested using one-way ANOVA. In all figures, * was used to indicate a p-value<0.05, ** for p<0.01, and *** for p<0.001. Statistical analysis and graphs were generated in Python 3.4 using SciPy and Seaborn packages respectively. Figures were generated in Adobe Illustrator CC.

Acknowledgements

We are grateful to T Schilling for unpublished driver lines, the Bloomington *Drosophila* Stock Center for fly lines and the *Drosophila* Genomics Resource Center (supported by NIH grant 2P40OD010949) for S2 cells; T Kornberg (UCSF) for the *actin-Gal4* plasmid for S2 cell culture and H Bellen for the Dα7-antibody. We thank W Essbauer for technical assistance with molecular work and R Kutlesa and I Ribeiro for help with the S2 cell culture; T Schilling and J Pujol-Marti for discussions and support throughout all stages of this project; I Ribeiro, A Mauss, L Groschner, G Ammer, J Malis, A Harbauer and A Barker for carefully reading the manuscript; M Drews and N Pirogova for helping with programming.

Additional information

Competing interests

Alexander Borst: Reviewing editor, *eLife*. The other authors declare that no competing interests exist.

Funding

Funder	Author
Max-Planck-Gesellschaft	Sandra Fendl Renee Marie Vieira Alexander Borst

The funders had no role in study design, data collection and interpretation, or the decision to submit the work for publication.

Author contributions

Sandra Fendl, Conceptualization, Formal analysis, Validation, Investigation, Visualization, Methodology, Writing - original draft, Project administration, Writing - review and editing, Conceived and designed the study, Imaged all data shown and processed confocal images, Wrote the manuscript and prepared the figures with the help of RMV and AB; Renee Marie Vieira, Conceptualization, Software, Formal analysis, Visualization, Methodology, Writing - review and editing, Conceived and designed the study; Analyzed and quantified all imaged data; Developed and created the UAS-lines and the FlpTag-construct and stocks with the help of SF; Alexander Borst, Conceptualization, Resources, Supervision, Project administration, Writing - review and editing

Author ORCIDs

Sandra Fendl https://orcid.org/0000-0001-6442-2542
Renee Marie Vieira https://orcid.org/0000-0001-8520-7382

Decision letter and Author response

Decision letter https://doi.org/10.7554/eLife.62953.sa1
Author response https://doi.org/10.7554/eLife.62953.sa2

Additional files

Supplementary files

- Supplementary file 1. Plasmid map of the full sequence of pJFRC7-20xUAS-GluClα-GFP.
- Supplementary file 2. Plasmid map of the full sequence of pJFRC7-20xUAS-Rdl-GFP.
- Supplementary file 3. Plasmid map of the full sequence of pUC57-FlpTag-GFP-ph0.
- Supplementary file 4. Plasmid map of the full sequence of pUC57-FlpTag-GFP-ph1.
- Supplementary file 5. Plasmid map of the full sequence of pUC57-FlpTag-GFP-ph2.
- Supplementary file 6. Plasmid map of the full sequence of pHD-FlpTag-DsRed-HDR-ph0.
- Supplementary file 7. Plasmid map of the full sequence of pHD-FlpTag-DsRed-HDR–ph1.
- Supplementary file 8. Plasmid map of the full sequence of pHD-FlpTag-DsRed-HDR-ph2.
- Supplementary file 9. 3D-image of a T4 dendrite (subtype d) (magenta) with GluClα::GFP (green).
- Supplementary file 10. 3D-image of a T4 dendrite (subtype d) (magenta) with Rdl::GFP (yellow).
- Supplementary file 11. 3D-image of a T4 dendrite (subtype d) (magenta) with Dα7::GFP (cyan).
- Transparent reporting form

Data availability

All data generated or analysed during this study are included in the manuscript and supporting files. Source data files have been provided for Figures 2, 3 and 4. Instructions on accessing the seven medulla column connectome data are available at https://github.com/janelia-flyem/Connectome-Hackathon2016/wiki/Accessing%20Optic%20Lobe%20Dataset%20using%20Google%20Cloud.

The following previously published dataset was used:

Author(s)	Year	Dataset title	Dataset URL	Database and Identifier
Shinomiya K	2019	Seven medulla column connectome	http://emdata.janelia.	https://emdata.

org/#/repo/medulla7column janelia.org/, 3b548

References

Ammer G, Leonhardt A, Bahl A, Dickson BJ, Borst A. 2015. Functional specialization of neural input elements to the *Drosophila* ON Motion Detector. *Current Biology* **25**:2247–2253. DOI: https://doi.org/10.1016/j.cub.2015.07.014, PMID: 26234212

Andlauer TFM, Scholz-Kornehl S, Tian R, Kirchner M, Babikir HA, Depner H, Loll B, Quentin C, Gupta VK, Holt MG, Dipt S, Cressy M, Wahl MC, Fiala A, Selbach M, Schwärzel M, Sigrist SJ. 2014. Drep-2 is a novel synaptic protein important for learning and memory. *eLife* **3**:e03895. DOI: https://doi.org/10.7554/eLife.03895

Arenz A, Drews MS, Richter FG, Ammer G, Borst A. 2017. The temporal tuning of the *Drosophila* Motion Detectors Is Determined by the Dynamics of Their Input Elements. *Current Biology* **27**:929–944. DOI: https://doi.org/10.1016/j.cub.2017.01.051, PMID: 28343964

Behnia R, Clark DA, Carter AG, Clandinin TR, Desplan C. 2014. Processing properties of ON and OFF pathways for *Drosophila* motion detection. *Nature* **512**:427–430. DOI: https://doi.org/10.1038/nature13427, PMID: 25043016

Bielopolski N, Amin H, Apostolopoulou AA, Rozenfeld E, Lerner H, Huetteroth W, Lin AC, Parnas M. 2019. Inhibitory muscarinic acetylcholine receptors enhance aversive olfactory learning in adult *Drosophila*. *eLife* **8**:e48264. DOI: https://doi.org/10.7554/eLife.48264, PMID: 31215865

Bolte S, Cordelières FP. 2006. A guided tour into subcellular colocalization analysis in light microscopy. *Journal of Microscopy* **224**:213–232. DOI: https://doi.org/10.1111/j.1365-2818.2006.01706.x, PMID: 17210054

Borst A. 2018. A biophysical mechanism for preferred direction enhancement in fly motion vision. *PLOS Computational Biology* **14**:e1006240. DOI: https://doi.org/10.1371/journal.pcbi.1006240, PMID: 29897917

Borst A, Helmstaedter M. 2015. Common circuit design in fly and mammalian motion vision. *Nature Neuroscience* **18**:1067–1076. DOI: https://doi.org/10.1038/nn.4050, PMID: 26120965

Chen Y, Akin O, Nern A, Tsui CY, Pecot MY, Zipursky SL. 2014. Cell-type-specific labeling of synapses in vivo through synaptic tagging with recombination. *Neuron* **81**:280–293. DOI: https://doi.org/10.1016/j.neuron.2013.12.021, PMID: 24462095

Chen Z, Wang Z. 2012. SCIENCE CHINA functional study of hyperpolarization activated channel (Ih) in *Drosophila* behavior. *Science China. Life Sciences* **55**:2–7. DOI: https://doi.org/10.1007/s11427-012-4270-6, PMID: 22314484

Cully DF, Paress PS, Liu KK, Schaeffer JM, Arena JP. 1996. Identification of a *Drosophila melanogaster* glutamate-gated chloride channel sensitive to the antiparasitic agent avermectin. *Journal of Biological Chemistry* **271**:20187–20191. DOI: https://doi.org/10.1074/jbc.271.33.20187, PMID: 8702744

Davis FP, Nern A, Picard S, Reiser MB, Rubin GM, Eddy SR, Henry GL. 2020. A genetic, genomic, and computational resource for exploring neural circuit function. *eLife* **9**:e50901. DOI: https://doi.org/10.7554/eLife.50901, PMID: 31939737

Diao F, Ironfield H, Luan H, Diao F, Shropshire WC, Ewer J, Marr E, Potter CJ, Landgraf M, White BH. 2015. Plug-and-play genetic access to *Drosophila* cell types using exchangeable exon cassettes. *Cell Reports* **10**:1410–1421. DOI: https://doi.org/10.1016/j.celrep.2015.01.059, PMID: 25732830

Drews MS, Leonhardt A, Pirogova N, Richter FG, Schuetzenberger A, Braun L, Serbe E, Borst A. 2020. Dynamic signal compression for robust motion vision in flies. *Current Biology* **30**:209–221. DOI: https://doi.org/10.1016/j.cub.2019.10.035, PMID: 31928873

Fayyazuddin A, Zaheer MA, Hiesinger PR, Bellen HJ. 2006. The nicotinic acetylcholine receptor Dalpha7 is required for an escape behavior in *Drosophila*. *PLOS Biology* **4**:e63. DOI: https://doi.org/10.1371/journal.pbio.0040063, PMID: 16494528

Ffrench-Constant RH, Rocheleau TA, Steichen JC, Chalmers AE. 1993. A point mutation in a *Drosophila* GABA receptor confers insecticide resistance. *Nature* **363**:449–451. DOI: https://doi.org/10.1038/363449a0, PMID: 8389005

Fisher YE, Leong JC, Sporar K, Ketkar MD, Gohl DM, Clandinin TR, Silies M. 2015a. A class of visual neurons with Wide-Field properties is required for local motion detection. *Current Biology* **25**:3178–3189. DOI: https://doi.org/10.1016/j.cub.2015.11.018, PMID: 26670999

Fisher YE, Silies M, Clandinin TR. 2015b. Orientation selectivity sharpens motion detection in *Drosophila*. *Neuron* **88**:390–402. DOI: https://doi.org/10.1016/j.neuron.2015.09.033, PMID: 26456048

Fisher YE, Yang HH, Isaacman-Beck J, Xie M, Gohl DM, Clandinin TR. 2017. FlpStop, a tool for conditional gene control in *Drosophila*. *eLife* **6**:e22279. DOI: https://doi.org/10.7554/eLife.22279, PMID: 28211790

Fritschy JM. 2008. Is my antibody-staining specific? how to deal with pitfalls of immunohistochemistry. *European Journal of Neuroscience* **28**:2365–2370. DOI: https://doi.org/10.1111/j.1460-9568.2008.06552.x, PMID: 19087167

George MS, Abbott LF, Siegelbaum SA. 2009. HCN hyperpolarization-activated cation channels inhibit EPSPs by interactions with M-type K+ channels. *Nature Neuroscience* **12**:577–584. DOI: https://doi.org/10.1038/nn.2307

Gordon MD, Scott K. 2009. Motor control in a *Drosophila* taste circuit. *Neuron* **61**:373–384. DOI: https://doi.org/10.1016/j.neuron.2008.12.033, PMID: 19217375

Gratz SJ, Ukken FP, Rubinstein CD, Thiede G, Donohue LK, Cummings AM, O'Connor-Giles KM. 2014. Highly specific and efficient CRISPR/Cas9-catalyzed homology-directed repair in *Drosophila*. *Genetics* **196**:961–971. DOI: https://doi.org/10.1534/genetics.113.160713, PMID: 24478335

Gruntman E, Romani S, Reiser MB. 2018. Simple integration of fast excitation and offset, delayed inhibition computes directional selectivity in *Drosophila*. *Nature Neuroscience* **21**:250–257. DOI: https://doi.org/10.1038/s41593-017-0046-4, PMID: 29311742

Gruntman E, Romani S, Reiser MB. 2019. The computation of directional selectivity in the *Drosophila* OFF motion pathway. *eLife* **8**:e50706. DOI: https://doi.org/10.7554/eLife.50706, PMID: 31825313

Haag J, Arenz A, Serbe E, Gabbiani F, Borst A. 2016. Complementary mechanisms create direction selectivity in the fly. *eLife* **5**:e17421. DOI: https://doi.org/10.7554/eLife.17421, PMID: 27502554

Haag J, Mishra A, Borst A. 2017. A common directional tuning mechanism of *Drosophila* motion-sensing neurons in the ON and in the OFF pathway. *eLife* **6**:e29044. DOI: https://doi.org/10.7554/eLife.29044, PMID: 28829040

Hörmann N, Schilling T, Ali AH, Serbe E, Mayer C, Borst A, Pujol-Martí J. 2020. A combinatorial code of transcription factors specifies subtypes of visual motion-sensing neurons in *Drosophila*. *Development* **147**: dev186296. DOI: https://doi.org/10.1242/dev.186296, PMID: 32238425

Hu W, Wang T, Wang X, Han J. 2015. Ih channels control feedback regulation from amacrine cells to photoreceptors. *PLOS Biology* **13**:e1002115. DOI: https://doi.org/10.1371/journal.pbio.1002115, PMID: 25831426

Joesch M, Schnell B, Raghu SV, Reiff DF, Borst A. 2010. ON and OFF pathways in *Drosophila* motion vision. *Nature* **468**:300–304. DOI: https://doi.org/10.1038/nature09545, PMID: 21068841

Kawasaki F, Zou B, Xu X, Ordway RW. 2004. Active zone localization of presynaptic calcium channels encoded by the cacophony locus of *Drosophila*. *Journal of Neuroscience* **24**:282–285. DOI: https://doi.org/10.1523/JNEUROSCI.3553-03.2004, PMID: 14715960

Kim M, Jang D, Yoo E, Oh Y, Sonn JY, Lee J, Ki Y, Son HJ, Hwang O, Lee C, Lim C, Choe J. 2017. Rogdi defines GABAergic control of a Wake-promoting dopaminergic pathway to sustain sleep in *Drosophila*. *Scientific Reports* **7**:1–14. DOI: https://doi.org/10.1038/s41598-017-11941-3

Kondo S, Takahashi T, Yamagata N, Imanishi Y, Katow H, Hiramatsu S, Lynn K, Abe A, Kumaraswamy A, Tanimoto H. 2020. Neurochemical organization of the *Drosophila* brain visualized by endogenously tagged neurotransmitter receptors. *Cell Reports* **30**:284–297. DOI: https://doi.org/10.1016/j.celrep.2019.12.018

Konstantinides N, Kapuralin K, Fadil C, Barboza L, Satija R, Desplan C. 2018. Phenotypic convergence: distinct transcription factors regulate common terminal features. *Cell* **174**:622–635. DOI: https://doi.org/10.1016/j.cell.2018.05.021, PMID: 29909983

Kuehn C, Duch C. 2013. Putative excitatory and putative inhibitory inputs are localised in different dendritic domains in a *Drosophila* flight motoneuron. *European Journal of Neuroscience* **37**:860–875. DOI: https://doi.org/10.1111/ejn.12104, PMID: 23279094

Lansdell SJ, Collins T, Goodchild J, Millar NS. 2012. The *Drosophila* nicotinic acetylcholine receptor subunits dα5 and dα7 form functional homomeric and heteromeric ion channels. *BMC Neuroscience* **13**:73. DOI: https://doi.org/10.1186/1471-2202-13-73, PMID: 22727315

Lansdell SJ, Millar NS. 2004. Molecular characterization of Dalpha6 and Dalpha7 nicotinic acetylcholine receptor subunits from *Drosophila*: formation of a high-affinity alpha-bungarotoxin binding site revealed by expression of subunit chimeras. *Journal of Neurochemistry* **90**:479–489. DOI: https://doi.org/10.1111/j.1471-4159.2004.02499.x, PMID: 15228604

Lee PT, Zirin J, Kanca O, Lin WW, Schulze KL, Li-Kroeger D, Tao R, Devereaux C, Hu Y, Chung V, Fang Y, He Y, Pan H, Ge M, Zuo Z, Housden BE, Mohr SE, Yamamoto S, Levis RW, Spradling AC, et al. 2018. A gene-specific *T2A-GAL4* library for *Drosophila*. *eLife* **7**:e35574. DOI: https://doi.org/10.7554/eLife.35574, PMID: 29565247

Littleton JT, Ganetzky B. 2000. Ion channels and synaptic organization: analysis of the *Drosophila* genome. *Neuron* **26**:35–43. DOI: https://doi.org/10.1016/s0896-6273(00)81135-6, PMID: 10798390

Liu X, Krause WC, Davis RL. 2007. GABAA receptor RDL *inhibits Drosophila* olfactory associative learning. *Neuron* **56**:1090–1102. DOI: https://doi.org/10.1016/j.neuron.2007.10.036, PMID: 18093529

Liu WW, Wilson RI. 2013. Glutamate is an inhibitory neurotransmitter in the *Drosophila* olfactory system. *PNAS* **110**:10294–10299. DOI: https://doi.org/10.1073/pnas.1220560110, PMID: 23729809

Luo J, Ting CY, Li Y, McQueen P, Lin TY, Hsu CP, Lee CH. 2020. Antagonistic regulation by insulin-like peptide and activin ensures the elaboration of appropriate dendritic field sizes of amacrine neurons. *eLife* **9**:e50568. DOI: https://doi.org/10.7554/eLife.50568, PMID: 32175842

Magee JC. 1999. Dendritic Ih normalizes temporal summation in hippocampal CA1 neurons. *Nature Neuroscience* **2**:508–514. DOI: https://doi.org/10.1038/9158, PMID: 10448214

Maisak MS, Haag J, Ammer G, Serbe E, Meier M, Leonhardt A, Schilling T, Bahl A, Rubin GM, Nern A, Dickson BJ, Reiff DF, Hopp E, Borst A. 2013. A directional tuning map of *Drosophila*. *Nature* **500**:212–216. DOI: https://doi.org/10.1038/nature12320

Mauss AS, Meier M, Serbe E, Borst A. 2014. Optogenetic and pharmacologic dissection of feedforward inhibition in *Drosophila* motion vision. *Journal of Neuroscience* **34**:2254–2263. DOI: https://doi.org/10.1523/JNEUROSCI.3938-13.2014, PMID: 24501364

Mauss AS, Pankova K, Arenz A, Nern A, Rubin GM, Borst A. 2015. Neural circuit to integrate opposing motions in the visual field. *Cell* **162**:351–362. DOI: https://doi.org/10.1016/j.cell.2015.06.035, PMID: 26186189

Mezler M, Müller T, Raming K. 2001. Cloning and functional expression of GABA(B) receptors from *Drosophila*. *The European Journal of Neuroscience* **13**:477–486. DOI: https://doi.org/10.1046/j.1460-9568.2001.01410.x, PMID: 11168554

Mosca TJ, Luo L. 2014. Synaptic organization of the *Drosophila* antennal lobe and its regulation by the teneurins. *eLife* **3**:e03726. DOI: https://doi.org/10.7554/eLife.03726, PMID: 25310239

Nagarkar-Jaiswal S, DeLuca SZ, Lee P-T, Lin W-W, Pan H, Zuo Z, Lv J, Spradling AC, Bellen HJ. 2015a. A genetic toolkit for tagging intronic MiMIC containing genes. *eLife* **4**:e08469. DOI: https://doi.org/10.7554/eLife.08469

Nagarkar-Jaiswal S, Lee P-T, Campbell ME, Chen K, Anguiano-Zarate S, Cantu Gutierrez M, Busby T, Lin W-W, He Y, Schulze KL, Booth BW, Evans-Holm M, Venken KJT, Levis RW, Spradling AC, Hoskins RA, Bellen HJ. 2015b. A library of MiMICs allows tagging of genes and reversible, spatial and temporal knockdown of proteins in *Drosophila*. *eLife* **4**:e05338. DOI: https://doi.org/10.7554/eLife.05338

Nagarkar-Jaiswal S, Manivannan SN, Zuo Z, Bellen HJ. 2017. A cell cycle-independent, conditional gene inactivation strategy for differentially tagging wild-type and mutant cells. *eLife* **6**:e26420. DOI: https://doi.org/10.7554/eLife.26420, PMID: 28561736

Pankova K, Borst A. 2016. RNA-Seq transcriptome analysis of Direction-Selective T4/T5 neurons in *Drosophila*. *PLOS ONE* **11**:e0163986. DOI: https://doi.org/10.1371/journal.pone.0163986, PMID: 27684367

Pankova K, Borst A. 2017. Transgenic line for the identification of cholinergic release sites in *Drosophila melanogaster*. *The Journal of Experimental Biology* **220**:1405–1410. DOI: https://doi.org/10.1242/jeb.149369, PMID: 28167805

Pavlowsky A, Schor J, Plaçais PY, Preat T. 2018. A GABAergic feedback shapes dopaminergic input on the *Drosophila* Mushroom Body to Promote Appetitive Long-Term Memory. *Current Biology* **28**:1783–1793. DOI: https://doi.org/10.1016/j.cub.2018.04.040, PMID: 29779874

Petzoldt AG, Lee YH, Khorramshahi O, Reynolds E, Plested AJ, Herzel H, Sigrist SJ. 2014. Gating characteristics control glutamate receptor distribution and trafficking in vivo. *Current Biology* **24**:2059–2065. DOI: https://doi.org/10.1016/j.cub.2014.07.051, PMID: 25131677

Pfeiffer BD, Ngo TT, Hibbard KL, Murphy C, Jenett A, Truman JW, Rubin GM. 2010. Refinement of tools for targeted gene expression in *Drosophila*. *Genetics* **186**:735–755. DOI: https://doi.org/10.1534/genetics.110.119917, PMID: 20697123

Raghu SV, Joesch M, Borst A, Reiff DF. 2007. Synaptic organization of lobula plate tangential cells in *Drosophila*: gamma-aminobutyric acid receptors and chemical release sites. *The Journal of Comparative Neurology* **502**:598–610. DOI: https://doi.org/10.1002/cne.21319, PMID: 17394161

Raghu SV, Joesch M, Sigrist SJ, Borst A, Reiff DF. 2009. Synaptic organization of lobula plate tangential cells in *Drosophila:* dalpha7 cholinergic receptors. *Journal of Neurogenetics* **23**:200–209. DOI: https://doi.org/10.1080/01677060802471684, PMID: 19306209

Richter FG, Fendl S, Haag J, Drews MS, Borst A. 2018. Glutamate signaling in the fly visual system. *iScience* **7**:85–95. DOI: https://doi.org/10.1016/j.isci.2018.08.019, PMID: 30267688

Sánchez-Soriano N, Bottenberg W, Fiala A, Haessler U, Kerassoviti A, Knust E, Löhr R, Prokop A. 2005. Are dendrites in *Drosophila* homologous to vertebrate dendrites? *Developmental Biology* **288**:126–138. DOI: https://doi.org/10.1016/j.ydbio.2005.09.026, PMID: 16223476

Sarov M, Barz C, Jambor H, Hein MY, Schmied C, Suchold D, Stender B, Janosch S, K J VV, Krishnan RT, Krishnamoorthy A, Ferreira IR, Ejsmont RK, Finkl K, Hasse S, Kämpfer P, Plewka N, Vinis E, Schloissnig S, Knust E, et al. 2016. A genome-wide resource for the analysis of protein localisation in *Drosophila*. *eLife* **5**:e12068. DOI: https://doi.org/10.7554/eLife.12068, PMID: 26896675

Schnütgen F, Doerflinger N, Calléja C, Wendling O, Chambon P, Ghyselinck NB. 2003. A directional strategy for monitoring Cre-mediated recombination at the cellular level in the mouse. *Nature Biotechnology* **21**:562–565. DOI: https://doi.org/10.1038/nbt811, PMID: 12665802

Serbe E, Meier M, Leonhardt A, Borst A. 2016. Comprehensive characterization of the major presynaptic elements to the *Drosophila* OFF Motion Detector. *Neuron* **89**:829–841. DOI: https://doi.org/10.1016/j.neuron.2016.01.006, PMID: 26853306

Sethuramanujam S, Matsumoto A, McIntosh JM, Jing M, Li Y, Berson D, Yonehara K, Awatramani GB. 2020. Rapid 'multi-directed' cholinergic transmission at central synapses. *bioRxiv*. DOI: https://doi.org/10.1101/2020.04.18.048330

Shinomiya K, Huang G, Lu Z, Parag T, Xu CS, Aniceto R, Ansari N, Cheatham N, Lauchie S, Neace E, Ogundeyi O, Ordish C, Peel D, Shinomiya A, Smith C, Takemura S, Talebi I, Rivlin PK, Nern A, Scheffer LK, et al. 2019. Comparisons between the ON- and OFF-edge motion pathways in the *Drosophila* brain. *eLife* **8**:e40025. DOI: https://doi.org/10.7554/eLife.40025, PMID: 30624205

Sigal YM, Speer CM, Babcock HP, Zhuang X. 2015. Mapping synaptic input fields of neurons with Super-Resolution imaging. *Cell* **163**:493–505. DOI: https://doi.org/10.1016/j.cell.2015.08.033, PMID: 26435106

Strother JA, Wu S-T, Wong AM, Nern A, Rogers EM, Le JQ, Rubin GM, Reiser MB. 2017. The emergence of directional selectivity in the visual motion pathway of *Drosophila*. *Neuron* **94**:168–182. DOI: https://doi.org/10.1016/j.neuron.2017.03.010

Strother JA, Wu ST, Rogers EM, Eliason JLM, Wong AM, Nern A, Reiser MB. 2018. Behavioral state modulates the ON visual motion pathway of *Drosophila*. *PNAS* **115**:E102–E111. DOI: https://doi.org/10.1073/pnas.1703090115, PMID: 29255026

Takemura SY, Karuppudurai T, Ting CY, Lu Z, Lee CH, Meinertzhagen IA. 2011. Cholinergic circuits integrate neighboring visual signals in a *Drosophila* motion detection pathway. *Current Biology : CB* **21**:2077–2084. DOI: https://doi.org/10.1016/j.cub.2011.10.053, PMID: 22137471

Takemura SY, Nern A, Chklovskii DB, Scheffer LK, Rubin GM, Meinertzhagen IA. 2017. The comprehensive connectome of a neural substrate for 'ON' motion detection in *Drosophila*. *eLife* **6**:e24394. DOI: https://doi.org/10.7554/eLife.24394, PMID: 28432786

Venken KJT, Schulze KL, Haelterman NA, Pan H, He Y, Evans-Holm M, Carlson JW, Levis RW, Spradling AC, Hoskins RA, Bellen HJ. 2011. MiMIC: a highly versatile transposon insertion resource for engineering *Drosophila melanogaster* genes. *Nature Methods* **8**:737–743 . DOI: https://doi.org/10.1038/nmeth.1662

Vogel C, Marcotte EM. 2012. Insights into the regulation of protein abundance from proteomic and transcriptomic analyses. *Nature Reviews Genetics* **13**:227–232 . DOI: https://doi.org/10.1038/nrg3185

Wienecke CFR, Leong JCS, Clandinin TR. 2018. Linear summation underlies direction selectivity in *Drosophila*. *Neuron* **99**:680–688. DOI: https://doi.org/10.1016/j.neuron.2018.07.005, PMID: 30057202

Willems J, de Jong APH, Scheefhals N, Mertens E, Catsburg LAE, Poorthuis RB, de Winter F, Verhaagen J, Meye FJ, MacGillavry HD. 2020. ORANGE: a CRISPR/Cas9-based genome editing toolbox for epitope tagging of endogenous proteins in neurons. *PLOS Biology* **18**:e3000665. DOI: https://doi.org/10.1371/journal.pbio.3000665, PMID: 32275651

Williams JL, Shearin HK, Stowers RS. 2019. Conditional synaptic vesicle markers for *Drosophila* . *G3: Genes, Genomes, Genetics* **9**:737–748. DOI: https://doi.org/10.1534/g3.118.200975

Xue M, Atallah BV, Scanziani M. 2014. Equalizing excitation-inhibition ratios across visual cortical neurons. *Nature* **511**:596–600. DOI: https://doi.org/10.1038/nature13321, PMID: 25043046

2.2 Manuscript 2: Anatomical distribution and functional roles of electrical synapses in *Drosophila*

Georg Ammer, **Renee Marie Vieira**, Sandra Fendl, Alexander Borst

Author contributions: G.A. conceived the study, performed and analyzed all experiments, and wrote the manuscript. R.M.V. helped with antibody design and validation. R.M.V. and S.F. generated fly lines. A.B. provided funding. A.B., R.M.V, and S.F. commented on the manuscript.

Renee Marie Vieira

Alexander Borst

Article

Current Biology

Anatomical distribution and functional roles of electrical synapses in *Drosophila*

Highlights

- An immunohistochemistry-based map of innexin gap junctions in the *Drosophila* CNS
- VS/HS cells are electrically coupled to large cell networks via shakB gap junctions
- Loss of electrical synapses from VS/HS cells induces voltage and calcium oscillations
- Electrical synapses play functional roles in both ON and OFF vision pathways

Authors

Georg Ammer, Renée M. Vieira, Sandra Fendl, Alexander Borst

Correspondence

gammer@neuro.mpg.de

In brief

Ammer et al. first map the broad distribution of electrical synapses in the fly nervous system. Next, they find that electrical synapses are required for the intrinsic stability of VS/HS cells. Furthermore, electrical synapses play differential roles in ON and OFF visual pathways but are not necessary for the emergence of direction selectivity.

Ammer et al., 2022, Current Biology *32*, 2022–2036
May 9, 2022
https://doi.org/10.1016/j.cub.2022.03.040

CellPress

CellPress
OPEN ACCESS

Current Biology

Article

Anatomical distribution and functional roles of electrical synapses in *Drosophila*

Georg Ammer,[1,2,*] Renée M. Vieira,[1] Sandra Fendl,[1] and Alexander Borst[1]
[1]Max Planck Institute of Neurobiology, Am Klopferspitz 18, 82152 Martinsried, Germany
[2]Lead contact
*Correspondence: gammer@neuro.mpg.de
https://doi.org/10.1016/j.cub.2022.03.040

SUMMARY

Electrical synapses are present in almost all organisms that have a nervous system. However, their brain-wide expression patterns and the full range of contributions to neural function are unknown in most species. Here, we first provide a light-microscopic, immunohistochemistry-based anatomical map of all innexin gap junction proteins—the building blocks of electrical synapses—in the central nervous system of *Drosophila melanogaster*. Of those innexin types that are expressed in the nervous system, some localize to glial cells, whereas others are predominantly expressed in neurons, with shakB being the most widely expressed neuronal innexin. We then focus on the function of shakB in VS/HS cells—a class of visual projection neurons—thereby uncovering an unexpected role for electrical synapses. Removing shakB from these neurons leads to spontaneous, cell-autonomous voltage and calcium oscillations, demonstrating that electrical synapses are required for these cells' intrinsic stability. Furthermore, we investigate the role of shakB-type electrical synapses in early visual processing. We find that the loss of shakB from the visual circuits upstream of VS/HS cells differentially impairs ON and OFF visual motion processing pathways but is not required for the computation of direction selectivity per se. Taken together, our study demonstrates that electrical synapses are widespread across the *Drosophila* nervous system and that they play essential roles in neuronal function and visual information processing.

INTRODUCTION

Neurons communicate via two fundamentally different types of synapses. At chemical synapses, neurotransmitters released from presynaptic sites activate receptors on postsynaptic neurons, leading to direct opening of ion channels or to an initiation of intracellular signaling cascades. In contrast, electrical synapses consist of channel-forming gap junction proteins, which allow for a direct, bidirectional flow of ions between two connected cells. In invertebrates, gap junctions are composed of innexin proteins, of which eight different types are encoded in the *Drosophila* genome.[1,2] Two hemichannels, composed of eight innexin proteins each, form a functional channel that bridges the cytoplasm of two cells.[3] Apart from forming electrical synapses between neurons, innexins play essential roles in other biological processes such as embryonic development,[4] stem cell division,[5] the formation of the blood-brain barrier,[6] or spermatogenesis.[7]

In *Drosophila*, the molecular components, physiology, and function of chemical synapses have been studied in great detail.[8] In addition, in recent years, large-scale efforts have been undertaken to generate a connectome of the *Drosophila* nervous system—a complete map of every chemical synaptic connection—based on electron-microscopic[9] reconstructions.[9–11] Conversely, the nervous-system-wide distribution of electrical synapses is unknown. Importantly, electrical synapses are completely absent from all published *Drosophila* connectomic studies. This is largely due to their small size of around 10–20 nm,[12] which is below the resolution of current electron microscopic imaging techniques used for generating large EM datasets. Thus, most of our knowledge about electrical synapses comes from studies that focused on particular cell types or small neural circuits. The best-studied example is the giant fiber escape circuit of *Drosophila*. Here, electrical connections formed by shakB-type gap junctions exist at all nodes of the circuit, from sensory neurons to interneurons to motor neurons.[13–17] The proposed function of the strong electrical coupling in the giant fiber circuit is to speed up signal transmission for enabling fast escape maneuvers, as electrical synapses essentially introduce no synaptic delay. Additional examples of electrical synaptic connections in the *Drosophila* brain include coupling between olfactory projection neurons[18] and coupling between different types of neurons in the mushroom body.[19–21]

Extensive electrical connections also exist in the fly visual system. Here, several studies have investigated the vertical system (VS) and horizontal system (HS) cells—subtypes of the lobula plate tangential cells (LPTCs)—in the blowfly *Calliphora*. LPTCs are wide-field neurons that project their axons from the optic lobe to the central brain or the contralateral optic lobe.[22] They receive direction-selective input from small-field T4 and T5 cells, the output neurons of ON and OFF motion pathways, which respond to moving luminance increments and decrements, respectively.[23] Spatial integration of these inputs renders LPTCs selective to a particular pattern of optic flow that is dependent on the neuronal subtype.[24] In addition to spatial integration, some LPTCs perform nonlinear amplification of

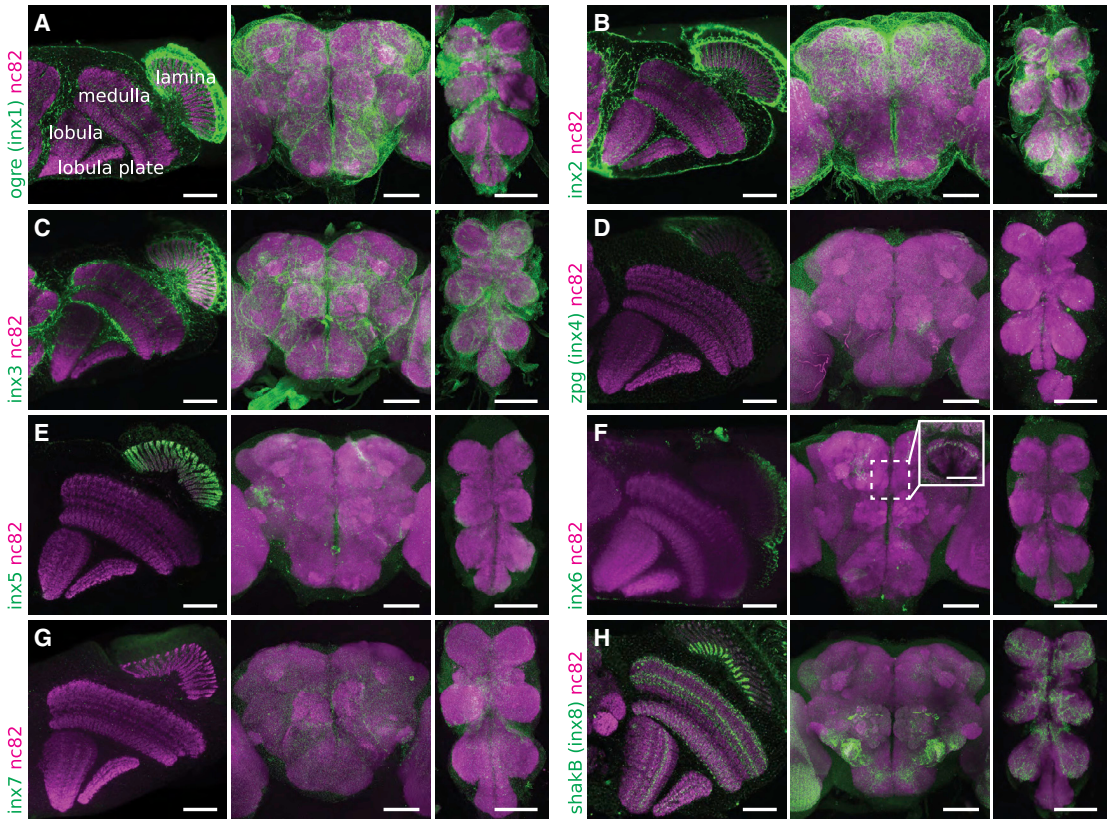

Figure 1. Expression patterns of innexin gap junction proteins in the *Drosophila* central nervous system

Immunostainings for the gap junction proteins ogre (inx1) (A), inx2 (B), inx3 (C), zpg (inx4) (D), inx5 (E), inx6 (F), inx7 (G), and shakB (inx8) (H). Horizontal sections of the optic lobes (left panels) and maximum intensity projections of the central brain (middle panels) and ventral nerve cord (right panels) are shown. Scale bars, 30 μm (optic lobe), 50 μm (central brain), 100 μm (VNC), and 40 μm (inset in F).
See also Figures S1–S3.

high-frequency inputs in the temporal domain.[25] Different subtypes of LPTCs form electrical synapses both with each other and with descending neurons.[26–29] Electrical coupling between the axons of VS cells broadens their axonal receptive fields and thereby increases the robustness of optic flow representation under noisy conditions.[30–34] Similarly, HS cells form electrical synapses with other HS cells and additionally with the H2 cell from the contralateral hemisphere.[35] However, which type of innexin is mediating the electrical coupling between LPTCs is unknown. Furthermore, experimental studies that directly test the effects of removing electrical synapses on the physiology of LPTCs are lacking.

Here, we first describe the distribution of innexins across the entire central nervous system (CNS) in adult *Drosophila*. Next, to assess the importance of electrical synapses in neuronal function, we investigate the role of shakB, the most widely expressed neuronal gap junction protein, in VS and HS cells. We find that loss of electrical synapses drives these cells into spontaneous membrane potential oscillations and induces large periodic calcium fluctuations. These oscillations arise cell autonomously and involve voltage-gated sodium channels (Na_v) and I_h channels. Moreover, we record from VS/HS cells and presynaptic T4/T5 cells and demonstrate that loss of shakB affects visual processing in both ON and OFF pathways.

RESULTS

A map of gap junction expression across the central nervous system

To determine the distribution of electrical synapses in the central nervous system of *Drosophila melanogaster*, we performed immunostainings against each of the eight innexin gap junction proteins (Figures 1 and S1–S3). We found that six of the eight innexins show expression in the nervous system (Figure 1). Three of those, ogre (inx1), inx2, and inx3, exclusively localized to glial cells (Figures 1A–1C). We performed colabeling of these innexins together with markers for glial subtypes. Consistent with earlier work, ogre localized to subperineural glia and partly to perineural glia, which are crucial components of the blood-brain barrier.[5,6] inx3 was detected exclusively and strongly in neuropil ensheathing glia, and inx2 colocalized with all of the three glial subtypes (Figure S2). Two of the other innexins showed only very sparse expression: whereas diffuse inx5 signal was visible only in the lamina (Figure 1E), inx6 was exclusively detected in the dorsal fan-shaped body in the central brain (Figures 1F and S3A).[21,36] In stark contrast, shakB (inx8) was broadly expressed in the optic lobes, in many regions of the central brain and in the ventral nerve cord (VNC) (Figure 1H). We obtained similar results by using a different set of antibodies (Figure S1). Together, these protein expression

patterns are largely in agreement with RNA sequencing data.[37–40] According to these studies, the mRNAs of ogre, inx2, inx3, and shakB are the most strongly expressed innexin transcripts in the nervous system, whereas zpg (inx4), inx5, inx6, and inx7 were either not detected at all or only at very low levels (Figure S3B).

Electrical synapses formed by shakB are widely distributed across the CNS

As shakB was broadly and strongly expressed in the neuropil, we analyzed the expression pattern of this innexin in more detail (Figures 2 and S1H–S1M). Correlation analysis between relative fluorescence intensities of shakB and nc82, a marker for chemical presynaptic sites, revealed a weak anticorrelation (Figure S3C). This suggests that the number of shakB electrical synapses does not simply scale with the number of chemical synapses but that these two types of synapses have distinct anatomical distributions. shakB localized to all four neuropils of the optic lobe in a layered fashion: the proximal lamina; layers 1, 3, 5, and 10 of the medulla; layer 3 of the lobula; and to the lobula plate (Figure 1H). In the central brain, we detected particularly strong expression of shakB in the anterior mechanosensory and motor center, the anterior ventrolateral protocerebrum, the wedge, the subesophageal ganglion, the giant fiber, the posterior slope, and the cervical connective. Additionally, we observed weaker expression in the antennal lobes, the optic tubercle, the superior medial protocerebrum, and the lateral horn (Figures 2A–2J). In the VNC, shakB localized to the leg neuropils, the tectulum, and the wing and haltere neuropils (Figure 2K). Importantly, no shakB immunolabeling was detected in shakB^{2}-mutant flies that carry a null allele for six of the eight shakB isoforms (Figure S3D).[41] This suggests that the remaining two isoforms (isoforms A, E) are either not expressed in the adult CNS or only at very low levels. Similarly, shakB staining was absent when we expressed an RNAi construct that targets all eight shakB isoforms pan-neuronally (Figure S3E), thereby confirming the specificity of the antibody. Given the abundant and widespread expression of shakB in the *Drosophila* nervous system, we focused our further investigations on this gap junction type.

Candidate cell types forming shakB-type electrical synapses

As a next step, we generated a genetic driver line that is based on the MiMIC-Trojan-Gal4 system (Figure S4A).[42] To do so, we used a published fly line in which a MiMIC transposon is inserted into an intron of the shakB gene that is common to the same six isoforms that are affected by the shakB^{2} mutation.[43] This MiMIC insertion was then exchanged with a Trojan-Gal4 exon that codes for a T2A-sequence followed by the Gal4 transcription factor. Consequently, every cell that expresses one of those shakB isoforms should express Gal4 as well, thereby allowing us to label most shakB-expressing cells. When using the shakB-Trojan-Gal4 line to drive GFP, we observed many labeled cells across the CNS (Figure 2L). The neuropil regions that showed strong shakB immunolabeling were also strongly innervated by neurons labeled by this line (Figures 2M–2O). A second fly line in which the Trojan-Gal4 cassette was integrated into a different intronic region revealed a highly similar expression pattern (Figures S4B–S4I). This confirms that shakB gap junctions are widely expressed in the central nervous system of the fly by a large number of different cell types.

LPTCs form large electrically coupled networks via shakB gap junctions

After describing the anatomical distribution of gap junctions across the *Drosophila* nervous system, we sought to study the functional role of electrical synapses in a restricted number of cells. We chose to investigate the VS and HS cells of the lobula plate tangential cell system for several reasons: First, these cells provide output from the optic lobes to the central brain. Given that shakB is strongly expressed in the optic lobes, we speculated that any effects of removing this protein would likely affect the response properties of LPTCs. Second, VS and HS cells have already been shown to be electrically coupled to each other and to other LPTCs.[26–28] Third, VS and HS cells are easily accessible by electrophysiological and functional imaging experiments.

VS and HS cells project their axons to the posterior slope in the central brain (Figure 3A). Since we observed shakB expression in this brain area, we reasoned that VS and HS cells might possess shakB gap junctions. When we visualized VS/HS cells with GFP and stained for shakB, we indeed observed colocalization between their axon terminals and shakB (Figure 3B). To identify the neurons that are coupled to VS and HS cells via shakB gap junctions, we performed whole-cell patch clamp recordings from individual cells and filled them with the gap junction-permeable molecule neurobiotin. Staining against neurobiotin revealed large dye-coupled neuronal networks, irrespective of the particular subtype of VS or HS cell (dye-coupling in 10/10 cells; Figures 3C, 3D, 3F, 3G, and S5A). VS and HS cells were dye-coupled to neighboring VS and HS cells, respectively, as described before.[27,28] Moreover, both cell types were strongly coupled to descending neurons.[29] Interestingly, in contrast to HS cells, VS cells were additionally coupled to dozens of smaller neurons (putatively lobula plate columnar cells) as revealed by the labeling of small cell bodies and thin neurites projecting to the central brain. Importantly, dye-coupling was abolished when injecting VS or HS cells in the shakB^{2}-mutant background (dye-coupling in 0/8 cells), demonstrating that electrical synapses between VS/HS cells and other cells are exclusively formed by shakB-type gap junctions (Figures 3E, 3H, and S5B). VS and HS cells are thus part of large electrically coupled networks connected by shakB gap junctions.

Spontaneous membrane potential oscillations in VS and HS cells of shakB-deficient flies

To investigate the functional relevance of electrical synapses in VS/HS cells and upstream visual circuits, we performed electrophysiological recordings from these neurons in control and shakB-deficient flies. Without visual stimulation, VS/HS cells from control flies showed small spontaneous membrane potential fluctuations, corresponding to excitatory postsynaptic potentials (EPSPs) and inhibitory postsynaptic potentials (IPSPs) but generally had stable resting potentials (Figures 4A and 4C). In contrast, a large fraction of recorded cells from shakB^{2}-mutant flies spontaneously displayed fast, high-amplitude membrane potential oscillations. Frequently, sudden, large drops in membrane potential, which again occurred periodically, interrupted these fast oscillations (Figure 4B). Both of these types of oscillations also occurred in flies in which the expression of shakB was knocked down pan-neuronally using RNA interference (hereafter referred to as shakB-RNAi flies) (Figure 4D). This makes it unlikely that secondary

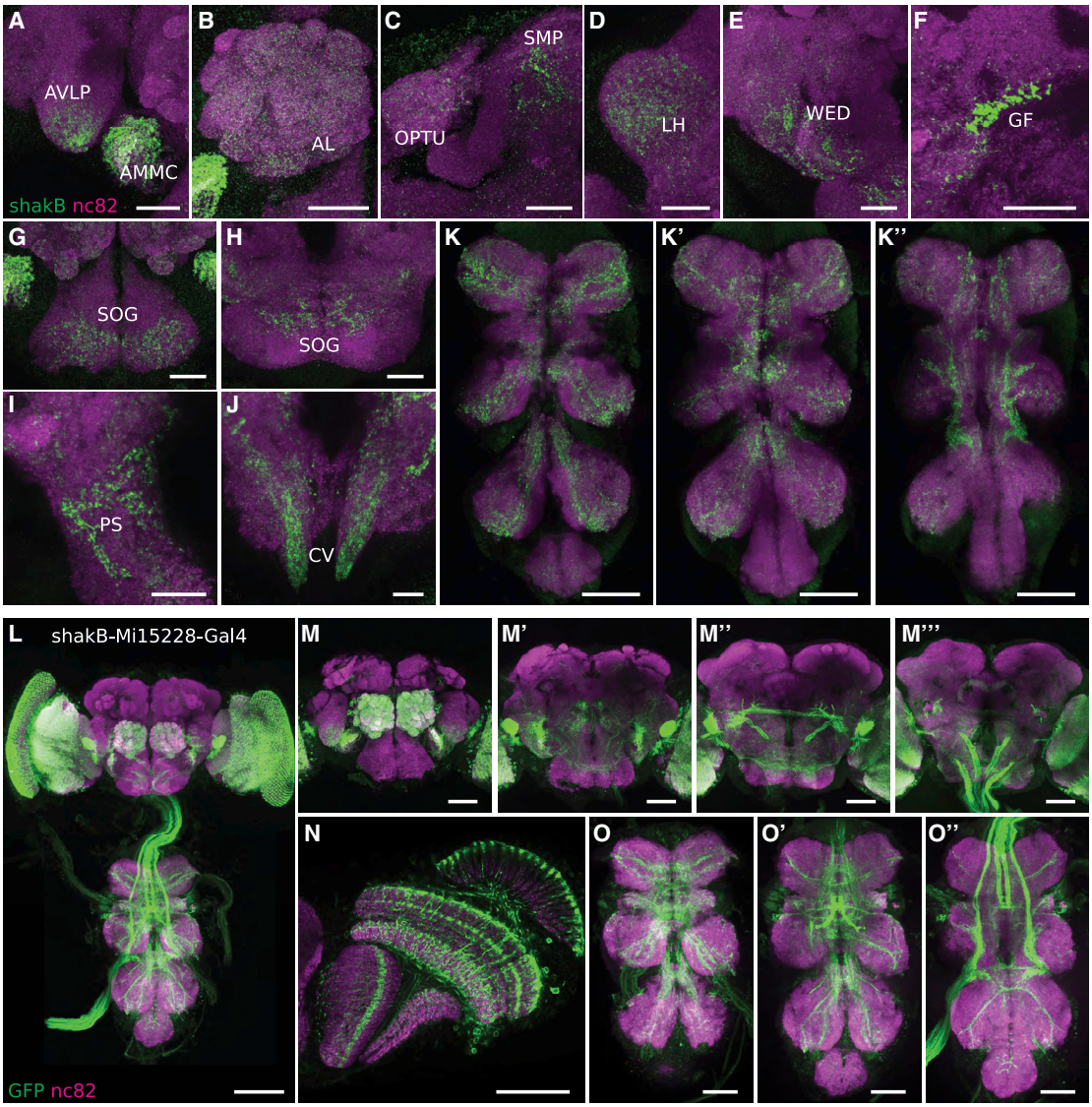

Figure 2. Distribution of shakB electrical synapses across the fly central nervous system

(A–J) In the central brain, shakB (green) is expressed in the antennal mechanosensory and motor center (AMMC) and anterior ventrolateral protocerebrum (AVLP) (A), the antennal lobe (AL) (B), the optic tubercle (OPTU) and superior medial protocerebrum (SMP) (C), the lateral horn (LH) (D), the wedge (WED) (E), the giant fiber (GF) (F), the subesophageal ganglion (SOG) (G and H), the posterior slope (PS) (I), and the cervical connective (CV) (J).

(K–K″) In the VNC, shakB localizes to regions in the ventral (K), medial (K′), and dorsal (K″) parts.

(L) Expression of GFP driven by shakB-Trojan-Gal4. Maximum intensity projection (MIP) of the brain and VNC.

(M–M‴) shakB-Trojan-Gal4-driven GFP expression in the central brain. MIPs of anterior (M), anteromedial (M′), posteromedial (M″), and posterior (M‴) parts.

(N) Cell types in the optic lobe labeled by the shakB-Trojan-Gal4 line (horizontal section).

(O–O″) Cell types in the VNC labeled by the shakB-Trojan-Gal4 line. MIPs of ventral (O), medial (O′), and dorsal (O″) regions are shown.

Scale bars, 20 μm (A–J), 50 μm (K), 100 μm (L), and 50 μm (M–O).

See also Figures S1I–S1M, S3, and S4.

mutations or off-target effects cause the oscillations. Although cells from control flies never displayed any of these two types of oscillations (CS-control: 0/21, RNAi-control: 0/16), both in mutant and knockdown flies, fast oscillations occurred in more than fifty percent of the neurons (shakB^{2}-mutant: 17/30, shakB-RNAi: 9/16), of which around half showed slow oscillations (shakB^{2}-mutant: 9/17, shakB-RNAi: 4/9) (Figure 4E). Importantly, neurons only oscillated slowly if they also exhibited fast oscillations, indicative of a functional link between these two oscillation types. We also noted that resting membrane potentials were slightly less negative in both types of flies that lacked shakB when compared with controls (Figure 4F). Why does only a subset of neurons oscillate spontaneously? Interestingly, we found that subtle current injections could switch neurons from a non-oscillatory into an oscillatory state and vice versa (Figures S5C–S5F). This suggests that most (or all) cells that lack shakB are intrinsically unstable,

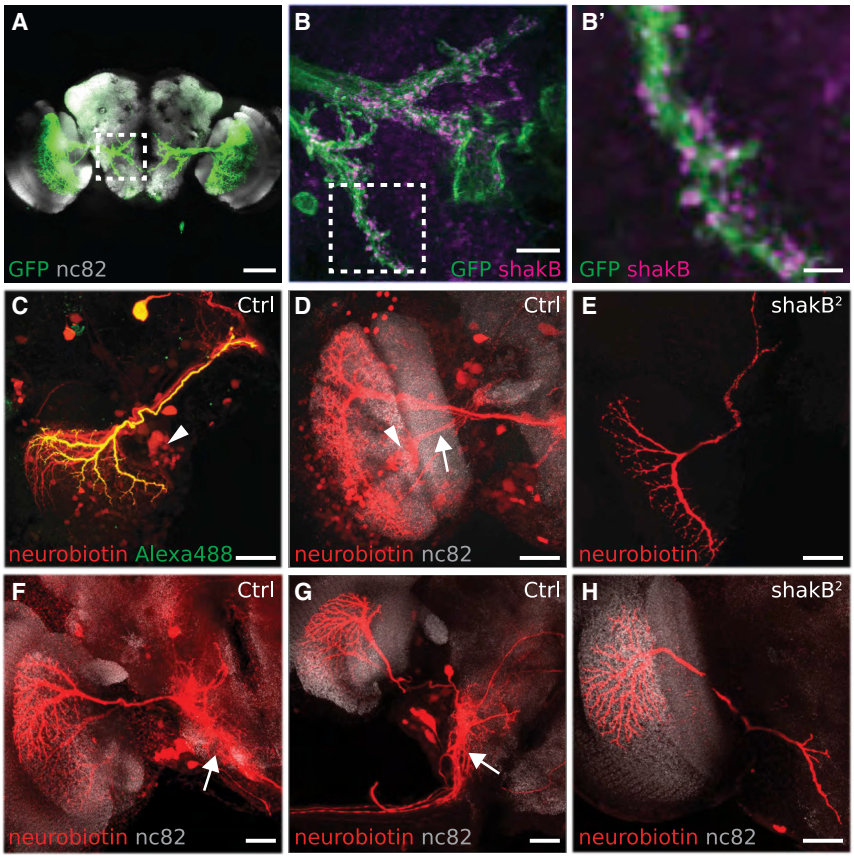

Figure 3. VS and HS cells form electrical synapses via shakB gap junctions

(A) Posterior view of the brain with VS and HS cells labeled with GFP.

(B) shakB localizes to the axon terminals of VS and HS cells. Brain area corresponds to boxed region in (A).

(B′) Magnification of HS cell terminals highlighted in (B).

(C and D) Neurobiotin injections (red) into single VS cells. In (C), we included the gap junction-impermeable dye Alexa 488 (green) in the electrode. The patched VS cell appears yellow because both neurobiotin (red) and Alexa 488 (green) are present. Arrows and arrowheads indicate neurites or somata of dye-coupled small neurons.

(E) Dye-coupling is abolished when injecting neurobiotin into a VS cell of a shakB^2-mutant fly.

(F–H) Similar to (C)–(E) but for HS cells. Note the strong coupling to descending neurons (arrows).

Scale bars, 50 μm (A), 10 μm (B), 3 μm (B'), and 25 μm (C–H).

See also Figures S5A and S5B.

however, yet unknown variables determine whether a given neuron oscillates spontaneously or not.

To analyze the amplitudes and frequencies of the spontaneous oscillations, we performed Fourier spectrum analysis of the cells' membrane potential fluctuations. Control flies showed a power spectrum that fell off with increasing frequency, indicative of pure low-pass filtering. In contrast, the power spectra of both shakB^2-mutant and shakB-RNAi flies exhibited two prominent peaks (Figures 4G and 4H). We defined two frequency bands around these peaks and named them ultraslow-wave (USW, 0.02–0.2 Hz) and β-oscillations (10–30 Hz), respectively, in accordance with the nomenclature of brain oscillations observed in the mammalian cortex.[44,45] The average power in both of these frequency bands was strongly increased in shakB-deficient flies when compared with control flies (Figures 4I and 4J). The median oscillation frequencies were 0.04 and 0.05 Hz for USW oscillations and 17.8 and 15.8 Hz for β-oscillations, for shakB^2-mutant and shakB-RNAi flies, respectively (Figures 4K and 4L). Notably, the oscillations in the β frequency band displayed maximum frequencies that were just around or above the corner frequency of the low-pass filter-like power spectrum of control flies (Figures 4G and 4H). Interestingly, this frequency range is highly reminiscent of the reported resonant frequency of HS cells.[25] Thus, VS and HS cells from flies that lack shakB often show spontaneous large-amplitude membrane potential oscillations, suggesting that, among others, one possible function of electrical synapses in LPTCs is to prevent their membrane from spontaneously falling into an unstable, oscillatory state.

Calcium oscillations in the VS and HS cells of shakB-deficient flies

Our electrophysiological experiments only allowed us to record from one cell at a time. To study the oscillations that arise in VS/HS cells at the network level and to link the membrane potential oscillations we observed after shakB removal to corresponding changes in intracellular calcium levels, we performed two-photon calcium imaging of VS and HS cells. Neurons from control flies did not show any spontaneous calcium activity without visual stimulation (Figure 5A). In contrast, neurons from shakB^2-mutant flies displayed slow, large periodic rises and decays in calcium levels (Figure 5B; Video S1). We observed calcium oscillations in the majority of cells (on average 5.2 [=57.8%] of maximally 9 labeled LPTCs per fly) in these flies. The calcium oscillations were not restricted to the soma but occurred synchronously throughout dendrites and axons as well (Video S2). Next, we performed pan-neuronal calcium imaging in flies that expressed both GCaMP6f and shakB-RNAi in all neurons. Again, LPTCs displayed large calcium oscillations—in fact, these cells were clearly distinguishable from all other labeled cells mainly because of their large fluorescence changes (Figure 5C; Video S3). We did not observe obvious large calcium transients in the rest of the lobula plate, suggesting that the induction of oscillations after shakB removal is specific to LPTCs (Video S3). In addition to shakB^2 mutant and shakB-RNAi flies, we also tested flies in which the pan-neuronal knockdown of shakB was restricted to adulthood by using the temperature-sensitive tubGal80^{ts} transgene (shakB-RNAi-tubGal80^{ts} flies). We confirmed that tubGal80^{ts} allowed for adult-specific RNAi knockdown by performing immunohistochemical and electrophysiological control experiments (Figures S6A–S6I). Importantly, shakB-RNAi-tubGal80^{ts} flies showed large spontaneous calcium oscillations similar to

CellPress
OPEN ACCESS

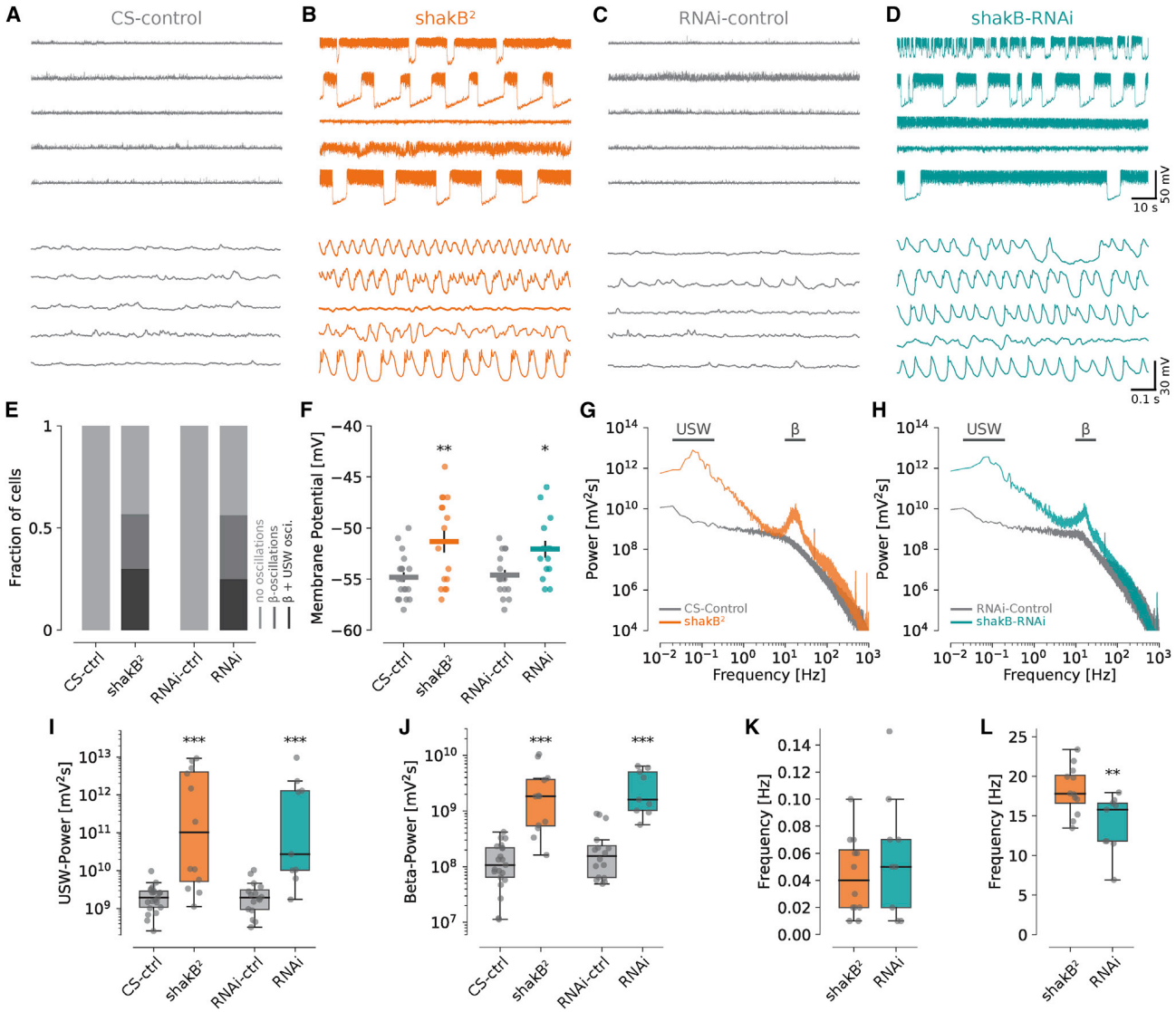

Figure 4. Electrophysiological recordings of VS/HS cells from shakB^2-mutant and shakB-RNAi flies

(A) Membrane potential traces of VS and HS cells from Canton-S control flies without visual stimulation. Traces below show zoom-ins of a stretch of traces above.

(B–D) Similar to (A) but for shakB^2-mutant (B), RNAi-control (C), and shakB-RNAi flies (D).

(E) Percentage of recorded cells showing none (light gray), only fast (β, medium gray), or fast and slow (β + USW, dark gray) membrane potential oscillations.

(F) Resting membrane potentials of indicated genotypes.

(G and H) Power spectra of membrane potentials for CS-control and shakB^2-mutant (G) or RNAi-control and shakB-RNAi flies (H).

(I and J) Average power in the ultraslow frequency band (I) and β frequency band (J).

(K and L) Maximum oscillation frequency in the ultraslow frequency band (K) and β frequency band (L).

Data in (E) are from CS-control, n = 21; shakB^2-mutant, n = 21; RNAi-control, n = 16; shakB-RNAi, n = 16 cells; in (F) from CS-control, n = 21; shakB^2-mutant, n = 16; RNAi-control, n = 16; shakB-RNAi, n = 14 cells; and in (G)–(L) from CS-control, n = 21; shakB^2-mutant, n = 12; RNAi-control, n = 16; shakB-RNAi, n = 9 cells. Data in (F) are mean ± SEM. Boxplots in (I)–(L) show median (horizontal line), interquartile range Q1–3 (boxes), and Q1/Q3–1.5*IQR (whiskers). Dots show data points from individual cells. Statistical analysis: (F) Welch's t test and (I–L) Mann-Whitney U test. *p < 0.05, **p < 0.01, ***p < 0.001.

See also Figures S5C–S5F.

shakB^2-mutant flies and flies in which RNAi expression occurred throughout development (Figure 5D). Thus, the oscillations were not due to a defect caused by depletion of shakB during development. Similar to the electrophysiological experiments, the power in the USW band was significantly higher in shakB^2-mutant and both shakB-RNAi fly lines when compared with control flies (Figures 5E and 5F). Power spectrum analysis revealed that the frequency of these slow oscillations (shakB^2-mutant: 0.035 Hz, shakB-RNAi: 0.030 Hz, shakB-RNAi-tubGal80^{ts}: 0.042 Hz) was similar to the USW oscillations of the cells' membrane potential, suggesting a correspondence between these two phenomena (Figure 5G). Importantly, the temporal properties of the calcium indicator excluded the detection of possible fast β-oscillations at the calcium level.

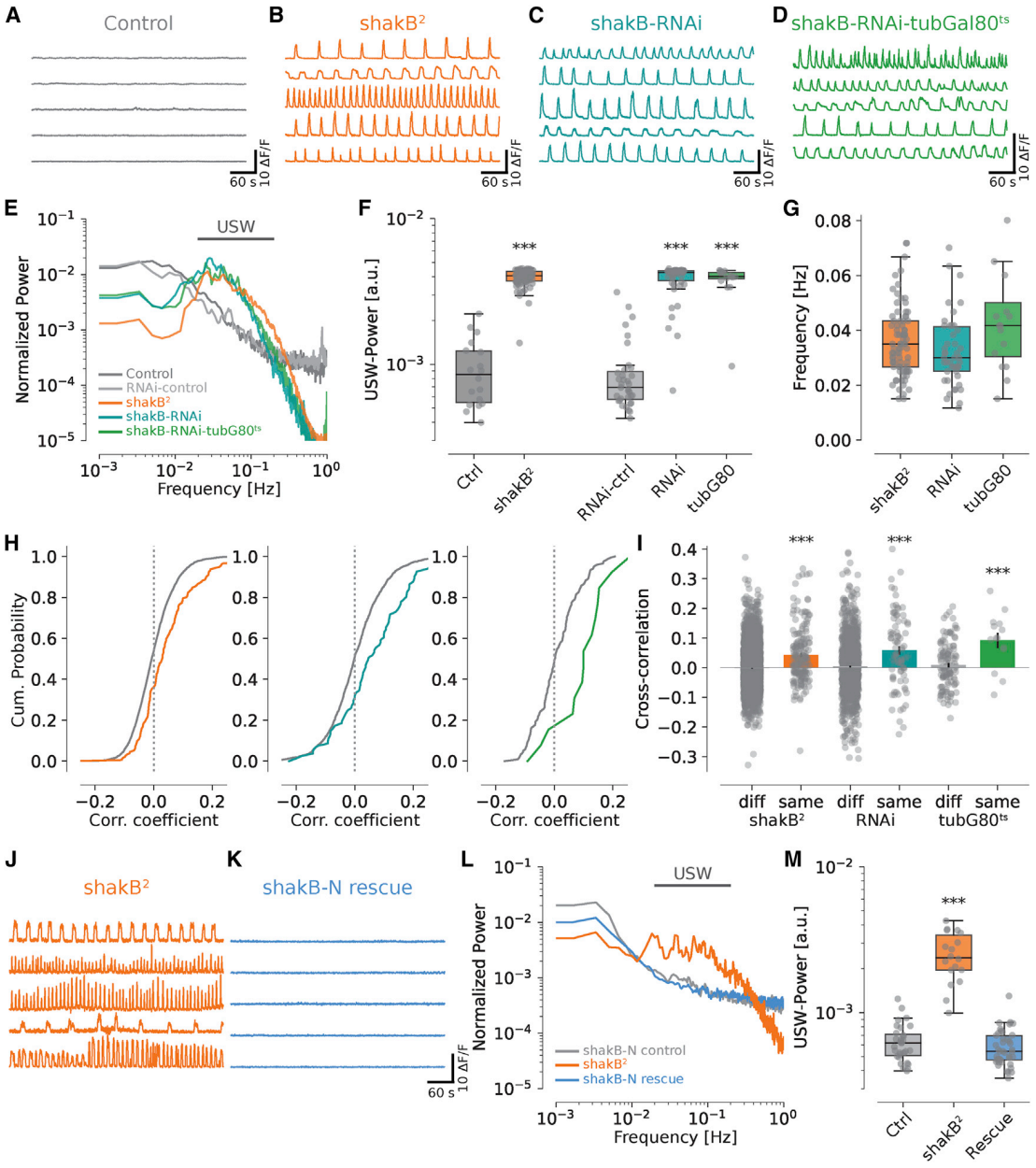

Figure 5. Calcium imaging of VS/HS cells from shakB^2-mutant, shakB-RNAi, and shakB-N rescue flies

(A–D) Calcium traces of VS and HS cells from control (A), shakB^2-mutant (B), shakB-RNAi (C), and shakB-RNAi-tub-Gal80^{ts} (D) flies.

(E) Power spectra of calcium traces.

(F) Average power in the ultraslow frequency band.

(G) Maximum oscillation frequency in the USW frequency band.

(H) Cumulative probability of the correlation coefficients for shakB^2-mutant (left), shakB-RNAi (middle), and shakB-RNAi-tubGal80^{ts} flies from cells within flies (colors) and across flies (gray).

(I) Average correlation coefficients within (same) and across (diff) flies.

(J and K) Calcium traces of VS/HS cells from shakB^2-mutant (J) and shakB-N rescue (K) flies.

(L and M) Power spectra (L) and USW power (M) of shakB-N control (gray), shakB^2-mutant (orange), and shakB-N rescue (light blue) flies.

Data in (E)–(I): Ctrl, n = 4/18; shakB^2-mutant, n = 16/83; shakB-RNAi-Ctrl, n = 7/35; shakB-RNAi, n = 11/46; shakB-RNAi-tubGal80^{ts}, n = 11/16 flies/cells. Data in (L) and (M): shakB-N control, n = 8/31; shakB^2, n = 11/18; shakB-N rescue, n = 10/41 flies/cells. Boxplots in (F), (G), and (M) show median (horizontal line), interquartile range Q1–3 (boxes), and Q1/Q3–1.5*IQR (whiskers). Data in (I) are mean ± SEM. Dots show data from individual cells (F and G) or pairwise correlations (I). Statistical test in (F), (G), and (I): Mann-Whitney U test (Holm-corrected when comparing >2 experimental groups). *p < 0.05, **p < 0.01, ***p < 0.001.

See also Figure S6 and Videos S1, S2, and S3.

As we could image several cell bodies in the same recording, we analyzed if, and to which extent, the calcium oscillations in different cells were synchronized. On average, we found only a weak, yet significant, positive cross-correlation between calcium signals in all shakB-deficient fly lines (Figures 5H and 5I). Thus, calcium levels in LPTCs do not oscillate in synchrony but still exhibit weak positive correlations.

So far, our experimental approach did not allow us to pinpoint the electrical connections whose loss induces oscillations. As cell-type-specific RNAi knockdown of shakB was unsuccessful (Figure S6L), we performed shakB-rescue experiments in VS and HS cells. To do so, we specifically overexpressed the shakB-N isoform in VS/HS cells in an otherwise shakB^2 mutant background (shakB-N rescue flies). Immunostainings confirmed that shakB was localized to the axon terminals of VS/HS cells but was absent from the rest of the brain (Figures S6J and S6K). Calcium imaging in these flies revealed that rescuing electrical synapses specifically between VS/HS cells prevents calcium oscillations (Figures 5J–5M). Thus, the loss of electrical synapses from VS/HS cells themselves (and not other cell types) is responsible for inducing an oscillatory state.

Cell-intrinsic mechanisms generate oscillations

The low correlation between calcium oscillations in different cells points toward a mainly cell-autonomous origin. To directly test if chemical synaptic connections between LPTCs themselves or chemical input from other cells drive or affect these oscillations, we used pharmacology to block chemical synaptic transmission. VS and HS cells receive mainly cholinergic, glutamatergic, and GABAergic inputs.[37] Therefore, we simultaneously applied mecamylamine (MEC) to block excitatory cholinergic input and picrotoxin (PTX) to interfere with inhibitory glutamatergic and GABAergic input.[46] By performing electrophysiological recordings, we confirmed that this pharmacological cocktail indeed blocked all fast synaptic input to these cells (Figures S7A–S7F). After blocking chemical synaptic input, LPTCs continued to display calcium oscillations with similar power and frequency as before (Figures 6A, 6B, 6E, 6I, and 6J; Videos S4 and S5). This suggests that after removal of electrical synapses, VS/HS cells start to oscillate spontaneously and cell autonomously, without any synaptic drive. Interestingly, we found that the average cross-correlation between calcium signals in these cells dropped to zero, suggesting that the weak correlation was caused by weakly synchronizing chemical synaptic input (Figures 6F and 6G). This could be due to common synaptic input from T4 and T5 cells or possible chemical connections between LPTCs themselves.

Voltage-gated sodium and I_h channels are involved in generating oscillations

Our finding that the calcium oscillations in VS/HS cells arise cell autonomously prompted us to investigate which cell-specific conductances generate these oscillations. Two prominent channels that were shown to be involved in many neuronal oscillators are hyperpolarization-activated I_h channels and voltage-gated sodium Na_v channels (in *Drosophila* termed "paralytic").[47] In addition, Na_v channels have been implicated in generating the frequency-dependent amplification of synaptic inputs in *Calliphora* HS cells mentioned earlier.[25] First, to test the involvement of I_h channels, we applied the I_h-antagonist ivabradine[48] together with MEC and PTX to block chemical synaptic input. After application of ivabradine, calcium oscillations did not cease but slowed down (Figures 6C and 6H–6J). Under the premise that ivabradine is similarly effective and specific at blocking *Drosophila* I_h as it is against rabbit I_h, these results suggest that I_h channels play a role in setting the frequency of these oscillations.

To test the potential role of Na_v channels, we blocked chemical synaptic input pharmacologically and then applied tetrodotoxin (TTX), a specific Na_v-channel blocker. Application of TTX led to a complete cessation of calcium oscillations in all cells, showing that Na_v channels are necessary for generating them (Figures 6D, 6H, and 6I). The dominant component of Na_v-currents rapidly inactivates within several milliseconds.[49] This, and our hypothesis that fast voltage oscillations and slow voltage/calcium oscillations are functionally linked, prompted us to test whether silencing Na_v channels also eliminates fast membrane potential oscillations. In line with this prediction, VS and HS cells from shakB^2 flies that displayed slow and/or fast oscillations turned completely silent after application of TTX (Figures 6K–6M). These experiments suggest that Na_v channels are directly involved in generating the fast spontaneous membrane potential oscillations. Notably, a subset of *Drosophila* Na_v channels exhibit persistent sodium currents[49] that could contribute to slow oscillations as well. However, Na_v channels alone cannot account for the large hyperpolarized phases of the slow oscillations. Thus, we propose that fast oscillations secondarily lead to slow voltage and calcium oscillations by a mechanism that might involve I_h channels among others.

Loss of electrical synapses impairs visual responses of VS and HS cells

Finally, we investigated whether VS and HS cells of flies that lack shakB-type electrical synapses still respond to visual stimuli, despite showing membrane potential oscillations. We performed electrophysiological recordings and excluded cells with slow membrane potential oscillations from the analysis. VS/HS cells of control flies responded to moving sine wave gratings in a direction-selective manner by depolarizing to their preferred direction and hyperpolarizing to their null direction. VS and HS cells from shakB-deficient flies still exhibited direction-selective responses, albeit at strongly reduced response amplitudes (Figures 7A–7D). Interestingly, direction selectivity, as calculated by the normalized vector sum of the responses ("LDir"), was unaffected (Figure 7E).

To test whether ON and OFF motion pathways are differentially affected by removing shakB, we stimulated VS/HS cells by showing moving ON or OFF edges. Responses to ON and OFF motion stimuli were both reduced, but the OFF pathway was affected more strongly (Figures 7F and 7G). In addition to direction-selective input via T4/T5 cells, VS and HS cells receive signals from a parallel luminance-sensitive pathway.[50] To investigate whether shakB gap junctions are important components of this "flicker pathway," we presented full field bright and dark flashes to the flies. Although ON flicker responses were left untouched by the loss of shakB, OFF flicker responses were strongly reduced (Figures 7H and 7I).

Are the effects on visual processing at the level of VS/HS cells caused by removing shakB from these cells themselves or rather by removing shakB from neurons in their upstream circuitry? To decide between these alternatives, we measured visual calcium

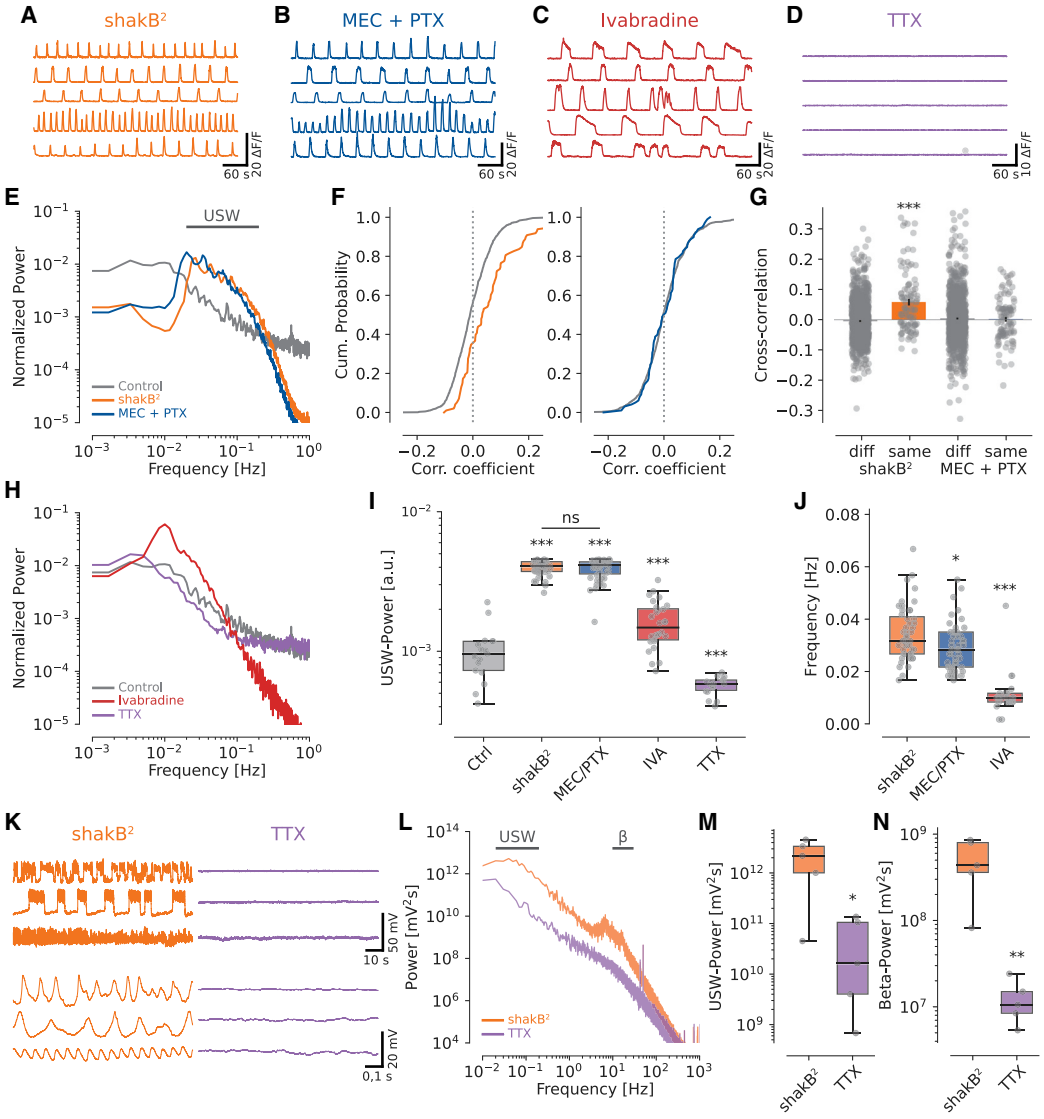

Figure 6. Pharmacological profile of calcium and voltage oscillations in VS/HS cells from shakB^2-mutant flies

(A–D) Calcium traces of VS and HS cells from shakB^2-mutant flies before (A) and after application of mecamylamine and picrotoxin (MEC + PTX) (B), ivabradine (IVA) (C), or tetrodotoxin (TTX) (D).

(E) Power spectra of calcium traces for control (gray) and shakB^2-mutant flies either untreated (orange) or after application of MEC + PTX (dark blue).

(F) Cumulative probability of the correlation coefficients for shakB^2-mutant flies before (left) and after MEC + PTX application calculated within same (colors) or across different flies (gray).

(G) Correlation coefficients within (same) and across (diff) shakB^2-mutant flies before and after application of MEC + PTX.

(H) Power spectra of calcium traces for indicated experiments.

(I) Average power in the ultraslow frequency band (USW).

(J) Maximum oscillation frequency in the USW frequency band.

(K) Representative voltage traces of VS/HS cells from shakB^2-mutant flies before (orange) and after treatment with TTX (purple).

(L) Power spectra of membrane potentials of shakB^2-mutant flies before (orange) and after application of TTX (purple).

(M and N) Average power in the USW frequency band (M) and β frequency band (N) for flies in (K) and (L).

Data in (E)–(J) are from Ctrl, n = 4/17; shakB^2-mutant, n = 9/48; shakB^2 MEC+PTX, n = 9/48; shakB^2 IVA, n = 6/31; shakB^2 TTX, n = 4/18 flies/cells. Data in (L)–(N) are from shakB^2-mutant, n = 5/5 cells/flies. Boxplots in (I), (J), (M), and (N) show median (horizontal line), interquartile range Q1–3 (boxes), and Q1/Q3–1.5*IQR (whiskers). Data in (G) are mean ± SEM. Dots show data from pairwise correlations (G) or individual cells (I, J, M, and N). Statistical test in (G), (I), (J), (M), and (N): Mann-Whitney U test (Holm-corrected when comparing >2 experimental groups). *p < 0.05, **p < 0.01, ***p < 0.001.

See also Figures S7A–S7F and Videos S4 and S5.

CellPress
OPEN ACCESS

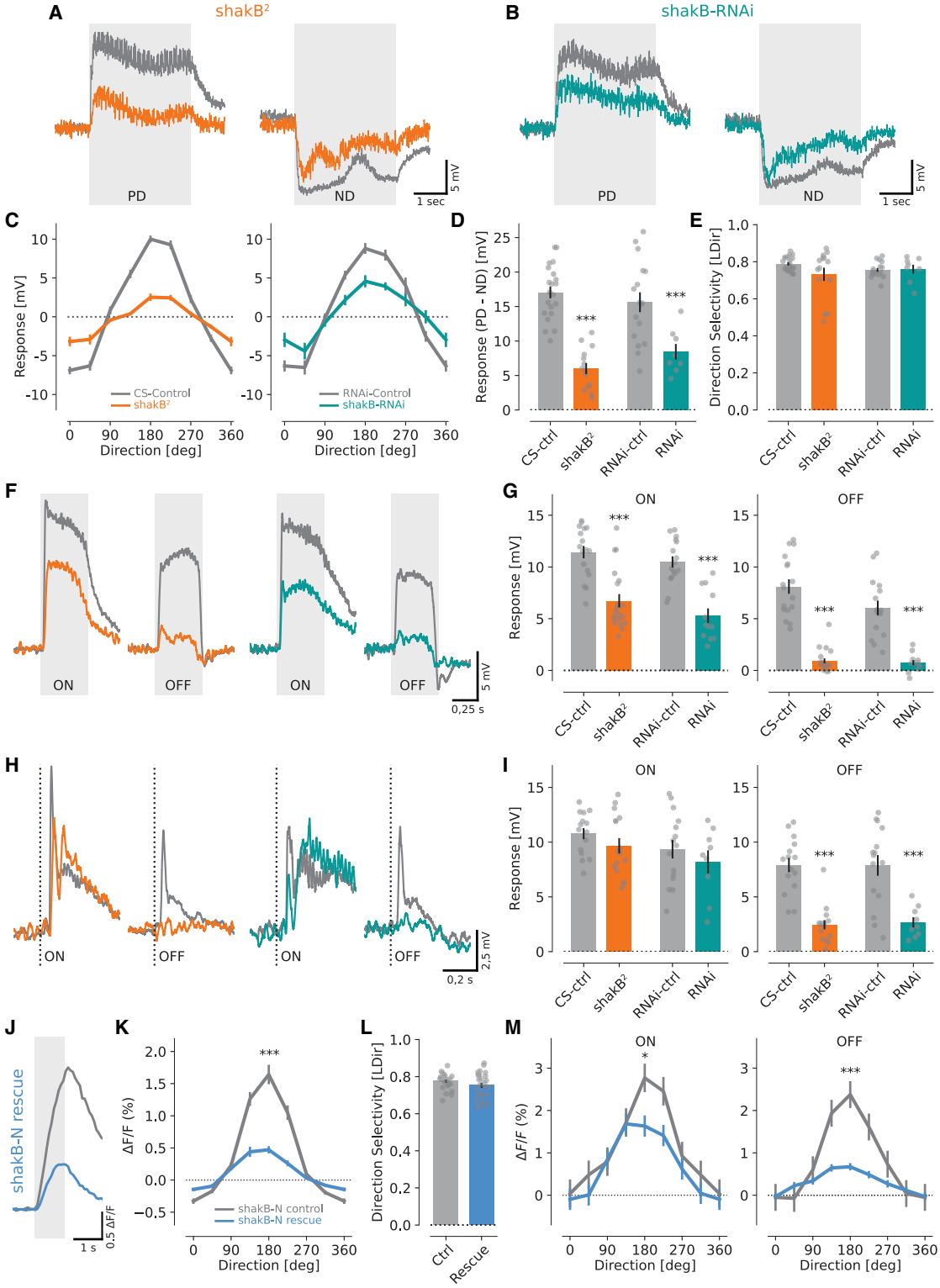

Figure 7. Electrophysiological responses of VS and HS cells from shakB^2-mutant and shakB-RNAi flies to visual stimuli

(A) Average voltage response traces of VS/HS cells from CS-control (gray) and shakB^2-mutant flies (orange) to preferred- (left) and null-direction grating motion.

(B) Similar to (A) but for VS/HS cells from RNAi-control (gray) and shakB-RNAi flies (turquoise).

(C) Directional tuning curves for CS-control and shakB^2-mutant flies (left) and RNAi-control and shakB-RNAi flies.

(D and E) Response strength (PD-ND) (D) and direction selectivity (E) of VS/HS cells to moving gratings.

(legend continued on next page)

responses in flies in which shakB-N was rescued in VS/HS cells. The results of these measurements closely resembled those of the electrophysiological experiments in shakB^2-mutant and shakB-RNAi flies: VS/HS cells from shakB-N rescue flies continued to show strongly reduced responses to drifting gratings, although their direction selectivity was unimpaired (Figures 7J–7L). Additionally, responses to moving ON and OFF edges were both reduced in amplitude, however, again with a much more pronounced effect on the OFF pathway (Figure 7M). Thus, the removal of electrical synapses from visual circuits upstream of VS/HS cells is responsible for their impaired responses to visual motion stimuli.

Visual responses of T4/T5 cells mirror VS/HS cell responses in shakB-deficient flies

The results of the previous section predict that similar effects of shakB removal should already be present at the level of the major presynaptic inputs to VS/HS cells—the T4 and T5 cells. To test this prediction, we performed two-photon calcium imaging from the axon terminals of upward-preferring T4/T5c cells[23] while presenting moving ON and OFF edges (Figures S7G–S7J). At the level of calcium, T4 and T5 neurons respond exclusively to either ON or OFF motion[51,52] allowing us to separate them by their responses to the stimulus. Calcium signals in the axon terminals of both T4 and T5 cells from control flies were narrowly tuned to upward motion. T4 and T5 cells from shakB^2-mutant flies also responded in a direction-selective manner. However, similar to the electrophysiological measurements in postsynaptic VS/HS cells, the response amplitudes were reduced in both T4 and T5, again with a slightly stronger, however more variable, effect on T5 cells (Figures S7H and S7I). When calculating the direction-selectivity index, no difference between controls and shakB^2-mutant flies was found (Figure S7J).

Taken together, these results suggest that shakB electrical synapses in the optic lobe—upstream of T4/T5 cells—play crucial roles in processing motion- and nonmotion-related visual information but are not essential for the emergence of direction selectivity.

DISCUSSION

Patterns of gap junction expression in the *Drosophila* central nervous system

Although large efforts have been made in generating a complete "chemical synaptic connectome" of the adult *Drosophila* nervous system,[9–11] surprisingly, no study has yet investigated the abundance and distribution of electrical synapses throughout that tissue. Here, we took the first steps in filling this gap.

We first described the expression patterns of all eight innexins in the adult central nervous system of *Drosophila* based on immunohistochemistry. We found that some innexins are not expressed, others exclusively in glial cells, and still others only sparsely in the CNS (Figures 1 and S1–S3). According to our immunostainings, shakB is the only innexin that is widely expressed in many neurons of the brain and VNC. Interestingly, both the immunostainings and the shakB-Trojan-Gal4 reporter lines suggest that shakB gap junctions are more abundant in primary and secondary sensory areas of the brain and much less so in higher brain centers such as the central complex or mushroom body.

Our immunohistochemical results are largely in agreement with published RNA sequencing datasets (Figure S3B):[37–40] Here, mRNAs for zpg, inx5, inx6, and inx7 were found to be not or only very weakly expressed. We did not detect zpg and inx7 protein, and inx5 and inx6 only localized sparsely to single brain regions. A study that performed cell-type-specific RNA sequencing of many cells in the optic lobes detected shakB mRNA in ca. 75% of tested cell types.[37] Although this is in qualitative agreement with our finding that shakB is widely expressed, our shakB-Trojan-Gal4 reporter lines clearly label less than 75% of cells in the optic lobes or CNS. Further differences to that study[37] exist as well: although inx3 mRNA was highly expressed in all sequenced cells, we detected inx3 protein only in neuropil ensheathing glia. Furthermore, we did not detect expression of inx7, despite high RNA levels in all photoreceptor subtypes. Whether such differences can be explained by the fact that high mRNA levels do not necessarily predict high protein levels or by limitations of one or the other method remains to be investigated.

Our description of innexin distribution based on immunostainings has obvious limitations: With the exception of shakB, we did not validate the signal specificity of the antibodies in genetic knockout fly lines. However, most of the antibodies that we obtained from other researchers were validated in publications from these labs.[4,7,20,21] Furthermore, we used two different antibodies per innexin and obtained similar results (Figures 1 and S1). One caveat of our immunohistochemical approach is that cells that weakly express innexin proteins might fall below the detection limit. This might explain, for example, why we did not detect clear innexin expression in the mushroom body, whereas

(F and G) Average response traces (F) and average response amplitudes (G) of VS/HS cells to ON and OFF motion stimuli moving in PD.
(H) Average voltage responses of VS/HS cells to full field ON (left) and OFF flicker stimuli. Vertical dotted lines indicate stimulus onset.
(I) Maximum responses to flicker stimuli calculated from the early response peak.
(J–L) Calcium response traces to PD-motion (J), directional tuning curves (K), and direction selectivity (L) of VS/HS cells from shakB-N control (gray) and shakB-N rescue (light blue) flies stimulated with moving gratings.
(M) Directional tuning curves of VS/HS cells from shakB-N-control and shakB-N rescue flies to moving ON and OFF edges measured with calcium imaging.
Data in (A)–(E): CS-control, n = 21; shakB^2-mutant, n = 14; RNAi-control, n = 17; shakB-RNAi, n = 8 cells. Data in (F) and (G): CS-control, n = 17; shakB^2-mutant, n = 20; RNAi-control, n = 16; shakB-RNAi, n = 12 cells. Data in (H) and (I): CS-control, n = 15; shakB^2-mutant, n = 16; RNAi-control, n = 15; shakB-RNAi, n = 9 cells. Data in (J)–(M): shakB-N control, n = 25 (J–L) or n = 27 (M); and shakB-N rescue, n = 26 (J–L) or n = 25 (M) cells. Data from VS and HS cells were pooled because no obvious differences in their responses were detected. Data in (C)–(E), (G), (I), and (K)–(M) are mean ± SEM. Dots indicate individual cells. Gray-shaded areas in (A), (B), (F), and (J) indicate stimulus motion. Statistical analysis: Welch's t test. Statistical testing in (K) and (M) was performed by comparing response strengths (PD-ND) similarly to (D). *p < 0.05, **p < 0.01, ***p < 0.001.
See also Figures S7G–S7J.

other studies have found several innexin subtypes to be involved in mushroom body function.[19–21] As another limitation, the spatial resolution of confocal microscopy does not allow for an unambiguous assignment of innexin expression to specific cell types. Here, a recent study suggests that the use of expansion microscopy can solve this problem.[53] Nonetheless, our approach can help to narrow down the list of candidate cells that might form electrical synaptic connections. Similarly, our shakB-Trojan-Gal4 reporter lines do not give definitive evidence about all cell types that express shakB but can serve as a useful guide for identifying cell types for closer investigation.

To circumvent some of the problems mentioned above, promising approaches include the generation of fly lines that allow for the conditional, endogenous tagging of innexin proteins.[43,54,55] Once a cell type has been identified to express gap junction proteins, the next step is to test if, and to which cells, it is electrically coupled. In this study, we used whole-cell patch clamp recordings and neurobiotin injections to identify the electrically coupled partners of VS and HS cells. This technique is labor intense and therefore not easily scalable. Alternative techniques that depend on the targeted delivery of gap junction-permeable molecules to a genetically defined cell population circumvent the manual injection step but suffer from low signal-to-noise ratios.[56,57] Unfortunately, with both approaches, the identification of coupled cell types is difficult because all connected cells are labeled simultaneously. In the end, improvements in EM technology, such as enhancing the resolution to detect gap junctions in large-scale datasets or genetic tagging of gap junction proteins combined with electron-dense labeling,[58] would solve many of the issues discussed above. Such a technique would not only allow for the identification of cells that form electrical synapses but also reveal all of their connected partners.

Intrinsic oscillations and function of electrical synapses in VS and HS cells

Removing shakB gap junctions through a null mutation or panneuronal knockdown induced fast and slow membrane potential oscillations as well as large calcium oscillations in VS and HS cells. This is unexpected because in many neural networks, exactly the opposite is the case—electrical coupling is necessary for generating network oscillations by synchronizing neural activity.[59,60] Similarly, gap junctions between cardiomyocytes function to stabilize and synchronize electrical activity throughout the myocardium.[61] In the present study, VS and HS cells continued to oscillate when isolated from synaptic input and ceased to do so when rescuing shakB cell type specifically. These two findings argue that the oscillations are not due to network effects but arise cell autonomously, owing to a loss of shakB from VS/HS cells themselves. Furthermore, adult-specific RNAi knockdown of shakB suggests that the oscillations are not caused by developmental defects. However, as immediate pharmacological block of gap junctions was unsuccessful (Figure S6M), we cannot rule out that the oscillations are in part shaped by adaptive mechanisms that occur on the timescales of hours or days.

We partially uncovered the biophysical mechanisms that generate oscillations by showing that Na_v channels are necessary and I_h channels influence their temporal dynamics. Interestingly, application of the Na_v antagonist TTX blocked both types of oscillations at the level of the membrane potential and at the level of calcium. Moreover, slow USW oscillations only occured in cells that show fast β-oscillations. Consequentially, we consider it plausible that the fast voltage oscillations directly induce the slow oscillations. The coupling between voltage and calcium oscillations could then potentially occur via calcium-activated potassium channels such as slowpoke. The exact mechanistic links between fast and slow voltage oscillations and calcium oscillations, however, are yet unknown and must be further investigated in the future.

What is the functional role of electrical synapses in the lobula plate network? We speculate that under normal conditions, these connections might form a safety net for VS and HS cells to keep their nonlinear membrane conductances in check by buffering cell-intrinsic noise via dissipating it through the coupled network. Only a synaptic stimulus of the right frequency and strength, acting on one or multiple connected cells synchronously, would engage the nonlinear mechanisms that lead to an amplification of these signals. If electrical synapses are missing, the cell-intrinsic noise itself is sufficient to induce spontaneous oscillations at the resonant frequency of these cells. Interestingly, it has been shown that active conductances in HS cells lead to an amplification of high-frequency inputs that would otherwise be attenuated by the low-pass properties of the passive membrane.[25] LPTCs receive such high-frequency inputs when the fly is confronted with fast visual motion. Thereby, this amplifying mechanism increases the dynamic range of these cells. Therefore, we consider it plausible that the spontaneous oscillations we observe in VS/HS cells after removal of shakB and the frequency-dependent amplification of synaptic inputs might be based on the same underlying conductance changes. This hypothesis, however, is difficult to test experimentally and must await further investigations.

Visual processing and electrical synapses

Several studies used the fly *Calliphora* to investigate how electrical coupling between LPTCs affects their complex receptive field structure.[31,32] Subsequent studies then built on these results and performed computational modeling to show that axo-axonal gap junctions between LPTCs can increase robustness and efficiency of coding.[30,33,34] The spontaneous oscillations, which arise in VS/HS cells without electrical synapses, complicate the detailed experimental investigation of these models. Thus, we chose to focus on the origin of these oscillations and on the role of electrical synapses in upstream visual circuits in this study.

Loss of shakB electrical synapses led to a reduction of the response magnitudes of T4/T5 and VS/HS cells to both ON and OFF motion stimuli and to an almost complete loss of OFF flicker sensitivity in VS/HS cells. Conversely, the degree of direction selectivity—that is, the sharpness of tuning—was unaffected. Thus, the elementary computation of motion direction does not directly depend on electrical synapses. How and at which level in the visual processing pathway do electrical synapses affect the responses T4/T5 and VS/HS cells? Since shakB mRNA is not or only very weakly expressed in T4/T5 cells,[37] the electrical connections responsible for these effects are likely to be found upstream in the medulla or lamina. Future investigations can now pinpoint the neural and synaptic substrates of these effects by identifying candidate cell types and connections. One such promising candidate is the lamina monopolar

cell L4. shakB colocalizes with the dendrites of L4 cells in the proximal lamina and a shakB-Trojan-Gal4 line labels this cell type (Figures S4F–S4I). Additionally, L4 cells are important for OFF motion detection both at the level of VS/HS cells and behavior.[62,63] The loss of electrical synapses from L4 cells might therefore contribute to the reduced responsiveness to OFF motion and flicker stimuli observed in VS and HS cells.

Notably, we only probed a narrow set of visual stimuli. It is likely that electrical synapses play further important roles in other visual regimes, such as under noisy, low-contrast or low-luminance conditions, as is the case for electrical synapses in the mammalian retina.[64] Moreover, in the mammalian retina, the strength of electrical coupling between neurons is dynamic and can change depending on ambient luminance or circadian rhythm.[65] It will be interesting to see if similar mechanisms are at work in invertebrate visual systems. Furthermore, we only tested the output of a single visual stream. Future research will show which functions electrical synapses exhibit in circuits for phototaxis, color vision, contrast vision, or small object detection but also in other regions of the nervous system such as the central brain or VNC.

Taken together, our study describes the anatomical distribution and demonstrates essential functional roles of electrical synapses in the *Drosophila* nervous system. Incorporating electrical synaptic connections into future connectomes[9] and brain-wide computational models,[66,67] and using the rich *Drosophila* tool kit to investigate the functional properties of these connections, will expand our understanding of their contribution to information processing in the fly brain and in nervous systems in general.

STAR★METHODS

Detailed methods are provided in the online version of this paper and include the following:

- KEY RESOURCES TABLE
- RESOURCE AVAILABILITY
  - Lead contact
  - Materials availability
  - Data and code availability
- EXPERIMENTAL MODEL AND SUBJECT DETAILS
  - Fly husbandry
- METHOD DETAILS
  - Generation of fly lines
  - Antibody generation
  - Immunohistochemistry
  - Confocal microscopy
  - Electrophysiology
  - Calcium imaging
  - Visual stimulation
  - Pharmacology
- QUANTIFICATION AND STATISTICAL ANALYSIS
  - Data analysis
  - Statistical analysis

SUPPLEMENTAL INFORMATION

Supplemental information can be found online at https://doi.org/10.1016/j.cub.2022.03.040.

ACKNOWLEDGMENTS

We thank Christoph Kapfer and Romina Kutlesa for generating the anti-shakB serum antibody; Lukas Groschner for proofreading the manuscript; John Tuthill and Anne Sustar for help with genotyping shakB flies; Guy Tanentzapf, Chia-Lin Wu, Ann-Shyn Chiang, and Reinhard Bauer for sharing anti-innexin antibodies; and Rodney Murphey for providing the shakB$^{2\text{-mutant}}$ fly line. This work was funded by the Max Planck Society.

AUTHOR CONTRIBUTIONS

G.A. conceived the study, performed and analyzed all experiments, and wrote the manuscript. R.V. helped with antibody design and validation. R.V. and S.F. generated fly lines. A.B. provided funding. A.B., R.V., and S.F. commented on the manuscript.

DECLARATION OF INTERESTS

The authors declare no competing interests.

INCLUSION AND DIVERSITY

One or more of the authors of this paper self-identifies as an underrepresented ethnic minority in science. One or more of the authors of this paper self-identifies as a member of the LGBTQ+ community.

Received: August 4, 2021
Revised: February 16, 2022
Accepted: March 14, 2022
Published: April 5, 2022

REFERENCES

1. Skerrett, I.M., and Williams, J.B. (2017). A structural and functional comparison of gap junction channels composed of connexins and innexins. Dev. Neurobiol. *77*, 522–547.
2. Alexopoulos, H., Böttger, A., Fischer, S., Levin, A., Wolf, A., Fujisawa, T., Hayakawa, S., Gojobori, T., Davies, J.A., David, C.N., and Bacon, J.P. (2004). Evolution of gap junctions: the missing link? Curr. Biol. *14*, R879–R880.
3. Oshima, A., Tani, K., and Fujiyoshi, Y. (2016). Atomic structure of the innexin-6 gap junction channel determined by cryo-EM. Nat. Commun. *7*, 13681.
4. Bohrmann, J., and Zimmermann, J. (2008). Gap junctions in the ovary of *Drosophila melanogaster*: localization of innexins 1, 2, 3 and 4 and evidence for intercellular communication via innexin-2 containing channels. BMC Dev. Biol. *8*, 111.
5. Spéder, P., and Brand, A.H. (2014). Gap junction proteins in the blood-brain barrier control nutrient-dependent reactivation of *Drosophila* neural stem cells. Dev. Cell *30*, 309–321.
6. Zhang, S.L., Yue, Z., Arnold, D.M., Artiushin, G., and Sehgal, A. (2018). A circadian clock in the blood-brain barrier regulates xenobiotic efflux. Cell *173*, 130–139.e10.
7. Smendziuk, C.M., Messenberg, A., Vogl, A.W., and Tanentzapf, G. (2015). Bi-directional gap junction-mediated soma-germline communication is essential for spermatogenesis. Development *142*, 2598–2609.
8. Harris, K.P., and Littleton, J.T. (2015). Transmission, development, and plasticity of synapses. Genetics *201*, 345–375.
9. Scheffer, L.K., Xu, C.S., Januszewski, M., Lu, Z., Takemura, S.Y., Hayworth, K.J., Huang, G.B., Shinomiya, K., Maitlin-Shepard, J., Berg, S., et al. (2020). A connectome and analysis of the adult *Drosophila* central brain. eLife *9*, e57443.
10. Zheng, Z., Lauritzen, J.S., Perlman, E., Robinson, C.G., Nichols, M., Milkie, D., Torrens, O., Price, J., Fisher, C.B., Sharifi, N., et al. (2018). A complete electron microscopy volume of the brain of adult *Drosophila melanogaster*. Cell *174*, 730–743.e22.

11. Phelps, J.S., Hildebrand, D.G.C., Graham, B.J., Kuan, A.T., Thomas, L.A., Nguyen, T.M., Buhmann, J., Azevedo, A.W., Sustar, A., Agrawal, S., et al. (2021). Reconstruction of motor control circuits in adult *Drosophila* using automated transmission electron microscopy. Cell *184*, 759–774.e18.

12. Oshima, A., Matsuzawa, T., Nishikawa, K., and Fujiyoshi, Y. (2013). Oligomeric structure and functional characterization of *Caenorhabditis elegans* Innexin-6 gap junction protein. J. Biol. Chem. *288*, 10513–10521.

13. Kennedy, T., and Broadie, K. (2018). Newly identified electrically coupled neurons support development of the *Drosophila* giant fiber model circuit. eNeuro *5*, ENEURO.0346-18.2018.

14. Pézier, A.P., Jezzini, S.H., Bacon, J.P., and Blagburn, J.M. (2016). Shaking B mediates synaptic coupling between auditory sensory neurons and the giant fiber of *Drosophila melanogaster*. PLoS One *11*, e0152211.

15. Phelan, P., Goulding, L.A., Tam, J.L., Allen, M.J., Dawber, R.J., Davies, J.A., and Bacon, J.P. (2008). Molecular mechanism of rectification at identified electrical synapses in the *Drosophila* giant fiber system. Curr. Biol. *18*, 1955–1960.

16. Phelan, P., Stebbings, L.A., Baines, R.A., Bacon, J.P., Davies, J.A., and Ford, C. (1998). *Drosophila* Shaking-B protein forms gap junctions in paired *Xenopus* oocytes. Nature *391*, 181–184.

17. Blagburn, J.M., Alexopoulos, H., Davies, J.A., and Bacon, J.P. (1999). Null mutation in shaking-B eliminates electrical, but not chemical, synapses in the *Drosophila* giant fiber system: a structural study. J. Comp. Neurol. *404*, 449–458.

18. Yaksi, E., and Wilson, R.I. (2010). Electrical coupling between olfactory glomeruli. Neuron *67*, 1034–1047.

19. Liu, Q., Yang, X., Tian, J., Gao, Z., Wang, M., Li, Y., and Guo, A. (2016). Gap junction networks in mushroom bodies participate in visual learning and memory in *Drosophila*. eLife *5*, e13238.

20. Shyu, W.H., Lee, W.P., Chiang, M.H., Chang, C.C., Fu, T.F., Chiang, H.C., Wu, T., and Wu, C.L. (2019). Electrical synapses between mushroom body neurons are critical for consolidated memory retrieval in *Drosophila*. PLoS Genet. *15*, e1008153.

21. Wu, C.L., Shih, M.F., Lai, J.S., Yang, H.T., Turner, G.C., Chen, L., and Chiang, A.S. (2011). Heterotypic gap junctions between two neurons in the *Drosophila* brain are critical for memory. Curr. Biol. *21*, 848–854.

22. Hausen, K. (1976). Functional characterization and anatomical identification of motion sensitive neurons in the lobula plate of the blowfly *Calliphora erythrocephala*. Z. Naturforsch. *31*, 629–634.

23. Maisak, M.S., Haag, J., Ammer, G., Serbe, E., Meier, M., Leonhardt, A., Schilling, T., Bahl, A., Rubin, G.M., Nern, A., et al. (2013). A directional tuning map of Drosophila elementary motion detectors. Nature *500*, 212–216.

24. Krapp, H.G., and Hengstenberg, R. (1996). Estimation of self-motion by optic flow processing in single visual interneurons. Nature *384*, 463–466.

25. Haag, J., and Borst, A. (1996). Amplification of high-frequency synaptic inputs by active dendritic membrane processes. Nature *379*, 639–641.

26. Haag, J., and Borst, A. (2005). Dye-coupling visualizes networks of large-field motion-sensitive neurons in the fly. J. Comp. Physiol. A Neuroethol. Sens. Neural Behav. Physiol. *191*, 445–454.

27. Joesch, M., Plett, J., Borst, A., and Reiff, D.F. (2008). Response properties of motion-sensitive visual interneurons in the lobula plate of *Drosophila melanogaster*. Curr. Biol. *18*, 368–374.

28. Schnell, B., Joesch, M., Forstner, F., Raghu, S.V., Otsuna, H., Ito, K., Borst, A., and Reiff, D.F. (2010). Processing of horizontal optic flow in three visual interneurons of the *Drosophila* brain. J. Neurophysiol. *103*, 1646–1657.

29. Suver, M.P., Huda, A., Iwasaki, N., Safarik, S., and Dickinson, M.H. (2016). An array of descending visual interneurons encoding self-motion in *Drosophila*. J. Neurosci. *36*, 11768–11780.

30. Cuntz, H., Haag, J., Forstner, F., Segev, I., and Borst, A. (2007). Robust coding of flow-field parameters by axo-axonal gap junctions between fly visual interneurons. Proc. Natl. Acad. Sci. USA *104*, 10229–10233.

31. Farrow, K., Borst, A., and Haag, J. (2005). Sharing receptive fields with your neighbors: tuning the vertical system cells to wide field motion. J. Neurosci. *25*, 3985–3993.

32. Haag, J., and Borst, A. (2004). Neural mechanism underlying complex receptive field properties of motion-sensitive interneurons. Nat. Neurosci. *7*, 628–634.

33. Wang, S., Borst, A., Zaslavsky, N., Tishby, N., and Segev, I. (2017). Efficient encoding of motion is mediated by gap junctions in the fly visual system. PLoS Comput. Biol. *13*, e1005846.

34. Elyada, Y.M., Haag, J., and Borst, A. (2009). Different receptive fields in axons and dendrites underlie robust coding in motion-sensitive neurons. Nat. Neurosci. *12*, 327–332.

35. Farrow, K., Haag, J., and Borst, A. (2006). Nonlinear, binocular interactions underlying flow field selectivity of a motion-sensitive neuron. Nat. Neurosci. *9*, 1312–1320.

36. Troup, M., Yap, M.H., Rohrscheib, C., Grabowska, M.J., Ertekin, D., Randeniya, R., Kottler, B., Larkin, A., Munro, K., Shaw, P.J., and van Swinderen, B. (2018). Acute control of the sleep switch in *Drosophila* reveals a role for gap junctions in regulating behavioral responsiveness. eLife *7*, e37105.

37. Davis, F.P., Nern, A., Picard, S., Reiser, M.B., Rubin, G.M., Eddy, S.R., and Henry, G.L. (2020). A genetic, genomic, and computational resource for exploring neural circuit function. eLife *9*, e50901.

38. Brown, J.B., Boley, N., Eisman, R., May, G.E., Stoiber, M.H., Duff, M.O., Booth, B.W., Wen, J., Park, S., Suzuki, A.M., et al. (2014). Diversity and dynamics of the *Drosophila* transcriptome. Nature *512*, 393–399.

39. Leader, D.P., Krause, S.A., Pandit, A., Davies, S.A., and Dow, J.A.T. (2018). FlyAtlas 2: a new version of the Drosophila melanogaster expression atlas with RNA-seq, miRNA-seq and sex-specific data. Nucleic Acids Res. *46*, D809–D815.

40. Robinson, S.W., Herzyk, P., Dow, J.A., and Leader, D.P. (2013). FlyAtlas: database of gene expression in the tissues of *Drosophila melanogaster*. Nucleic Acids Res. *41*, D744–D750.

41. Krishnan, S.N., Frei, E., Swain, G.P., and Wyman, R.J. (1993). Passover: a gene required for synaptic connectivity in the giant fiber system of *Drosophila*. Cell *73*, 967–977.

42. Diao, F., Ironfield, H., Luan, H., Diao, F., Shropshire, W.C., Ewer, J., Marr, E., Potter, C.J., Landgraf, M., and White, B.H. (2015). Plug-and-play genetic access to *Drosophila* cell types using exchangeable exon cassettes. Cell Rep. *10*, 1410–1421.

43. Nagarkar-Jaiswal, S., Lee, P.T., Campbell, M.E., Chen, K., Anguiano-Zarate, S., Gutierrez, M.C., Busby, T., Lin, W.W., He, Y., Schulze, K.L., et al. (2015). A library of MiMICs allows tagging of genes and reversible, spatial and temporal knockdown of proteins in Drosophila. eLife *4*, e05338.

44. Engel, A.K., and Fries, P. (2010). Beta-band oscillations – signalling the status quo? Curr. Opin. Neurobiol. *20*, 156–165.

45. Penttonen, M., Nurminen, N., Miettinen, R., Sirviö, J., Henze, D.A., Csicsvári, J., and Buzsáki, G. (1999). Ultra-slow oscillation (0.025 Hz) triggers hippocampal afterdischarges in Wistar rats. Neuroscience *94*, 735–743.

46. Mauss, A.S., Meier, M., Serbe, E., and Borst, A. (2014). Optogenetic and pharmacologic dissection of feedforward inhibition in Drosophila motion vision. J. Neurosci. *34*, 2254–2263.

47. Hutcheon, B., and Yarom, Y. (2000). Resonance, oscillation and the intrinsic frequency preferences of neurons. Trends Neurosci. *23*, 216–222.

48. Bucchi, A., Baruscotti, M., and DiFrancesco, D. (2002). Current-dependent block of rabbit sino-atrial node I_f channels by ivabradine. J. Gen. Physiol. *120*, 1–13.

49. Lin, W.H., Wright, D.E., Muraro, N.I., and Baines, R.A. (2009). Alternative splicing in the voltage-gated sodium channel DmNav regulates activation, inactivation, and persistent current. J. Neurophysiol. *102*, 1994–2006.

50. Schnell, B., Raghu, S.V., Nern, A., and Borst, A. (2012). Columnar cells necessary for motion responses of wide-field visual interneurons in

Drosophila. J. Comp. Physiol. A Neuroethol. Sens. Neural Behav. Physiol. *198*, 389–395.

51. Leonhardt, A., Ammer, G., Meier, M., Serbe, E., Bahl, A., and Borst, A. (2016). Asymmetry of Drosophila ON and OFF motion detectors enhances real-world velocity estimation. Nat. Neurosci. *19*, 706–715.
52. Fisher, Y.E., Silies, M., and Clandinin, T.R. (2015). Orientation selectivity sharpens motion detection in *Drosophila*. Neuron *88*, 390–402.
53. Lillvis, J.L., Otsuna, H., Ding, X., Pisarev, I., Kawase, T., Colonell, J., Rokicki, K., Goina, C., Gao, R., Hu, A., et al. (2021). Rapid reconstruction of neural circuits using tissue expansion and lattice light sheet microscopy. Preprint at bioRxiv. https://doi.org/10.1101/2021.11.14.468535.
54. Fendl, S., Vieira, R.M., and Borst, A. (2020). Conditional protein tagging methods reveal highly specific subcellular distribution of ion channels in motion-sensing neurons. eLife *9*, e62953.
55. Li, Y., Chen, P.J., Lin, T.Y., Ting, C.Y., Muthuirulan, P., Pursley, R., Ilić, M., Pirih, P., Drews, M.S., Menon, K.P., et al. (2021). Neural mechanism of spatio-chromatic opponency in the *Drosophila* amacrine neurons. Curr. Biol. *31*, 3040–3052.e9.
56. Qiao, M., and Sanes, J.R. (2015). Genetic method for labeling electrically coupled cells: application to retina. Front. Mol. Neurosci. *8*, 81.
57. Tian, L., Yang, Y., Wysocki, L.M., Arnold, A.C., Hu, A., Ravichandran, B., Sternson, S.M., Looger, L.L., and Lavis, L.D. (2012). Selective esterase-ester pair for targeting small molecules with cellular specificity. Proc. Natl. Acad. Sci. USA *109*, 4756–4761.
58. Atasoy, D., Betley, J.N., Li, W.P., Su, H.H., Sertel, S.M., Scheffer, L.K., Simpson, J.H., Fetter, R.D., and Sternson, S.M. (2014). A genetically specified connectomics approach applied to long-range feeding regulatory circuits. Nat. Neurosci. *17*, 1830–1839.
59. Connors, B.W. (2017). Synchrony and so much more: diverse roles for electrical synapses in neural circuits. Dev. Neurobiol. *77*, 610–624.
60. Tchumatchenko, T., and Clopath, C. (2014). Oscillations emerging from noise-driven steady state in networks with electrical synapses and subthreshold resonance. Nat. Commun. *5*, 5512.
61. Bernstein, S.A., and Morley, G.E. (2006). Gap junctions and propagation of the cardiac action potential. Adv. Cardiol. *42*, 71–85.
62. Tuthill, J.C., Nern, A., Holtz, S.L., Rubin, G.M., and Reiser, M.B. (2013). Contributions of the 12 neuron classes in the fly lamina to motion vision. Neuron *79*, 128–140.
63. Meier, M., Serbe, E., Maisak, M.S., Haag, J., Dickson, B.J., and Borst, A. (2014). Neural circuit components of the *Drosophila* OFF motion vision pathway. Curr Biol *24*, 385–392.
64. Bloomfield, S.A., and Völgyi, B. (2009). The diverse functional roles and regulation of neuronal gap junctions in the retina. Nat. Rev. Neurosci. *10*, 495–506.
65. Ribelayga, C., Cao, Y., and Mangel, S.C. (2008). The circadian clock in the retina controls rod-cone coupling. Neuron *59*, 790–801.
66. Lazar, A.A., Liu, T., Turkcan, M.K., and Zhou, Y. (2021). Accelerating with FlyBrainLab the discovery of the functional logic of the *Drosophila* brain in the connectomic and synaptomic era. eLife *10*, e62362.
67. Givon, L.E., and Lazar, A.A. (2016). Neurokernel: an open source platform for emulating the fruit fly brain. PLOS One *11*, e0146581.
68. Mauss, A.S., and Borst, A. (2016). Electrophysiological recordings from lobula plate tangential cells in *Drosophila*. Methods Mol. Biol. *1478*, 321–332.
69. Arenz, A., Drews, M.S., Richter, F.G., Ammer, G., and Borst, A. (2017). The temporal tuning of the *Drosophila* motion detectors is determined by the dynamics of their input elements. Curr. Biol. *27*, 929–944.

STAR★METHODS

KEY RESOURCES TABLE

REAGENT or RESOURCE	SOURCE	IDENTIFIER
Antibodies		
anti-ogre rabbit polyclonal antibody	This paper	N/A
anti-inx2 rabbit polyclonal antibody	This paper	N/A
anti-inx3 rabbit polyclonal antibody	This paper	N/A
anti-zpg rabbit polyclonal antibody	This paper	N/A
anti-inx5 rabbit polyclonal antibody	This paper	N/A
anti-inx6 rabbit polyclonal antibody	This paper	N/A
anti-inx7 rabbit polyclonal antibody	This paper	N/A
anti-shakB rabbit polyclonal antibody	This paper	N/A
anti-shakB rabbit polyclonal serum antibody	This paper	N/A
anti-ogre rabbit polyclonal antibody	Reinhard Bauer[4]	N/A
anti-inx2 rabbit polyclonal antibody	Reinhard Bauer[4]	N/A
anti-inx3 rabbit polyclonal antibody	Reinhard Bauer[4]	N/A
anti-zpg guinea pig polyclonal antibody	Guy Tanentzapf[7]	N/A
anti-inx5 rabbit polyclonal antibody	Chia-Lin Wu[20]	N/A
anti-inx6 rabbit polyclonal antibody	Ann Shyn-Chiang[21]	N/A
anti-inx7 rabbit polyclonal antibody	Ann Shyn-Chiang[21]	N/A
anti-nc82 mouse monoclonal antibody	DSHB	RRID: AB_2314866
anti-GFP rabbit polyclonal antibody	Invitrogen	Cat# A-11122; RRID: AB_221569
anti-GFP chicken polyclonal antibody	Rockland	Cat# 600-901-215S; RRID: AB_1537403
goat anti-rabbit-Alexa-488	Invitrogen	Cat# A32731; RRID: AB_2633280
donkey anti-chicken-Alexa-488	Jackson Immuno Research	Cat# 703-545-155; RRID: AB_2340375
goat anti-rabbit-Alexa-568	Invitrogen	Cat# A-11011; RRID: AB_2535730
goat anti-mouse-Alexa-647	Invitrogen	Cat# A32728; RRID: AB_2633282
streptavidin-Alexa-568	Invitrogen	Cat# S11226; RRID: AB_2315774
streptavidin-Alexa-633	Invitrogen	Cat# S21375; RRID: AB_2313500
Chemicals, peptides, and recombinant proteins		
Tetrodotoxin citrate	Abcam	Cat# ab120055
Picrotoxin	TCI	Cat# C0375
Ivabradine hydrochloride	Sigma	Cat# SML0281
Mecamylamine hydrochloride	Sigma	Cat# M9020
Carbenoxolone	Sigma	Cat# C4790
Neurobiotin tracer	VectorLabs	Cat# SP-1120; RRID: AB_2313575
Deposited data		
Raw and analyzed data	This paper	https://gin.g-node.org/gammer/Ammer_et_al_2022.git
Experimental models: Organisms/strains		
Canton S (wildtype)	BDSC	RRID: BDSC_64349
MiMIC02168-shakB; +; +	BDSC	RRID: BDSC_34285
MiMIC15228-shakB; +; +	BDSC	RRID: BDSC_60999
MiMiC02168-shakB-Trojan-Gal4; +; +	This paper	N/A
MiMiC15228-shakB-Trojan-Gal4; +; +	This paper	N/A
w-; +; R57C10-Gal4 (pan-neuronal)	BDSC	RRID: BDSC_39171
w-; +; R24E09-Gal4 (VS/HS cells)	BDSC	RRID: BDSC_49083
w-; +; R54C07-Gal4 (SPG glia)	BDSC	RRID: BDSC_50472

(*Continued on next page*)

Continued

REAGENT or RESOURCE	SOURCE	IDENTIFIER
w-; +; R56F03-Gal4 (EGN glia)	BDSC	RRID: BDSC_39157
w-; +; R85G01-Gal4 (PNG glia)	BDSC	RRID: BDSC_40436
w-; VT058487-AD/ +; R35G07-DBD/ + (VS/HS cells)	Janelia FlyLight (https://splitgal4.janelia.org)	SS04438
w-; +; VT50384-lexA (T4/T5 cells)	Barry Dickson[68]	N/A
w-; +; VT40547-Gal4 (L4 cells)	Janelia FlyLight (https://flweb.janelia.org/)	N/A
shakB^{2}; +; +	Rodney Murphey[41]	N/A
w-; +; 20xUAS-Valium20-shakB-RNAi	BDSC	RRID: BDSC_57706
w-; +; 20xUAS-Valium20-GFP-RNAi	BDSC	RRID: BDSC_41553
w-; 20xUAS-IVS-GCaMP6f; +	BDSC	RRID: BDSC_42747
w-; +; 13xlexAop-IVS-GCaMP6m	BDSC	RRID: BDSC_44277
w-; tubGal80^{ts}; +	BDSC	RRID: BDSC_7019
w-; +; UAS-shakB-N	Jonathan Bacon[15]	N/A
Recombinant DNA		
pBS-KS-attB2-SA(2)-T2A-Gal4-Hsp70	DGRC	DGRC# 1410
pBS-KS-attB2-SA(0)-T2A-Gal4-Hsp70	DGRC	DGRC# 1412
Software and algorithms		
MATLAB	MathWorks	https://www.mathworks.com/
Python 2.7.15 and 3.8.8	Python	https://www.python.org/
ScanImage 3.8	Vidrio Technologies	http://scanimage.vidriotechnologies.com/
ImageJ/Fiji	National Institutes of Health	https://imagej.net/software/fiji/
Code used for analysis	This paper	https://gin.g-node.org/gammer/Ammer_et_al_2022.git

RESOURCE AVAILABILITY

Lead contact

Further information and requests for resources and reagents should be directed and will be fulfilled by the Lead Contact, Georg Ammer (gammer@neuro.mpg.de).

Materials availability

Newly generated fly lines and antibodies are available from the lead contact upon request.

Data and code availability

All data reported in this paper and codes used for analysis are publicly available at: https://gin.g-node.org/gammer/Ammer_et_al_2022.git

EXPERIMENTAL MODEL AND SUBJECT DETAILS

Fly husbandry

All flies were raised on standard cornmeal agar medium at 60% humidity on a 12 h light/12 h dark cycle throughout development. Except when noted otherwise, flies were raised at 25° C. We used female flies for all experiments except for those in which shakB was rescued in VS/HS cells, which were performed with males. For electrophysiology, we used flies that were between 6 hours and 2 days old. For calcium imaging experiments, in order to enhance expression of transgenes, flies were transferred to 29° C after eclosion and then imaged at an age between 4 and 7 days. Flies carrying a tubGal80^{ts} transgene were raised at 18° C. For inducing Gal4 expression, tubGal80^{ts} flies were transferred to 31° C after eclosion, and imaged when 7 days old. For tubGal80^{ts} control experiments, flies were left at 18° C until the beginning of the experiment. The full genotypes of flies used in this study are listed in Table S1.

METHOD DETAILS

Generation of fly lines

For generating Trojan-Gal4 lines the T2A-TrojanGal4 plasmid with the correct reading frame[42] was injected into embryos of the respective MiMIC insertion lines:[43]

pBS-KS-attB2-SA(2)-T2A-Gal4-Hsp70 (DGRC#1410) was injected into y[1] w[*] Mi{y[+mDint2]=MIC}shakB[MI15228] (RRID: BDSC_60999)
pBS-KS-attB2-SA(0)-T2A-Gal4-Hsp70 (DGRC#1412) was injected into y[1] w[*] Mi{y[+mDint2]=MIC}shakB[MI02168] (RRID: BDSC_34285)

Injections were performed by BestGene (https://www.thebestgene.com/).

Antibody generation

We generated polyclonal rabbit antibodies against different innexin proteins by immunizing against the following peptides:

- ogre (inx1): CFAKQVEPSKHDRAK
- inx2: CMSGDEHSAHKRPFD
- inx3: CPPVETFGGGKETET
- zpg (inx4): CAQSLIKIPPGADKI
- inx5: CLRTSASGSTLESPV
- inx6: IAEGVGPETRGVTKC
- inx7: CEAPPTPAKNRYPEL
- shakB (inx8) purified antibody: CQHHRVPGLKGEIQD
- shakB (inx8) serum antibody: CQHHRVPGLKGEIQD

Both shakB antibodies were raised against a part of the C-terminal sequence that is common to all protein isoforms. The shakB serum antibody was generated in our laboratory using standard procedures. The other eight antibodies were generated by the company GenScript (https://www.genscript.com/).

Immunohistochemistry

Brains (and ventral nerve cords) were dissected in cold phosphate-buffered saline (PBS) and fixed in 4% PFA (in PBS with 0.1% Triton X). Brains were washed three times in PBT (PBS + 0.3% Triton X), blocked in 10% normal goat serum (NGS) in PBT and incubated in the primary antibody solution (antibody in 5% NGS in PBT) for 36-48 hours. Afterwards, brains were washed in PBT overnight and then incubated in the secondary antibody solution for 48-72 hours. Brains were washed in PBT overnight, washed in PBS and then mounted in Vectashield medium (VectorLabs).

Primary antibodies were used at the following dilutions: anti-nc82 (1:25), anti-GFP (1:1000), anti-inx1-genscript (1:1000), anti-inx2-genscript (1:1000), anti-inx3-genscript (1:1000), anti-inx4-Tanentzapf (1:2000), anti-inx5-Wu (1:1000), anti-inx6-Chiang (1:2500), anti-inx7-Chiang (1:200), anti-shakB-serum (1:800), anti-ogre-Bauer (1:50), anti-inx2-Tanentzapf (1:1000), anti-inx3-Bauer (1:50), anti-zpg-genscript (1:1000), anti-inx5-genscript (1:500), anti-inx6-genscript (1:1000), anti-inx7-genscript (1:2000), anti-shakB-genscript (1:2000). All secondary antibodies were used at a dilution of 1:500 or 1:1000.

The specific innexin antibodies that were used in each Figure panel are listed in Table S2.

Confocal microscopy

Images were acquired on a Leica SP5 or SP8 confocal microscope with either a 20× (Leica #115063643) or 63× (Leica #11506353) glycerol immersion objective or a 40× (Leica #11506358) oil immersion objective at a resolution of 1024x1024 pixels. Image processing was performed with Fiji.

Electrophysiology

Electrophysiological whole-cell patch clamp recordings were done as previously described.[68] Briefly, flies were waxed to a plexiglas holder with bees wax and the head inserted into an opening in aluminum foil that was mounted in a recording chamber. External saline was added to the preparation, a part of the cuticle on the posterior side of the head removed with a fine needle, and the muscle covering the LPTC cell bodies severed. The glial sheath on the surface of the brain was locally digested by applying Collagenase IV (Gibco) through a pipette with a ~5 μm opening. When the somata of LPTCs were exposed, whole cell recordings were performed with patch electrodes (TW-150F-4, WPI) pulled to a resistance of 5-9 MOhm. Signals were amplified with a BA-1s amplifier (npi electronics), low-pass filtered with a cut-off frequency of 3 kHz and digitized at 10 kHz. Data acquisition was performed with Matlab R2011b (Mathworks) and data analysis was done with Matlab R2011b (Mathworks), Python 2.7.15 and Python 3.8.8. External saline contained the following (in mM): 103 NaCl, 3 KCl, 5 TES, 10 trehalose, 10 glucose, 3 sucrose, 26 $NaHCO_3$, 1 NaH_2PO_4, 1.5 $CaCl_2$, and 4 $MgCl_2$. The pH of the solution was 7.3 – 7.35 and the osmolarity was around 285 mOsmol. External saline was oxygenated with 95% O_2/5% CO_2. Internal solution contained the following (in mM): 140 K-aspartate, 10 HEPES, 4 MgATP, 0.5 Na_3GTP, 1 EGTA, 1 KCl, and 0.2 Alexa Fluor 568 hydrazide. The pH of the internal solution was adjusted to 7.26 and the osmolarity to ca. 265 mOsmol. Cell types were identified based on the typical response profiles of VS and HS cells to moving gratings and - in most cases - anatomically when cells were properly filled with the Alexa dye. For neurobiotin coupling experiments, we included 2% neurobiotin (VectorLabs) in the patch pipette.

Calcium imaging

For functional imaging, we used a custom-built two-photon laser scanning microscope as described previously.[23] Flies were dissected identically to the electrophysiological experiments and imaged in the same extracellular saline. Images were typically recorded at a resolution of 128 × 128 pixels and a frame rate of 3,76 Hz. Some experiments were done at a resolution of 64 × 64 pixels and a frame rate of 12,6 Hz. Data acquisition was performed in Matlab R2013b (MathWorks) using ScanImage 3.8. Data analysis was performed in Matlab R2013b (MathWorks), Python 2.7.15, and Python 3.8.8.

Visual stimulation

For electrophysiological recordings, a custom-built LED arena was used for visual stimulation.[27] The arena spanned 170° in azimuth and 90° in elevation, allowed refresh rates up to 600 Hz and had a maximum luminance of 80 cd/m^2. Moving sine wave gratings were displayed at full contrast, had a spatial wavelength of 30° and moved at a temporal frequency of 0.5 Hz for 3 s. For stimulating ON and OFF pathways independently, we used multiple moving ON or OFF edges. The stimulus started with a standing vertical or horizontal square wave grating that had a wavelength of 42°. Then, either all bright or all dark edges moved for 0.45 s with a velocity of 50°/s. Flicker stimuli consisted of full field flashes at maximum luminance that lasted for 3 s. Stimuli were presented in a randomized manner.

For functional calcium imaging, we used a custom built projector-based arena.[69] Visual stimuli were projected onto the back of an opaque cylindrical screen with two micro-projectors (TI DLP Lightcrafter 3000). The arena covered 180° in azimuth and 105° in elevation. Visual stimuli were displayed with a refresh rate of 180 Hz and a maximum luminance of 276 ± 48 cd/m^2. For stimulating VS/HS or T4/T5 cells we presented moving ON or OFF edges at full contrast moving with a velocity of 15°/s. Moving gratings had a spatial wavelength of 30° and were shown for 1 s at 1 Hz temporal frequency. Stimuli were presented in a randomized fashion. For imaging spontaneous calcium oscillations in VS and HS cells, the arena was completely dark i.e. no visual stimulus was displayed. Spontaneous activity of VS/HS cells was recorded for 2500 frames at 3.76 Hz which amounts to ca. 663 s.

Pharmacology

The following pharmacological substances were used in this study. Tetrodotoxin (TTX, Abcam) 1 mM stock in H_2O, used at a final concentration of 1 μM. Picrotoxin (PTX, TCI) 50 mM stock in DMSO, final concentration 2.5 μM. Mecamylamine (MEC, Sigma) 100 mM stock in H_2O, final concentration: 200 μM. Ivabradine (IVA, Sigma) 20 mM stock in H_2O, final concentration: 200 μM. Carbenoxolone (CBX, Sigma) 5 mM stock in H_2O used at a final concentration of 200 μM. Aliquoted stocks were kept at -20°C, freshly diluted in external saline at the day of the experiment, and added directly to the preparation with a pipette. Recordings were started at least 10 min after addition of the pharmacological substances to allow for diffusion. Carbenoxolone was added to the saline 20 min before the whole cell recording was established.

QUANTIFICATION AND STATISTICAL ANALYSIS

Data analysis

Electrophysiology

For responses to visual motion stimuli, we computed the mean response over the whole stimulation period and averaged that value over sweeps. For responses to full flied flicker stimuli, we detected the extrema during the first 500 ms of the response and averaged this value over sweeps. Power spectra were computed using fast Fourier transformations. We classified cells as exhibiting USW- and/or β-oscillations by visually inspecting their membrane potential traces and power spectra.

Calcium Imaging

Baseline subtraction and calculation of ΔF/F was performed as previously described.[69] In contrast to electrophysiology, for power spectra we first z-scored the ΔF/F values. This was done because ΔF/F values are relative measures and can vary depending on expression strength, depth of imaging, size of regions of interest (ROIs) and other factors. We then used fast Fourier transformations to calculate power spectra. Cells were classified as active/oscillatory when the variance of their ΔF/F signal was > 0.15 during the whole imaging period and when they exhibited a clear peak in the USW-power spectrum. For T4/T5 imaging we first averaged the response traces over sweeps and then took the maximum ΔF/F value during the stimulation period. The direction selectivity index "LDir" was calculated as the length of the normalized response vector:

$$L_{Dir} = \left| \frac{\sum_{\varphi} \vec{r}(\varphi)}{\sum_{\varphi} |\vec{r}(\varphi)|} \right|$$

where $\vec{r}(\varphi)$ is a vector with the stimulus direction φ as its angle and the corresponding neuronal response as its length.

Statistical analysis

Gaussianity of data point distributions was assessed by performing Shapiro-Wilk's test. Based on the outcome we performed either Welch's t test or Mann-Whitney's U test and applied Holm's post-hoc correction when comparing more than two experimental groups. Statistical analysis was performed in Python 3.8.8 using scipy 1.6.2, statsmodels 0.12.2 and scikit_posthocs 0.6.7 packages. More details on the statistical analysis are provided in Table S3.

Chapter 3

Discussion

3.1 Protein Tagging Considerations

Neurotransmitter receptors and ion channels are critical in shaping the electrical properties of neurons, determining whether a neuron's response to a signal is excitatory or inhibitory, and modulating the overall dynamics of neuronal activity. Additionally, gap junctions, which form direct electrical connections between neurons, play a vital role in stabilising neuronal activity and further influencing the overall function of neural circuits. Therefore, it is essential to identify the specific neurotransmitter receptors, ion channels, and gap junctions within a particular cell type and precisely locate them within cellular compartments such as the dendrite, soma, or axon. Motion-sensing T4/T5 neurons receive input from multiple other neurons, and due to their densely packed and overlapping dendrites, studying these neurotransmitter receptors at the single-cell level is crucial for accurately understanding their localisation and function. In Manuscript 1, we developed two methods to achieve this in *Drosophila*: flippase-dependent expression of GFP-tagged receptor subunits in individual neurons and a versatile new tool called 'FlpTag' for conditional labelling of endogenous proteins. Due to the complexity of tagging gap junctions, in Manuscript 2, we opted to generate antibodies against various *Drosophila* innexins, enabling us to map their distribution throughout the CNS. When choosing to tag a protein, two of the most important components to consider are where the tag will be placed and what type of tag will be used, especially when tagging transmembrane proteins. In the following sections, I will discuss tag placement and choice as it relates to transmembrane proteins. Additionally, I will discuss current tools for tagging in a cell-type-specific endogenous manner and how they compare to the tools generated in this thesis.

3.1.1 Structure of Transmembrane Proteins

Understanding the general structure of a protein is a prerequisite for determining the optimal site for tag placement. This consideration is particularly important in large-scale tagging initiatives, such as the FlyORF project, where the goal is to identify the most generalisable tag position (Bischof et al., 2013). However, examining the specific structure of individual proteins is important for creating a precise and refined tagging strategy. Generating structural data for proteins, especially transmembrane channels, has historically been difficult due to their amphiphilic nature and large size (Choy et al., 2021). Traditional methods such as X-ray crystallography and nuclear magnetic resonance (NMR) techniques have been difficult to apply effectively to these proteins because they require stable, homogeneous samples that are often hard to achieve outside of a membrane environment (Terlau & Stühmer, 1998). As a result, initial structural data for these complex proteins were often obtained through electron microscopy, a technique that allows visualisation in near-native conditions without the need for crystallisation. However, very few transmembrane structures have been resolved in *Drosophila*, with the exception of Shaker, which has been cited as a landmark achievement (Long et al., 2005). Alternatively, utilising tools that display known protein structures or predict protein configurations can significantly improve the likelihood of successful tag expression while minimising disruption to the protein's function (Leaver-Fay et al., 2011; Källberg et al., 2012; Kelley et al., 2015; Waterhouse et al., 2018; Jumper et al., 2021). Before the recent advancements in AI, tools like SWISS-MODEL were commonly used to predict protein structures based on homology to known templates (Waterhouse et al., 2018). This process involved obtaining the cDNA sequence of a protein, inputting it into a model generator, and aligning the sequence with known protein structures to predict its 3D configuration. While effective, this approach depended heavily on the availability of similar templates and was limited by the accuracy of homology modelling (Bienert et al., 2017). Today, AlphaFold has become the gold standard in protein modelling, leveraging AI to predict protein structures with remarkable accuracy directly from amino acid sequences, surpassing traditional methods that relied on homology (Jumper et al., 2021).

Given the structural diversity among neuronal membrane proteins in *Drosophila*, it is important to consider the specific characteristics of each protein group when determining the optimal location for its tag. Gap junction channels, formed by innexins, consist of two extracellular loop domains, four hydrophobic transmembrane domains, and three cytoplasmic domains, including an intracellular loop and amino- (N) and carboxy (C) termini (Skerrett & Williams, 2017). Placing a tag at either of the extracellular domains in gap junctions is not advisable because

the docking of two hemichannels, each contributed by one of two adjacent cells, occurs head-to-head in the extracellular space. It is crucial not to place a tag close to the two conserved cysteine residues in the two extracellular domains, as this is where the disulphide bonds connect the hemichannels (Qu & Dahl, 2002; Rahman & Evans, 1991). It has also been demonstrated that the N-terminal domain is essential for insertion into the membrane and for oligomerisation (Ahmad et al., 2001). While the C-terminal domain is suggested to be involved in linking channel subunits to form either homotypic or heterotypic channels, making N or C terminal tags less than ideal (Ahmad et al., 2001). Although the intracellular loop is well-ordered and has a stable, defined three-dimensional structure, it theoretically offers the most suitable target for tagging innexins (Unger et al., 1999). For Manuscript 2, we attempted to make a UAS-*ShakB::GFP* line, but both of our attempts failed to show any expression. We first attempted to tag the intracellular loop of ShakB between exons 7 and 8 as it is the least ordered region. However, we failed to see any protein expression. Since tagging the N-terminus is often more disruptive, we opted to generate a C-terminal UAS-*ShakB::GFP* construct for our next attempt. Unfortunately, this also resulted in undetectable protein expression. Lastly, we tested an available ShakB MiMIC line with a GFP insertion near the N-terminus (MI02168-GFSTF.2); unfortunately, this line also failed to show detectable expression. To date, no *Drosophila* innexin has been successfully tagged, highlighting the particular challenges associated with tagging these channels.

Voltage-gated ion channels exhibit more complex and diverse structures than gap junctions, yet they still share a common structural framework. The α subunit, which is the main pore-forming subunit, usually consists of four homologous domains (I-IV), each containing six α helix transmembrane segments (S1-S6) (Catterall, 2010). In general, extracellular loops of ion channels are unsuitable for protein tagging. The extracellular loops between S1-S4 serve as voltage sensors and engage with various modulatory molecules or ions that control channel gating, making these regions essential for proper channel function (Catterall, 2014). Similarly, the S5-S6 segments form a reentrant loop that dips into the transmembrane region to create the pore domain, making it unsuitable for tagging, as the tag would be concealed within the pore (Catterall, 2014). Therefore, intracellular loops and termini, particularly the C-terminus, are more suitable sites for tagging, as they are less likely to interfere with the channel's function. In Manuscript 1, we successfully used available MiMIC lines to tag ion channels para and Ih at the intracellular loop between S1 and S2 via RMCE with FlpTag.

Ionotropic channels typically comprise multiple subunits, usually 4 or 5, which assemble to form a central ion-conducting pore (Sine & Engel, 2006; Benton et

al., 2009). These subunits can form either homomeric or heteromeric channels. Each subunit generally contains four transmembrane segments (TMs), labelled M1 through M4 (Ortells et al., 1997). The M2 segment of each subunit lines the central pore and plays a crucial role in ion selectivity and conductance (Ortells et al., 1997; Benton et al., 2006). The extracellular domain contains the ligand-binding sites, where neurotransmitters or other ligands bind to initiate channel opening (Ortells et al., 1997; Benton et al., 2006). The N- and C-termini are typically located on the extracellular and intracellular sides of the membrane, respectively. Tagging strategies often target the extracellular or intracellular termini and intracellular loops (Drenan et al., 2008; Nashmi et al., 2003; Raghu et al., 2009). However, depending on the specific channel, the C-terminus may be embedded within the cell membrane, which can mask any expression (Jones & Sattelle, 2006). For instance, our initial attempts to tag the neurotransmitter receptor GluClα by generating a UAS-*GluClα::GFP* line at the C-terminus were unsuccessful. Subsequent analysis of a predicted protein structure model revealed that the C-terminus of GluClα terminates within the membrane, thus masking the expression of GFP. As detailed in Manuscript 1, we successfully tagged GluClα at a disordered intracellular loop, overcoming this challenge.

GPCRs are characterised by having seven transmembrane α-helices (7TM) (Brody & Cravchik, 2000). These helices, labelled from TM1 to TM7, span the cell membrane in a serpentine fashion. The helices are connected by three extracellular loops (ECL1-ECL3) and three intracellular loops (ICL1-ICL3). The N-terminus of the GPCR is located on the extracellular side of the membrane. This region can be involved in ligand binding, particularly in receptors that bind large or complex ligands. The C-terminus of GPCRs often contains sites for post-translational modifications, such as phosphorylation, and interacts with G-proteins and other intracellular signalling molecules. GPCRs are typically tagged at the C-terminus or the intracellular loops. In Manuscript 1, we tested an available MiMIC line for Gaba-b-r1 with a GFP insertion near the N-terminus. Surprisingly, we could detect fluorescence despite this not being the ideal location for tagging GPCRs.

3.1.2 Types of Protein Tags

Another important factor to consider when visualising a protein is the choice of tag. Although many types of tags are available, the two most commonly used are peptide antigens known as epitopes and fluorescent proteins. Fluorescent protein tags have historically been the preferred option for protein labelling. They enable real-time visualisation of protein dynamics without requiring tissue fixation. They also offer

high sensitivity, meaning even low levels of tagged proteins can be detected with standard confocal microscopy. Additionally, the availability of various fluorescent proteins in different colours facilitates multicolour labelling, making it possible to simultaneously label a transmembrane protein and the specific cell type in which it is expressed within the same experiment. In Manuscript 1, we used EGFP, a modified version of the original GFP that is brighter, folds more efficiently, and is more photostable (Shimomura et al., 1962; Tsien, 1998; Cinelli et al., 2000). One of the primary reasons we chose a fluorescent protein over an epitope tag is the ease of screening new lines. This approach eliminates the need for antibody staining, which often leads to cross-reactivity and non-specific staining, thereby significantly speeding up the verification time of new lines (Chalfie et al., 1994; Tsien, 1998). Using GFP was particularly effective when studying neurotransmitter receptors because they are often clustered at the postsynaptic membrane, thus amplifying the GFP signal in these sites.

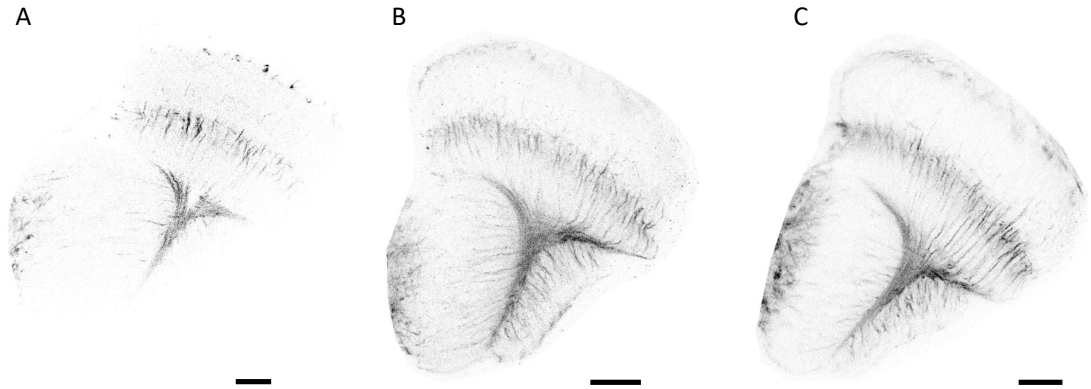

Figure 3.1: These images show the differences in detectable fluorescence when labelling the protein para with different fluorescent tags. (A) para is labelled with the fluorescent protein EGFP. (B) para is labelled with the common epitope tag V5. (C) para is labelled with multiple V5 epitope tags inserted into a fluorescent protein scaffold with a darkened chromophore (smV5). Scale bar represents 20 μm.

However, the main drawback of using fluorescent proteins is their susceptibility to photobleaching when exposed to high laser power, particularly when the labelled proteins are sparse (Tsien, 1998; Viswanathan et al., 2015). This issue is especially relevant when labelling ion channels, which tend to be dispersed rather than clustered, as demonstrated by the weak GFP expression in the FlpTag Ih line in Manuscript 1. Therefore, there is a need for brighter and more photostable labels. Epitope tags offer an advantage in this regard. The antibodies that bind to epitope

tags can be conjugated with brighter and more photostable fluorescent dyes, such as Atto or Alexa dyes, providing enhanced fluorescence (Viswanathan et al., 2015). Additionally, the small size of the tag, generally 8-12 amino acids, allows multiple copies to be added, amplifying the fluorescent signal without affecting protein folding (Viswanathan et al., 2015). Another method to amplify fluorescence signals is by using "Spaghetti monster" fluorescent proteins (smFPs), engineered to contain multiple epitope tags, enabling them to bind numerous antibodies simultaneously and significantly enhance signal detection (Viswanathan et al., 2015). This strategy considerably boosts fluorescence intensity, making it a powerful alternative to single fluorescent proteins.

3.1.3 Tagging Strategies

The most straightforward way to visualise the localisation of a receptor in a specific neuron is by tagging the protein in the cell type of interest using the UAS-Gal4 system. In a previous study, the UAS-Dα7::GFP line was generated to investigate the subcellular distribution of the receptor in LPTCs (Raghu et al., 2009). Although overexpression lines can result in mislocalised protein expression, this particular line accurately localised the acetylcholine receptor to endogenous synapses, as confirmed by antibody staining and comparison with endogenous bruchpilot (Brp) puncta (Kuehn & Duch, 2013; Mosca & Luo, 2014). In our experiments, the UAS-Dα7::GFP line appeared to localise specifically to cholinergic synapses. However, since nicotinic acetylcholine receptors can form heteromers, it is unclear whether the overexpression of Dα7 causes it to localise to more cholinergic synapses than it natively would. A study on the postsynaptic density protein PSD95 showed that overexpression altered its quantitative levels but did not qualitatively change its localisation (Willems et al., 2020). In the case of receptors that can form heteromers, a quantitative change in the expression of a particular subunit can lead to qualitative changes by altering the composition of the heteromeric receptors. However, the UAS-Rdl::GFP and UAS-GluClα::GFP lines generated matched the GABAergic and glutamatergic input synapses predicted from EM studies (personal communication, K. Shinomiya, May 2020). Additionally, the UAS-GluClα::GFP line demonstrated the same distribution patterns as endogenously tagged control lines. The main advantage of the UAS-Gal4 system for tagging these receptors is its ability to easily visualise receptors in single cells. This was accomplished by utilising an FRT-Gal80-FRT cassette along with hs-FLP recombinase, ensuring that the expression of both the cell marker, UAS-myr::tdTomato, and UAS-receptor::GFP is dependent on the same stochastic FLP recombinase event. However, making generalisations about UAS overexpression lines and their correct localisations is

challenging. It is imperative that each line is carefully controlled, as the outcomes may vary depending on the specific case.

Strategies have been developed to tag proteins at their endogenous loci, circumventing the potential protein mislocalisation that can result from overexpression. Large-scale projects, such as the MiMIC and CRIMIC libraries, utilise transposon elements and direct insertion via CRISPR/Cas-mediated genome editing, respectively, to introduce Swappable Insertion Cassettes consisting of *attP* sites into the endogenous loci of a gene (Nagarkar-Jaiswal, et al., 2015; Lee et al., 2018; Kanca et al., 2022). Thousands of lines have been generated that allow the original cassette to be replaced with virtually any DNA sequence of choice through RMCE using ϕC31 integrase (Bateman et al., 2006). These MiMIC and CRIMIC lines specifically target introns to create an artificial exon with a splice donor and splice acceptor, resulting in the internal tagging of proteins with the multi-tag cassette EGFP-FlAsH-StrepII-TEV-3xFlag (GFSTF) (Venken et al., 2011). However, not all existing MiMIC and CRIMIC GFSTF lines display a detectable GFP signal. As previously discussed, successful expression and detec-tion depend on both the protein's structure and the placement of the tag. In the case of MiMIC insertions, the tag's location is determined randomly, without consideration for optimal insertion positioning (Nagarkar-Jaiswal, et al., 2015). The optimal tag placement was considered for the generation of the CRIMIC collection, yielding a higher chance of GFP detection (Lee et al., 2018). As an alternative to internal tagging, 75 neurotransmitter receptor genes were modified with a C-terminal T2A-Gal4 gene trap cassette, which can be easily swapped for a fluorescent tag like Venus (Kondo et al., 2020). Although C-terminal tags have traditionally been the preferred tagging position for transmembrane proteins, particularly neurotransmitter receptors, the C-terminus often resides within the membrane, making the tag undetectable. Nonetheless, these resources offer the capability to generate tagged proteins almost effortlessly, eliminating the need for cloning or additional wet lab work. The primary disadvantage of these endogenous strategies is that they label the protein in every cell rather than targeting specific cell types. This widespread tagging can make it harder to pinpoint exactly where the protein is located within a specific cell type or in particular subcellular areas, such as dendrites or axons, especially in areas where neurons are densely packed.

The optimal strategy for labelling transmembrane proteins would combine both cell-type specificity and endogenous expression. This approach ensures the protein is tagged within its natural cellular environment and expressed at physiological levels, minimising potential artefacts associated with overexpression or ectopic expression. By targeting the tag to specific neuronal cell types, the subcellular

localisation of transmembrane proteins can be observed within distinct neuronal compartments. Few strategies for labelling proteins have successfully achieved both cell-type specificity and endogenous expression, and those that have been applied are not widely generalisable.

The first of these strategies to be developed was Synaptic Tagging with Recombination (STaR), a method designed for cell-type-specific labelling of synapses (Chen et al., 2014). In this approach, the genomic regions of the *brp* and *ort* genes were modified to include an FRT-Stop-FRT-tag cassette, along with a 2A-LexA. The FRT-Stop-FRT cassette prevents the translation of the receptor until the stop cassette is flipped out by a cell-specific FLP recombinase. The 2A-LexA allows for the co-translation of LexA, which drives the expression of myr-tdTomato from the LexAoP enhancer, labelling the cell. However, in the case of *ort*, the insertion of the 2A-LexA sequence at the 3' end of the *ort* open reading frame disrupted Ort protein expression, making it impossible to use this strategy to assess the morphology of the cell. This highlights the disadvantage of using 2A-LexA for co-labelling cells, as it can potentially disrupt protein expression. Another caveat of this approach is that transgene insertion of BACs is not truly endogenous. They introduce an additional copy of a gene at a non-native location in the genome, rather than modifying the gene at its chromosomal locus. This can lead to non-physiological levels of protein expression and disruption of other genes, resulting in off-target effects which can alter gene expression. A recent improvement to the STaR method has been published, addressing the major concerns of the original approach (Sanfilippo et al., 2024). In this updated version, the stop cassette followed by the tag is inserted directly into the genomic locus, specifically within an exon region, creating a truly endogenous tag. To circumvent issues related to co-labelling, a UAS-FRT-Stop-FRT-myrFP cassette has been designed, enabling dependent labelling of both the receptor and the cell based on the cell type-specific promoter used. However, introducing a stop cassette internally within a receptor leads to a loss-of-function allele, producing truncated proteins until the receptor is crossed with the desired driver line. Depending on the timing of expression of the driver line used, this can result in developmental defects, delayed phenotypic rescue, or altered physiological processes that might affect the overall interpretation of the receptor's function in specific tissues. Despite this limitation, a significant advantage of this method is the ability to achieve single-cell labelling by titrating the expression of FLP recombinase. This method successfully tagged alleles of 11 neurotransmitter receptor subunits belonging to the cys-loop superfamily (Sanfilippo et al., 2024).

The GRASP method, originally developed to label synaptic contact sites, inspired the methods developed by Kondo et al. (2020) and Luo et al. (2020) for cell-type-specific fluorescent labelling. Both approaches involve the expression of split GFP, where GFP is divided into two non-fluorescent fragments: GFP1-10, the larger fragment, and GFP11, the smaller fragment. In *Drosophila*, GFP1-10 is typically expressed in a cell type-specific manner in presynaptic neurons using the UAS-GAL4 system. At the same time, GFP11 is tethered to a neurotransmitter receptor in postsynaptic neurons via CRISPR/Cas9-mediated genomic insertion. When these neurons form synaptic contacts, the GFP fragments come into close proximity and reconstitute into a functional GFP, marking the synapse. To further enhance specificity at the single-cell level, an FRT-Stop-FRT cassette is placed upstream of GFP11, allowing its expression to be controlled by the presence of FLP recombinase. Though these tools provide a valuable means for visualising membrane proteins, they have several drawbacks. Tethering GFP fragments to neurotransmitter receptors can result in incomplete GFP reconstitution, leading to weak or inconsistent signals. Additionally, there is a risk of false positives arising from non-specific reconstitution of GFP fragments, which can produce misleading signals. Furthermore, these methods lack a generalisable insertion cassette that could be applied to tag other membrane proteins of interest. Lastly, the study by Kondo et al. (2020) tagged neurotransmitter receptor genes exclusively at the C-terminus, which, as previously discussed, may obscure the expression of the reconstituted GFP within the transmembrane domain.

In our effort to observe the spatial distribution of membrane proteins in *Drosophila*, we developed FlpTag, a cell-type-specific tool that is endogenous and generalisable (Manuscript 1). FlpTag leverages the thousands of available MiMIC and CRIMIC gene trap lines by inserting a GFP tag into an intronic region of a gene flanked by FRT sites. In its initial configuration, the FlpTag cassette is oriented oppositely to the gene's direction, resulting in no GFP expression. However, when Flp recombinase is expressed in a cell-type-specific manner, it inverts the cassette, positioning the GFP tag flanked by splice acceptor and donor sites in the correct orientation for gene expression. The primary advantage of FlpTag is its versatility, as it can be applied to many genes of interest by inserting the FlpTag cassette into MiMIC/CRIMIC sites or through CRISPR/Cas9-mediated integration. In contrast, other existing methods have primarily targeted specific genes and do not offer a general plasmid or cassette that can be easily used for genome insertion. Moreover, no specialised cassette is required for cell-dependent labelling, as any UAS-FP line can be employed effectively. To add further flexibility, the FlpTag cassette can be easily modified to incorporate different tags. Recently, we developed

two additional versions of FlpTag featuring epitope tags: FlpTag::3xV5 and FlpTag::smV5 (unpublished). The FlpTag::3xV5 version introduces a smaller tag that reduces steric hindrance, minimising the potential for disrupting protein function. Additionally, it avoids issues related to fluorescence quenching or photobleaching associated with GFP, making it more suitable for long-term or high-sensitivity applications, such as single-cell imaging. The FlpTag::smV5 version was developed to enhance signal intensity by incorporating multiple V5 epitopes, enabling it to bind numerous antibodies simultaneously. This feature is particularly advantageous for visualising weakly expressed proteins that might be challenging to detect with regular GFP. Since the publication of Manuscript 1, we have also developed a strategy to achieve single-cell labelling without altering the original FlpTag cassette. The new approach, called singleFlp, utilises a titratable recombinase system. KD-Recombinase-PEST, controlled by a heat-shock promoter, enables adjustable excision levels that can be fine-tuned to selectively induce recombination in a limited number of cells. Following this, FLP-recombinase is activated, leading to the dependent expression of the tagged protein by inverting FlpTag and removing the stop cassette, effectively labelling the targeted cell. This demonstrates the broad versatility and ease with which FlpTag can be applied and modified to tag nearly any protein of choice, enabling visualisation across a spectrum of specificity, from entire cell populations to individual cells. Like all methods, FlpTag has its limitations, with the most significant being the requirement for a coding intron for insertion. A coding intron, flanked by two coding exons, is essential for the integration of the FlpTag cassette and the subsequent activation of GFP, as it is incorporated into the protein as an artificial exon. Additionally, the introduction of FlpTag as an artificial exon is only feasible for genes with a sufficiently large coding intron, typically 100 nucleotides or more (Lee et al., 2018). Due to its requirement for insertion into a coding intron, FlpTag is not suitable for producing N- or C-terminal tags. However, this limitation is less of a concern when tagging transmembrane proteins, where internal cytosolic tags are generally preferred.

Advancements in protein tagging methods are instrumental to our understanding of neuronal computations and subcellular mechanisms across various fields of study. Research progress has consistently been driven by the development of accessible and user-friendly techniques and technologies, and this is especially true for the tools used to label proteins of interest. The introduction of FlpTag has further expanded the protein tagging toolkit, offering a versatile method for tagging proteins in a cell-type-specific and endogenous manner. While no single technique is perfect, choosing the right approach is essential for achieving the desired outcome and requires careful consideration of each method's strengths and limitations.

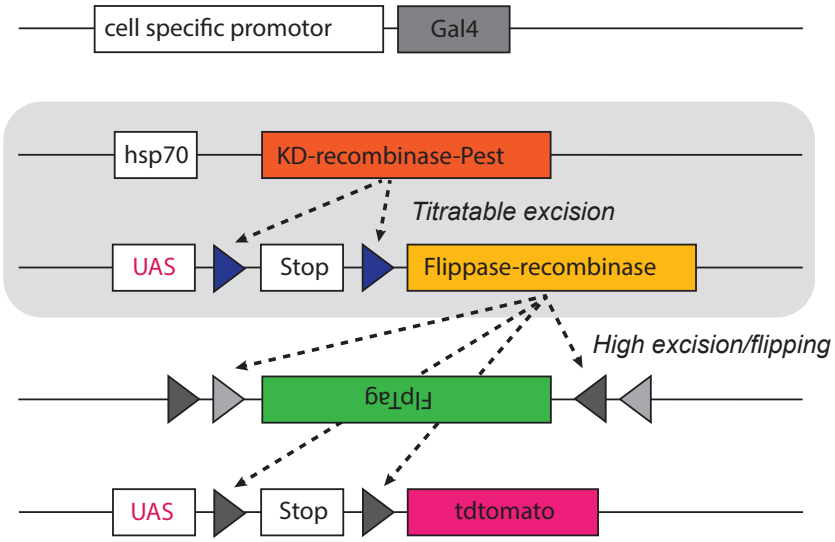

Figure 3.2: The diagram illustrates singleFlp, a conditional, cell-type-specific labelling system. The GAL4 transcription factor drives the expression of Flp recombinase and a cell marker, both of which are activated by titratable KD recombinase through heat shock induction. This system facilitates the labelling of sparse cells by linking protein tagging through FlpTag inversion and cell labelling via the removal of a stop cassette, enabling sparse labelling of both proteins of interest and the cell.

3.2 Adapting FlpTag for Conditional Tagging in Vertebrate Models

The FlpTag technique, developed in Manuscript 1, holds great potential for adaptation in vertebrate models like zebrafish and mice. These model organisms possess comparable genetic techniques that can be employed for the integration and expression of FlpTag. Furthermore, zebrafish and mice benefit from high-resolution imaging technologies, such as live imaging, confocal microscopy, and super-resolution microscopy, making them ideal models for imaging protein localization and studying protein dynamics across various tissues. This adaptation could significantly enhance the genetic toolkit of these model organisms.

3.2.1 FlpTag Integration in Zebrafish

A key advantage of using zebrafish in neuroscience research, particularly for imaging, is their optical transparency during early development, which allows for

real-time, high-resolution visualisation of neural activity and structural changes in a living organism. This makes zebrafish a valuable candidate for incorporating the FlpTag system. A key component for integrating the FlpTag system into zebrafish is the ability to generate cell-type specificity. Similar to *Drosophila*, zebrafish have adopted the UAS-GAL4 system, though more recently and less extensively (Halpern et al., 2008). The introduction of the Tol2 transposon has significantly advanced genetic manipulation, enabling the creation of GAL4 gene trap lines to drive expression in specific cell types (Kawakami et al., 2016). This makes the application of FlpTag more feasible, as tissue-specific drivers can now be combined with other transgenes for controlled expression in zebrafish. Another critical element required is the compatibility of recombinase systems. Zebrafish currently utilise three main recombinase systems—Cre/loxP, Flp/FRT, and PhiC31 recombinase—which allow precise recombination events for genetic manipulation. These systems, particularly Flp/FRT, are essential for integrating FlpTag, as they provide spatial and temporal control of transgene activation. The CRISPR/Cas9 system has further enhanced genetic editing in zebrafish by enabling efficient intron-targeting knock-ins, which maintain the integrity of endogenous genes without disrupting their natural expression (Li et al., 2015). For FlpTag, this means that CRISPR-mediated knock-ins can be used to insert the FlpTag cassette at precise locations, particularly in intronic regions of the protein of interest.

Conveniently, all the necessary transgenes are already available to implement FlpTag in zebrafish. A cell-type-specific driver line, such as ChAT-Gal4 for cholinergic neurons, can be used to direct expression of UAS-driven constructs. The FlpTag plasmid can be integrated into the genome using CRISPR/Cas9-mediated knock-ins at the protein of interest intron. Additionally, UAS-based reporters, such as UAS-myr-tdTomato, would be used for visualising specific cell populations, while Flp recombinase expressed under the UAS promoter (e.g., UAS-Flp) will facilitate recombination events necessary for FlpTag function. Stable zebrafish lines can be generated using Tol2-mediated transgenesis, ensuring the proper incorporation of all genetic components. By crossing these lines, researchers can achieve endogenous, cell-type-specific FlpTag expression, with the only variable differing from *Drosophila* being the specific GAL4 line used to drive expression. This approach leverages existing zebrafish genetic tools, making the integration of FlpTag relatively straightforward.

3.2.2 FlpTag-like Implementation in Mice

While flies and zebrafish offer advantages in terms of simplicity and optical transparency, mice provide a more relevant model for imaging neuronal signalling elements due to their closer genetic and physiological resemblance to humans. This approach could facilitate a more detailed investigation of mammalian-specific neurotransmission through chemical and electrical synaptic pathways and their roles in behaviour and neurological disorders. However, adapting such labelling systems in mice is more challenging due to the increased complexity of the organism. The main drawbacks are the longer time required to generate transgenes and perform gene editing, as well as the significantly greater resources needed to carry out these processes. Additionally, as discussed earlier, not every attempt to tag a protein of interest will be successful, making it critical to weigh whether generating a transgenic mouse is worth the investment of both time and resources.

With the above considerations in mind, implementing a FlpTag-like method for cell type-specific endogenous labelling in mice is plausible, especially with some modifications. As stated above, the current implementation of FlpTag in *Drosophila* requires four components: a cell type-specific driver line, FlpTag integrated into the protein of interest, a UAS-reporter for cell labelling, and Flp recombinase under UAS control. In FlpTag's current form, this would require generating a quadruple transgenic mouse line. While possible, this is extremely difficult. As a modification of the Flippase-based FlpTag, Cre recombinase could be used instead, as it is more widely applied in mice. A modified Cre system would induce cell type specificity by being expressed under a particular promoter (promoter-Cre). Cell labelling would be achieved by integrating a loxP-Stop-loxP-tdTomato transgene, which would only be expressed in Cre-expressing cells. Using CRISPR/Cas9-mediated knock-in, a modified FlpTag cassette could be integrated into the intronic region of the protein of interest. It would consist of opposing non-compatible loxP sites flanking an inverted GFP (Langer et al., 2002). The GFP would be positioned between mouse-specific splice acceptor and donor sites, allowing the inversion of GFP and thus labelling the protein of interest only in Cre-expressing cells. Alternatively, this system could be further simplified to require only two transgenes if cell type-specific Cre is introduced via viral injection. In this case, only one new mouse line, the FlpTag-like line, would need to be generated, as the Stop-tdTomato line already exists. Though in theory this may sound straightforward, especially for those familiar with *Drosophila* and zebrafish genetics, it would be a significant endeavour in mice. However, it is potentially a worthwhile one.

3.3 Membrane Channel Relevance in Motion Detection

Understanding the subcellular mechanisms behind motion detection is vital for uncovering how organisms process sensory information. As demonstrated in this thesis, recent progress in molecular biology and genetics have provided deeper insights into the roles of neurotransmitter systems, receptors, and ion channels in shaping neural responses to visual stimuli. In *Drosophila*, key components such as inhibitory and excitatory receptors, along with electrical synapses, play vital roles in motion detection.

3.3.1 Neurotransmitter Receptors

Understanding motion detection in *Drosophila* has significantly advanced over the years, with early research predominantly relying on classical neurophysiological techniques that probed neuronal activity at the level of the whole cell to better understand the mechanisms underlying visual processing and motion detection (Maisak et al., 2013; Serbe et al., 2016). These approaches provided foundational insights into the roles of T4 and T5 neurons in detecting motion direction; however, this information alone is not enough to truly understand how motion vision is processed. Recent advancements in molecular biology and genetics have driven a shift towards more molecular-focused approaches, such as improved protein tagging techniques and RNA sequencing, enabling a deeper understanding of the subcellular substrates involved in motion vision computation (Pankova & Borst, 2016; Davis et al., 2020; Hörmann et al., 2020). With these advances, we can now map out specific neurotransmitter systems and receptor profiles that contribute to the complex motion detection circuitry in *Drosophila*, offering a more detailed and nuanced view of the underlying mechanisms.

Of particular interest to the motion vision system are the neurotransmitter receptors expressed on the dendrites of T4/T5 neurons, as they define the functional properties of synaptic connections within the motion detection pathway. Neurotransmitter receptors play a crucial role in defining the synaptic sign and determining whether a synapse is excitatory or inhibitory. Ionotropic receptors, which are fast-acting, directly gate ion channels upon neurotransmitter binding, leading to rapid changes in neuronal conductance. This can result in either excitatory postsynaptic potentials, such as through sodium influx, or inhibitory potentials, such as through chloride influx. In contrast, metabotropic receptors induce slower, more sustained effects by activating intracellular signalling cascades,

which modulate various aspects of neuronal function and influence long-term synaptic activity. Additionally, receptors can also influence the temporal dynamics of synaptic transmission. Ionotropic receptors facilitate rapid synaptic transmission, while metabotropic receptors contribute to slower, longer-lasting, and modulatory effects.

As described earlier, the three-arm detector model serves as the current framework for explaining motion detection in *Drosophila*. Refining this model involves understanding the precise localisation of neurotransmitters and their receptors within T4/T5 neurons. Using the genetic strategies developed in Manuscript 1, we visualised the distribution of key receptors along the dendrites of these neurons. Our findings confirmed that the glutamatergic synapse between the Mi9 neuron and T4 dendrites is mediated by the inhibitory receptor GluClα, which is localised to the distal tips of T4 dendrites. This localisation aligns with previous EM studies that mapped the synaptic contacts to this region. The input from Mi9 to T4 is inhibitory, thus it has a negative sign; however, because Mi9 is responsive to OFF stimuli, the inhibition is reversed during ON stimuli. This reversal results in a release of inhibition in T4 neurons, allowing them to become more active in response to ON stimuli. In the central part of T4 dendrites, cholinergic inputs from neurons like Mi1 and Tm3 are excitatory and are mediated by the Dα7 receptor, contributing significantly to the excitation of T4 neurons in response to visual stimuli. Additionally, GABAergic inputs from neurons such as Mi4, C3, and CT1, mediated through the Rdl receptor, provide inhibitory signals.

For T5 neurons, which receive a more limited variety of inputs, the cholinergic inputs via neurons such as Tm1, Tm2, Tm4, and Tm9 are predominantly excitatory. These inputs are mediated by the Dα7 receptor, mainly distributed in the central regions of T5 dendrites but with a lesser presence towards the distal tips. We observed fewer Dα7 puncta than expected relative to the number of cholinergic synapses, suggesting the involvement of other cholinergic receptor subunits. This hypothesis is supported by recent findings from (Sanfilippo et al., 2024), which demonstrated the expression of Dα5 in the central compartment of T5 dendrites, overlapping with the areas where Tm1, Tm2, and Tm4 neurons synapse. Additionally, Dα1 and Dβ1 were localised specifically to the distal tips of T5 dendrites, where Tm9 neurons and recurrent T5-T5 connections occur. Moreover, the only GABAergic input to T5, provided by CT1, was confirmed to mediate inhibition through the Rdl receptor subunit.

Another component of the three-arm detector model is the delay between inputs from different synapses along the dendrite. This delay allows the neuron to compare inputs received at different times. Delays can occur at the level of the presynaptic

neurons that provide input to the T4 and T5 neurons. These presynaptic delays can be due to cell-intrinsic mechanisms, meaning they can be inherent properties of the input neurons themselves. Several studies have documented these presynaptic delays in neurons that connect to T4/T5, which contribute to the timing of the inputs these neurons receive (Ammer et al., 2015; Serbe et al., 2016; Arenz et al., 2017). However, another way to introduce temporal delays is through postsynaptic mechanisms on the dendrites of T4/T5 neurons. Metabotropic receptors can create delays via their slower action compared to ionotropic receptors. These receptors operate through second-messenger systems, which take longer to induce cellular responses, thus introducing a temporal delay (Reiner & Levitz, 2018). For T5 neurons, some of the cholinergic inputs could be delayed by metabotropic acetylcholine receptors, such as muscarinic receptors. These receptors are slower-acting and might create the necessary delays for enhanced motion detection (Shinomiya et al., 2014). Recent RNA sequencing studies have shown that both T4 and T5 neurons express metabotropic receptors for acetylcholine and gamma-aminobutyric acid. These findings suggest that these neurons have the molecular machinery necessary for postsynaptic delays, although further investigation is needed to fully understand their roles (Pankova & Borst, 2016; Davis et al., 2020). While current simulations of motion detection already perform well using the delays measured in presynaptic inputs (Serbe et al., 2016; Arenz et al., 2017; Drews et al., 2020), postsynaptic delays introduced by metabotropic receptors could add another layer of temporal modulation, further refining the accuracy of current models.

The three-arm detector model incorporates both PD enhancement and ND suppression as central mechanisms for motion detection in *Drosophila*. This model postulates that neurotransmitters and their corresponding receptors are distributed along T4/T5 neurons in a way that facilitates these non-linear computations. PD enhancement occurs when the response to motion in the preferred direction is greater than the sum of individual responses to flickering stimuli. This enhancement is achieved through a combination of excitatory and inhibitory synaptic inputs, focusing on the interaction between cholinergic and glutamatergic inputs. The multiplication-like nonlinearity observed in T4 neurons arises from the coincidence of cholinergic excitation and release from glutamatergic inhibition, which is mediated by the glutamate-gated chloride channel GluClα. This interaction increases the input resistance of T4 neurons, amplifying the response to subsequent excitatory inputs from cholinergic neurons like Mi1 and Tm3 during motion in the preferred direction. This mechanism effectively sharpens the directional tuning of the neurons, allowing them to respond more robustly to motion in the preferred direction. On the other hand, ND suppression occurs through shunting inhibition,

where inhibitory inputs reduce excitatory signals by lowering membrane resistance, dampening input without significantly changing the membrane potential. GABAergic inputs, mediated by the Rdl receptor in T4 and T5 neurons, provide this strong shunting inhibition, particularly in response to motion in the null direction. This inhibition helps suppress responses to motion in the opposite direction, enhancing the neuron's ability to detect motion in the preferred direction. This precise arrangement of excitatory and inhibitory inputs across the dendritic tree of T4/T5 neurons sharpens their directional tuning, enhancing the ability to detect the direction of motion.

3.3.2 Voltage Gated Ion Channels

Ih channels, also known as hyperpolarisation-activated cyclic nucleotide-gated (HCN) channels, were found on the dendrites of both T4 and T5 neurons. Although the role of Ih in motion vision has not been experimentally verified, we can speculate about its function. In T4 neurons, Ih channels could serve as a key mechanism for PD enhancement via rebound excitation following the release of T4 neurons from inhibitory inputs. When a moving bright edge stimulates T4 neurons, these neurons are initially inhibited by the Mi9 neuron via the GluClα receptor. As the stimulus continues to move in the preferred direction, this inhibition is released. Ih channels, which are activated by hyperpolarisation, could then become active upon this release from inhibition. This activation might lead to a rebound excitation, where the neuron experiences a rapid depolarisation following the initial hyperpolarisation. This rebound could contribute to a non-linear enhancement of the depolarisation in T4 neurons as they begin to receive excitatory inputs from cholinergic neurons like Mi1 and Tm3 in the central area of their dendrites. The enhanced depolarisation caused by this rebound excitation could amplify the response of T4 neurons to stimuli moving in the preferred direction, resulting in the observed PD enhancement. This would align with the notion that Ih channels can support sustained depolarisation and reduce response latency, which is critical for the rapid and selective detection of motion direction (Magee, 1998; Robinson & Siegelbaum, 2003). In T5 neurons, while the specific role of Ih is less clear, these channels could similarly contribute to the processing of motion signals by shaping the timing and integration of synaptic inputs. Given the cholinergic inputs from neurons like Tm1, Tm2, Tm4, and Tm9, which are distributed across the central and distal regions of T5 dendrites, Ih could modulate how these inputs are integrated, potentially influencing both PD enhancement and ND suppression (Lüthi & McCormick, 1998; Hutcheon & Yarom, 2000). In summary, Ih channels may help enhance responses to motion in the preferred

direction while also stabilising neural activity and modulating signal integration. However, future studies are required to fully elucidate the specific contributions of Ih channels to direction selectivity in T4/T5 neurons.

para is the only gene in *Drosophila* that encodes voltage-gated sodium channels, which are typically involved in the rapid depolarisation phase of action potentials, crucial for the fast transmission of electrical signals in many types of neurons (Loughney et al., 1989; Pankova & Borst, 2016; Davis et al., 2020). In Manuscript 1, we observed that para is specifically localised to the axonal fibres that connect the dendrites to the axon terminals in T4/T5 neurons. This localisation suggests that para might play a significant role in the conduction of electrical signals along these axonal fibres, potentially influencing how information is transmitted from the dendrites to the axon terminals. However, it remains unclear whether T4/T5 neurons generate traditional action potentials, leaving the exact role of para somewhat speculative. Even in the absence of traditional action potentials, para-encoded sodium channels could contribute to non-linear signal processing, where graded potentials become significantly stronger once a certain threshold of excitatory input is reached. This non-linearity could be crucial in distinguishing between preferred and null direction stimuli, ensuring that only sufficiently strong or well-timed inputs result in large graded potentials. This mechanism would support direction selectivity by enhancing responses to motion in the preferred direction while minimising responses in the null direction, as suggested by the current motion vision model.

The ongoing research into motion detection in *Drosophila* highlights the complexity of the underlying neural mechanisms. Early studies laid the foundation by using classical neurophysiological techniques to explore the roles of T4 and T5 neurons in detecting motion direction. However, recent advancements in molecular biology and genetics have allowed for a more detailed understanding of the specific neurotransmitter systems, receptor profiles, and ion channel functions that contribute to this process. We elucidated crucial roles within the motion detection circuitry, such as GluClα mediation of inhibitory inputs, the potential involvement of Ih channels in PD enhancement, and the potential function of para channels in signal conduction. Future studies should investigate other neurotransmitter receptors and ion channels that may partake in the computation of motion vision to further our understanding of this neuronal circuit. This growing body of knowledge deepens our understanding of motion vision in *Drosophila* and provides a framework for exploring similar processes in other organisms, ultimately contributing to a broader comprehension of sensory processing in the brain.

3.3.3 Gap Junctions

Neurons communicate through two types of synapses: chemical and electrical. Chemical synapses use neurotransmitters to transmit signals from the presynaptic to the postsynaptic neuron, either by directly opening ion channels or by triggering intracellular signalling cascades. In contrast, electrical synapses use gap junctions to allow ions to flow directly between neurons, enabling rapid, bidirectional communication. Extensive research on *Drosophila* has been conducted on the molecular components, physiology, and function of chemical synapses, resulting in a detailed understanding of these connections. Conversely, very little was known about the distribution and functional role of electrical synapses throughout the *Drosophila* nervous system. Most existing knowledge derives from studies focused on specific cell types or small neural circuits, leaving a significant gap in understanding how these synapses contribute to broader neural network function. In Manuscript 2, we aimed to close this gap by generating an immunohistochemistry-based anatomical map of all innexin gap junction proteins. After evaluating innexin expression, we focused on ShakB, one of the most widely expressed neuronal innexins in the *Drosophila* nervous system. This detailed investigation of ShakB explored its specific roles in neural circuits, particularly concerning its contribution to the stability and functional role within visual projection neurons. By examining the effects of ShakB removal, valuable insights were gained into how ShakB influences the dynamics of electrical synapses and the overall neural circuitry involved in motion detection.

When ShakB gap junctions were removed through either a null mutation or pan-neuronal knockdown, VS and HS cells exhibited both fast and slow membrane potential oscillations and large calcium oscillations. This outcome was surprising because, in many neural networks, electrical synapses are typically required to generate and synchronise oscillations, not prevent them (Tchumatchenko & Clopath, 2014; Connors, 2017). The fact that these oscillations occurred when ShakB was absent suggests that ShakB normally stabilises these neurons by preventing such oscillations. To better understand how these oscillations arose, the role of specific ions and their potential influence on the observed phenomena was investigated. The focus was on voltage-gated sodium (Nav) channels, essential for initiating fast membrane potential oscillations, and hyperpolarisation-activated cyclic nucleotide-gated (Ih) channels, which modulate the timing and dynamics of these oscillations. The addition of the Nav antagonist TTX effectively halted both fast and slow oscillations, indicating that these channels are integral to the oscillatory activity in the absence of ShakB-mediated electrical synapses. However, the exact mechanisms linking fast and slow voltage oscillations to calcium oscillations remain unclear and

require further investigation. These findings suggest that under normal conditions, ShakB-mediated electrical synapses help maintain the stability of VS/HS cells by buffering intrinsic noise and dissipating it across the network. This mechanism prevents spontaneous oscillations unless a synaptic stimulus of the appropriate frequency and strength engages the cell's non-linear conductances. Without these electrical synapses, the intrinsic noise within the cells may be sufficient to trigger spontaneous oscillations at the cells' resonant frequency.

To probe the role of ShakB-mediated electrical synapses in direction selectivity, targeted experiments were conducted to assess how the removal or alteration of these synapses affected the ability of *Drosophila* neurons, particularly T4/T5 and VS/HS cells, to process directional visual stimuli. Interestingly, the loss of ShakB-mediated electrical synapses resulted in a significant reduction in the response magnitude of T4/T5 and VS/HS cells to both ON and OFF motion stimuli. Additionally, it led to an almost complete loss of sensitivity to OFF flicker stimuli in VS/HS cells. Despite these changes, the direction selectivity, defined as the sharpness of tuning to motion direction, of these neurons remained unaffected. This indicates that while electrical synapses are not directly involved in the basic computation of motion direction, they are crucial for maintaining the strength of responses to visual stimuli. Since ShakB mRNA is only weakly expressed in T4/T5 cells, this suggests that the electrical synapses influencing these responses are likely located upstream in the visual processing pathway, such as in the medulla or lamina (Davis et al., 2020). One potential candidate for these upstream connections is the lamina monopolar cell L4, which is important for OFF motion detection. The co-localisation of ShakB with L4 dendrites suggests that the loss of electrical synapses in these cells might contribute to the reduced responsiveness observed in VS/HS cells. Moving forward in Manuscript 2, only a narrow range of visual stimuli was tested, which leaves unexplored the potential role that electrical synapses might play in other visual conditions, such as noisy, low-contrast, or low-luminance environments. Further research is needed to better understand the role these synapses might have in the broader context of visual circuits. However, Manuscript 2 has laid a solid foundation by identifying key aspects of how electrical synapses function within the visual system, setting the stage for future investigations to explore their roles under a wider variety of visual conditions and in other neural circuits.

3.4 Summary and Outlook

Investigating the subcellular localisation and distribution of neurotransmitter receptors, ion channels, and gap junctions across neuronal compartments is essential for understanding their functional roles and how they contribute to neural circuit dynamics. In this thesis, I developed tools to investigate the distribution of various transmembrane proteins in *Drosophila* neurons, with a particular focus on their expression in T4/T5 neurons, which are involved in motion detection. Using methods like flippase-dependent expression and the novel FlpTag tool for conditional, cell-type-specific tagging, I provided insights into the localisation of receptors such as GluClα, Rdl, Dα7 and the ion channels para and Ih.

As a next step, the precise roles of these channels can be further validated through loss-of-function experiments using RNAi-mediated knockdown or CRISPR-based knockout techniques. These approaches can selectively deplete neurotransmitter receptors and ion channels in specific neuronal populations, followed by functional analysis using calcium imaging with GCaMP or electrophysiological recordings. As demonstrated by Groschner et al. (2022), the researchers used in vivo patch-clamp recordings to show that T4 neurons exhibit a multiplication-like nonlinearity from the coincidence of cholinergic excitation and release from glutamatergic inhibition. Paired with RNAi silencing of GluClα, this revealed that GluClα is crucial for sharpening the directional tuning of T4 neurons. Using a similar experimental framework, the role of Rdl and other channels can be explained. It is predicted that depleting the Rdl receptor, which is localised to T4/T5 dendrites, would lead to diminished ND suppression and a marked reduction in direction selectivity.

Beyond the work presented in this thesis, these tools can be expanded to investigate additional receptors and ion channels even with different model organisms. RNA sequencing data indicates that other ionotropic and metabotropic receptors, as well as voltage-gated ion channels, are expressed in T4/T5 neurons, some of which remain uncharacterised. Using FlpTag allows for endogenous conditional tagging of these proteins, enabling a detailed investigation of their localisation at synaptic sites. Future work can utilise these tools to uncover the subcellular distribution of these receptors across different neuronal compartments, further elucidating their roles in synaptic transmission and neural computation.

References

Adams, M. D., Celniker, S. E., Holt, R. A., Evans, C. A., Gocayne, J. D., Amanatides, P. G., ... Venter, J. C. (2000, March). The Genome Sequence of *Drosophila Melanogaster*. *Science*, *287*(5461), 2185–2195.

Ahmad, S., Martin, P. E. M., & Evans, W. H. (2001). Assembly of gap junction channels. *European Journal of Biochemistry*, *268*(16), 4544–4552.

Alekseyenko, O. V., Chan, Y.-B., Li, R., & Kravitz, E. A. (2013, April). Single dopaminergic neurons that modulate aggression in *Drosophila*. *Proceedings of the National Academy of Sciences of the United States of America*, *110*(15), 6151–6156.

Alekseyenko, O. V., Lee, C., & Kravitz, E. A. (2010, May). Targeted Manipulation of Serotonergic Neurotransmission Affects the Escalation of Aggression in Adult Male *Drosophila Melanogaster*. *PLoS ONE*, *5*(5), e10806.

Alexopoulos, H., Böttger, A., Fischer, S., Levin, A., Wolf, A., Fujisawa, T., ... Bacon, J. P. (2004, October). Evolution of gap junctions: The missing link? *Current Biology*, *14*(20), R879-R880.

Ammer, G., Leonhardt, A., Bahl, A., Dickson, B. J., & Borst, A. (2015, August). Functional Specialization of Neural Input Elements to the *Drosophila* ON Motion Detector. *Current Biology*, *25*(17), 2247–2253.

Anholt, R. R. H., Lyman, R. F., & Mackay, T. F. C. (1996, May). Effects of Single P-Element Insertions on Olfactory Behavior in *Drosophila Melanogaster*. *Genetics*, *143*(1), 293–301.

Arenz, A., Drews, M. S., Richter, F. G., Ammer, G., & Borst, A. (2017, April). The Temporal Tuning of the *Drosophila* Motion Detectors Is Determined by the Dynamics of Their Input Elements. *Current Biology*, *27*(7), 929–944.

Aronstein, K., & Ffrench-Constant, R. (1995). Immunocytochemistry of a novel GABA receptor subunit Rdl in *Drosophila Melanogaster*. *Invertebrate neuroscience: IN*, *1*(1), 25–31.

Aso, Y., Hattori, D., Yu, Y., Johnston, R. M., Iyer, N. A., Ngo, T.-T., ... Rubin, G. M. (2014, December). The neuronal architecture of the mushroom body provides a logic for associative learning. *eLife*, *3*, e04577.

Baez, M. V., Cercato, M. C., & Jerusalinsky, D. A. (2018). NMDA Receptor Subunits Change after Synaptic Plasticity Induction and Learning and Memory Acquisition. *Neural Plasticity*, *2018*, 5093048.

Bahl, A., Ammer, G., Schilling, T., & Borst, A. (2013, June). Object tracking in motion-blind flies. *Nature Neuroscience*, *16*(6), 730–738.

Baines, R. A., Uhler, J. P., Thompson, A., Sweeney, S. T., & Bate, M. (2001, March). Altered electrical properties in *Drosophila* neurons developing without synaptic transmission. *The Journal of Neuroscience: The Official Journal of the Society for Neuroscience*, *21*(5), 1523–1531.

Balfanz, S., Strünker, T., Frings, S., & Baumann, A. (2005, April). A family of octopamine [corrected] receptors that specifically induce cyclic AMP production or Ca2+ release in *Drosophila Melanogaster*. *Journal of Neurochemistry*, *93*(2), 440–451.

Barlow, H. B., & Levick, W. R. (1965, June). The mechanism of directionally selective units in rabbit's retina. *The Journal of Physiology*, *178*(3), 477–504.

Bateman, J. R., Lee, A. M., & Wu, C.-t. (2006, June). Site-Specific Transformation of *Drosophila* via ϕC31 Integrase-Mediated Cassette Exchange. *Genetics*, *173*(2), 769–777.

Bausenwein, B., Dittrich, A. P. M., & Fischbach, K. F. (1992, January). The optic lobe of *Drosophila Melanogaster*. *Cell and Tissue Research*, *267*(1), 17–28.

Bear, M., Connors, B., & Paradiso, M. A. (2020). *Neuroscience: Exploring the Brain, Enhanced Edition: Exploring the Brain, Enhanced Edition*. Jones & Bartlett Learning.

Benton, R., Sachse, S., Michnick, S. W., & Vosshall, L. B. (2006, January). Atypical Membrane Topology and Heteromeric Function of *Drosophila* Odorant Receptors In Vivo. *PLOS Biology*, *4*(2), e20.

Benton, R., Vannice, K. S., Gomez-Diaz, C., & Vosshall, L. B. (2009, January). Variant Ionotropic Glutamate Receptors as Chemosensory Receptors in *Drosophila*. *Cell*, *136*(1), 149–162.

Berry, J. A., Cervantes-Sandoval, I., Chakraborty, M., & Davis, R. L. (2015, June). Sleep Facilitates Memory by Blocking Dopamine Neuron-Mediated Forgetting. *Cell*, *161*(7), 1656–1667.

Bicker, G., & Menzel, R. (1989, January). Chemical codes for the control of behaviour in arthropods. *Nature*, *337*(6202), 33–39.

Bielopolski, N., Amin, H., Apostolopoulou, A. A., Rozenfeld, E., Lerner, H., Huetteroth, W., ... Parnas, M. (2019, June). Inhibitory muscarinic acetylcholine receptors enhance aversive olfactory learning in adult *Drosophila*. *eLife*, *8*, e48264.

Bienert, S., Waterhouse, A., de Beer, T. A. P., Tauriello, G., Studer, G., Bordoli, L., & Schwede, T. (2017, January). The SWISS-MODEL Repository-new features and functionality. *Nucleic Acids Research*, *45*(D1), D313-D319.

Bischof, J., Björklund, M., Furger, E., Schertel, C., Taipale, J., & Basler, K. (2013, June). A versatile platform for creating a comprehensive UAS-ORFeome library in *Drosophila*. *Development*, *140*(11), 2434–2442.

Bishop, L. G., & Keehn, D. G. (1966, December). Two Types of Neurones Sensitive to Motion in the Optic Lobe of the Fly. *Nature*, *212*(5068), 1374–1376.

Bogdanik, L., Mohrmann, R., Ramaekers, A., Bockaert, J., Grau, Y., Broadie, K., & Parmentier, M.-L. (2004, October). The *Drosophila* metabotropic glutamate receptor DmGluRA regulates activity-dependent synaptic facilitation and fine synaptic morphology. *The Journal of Neuroscience: The Official Journal of the Society for Neuroscience*, *24*(41), 9105–9116.

Bohrmann, J., & Zimmermann, J. (2008). Gap junctions in the ovary of *Drosophila Melanogaster*: Localization of innexins 1, 2, 3 and 4 and evidence for intercellular communication via innexin-2 containing channels. *BMC Developmental Biology*, *8*, 111.

Borst, A., & Egelhaaf, M. (1989, August). Principles of visual motion detection. *Trends in Neurosciences*, *12*(8), 297–306.

Borst, A., & Groschner, L. N. (2023, July). How Flies See Motion. *Annual Review of Neuroscience*, *46*(Volume 46, 2023), 17–37.

Braitenberg, V. (1966, June). Unsymmetrische Projektion der Retinulazellen auf die Lamina ganglionaris bei der Fliege Musca domestica. *Zeitschrift für vergleichende Physiologie*, *52*(2), 212–214.

Braitenberg, V. (1967, March). Patterns of projection in the visual system of the fly. I. Retina-lamina projections. *Experimental Brain Research*, *3*(3), 271–298.

Brand, A. H., & Perrimon, N. (1993, June). Targeted gene expression as a means of altering cell fates and generating dominant phenotypes. *Development (Cambridge, England)*, *118*(2), 401–415.

Brody, T., & Cravchik, A. (2000, July). *Drosophila Melanogaster* g protein–Coupled Receptors. *The Journal of Cell Biology*, *150*(2), 83–88.

Buchner, E., Buchner, S., Burg, M. G., Hofbauer, A., Pak, W. L., & Pollack, I. (1993, July). Histamine is a major mechanosensory neurotransmitter candidate in *Drosophila Melanogaster*. *Cell and Tissue Research*, *273*(1), 119–125.

Buschbeck, E. K., & Strausfeld, N. J. (1997). The relevance of neural architecture to visual performance: Phylogenetic conservation and variation in dipteran visual systems. *Journal of Comparative Neurology*, *383*(3), 282–304.

Butler, A., Wei, A., Baker, K., & Salkoff, L. (1989, February). A Family of Putative Potassium Channel Genes in *Drosophila*. *Science*, *243*(4893), 943–947.

Castle, W. E., Carpenter, F. W., Clark, A. H., Mast, S. O., & Barrows, W. M. (1906). The Effects of Inbreeding, Cross-Breeding, and Selection upon the Fertility and Variability of *Drosophila*. *Proceedings of the American Academy of Arts and Sciences*, *41*(33), 731–786.

Catterall, W. A. (2010, September). Ion Channel Voltage Sensors: Structure, Function, and Pathophysiology. *Neuron*, *67*(6), 915–928.

Catterall, W. A. (2014). Structure and function of voltage-gated sodium channels at atomic resolution. *Experimental Physiology*, *99*(1), 35–51.

Chalfie, M., Tu, Y., Euskirchen, G., Ward, W. W., & Prasher, D. C. (1994, February). Green Fluorescent Protein as a Marker for Gene Expression. *Science*, *263*(5148), 802–805.

Chen, X., Zaro, J. L., & Shen, W.-C. (2013, October). Fusion protein linkers: Property, design and functionality. *Advanced Drug Delivery Reviews*, *65*(10), 1357–1369.

Chen, Y., Akin, O., Nern, A., Tsui, C. Y. K., Pecot, M. Y., & Zipursky, S. L. (2014, January). Cell-type-specific labeling of synapses in vivo through synaptic tagging with recombination. *Neuron*, *81*(2), 280–293.

Choy, B. C., Cater, R. J., Mancia, F., & Pryor, E. E. (2021, March). A 10-Year Meta-Analysis Of Membrane Protein Structural Biology: Detergents, Membrane Mimetics, And Structure Determination Techniques. *Biochimica et biophysica acta. Biomembranes*, *1863*(3), 183533.

Chudakov, D. M., Matz, M. V., Lukyanov, S., & Lukyanov, K. A. (2010, July). Fluorescent proteins and their applications in imaging living cells and tissues. *Physiological Reviews*, *90*(3), 1103–1163.

Cinelli, R. A., Ferrari, A., Pellegrini, V., Tyagi, M., Giacca, M., & Beltram, F. (2000, June). The enhanced green fluorescent protein as a tool for the analysis of protein dynamics and localization: Local fluorescence study at the single-molecule level. *Photochemistry and Photobiology*, *71*(6), 771–776.

Connors, B. W. (2017). Synchrony and so much more: Diverse roles for electrical synapses in neural circuits. *Developmental Neurobiology*, *77*(5), 610–624.

Coons, A. H., Creech, H. J., & Jones, R. N. (1941, June). Immunological Properties of an Antibody Containing a Fluorescent Group. *Proceedings of the Society for Experimental Biology and Medicine*, *47*(2), 200–202.

Covarrubias, M., Wei, A., & Salkoff, L. (1991, November). Shaker, Shal, Shab, and Shaw express independent K+ current systems. *Neuron*, *7*(5), 763–773.

Dana, H., Sun, Y., Mohar, B., Hulse, B. K., Kerlin, A. M., Hasseman, J. P., ... Kim, D. S. (2019, July). High-performance calcium sensors for imaging activity in neuronal populations and microcompartments. *Nature Methods*, *16*(7), 649–657.

Daniels, R. W., Collins, C. A., Gelfand, M. V., Dant, J., Brooks, E. S., Krantz, D. E., & DiAntonio, A. (2004, November). Increased Expression of the *Drosophila* Vesicular Glutamate Transporter Leads to Excess Glutamate Release and a Compensatory Decrease in Quantal Content. *Journal of Neuroscience*, *24*(46), 10466–10474.

Das, A., Chiang, A., Davla, S., Priya, R., Reichert, H., VijayRaghavan, K., & Rodrigues, V. (2011, January). Identification and analysis of a glutamatergic local interneuron lineage in the adult *Drosophila* olfactory system. *Neural Systems & Circuits*, *1*(1), 4.

Das, S., Sadanandappa, M. K., Dervan, A., Larkin, A., Lee, J. A., Sudhakaran, I. P., ... Ramaswami, M. (2011, September). Plasticity of local GABAergic interneurons drives olfactory habituation. *Proceedings of the National Academy of Sciences*, *108*(36), E646-E654.

David, J.-C., & Coulon, J.-F. (1985, January). Octopamine in invertebrates and vertebrates. A review. *Progress in Neurobiology*, *24*(2), 141–185.

Davis, F. P., Nern, A., Picard, S., Reiser, M. B., Rubin, G. M., Eddy, S. R., & Henry, G. L. (2020, January). A genetic, genomic, and computational resource for exploring neural circuit function. *eLife*, *9*, e50901.

Deng, B., Li, Q., Liu, X., Cao, Y., Li, B., Qian, Y., ... Rao, Y. (2019, March). Chemoconnectomics: Mapping Chemical Transmission in *Drosophila*. *Neuron*, *101*(5), 876-893.e4.

Dierick, H. A., & Greenspan, R. J. (2007, May). Serotonin and neuropeptide F have opposite modulatory effects on fly aggression. *Nature Genetics*, *39*(5), 678–682.

Dietrich, W. (1909). *Die Facettenaugen der Dipteren.*

Dietzl, G., Chen, D., Schnorrer, F., Su, K.-C., Barinova, Y., Fellner, M., ... Dickson, B. J. (2007, July). A genome-wide transgenic RNAi library for conditional gene inactivation in *Drosophila*. *Nature*, *448*(7150), 151–156.

Dorkenwald, S., McKellar, C. E., Macrina, T., Kemnitz, N., Lee, K., Lu, R., ... Seung, H. S. (2022, January). FlyWire: Online community for whole-brain connectomics. *Nature Methods*, *19*(1), 119–128.

Drenan, R. M., Nashmi, R., Imoukhuede, P., Just, H., McKinney, S., & Lester, H. A. (2008, January). Subcellular Trafficking, Pentameric Assembly, and Subunit Stoichiometry of Neuronal Nicotinic Acetylcholine Receptors Containing Fluorescently Labeled *A*6 and *B*3 Subunits. *Molecular Pharmacology*, *73*(1), 27–41.

Drews, M. S., Leonhardt, A., Pirogova, N., Richter, F. G., Schuetzenberger, A., Braun, L., ... Borst, A. (2020, January). Dynamic Signal Compression for Robust Motion Vision in Flies. *Current Biology*, *30*(2), 209-221.e8.

Dvorak, D. R., Bishop, L. G., & Eckert, H. E. (1975, January). On the identification of movement detectors in the fly optic lobe. *Journal of comparative physiology*, *100*(1), 5–23.

Eckstein, N., Bates, A. S., Champion, A., Du, M., Yin, Y., Schlegel, P., ... Funke, J. (2024, May). Neurotransmitter classification from electron microscopy images at synaptic sites in *Drosophila Melanogaster*. *Cell*, *187*(10), 2574-2594.e23.

Enell, L., Hamasaka, Y., Kolodziejczyk, A., & Nässel, D. R. (2007, November). Gamma-Aminobutyric acid (GABA) signaling components in *Drosophila*: Immunocytochemical localization of GABA(B) receptors in relation to the GABA(A) receptor subunit RDL and a vesicular GABA transporter. *The Journal of Comparative Neurology*, *505*(1), 18–31.

Evans, P. D., & Maqueira, B. (2005, November). Insect octopamine receptors: A new classification scheme based on studies of cloned *Drosophila* G-protein coupled receptors. *Invertebrate Neuroscience*, *5*(3), 111–118.

Evans, P. D., & Robb, S. (1993, August). Octopamine receptor subtypes and their modes of action. *Neurochemical Research*, *18*(8), 869–874.

Fayyazuddin, A., Zaheer, M. A., Hiesinger, P. R., & Bellen, H. J. (2006, February). The Nicotinic Acetylcholine Receptor Dα7 Is Required for an Escape Behavior in *Drosophila*. *PLOS Biology*, *4*(3), e63.

Fedorov, Y., Anderson, E. M., Birmingham, A., Reynolds, A., Karpilow, J., Robinson, K., ... Khvorova, A. (2006, July). Off-target effects by siRNA can induce toxic phenotype. *RNA*, *12*(7), 1188–1196.

Fei, H., Chow, D. M., Chen, A., Romero-Calderón, R., Ong, W. S., Ackerson, L. C., ... Krantz, D. E. (2010, May). Mutation of the *Drosophila* vesicular GABA transporter disrupts visual figure detection. *The Journal of Experimental Biology*, *213*(10), 1717–1730.

Feinberg, E. H., VanHoven, M. K., Bendesky, A., Wang, G., Fetter, R. D., Shen, K., & Bargmann, C. I. (2008, February). GFP Reconstitution Across Synaptic Partners (GRASP) Defines Cell Contacts and Synapses in Living Nervous Systems. *Neuron*, *57*(3), 353–363.

Fischbach, K. F., & Dittrich, A. P. M. (1989, December). The optic lobe of *Drosophila Melanogaster*. I. A Golgi analysis of wild-type structure. *Cell and Tissue Research*, *258*(3), 441–475.

Fisher, Y. E., Silies, M., & Clandinin, T. R. (2015, October). Orientation Selectivity Sharpens Motion Detection in *Drosophila*. *Neuron*, *88*(2), 390–402.

Freifeld, L., Clark, D. A., Schnitzer, M. J., Horowitz, M. A., & Clandinin, T. R. (2013, June). GABAergic Lateral Interactions Tune the Early Stages of Visual Processing in *Drosophila*. *Neuron*, *78*(6), 1075–1089.

Gateff, E. (1978, June). Malignant Neoplasms of Genetic Origin in *Drosophila Melanogaster*. *Science*, *200*(4349), 1448–1459.

Gengs, C., Leung, H.-T., Skingsley, D. R., Iovchev, M. I., Yin, Z., Semenov, E. P., ... Pak, W. L. (2002, November). The Target of *Drosophila* Photoreceptor Synaptic Transmission Is a Histamine-gated Chloride Channel Encoded by*ort* (*hclA*)*. *Journal of Biological Chemistry*, *277*(44), 42113–42120.

Germeraad, S., O'dowd, D., & Aldrich, R. W. (1992, January). Functional Assay of a Putative *Drosophila* Sodium Channel Gene in Homozygous Deficiency Neurons. *Journal of Neurogenetics*, *8*(1), 1–16.

Gisselmann, G., Plonka, J., Pusch, H., & Hatt, H. (2004, June). *Drosophila melanogaster* GRD and LCCH3 subunits form heteromultimeric GABA-gated cation channels. *British Journal of Pharmacology*, *142*(3), 409–413.

Gisselmann, G., Pusch, H., Hovemann, B. T., & Hatt, H. (2002, January). Two cDNAs coding for histamine-gated ion channels in D. melanogaster. *Nature Neuroscience*, *5*(1), 11–12.

Gohl, D. M., Silies, M. A., Gao, X. J., Bhalerao, S., Luongo, F. J., Lin, C.-C., ... Clandinin, T. R. (2011, March). A versatile in vivo system for directed dissection of gene expression patterns. *Nature Methods*, *8*(3), 231–237.

Götz, K. G. (1964, June). Optomotorische Untersuchung des visuellen systems einiger Augenmutanten der Fruchtfliege *Drosophila*. *Kybernetik*, *2*(2), 77–92.

Groschner, L. N., Malis, J. G., Zuidinga, B., & Borst, A. (2022, March). A biophysical account of multiplication by a single neuron. *Nature*, *603*(7899), 119–123.

Gruntman, E., Romani, S., & Reiser, M. B. (2018, February). Simple integration of fast excitation and offset, delayed inhibition computes directional selectivity in *Drosophila*. *Nature neuroscience*, *21*(2), 250–257.

Gruntman, E., & Turner, G. C. (2013, December). Integration of the olfactory code across dendritic claws of single mushroom body neurons. *Nature neuroscience*, *16*(12), 1821–1829.

Gu, H., & O'Dowd, D. K. (2006, January). Cholinergic Synaptic Transmission in Adult *Drosophila* Kenyon Cells In Situ. *The Journal of Neuroscience*, *26*(1), 265–272.

Haag, J., Arenz, A., Serbe, E., Gabbiani, F., & Borst, A. (2016, August). Complementary mechanisms create direction selectivity in the fly. *eLife*, *5*, e17421.

Haag, J., & Borst, A. (2002, April). Dendro-dendritic interactions between motion-sensitive large-field neurons in the fly. *The Journal of Neuroscience: The Official Journal of the Society for Neuroscience*, *22*(8), 3227–3233.

Haag, J., & Borst, A. (2004, June). Neural mechanism underlying complex receptive field properties of motion-sensitive interneurons. *Nature Neuroscience*, *7*(6), 628–634.

Haag, J., Mishra, A., & Borst, A. (2017, August). A common directional tuning mechanism of *Drosophila* motion-sensing neurons in the ON and in the OFF pathway. *eLife*, *6*, e29044.

Häcker, U., Nystedt, S., Barmchi, M. P., Horn, C., & Wimmer, E. A. (2003, June). piggyBac-based insertional mutagenesis in the presence of stably integrated P elements in *Drosophila*. *Proceedings of the National Academy of Sciences of the United States of America*, *100*(13), 7720–7725.

Halpern, M. E., Rhee, J., Goll, M. G., Akitake, C. M., Parsons, M., & Leach, S. D. (2008, June). Gal4/UAS Transgenic Tools and Their Application to Zebrafish. *Zebrafish*, *5*(2), 97–110.

Hamasaka, Y., Rieger, D., Parmentier, M.-L., Grau, Y., Helfrich-Förster, C., & Nässel, D. R. (2007). Glutamate and its metabotropic receptor in *Drosophila* clock neuron circuits. *Journal of Comparative Neurology*, *505*(1), 32–45.

Hanlon, C. D., & Andrew, D. J. (2015, October). Outside-in signaling – a brief review of GPCR signaling with a focus on the *Drosophila* GPCR family. *Journal of Cell Science*, *128*(19), 3533–3542.

Hardie, R. C. (1989, June). A histamine-activated chloride channel involved in neurotransmission at a photoreceptor synapse. *Nature*, *339*(6227), 704–706.

Harris, W. A., Stark, W. S., & Walker, J. A. (1976, April). Genetic dissection of the photoreceptor system in the compound eye of *Drosophila* melanogaster. *The Journal of Physiology*, *256*(2), 415–439.

Hassenstein, B., & Reichardt, W. (1956, October). Systemtheoretische Analyse der Zeit-, Reihenfolgen- und Vorzeichenauswertung bei der Bewegungsperzeption des Rüsselkäfers Chlorophanus. *Zeitschrift für Naturforschung B*, *11*(9-10), 513–524.

Hausen, K. (1976, October). Functional Characterization and Anatomical Identification of Motion Sensitive Neurons in the Lobula plate of the Blowfly Calliphora erythrocephala. *Zeitschrift für Naturforschung C*, *31*(9-10), 629–634.

Hearn, M. G., Ren, Y., McBride, E. W., Reveillaud, I., Beinborn, M., & Kopin, A. S. (2002, October). A *Drosophila* dopamine 2-like receptor: Molecular characterization and identification of multiple alternatively spliced variants. *Proceedings of the National Academy of Sciences of the United States of America*, *99*(22), 14554–14559.

Heidenreich, M., & Zhang, F. (2016, January). Applications of CRISPR-Cas systems in neuroscience. *Nature Reviews. Neuroscience*, *17*(1), 36–44.

Heisenberg, M., & Buchner, E. (1977, January). The rôle of retinula cell types in visual behavior of *Drosophila* melanogaster. *Journal of comparative physiology*, *117*(2), 127–162.

Hiesinger, P. R., Reiter, C., Schau, H., & Fischbach, K.-F. (1999, September). Neuropil Pattern Formation and Regulation of Cell Adhesion Molecules in *Drosophila* Optic Lobe Development Depend on Synaptobrevin. *The Journal of Neuroscience*, *19*(17), 7548–7556.

Hille, B. (1992). *Ionic channels of excitable membranes* (2nd edition ed.). Sunderland, Massachusetts USA: Sinauer Associates Inc.

Hirsh, J., & Davidson, N. (1981, June). Isolation and characterization of the dopa decarboxylase gene of *drosophila melanogaster*. *Molecular and Cellular Biology*, *1*(6), 475–485.

Hong, C. S., & Ganetzky, B. (1994, September). Spatial and temporal expression patterns of two sodium channel genes in *Drosophila*. *Journal of Neuroscience*, *14*(9), 5160–5169.

Hörmann, N., Schilling, T., Ali, A. H., Serbe, E., Mayer, C., Borst, A., & Pujol-Martí, J. (2020, May). A combinatorial code of transcription factors specifies subtypes of visual motion-sensing neurons in *Drosophila*. *Development (Cambridge, England)*, *147*(9), dev186296.

Housden, B. E., Muhar, M., Gemberling, M., Gersbach, C. A., Stainier, D. Y. R., Seydoux, G., ... Perrimon, N. (2017, January). Loss-of-function genetic tools for animal models: Cross-species and cross-platform differences. *Nature Reviews. Genetics*, *18*(1), 24–40.

Huang, W., Liu, M., Yan, S. F., & Yan, N. (2017, June). Structure-based assessment of disease-related mutations in human voltage-gated sodium channels. *Protein & Cell*, *8*(6), 401–438.

Hutcheon, B., & Yarom, Y. (2000, May). Resonance, oscillation and the intrinsic frequency preferences of neurons. *Trends in Neurosciences*, *23*(5), 216–222.

Ishimoto, H., Wang, Z., Rao, Y., Wu, C.-F., & Kitamoto, T. (2013, October). A Novel Role for Ecdysone in *Drosophila* Conditioned Behavior: Linking GPCR-Mediated Non-canonical Steroid Action to cAMP Signaling in the Adult Brain. *PLoS Genetics*, *9*(10).

Ito, K., Okada, R., Tanaka, N. K., & Awasaki, T. (2003). Cautionary observations on preparing and interpreting brain images using molecular biology-based staining techniques. *Microscopy Research and Technique*, *62*(2), 170–186.

Jackson, F. R., Newby, L. M., & Kulkarni, S. J. (1990). *Drosophila* GABAergic Systems: Sequence and Expression of Glutamic Acid Decarboxylase. *Journal of Neurochemistry*, *54*(3), 1068–1078.

Jan, L. Y., & Jan, Y. N. (1976). L-glutamate as an excitatory transmitter at the *Drosophila* larval neuromuscular junction. *The Journal of Physiology*, *262*(1), 215–236.

Jenett, A., Rubin, G. M., Ngo, T.-T. B., Shepherd, D., Murphy, C., Dionne, H., ... Zugates, C. T. (2012, October). A GAL4-Driver Line Resource for *Drosophila* Neurobiology. *Cell reports*, *2*(4), 991–1001.

Jin, L., Han, Z., Platisa, J., Wooltorton, J. R. A., Cohen, L. B., & Pieribone, V. A. (2012, September). Single Action Potentials and Subthreshold Electrical Events Imaged in Neurons with a Fluorescent Protein Voltage Probe. *Neuron*, *75*(5), 779–785.

Joesch, M., Plett, J., Borst, A., & Reiff, D. F. (2008, March). Response Properties of Motion-Sensitive Visual Interneurons in the Lobula Plate of *Drosophila Melanogaster*. *Current Biology*, *18*(5), 368–374.

Joesch, M., Schnell, B., Raghu, S. V., Reiff, D. F., & Borst, A. (2010, November). ON and OFF pathways in *Drosophila* motion vision. *Nature*, *468*(7321), 300–304.

Johnson, O., Becnel, J., & Nichols, C. D. (2009, February). Serotonin 5-HT2 and 5-HT1A-like receptors differentially modulate aggressive behaviors in *Drosophila Melanogaster*. *Neuroscience*, *158*(4), 1292–1300.

Jones, A. K., & Sattelle, D. B. (2006, September). The cys-loop ligand-gated ion channel superfamily of the honeybee, Apis mellifera. *Invertebrate Neuroscience*, *6*(3), 123–132.

Jumper, J., Evans, R., Pritzel, A., Green, T., Figurnov, M., Ronneberger, O., ... Hassabis, D. (2021, August). Highly accurate protein structure prediction with AlphaFold. *Nature*, *596*(7873), 583–589.

Juusola, M., & Hardie, R. C. (2001, January). Light Adaptation in *Drosophila* Photoreceptors. *The Journal of General Physiology*, *117*(1), 3–25.

Källberg, M., Wang, H., Wang, S., Peng, J., Wang, Z., Lu, H., & Xu, J. (2012, August). Template-based protein structure modeling using the RaptorX web server. *Nature Protocols*, *7*(8), 1511–1522.

Kanca, O., Zirin, J., Garcia-Marques, J., Knight, S. M., Yang-Zhou, D., Amador, G., ... Bellen, H. J. (2019, November). An efficient CRISPR-based strategy to insert small and large fragments of DNA using short homology arms. *eLife*, *8*, e51539.

Kanca, O., Zirin, J., Hu, Y., Tepe, B., Dutta, D., Lin, W.-W., ... Bellen, H. J. (2022, June). An expanded toolkit for *Drosophila* gene tagging using synthesized homology donor constructs for CRISPR-mediated homologous recombination. *eLife*, *11*, e76077.

Kandel, E. R. (2013). *Principles of Neural Science, Fifth Edition*. McGraw Hill Professional.

Kaplan, D. D., Zimmermann, G., Suyama, K., Meyer, T., & Scott, M. P. (2008, July). A nucleostemin family GTPase, NS3, acts in serotonergic neurons to regulate insulin signaling and control body size. *Genes & Development*, *22*(14), 1877–1893.

Kaplan, W. D., & Trout, W. E. (1969, February). The Behavior of Four Neurological Mutants of *Drosophila*. *Genetics*, *61*(2), 399–409.

Kasture, A. S., Hummel, T., Sucic, S., & Freissmuth, M. (2018, June). Big Lessons from Tiny Flies: *Drosophila Melanogaster* as a Model to Explore Dysfunction of Dopaminergic and Serotonergic Neurotransmitter Systems. *International Journal of Molecular Sciences*, *19*(6), 1788.

Kawakami, K., Asakawa, K., Hibi, M., Itoh, M., Muto, A., & Wada, H. (2016, January). Chapter Three - Gal4 Driver Transgenic Zebrafish: Powerful Tools to Study Developmental Biology, Organogenesis, and Neuroscience. In N. S. Foulkes (Ed.), *Advances in Genetics* (Vol. 95, pp. 65–87). Academic Press.

Kawasaki, F., Collins, S. C., & Ordway, R. W. (2002, July). Synaptic Calcium-Channel Function in *Drosophila*: Analysis and Transformation Rescue of

Temperature-Sensitive Paralytic and Lethal Mutations of Cacophony. *The Journal of Neuroscience*, *22*(14), 5856–5864.

Kelley, L. A., Mezulis, S., Yates, C. M., Wass, M. N., & Sternberg, M. J. E. (2015, June). The Phyre2 web portal for protein modeling, prediction and analysis. *Nature Protocols*, *10*(6), 845–858.

Ki, Y., & Lim, C. (2019, July). Sleep-promoting effects of threonine link amino acid metabolism in *Drosophila* neuron to GABAergic control of sleep drive. *eLife*, *8*, e40593.

Kim, J. S., Greene, M. J., Zlateski, A., Lee, K., Richardson, M., Turaga, S. C., ... Seung, H. S. (2014, May). Space–time wiring specificity supports direction selectivity in the retina. *Nature*, *509*(7500), 331–336.

Kitamoto, T. (2001, May). Conditional modification of behavior in *Drosophila* by targeted expression of a temperature-sensitive shibire allele in defined neurons. *Journal of Neurobiology*, *47*(2), 81–92.

Klapoetke, N. C., Murata, Y., Kim, S. S., Pulver, S. R., Birdsey-Benson, A., Cho, Y. K., ... Boyden, E. S. (2014, March). Independent optical excitation of distinct neural populations. *Nature Methods*, *11*(3), 338–346.

Köhler, G., & Milstein, C. (1975, August). Continuous cultures of fused cells secreting antibody of predefined specificity. *Nature*, *256*(5517), 495–497.

Kondo, S., Takahashi, T., Yamagata, N., Imanishi, Y., Katow, H., Hiramatsu, S., ... Tanimoto, H. (2020, January). Neurochemical Organization of the *Drosophila* Brain Visualized by Endogenously Tagged Neurotransmitter Receptors. *Cell Reports*, *30*(1), 284-297.e5.

Koushika, S. P., Lisbin, M. J., & White, K. (1996, December). ELAV, a *Drosophila* neuron-specific protein, mediates the generation of an alternatively spliced neural protein isoform. *Current Biology*, *6*(12), 1634–1641.

Krapp, H. G., & Hengstenberg, R. (1996, December). Estimation of self-motion by optic flow processing in single visual interneurons. *Nature*, *384*(6608), 463–466.

Kuehn, C., & Duch, C. (2013, March). Putative Excitatory and Putative Inhibitory Inputs Localize to Different Dendritic Domains in a *Drosophila* Flight Motoneuron. *The European journal of neuroscience*, *37*(6), 860–875.

Kulkarni, N. H., Yamamoto, A. H., Robinson, K. O., Mackay, T. F. C., & Anholt, R. R. H. (2002, August). The DSC1 Channel, Encoded by the smi60E Locus,

Contributes to Odor-Guided Behavior in *Drosophila Melanogaster*. *Genetics*, *161*(4), 1507–1516.

Kunishima, N., Shimada, Y., Tsuji, Y., Sato, T., Yamamoto, M., Kumasaka, T., ... Morikawa, K. (2000, October). Structural basis of glutamate recognition by a dimeric metabotropic glutamate receptor. *Nature*, *407*(6807), 971–977.

Kvon, E. Z., Kazmar, T., Stampfel, G., Yáñez-Cuna, J. O., Pagani, M., Schernhuber, K., ... Stark, A. (2014, August). Genome-scale functional characterization of *Drosophila* developmental enhancers in vivo. *Nature*, *512*(7512), 91–95.

Langer, S. J., Ghafoori, A. P., Byrd, M., & Leinwand, L. (2002, July). A genetic screen identifies novel non-compatible loxP sites. *Nucleic Acids Research*, *30*(14), 3067–3077.

Lansdell, S. J., Collins, T., Goodchild, J., & Millar, N. S. (2012). The *Drosophila* nicotinic acetylcholine receptor subunits Dα5 and Dα7 form functional homomeric and heteromeric ion channels. *BMC Neuroscience*, *13*, 73.

Lansdell, S. J., & Millar, N. S. (2004). Molecular characterization of Dα6 and Dα7 nicotinic acetylcholine receptor subunits from *Drosophila*: Formation of a high-affinity α-bungarotoxin binding site revealed by expression of subunit chimeras. *Journal of Neurochemistry*, *90*(2), 479–489.

Leaver-Fay, A., Tyka, M., Lewis, S. M., Lange, O. F., Thompson, J., Jacak, R., ... Bradley, P. (2011). ROSETTA3: An object-oriented software suite for the simulation and design of macromolecules. *Methods in Enzymology*, *487*, 545–574.

Lee, D., & O'Dowd, D. K. (1999, July). Fast Excitatory Synaptic Transmission Mediated by Nicotinic Acetylcholine Receptors in *Drosophila* Neurons. *Journal of Neuroscience*, *19*(13), 5311–5321.

Lee, D., Su, H., & O'Dowd, D. K. (2003, June). GABA Receptors Containing Rdl Subunits Mediate Fast Inhibitory Synaptic Transmission in *Drosophila* Neurons. *Journal of Neuroscience*, *23*(11), 4625–4634.

Lee, H. K., Barbarosie, M., Kameyama, K., Bear, M. F., & Huganir, R. L. (2000, June). Regulation of distinct AMPA receptor phosphorylation sites during bidirectional synaptic plasticity. *Nature*, *405*(6789), 955–959.

Lee, P. T., Zirin, J., Kanca, O., Lin, W.-W., Schulze, K. L., Li-Kroeger, D., ... Bellen, H. J. (2018, March). A gene-specific T2A-GAL4 library for *Drosophila*. *eLife*, *7*, e35574.

Leong, J. C. S., Esch, J. J., Poole, B., Ganguli, S., & Clandinin, T. R. (2016, August). Direction Selectivity in *Drosophila* Emerges from Preferred-Direction Enhancement and Null-Direction Suppression. *The Journal of Neuroscience: The Official Journal of the Society for Neuroscience*, *36*(31), 8078–8092.

Li, H.-H., Kroll, J. R., Lennox, S. M., Ogundeyi, O., Jeter, J., Depasquale, G., & Truman, J. W. (2014, August). A GAL4 Driver Resource for Developmental and Behavioral Studies on the Larval CNS of *Drosophila*. *Cell Reports*, *8*(3), 897–908.

Li, J., bing Zhang, B., gang Ren, Y., ye Gu, S., hang Xiang, Y., Huang, C., & Du, J.-l. (2015, May). Intron targeting-mediated and endogenous gene integrity-maintaining knockin in zebrafish using the CRISPR/Cas9 system. *Cell Research*, *25*(5), 634–637.

Lin, W.-H., Günay, C., Marley, R., Prinz, A. A., & Baines, R. A. (2012, May). Activity-Dependent Alternative Splicing Increases Persistent Sodium Current and Promotes Seizure. *The Journal of Neuroscience*, *32*(21), 7267–7277.

Lin, W.-H., Wright, D. E., Muraro, N. I., & Baines, R. A. (2009, September). Alternative Splicing in the Voltage-Gated Sodium Channel DmNav Regulates Activation, Inactivation, and Persistent Current. *Journal of Neurophysiology*, *102*(3), 1994–2006.

Littleton, J. T., & Ganetzky, B. (2000, April). Ion channels and synaptic organization: Analysis of the *Drosophila* genome. *Neuron*, *26*(1), 35–43.

Liu, W. W., & Wilson, R. I. (2013, June). Glutamate is an inhibitory neurotransmitter in the *Drosophila* olfactory system. *Proceedings of the National Academy of Sciences of the United States of America*, *110*(25), 10294–10299.

Liu, X., Krause, W. C., & Davis, R. L. (2007, December). GABAA receptor RDL inhibits *Drosophila* olfactory associative learning. *Neuron*, *56*(6), 1090–1102.

Livingstone, M. S., & Tempel, B. L. (1983). Genetic dissection of monoamine neurotransmitter synthesis in *Drosophila*. *Nature*, *303*(5912), 67–70.

Long, S. B., Campbell, E. B., & MacKinnon, R. (2005, August). Crystal Structure of a Mammalian Voltage-Dependent Shaker Family K+ Channel. *Science*, *309*(5736), 897–903.

Loughney, K., Kreber, R., & Ganetzky, B. (1989, September). Molecular analysis of the *para* locus, a sodium channel gene in *Drosophila*. *Cell*, *58*(6), 1143–1154.

Luo, J., Ting, C.-Y., Li, Y., McQueen, P., Lin, T.-Y., Hsu, C.-P., & Lee, C.-H. (2020, March). Antagonistic regulation by insulin-like peptide and activin ensures the elaboration of appropriate dendritic field sizes of amacrine neurons. *eLife*, *9*, e50568.

Lüthi, A., & McCormick, D. A. (1998, July). H-current: Properties of a neuronal and network pacemaker. *Neuron*, *21*(1), 9–12.

Magee, J. C. (1998, October). Dendritic Hyperpolarization-Activated Currents Modify the Integrative Properties of Hippocampal CA1 Pyramidal Neurons. *Journal of Neuroscience*, *18*(19), 7613–7624.

Maisak, M. S., Haag, J., Ammer, G., Serbe, E., Meier, M., Leonhardt, A., ... Borst, A. (2013, August). A directional tuning map of *Drosophila* elementary motion detectors. *Nature*, *500*(7461), 212–216.

Manning, L., Heckscher, E. S., Purice, M. D., Roberts, J., Bennett, A. L., Kroll, J. R., ... Doe, C. Q. (2012, October). A Resource for Manipulating Gene Expression and Analyzing *cis*-Regulatory Modules in the *Drosophila* CNS. *Cell Reports*, *2*(4), 1002–1013.

Manseau, L., Baradaran, A., Brower, D., Budhu, A., Elefant, F., Phan, H., ... Selleck, S. (1997). GAL4 enhancer traps expressed in the embryo, larval brain, imaginal discs, and ovary of *Drosophila*. *Developmental Dynamics*, *209*(3), 310–322.

Maqueira, B., Chatwin, H., & Evans, P. D. (2005). Identification and characterization of a novel family of *Drosophila*β-adrenergic-like octopamine G-protein coupled receptors. *Journal of Neurochemistry*, *94*(2), 547–560.

Martin, C. A., & Krantz, D. E. (2014, July). *Drosophila melanogaster* as a genetic model system to study neurotransmitter transporters. *Neurochemistry International*, *73*, 71–88.

Marty, A. (1983, February). Blocking of large unitary calcium-dependent potassium currents by internal sodium ions. *Pflügers Archiv*, *396*(2), 179–181.

Matz, M. V., Fradkov, A. F., Labas, Y. A., Savitsky, A. P., Zaraisky, A. G., Markelov, M. L., & Lukyanov, S. A. (1999, October). Fluorescent proteins from nonbioluminescent Anthozoa species. *Nature Biotechnology*, *17*(10), 969–973.

Mauss, A. S., Busch, C., & Borst, A. (2017, October). Optogenetic Neuronal Silencing in *Drosophila* during Visual Processing. *Scientific Reports*, *7*(1), 13823.

Mauss, A. S., Meier, M., Serbe, E., & Borst, A. (2014, February). Optogenetic and Pharmacologic Dissection of Feedforward Inhibition in *Drosophila* Motion Vision. *Journal of Neuroscience*, *34*(6), 2254–2263.

Mauss, A. S., Pankova, K., Arenz, A., Nern, A., Rubin, G. M., & Borst, A. (2015, July). Neural Circuit to Integrate Opposing Motions in the Visual Field. *Cell*, *162*(2), 351–362.

McGuire, S. E., Mao, Z., & Davis, R. L. (2004, February). Spatiotemporal gene expression targeting with the TARGET and gene-switch systems in *Drosophila*. *Science's STKE: signal transduction knowledge environment*, *2004*(220), pl6.

Meier, M., Serbe, E., Maisak, M. S., Haag, J., Dickson, B. J., & Borst, A. (2014, February). Neural Circuit Components of the *Drosophila* OFF Motion Vision Pathway. *Current Biology*, *24*(4), 385–392.

Meinertzhagen, I. A., & O'Neil, S. D. (1991). Synaptic organization of columnar elements in the lamina of the wild type in *Drosophila* melanogaster. *Journal of Comparative Neurology*, *305*(2), 232–263.

Mezler, M., Müller, T., & Raming, K. (2001, February). Cloning and functional expression of GABA(B) receptors from *Drosophila*. *The European Journal of Neuroscience*, *13*(3), 477–486.

Millar, N. S., Baylis, H. A., Reaper, C., Bunting, R., Mason, W. T., & Sattelle, D. B. (1995, September). Functional expression of a cloned *Drosophila* muscarinic acetylcholine receptor in a stable *Drosophila* cell line. *The Journal of Experimental Biology*, *198*(Pt 9), 1843–1850.

Miller, A. C., & Pereda, A. E. (2017, May). The electrical synapse – molecular complexities at the gap and beyond. *Developmental neurobiology*, *77*(5), 562.

Mirzoyan, Z., Sollazzo, M., Allocca, M., Valenza, A. M., Grifoni, D., & Bellosta, P. (2019, March). *Drosophila melanogaster*: A Model Organism to Study Cancer. *Frontiers in Genetics*, *10*, 51.

Mitri, C., Parmentier, M.-L., Pin, J.-P., Bockaert, J., & Grau, Y. (2004, March). Divergent Evolution in Metabotropic Glutamate Receptors: A NEW RECEPTOR ACTIVATED BY AN ENDOGENOUS LIGAND DIFFERENT FROM GLUTAMATE IN INSECTS*. *Journal of Biological Chemistry*, *279*(10), 9313–9320.

Molina-Obando, S., Vargas-Fique, J. F., Henning, M., Gür, B., Schladt, T. M., Akhtar, J., ... Silies, M. (2019, September). ON selectivity in the *Drosophila* visual system is a multisynaptic process involving both glutamatergic and GABAergic inhibition. *eLife*, *8*, e49373.

Morante, J., & Desplan, C. (2008, April). The Color-Vision Circuit in the Medulla of *Drosophila*. *Current Biology*, *18*(8), 553–565.

Moreno, E., Basler, K., & Morata, G. (2002, April). Cells compete for Decapentaplegic survival factor to prevent apoptosis in *Drosophila* wing development. *Nature*, *416*(6882), 755–759.

Morgan, T., & Cattell, E. (1912). Data for the Study of Sex-linked Inheritance in *Drosophila*. *Journal of Experimental Zoology*, *13*, 79–102.

Mosca, T. J., & Luo, L. (2014, October). Synaptic organization of the *Drosophila* antennal lobe and its regulation by the Teneurins. *eLife*, *3*, e03726.

Myers, E. W., Sutton, G. G., Delcher, A. L., Dew, I. M., Fasulo, D. P., Flanigan, M. J., ... Venter, J. C. (2000, March). A Whole-Genome Assembly of *Drosophila*. *Science*, *287*(5461), 2196–2204.

Nagarkar-Jaiswal, S., DeLuca, S. Z., Lee, P.-T., Lin, W.-W., Pan, H., Zuo, Z., ... Bellen, H. J. (2015, June). A genetic toolkit for tagging intronic MiMIC containing genes. *eLife*, *4*, e08469.

Nagarkar-Jaiswal, S., Lee, P.-T., Campbell, M. E., Chen, K., Anguiano-Zarate, S., Cantu Gutierrez, M., ... Bellen, H. J. (2015, March). A library of MiMICs allows tagging of genes and reversible, spatial and temporal knockdown of proteins in *Drosophila*. *eLife*, *4*, e05338.

Nagel, G., Szellas, T., Huhn, W., Kateriya, S., Adeishvili, N., Berthold, P., ... Bamberg, E. (2003, November). Channelrhodopsin-2, a directly light-gated cation-selective membrane channel. *Proceedings of the National Academy of Sciences of the United States of America*, *100*(24), 13940–13945.

Nakai, J., Ohkura, M., & Imoto, K. (2001, February). A high signal-to-noise Ca2+ probe composed of a single green fluorescent protein. *Nature Biotechnology*, *19*(2), 137–141.

Nakane, P. K., & Pierce, G. B. (1967, May). Enzyme-labeled antibodies for the light and electron microscopic localization of tissue antigens. *The Journal of Cell Biology*, *33*(2), 307–318.

Nashmi, R., Dickinson, M. E., McKinney, S., Jareb, M., Labarca, C., Fraser, S. E., & Lester, H. A. (2003, December). Assembly of $A4\beta2$ Nicotinic Acetylcholine Receptors Assessed with Functional Fluorescently Labeled Subunits: Effects of Localization, Trafficking, and Nicotine-Induced Upregulation in Clonal Mammalian Cells and in Cultured Midbrain Neurons. *Journal of Neuroscience*, *23*(37), 11554–11567.

Neckameyer, W. S., Coleman, C. M., Eadie, S., & Goodwin, S. F. (2007). Compartmentalization of neuronal and peripheral serotonin synthesis in *Drosophila Melanogaster*. *Genes, Brain and Behavior*, *6*(8), 756–769.

Neckameyer, W. S., & White, K. (1992, February). A single locus encodes both phenylalanine hydroxylase and tryptophan hydroxylase activities in *Drosophila*. *Journal of Biological Chemistry*, *267*(6), 4199–4206.

Nern, A., Pfeiffer, B. D., & Rubin, G. M. (2015, June). Optimized tools for multicolor stochastic labeling reveal diverse stereotyped cell arrangements in the fly visual system. *Proceedings of the National Academy of Sciences of the United States of America*, *112*(22), E2967-2976.

Ni, J.-Q., Liu, L.-P., Binari, R., Hardy, R., Shim, H.-S., Cavallaro, A., ... Perrimon, N. (2009, August). A *Drosophila* resource of transgenic RNAi lines for neurogenetics. *Genetics*, *182*(4), 1089–1100.

Nichols, C. D. (2007, May). 5-HT2 receptors in *Drosophila* are expressed in the brain and modulate aspects of circadian behaviors. *Developmental Neurobiology*, *67*(6), 752–763.

Nienhaus, K., & Nienhaus, G. U. (2022, July). Genetically encodable fluorescent protein markers in advanced optical imaging. *Methods and Applications in Fluorescence*, *10*(4).

Nitz, D. A., van Swinderen, B., Tononi, G., & Greenspan, R. J. (2002, November). Electrophysiological Correlates of Rest and Activity in *Drosophila Melanogaster*. *Current Biology*, *12*(22), 1934–1940.

Okamoto, H., Sakai, K., Goto, S., Takasu-Ishikawa, E., & Hotta, Y. (1987). Isolation of *Drosophila* Genomic Clones Homologous to the Eel Sodium Channel Gene. *Proceedings of the Japan Academy, Series B*, *63*(7), 284–288.

Olsen, S. R., & Wilson, R. I. (2008, October). Cracking neural circuits in a tiny brain: New approaches for understanding the neural circuitry of *Drosophila*. *Trends in Neurosciences*, *31*(10), 512–520.

Ortells, M. O., Barrantes, G. E., Wood, C., Lunt, G. G., & Barrantes, F. J. (1997, May). Molecular modelling of the nicotinic acetylcholine receptor transmembrane region in the open state. *Protein Engineering*, *10*(5), 511–517.

O'Tousa, J. E., Baehr, W., Martin, R. L., Hirsh, J., Pak, W. L., & Applebury, M. L. (1985, April). The *Drosophila ninaE* gene encodes an opsin. *Cell*, *40*(4), 839–850.

Pankova, K., & Borst, A. (2016, September). RNA-Seq Transcriptome Analysis of Direction-Selective T4/T5 Neurons in *Drosophila*. *PLOS ONE*, *11*(9), e0163986.

Pankova, K., & Borst, A. (2017, April). Transgenic line for the identification of cholinergic release sites in *Drosophila Melanogaster*. *The Journal of Experimental Biology*, *220*(8), 1405–1410.

Papatsenko, D., Sheng, G., & Desplan, C. (1997, May). A new rhodopsin in R8 photoreceptors of *Drosophila*: Evidence for coordinate expression with Rh3 in R7 cells. *Development*, *124*(9), 1665–1673.

Perkins, L. A., Holderbaum, L., Tao, R., Hu, Y., Sopko, R., McCall, K., ... Perrimon, N. (2015, November). The Transgenic RNAi Project at Harvard Medical School: Resources and Validation. *Genetics*, *201*(3), 843–852.

Pfeiffer, B. D., Jenett, A., Hammonds, A. S., Ngo, T.-T. B., Misra, S., Murphy, C., ... Rubin, G. M. (2008, July). Tools for neuroanatomy and neurogenetics in *Drosophila*. *Proceedings of the National Academy of Sciences of the United States of America*, *105*(28), 9715–9720.

Pfeiffer, B. D., Ngo, T.-T. B., Hibbard, K. L., Murphy, C., Jenett, A., Truman, J. W., & Rubin, G. M. (2010, October). Refinement of Tools for Targeted Gene Expression in *Drosophila*. *Genetics*, *186*(2), 735–755.

Port, F., Chen, H.-M., Lee, T., & Bullock, S. L. (2014, July). Optimized CRISPR/Cas tools for efficient germline and somatic genome engineering in *Drosophila*. *Proceedings of the National Academy of Sciences of the United States of America*, *111*(29), E2967-2976.

Port, F., Strein, C., Stricker, M., Rauscher, B., Heigwer, F., Zhou, J., ... Boutros, M. (2020, February). A large-scale resource for tissue-specific CRISPR mutagenesis in *Drosophila*. *eLife*, *9*, e53865.

Purves, D., Augustine, G. J., Fitzpatrick, D., Katz, L. C., LaMantia, A.-S., O McNamara, J., & Williams, M. (2001). *Neuroscience* (2nd ed.). Sinauer Associates.

Qin, B., Humberg, T.-H., Kim, A., Kim, H. S., Short, J., Diao, F., ... Yuan, Q. (2019, September). Muscarinic acetylcholine receptor signaling generates OFF selectivity in a simple visual circuit. *Nature Communications*, *10*, 4093.

Qu, Y., & Dahl, G. (2002, January). Function of the voltage gate of gap junction channels: Selective exclusion of molecules. *Proceedings of the National Academy of Sciences*, *99*(2), 697–702.

Raghu, S. V., Joesch, M., Sigrist, S. J., Borst, A., & Reiff, D. F. (2009, January). Synaptic Organization of Lobula Plate Tangential Cells in *Drosophila*: Dα7 Cholinergic Receptors. *Journal of Neurogenetics*, *23*(1-2), 200–209.

Rahman, S., & Evans, W. H. (1991, November). Topography of connexin32 in rat liver gap junctions : Evidence for an intramolecular disulphide linkage connecting the two extracellular peptide loops. *Journal of Cell Science*, *100*(3), 567–578.

Ramón y Cajal, S., Sánchez, D. D., & Universidad Complutense de Madrid. Laboratorio de Investigaciones Biológicas. (1915). *Contribución al conocimiento de los centros nerviosos de los insectos*. Madrid : Imprenta de Hijos de Nicolás Moya.

Ranson, D. C., Ayoub, S. S., Corcoran, O., & Casalotti, S. O. (2020, March). Pharmacological targeting of the GABAB receptor alters *Drosophila*'s behavioural responses to alcohol. *Addiction Biology*, *25*(2).

Ready, D. F., Hanson, T. E., & Benzer, S. (1976, October). Development of the *drosophila* retina, a neurocrystalline lattice. *Developmental Biology*, *53*(2), 217–240.

Reiner, A., & Levitz, J. (2018, June). Glutamatergic Signaling in the Central Nervous System: Ionotropic and Metabotropic Receptors in Concert. *Neuron*, *98*(6), 1080–1098.

Riemensperger, T., Isabel, G., Coulom, H., Neuser, K., Seugnet, L., Kume, K., ... Birman, S. (2011, January). Behavioral consequences of dopamine deficiency in the *Drosophila* central nervous system. *Proceedings of the National Academy of Sciences of the United States of America*, *108*(2), 834–839.

Robinson, R. B., & Siegelbaum, S. A. (2003). Hyperpolarization-activated cation currents: From molecules to physiological function. *Annual Review of Physiology*, *65*, 453–480.

Root, C. M., Masuyama, K., Green, D. S., Enell, L. E., Nässel, D. R., Lee, C.-H., & Wang, J. W. (2008, July). A presynaptic gain control mechanism fine-tunes olfactory behavior. *Neuron*, *59*(2), 311–321.

Sanfilippo, P., Kim, A. J., Bhukel, A., Yoo, J., Mirshahidi, P. S., Pandey, V., ... Zipursky, S. L. (2024, March). Mapping of multiple neurotransmitter receptor subtypes and distinct protein complexes to the connectome. *Neuron*, *112*(6), 942-958.e13.

Sarov, M., Barz, C., Jambor, H., Hein, M. Y., Schmied, C., Suchold, D., ... Schnorrer, F. (2016, February). A genome-wide resource for the analysis of protein localisation in *Drosophila*. *eLife*, *5*, e12068.

Scheffer, L. K., Xu, C. S., Januszewski, M., Lu, Z., Takemura, S.-y., Hayworth, K. J., ... Plaza, S. M. (2020, September). A connectome and analysis of the adult *Drosophila* central brain. *eLife*, *9*, e57443.

Schilling, T., & Borst, A. (2015, July). Local motion detectors are required for the computation of expansion flow-fields. *Biology Open*, *4*(9), 1105–1108.

Schnell, B., Joesch, M., Forstner, F., Raghu, S. V., Otsuna, H., Ito, K., ... Reiff, D. F. (2010, March). Processing of horizontal optic flow in three visual interneurons of the *Drosophila* brain. *Journal of Neurophysiology*, *103*(3), 1646–1657.

Schnell, B., Raghu, S. V., Nern, A., & Borst, A. (2012). Columnar cells necessary for motion responses of wide-field visual interneurons in *Drosophila*. *Journal of Comparative Physiology. A, Neuroethology, Sensory, Neural, and Behavioral Physiology*, *198*(5), 389–395.

Schwaerzel, M., Monastirioti, M., Scholz, H., Friggi-Grelin, F., Birman, S., & Heisenberg, M. (2003, November). Dopamine and octopamine differentiate between aversive and appetitive olfactory memories in *Drosophila*. *The Journal of Neuroscience: The Official Journal of the Society for Neuroscience*, *23*(33), 10495–10502.

Scott, E. K., Raabe, T., & Luo, L. (2002). Structure of the vertical and horizontal system neurons of the lobula plate in *Drosophila*. *Journal of Comparative Neurology*, *454*(4), 470–481.

Serbe, E., Meier, M., Leonhardt, A., & Borst, A. (2016, February). Comprehensive Characterization of the Major Presynaptic Elements to the *drosophila* OFF Motion Detector. *Neuron*, *89*(4), 829–841.

Shemetov, A. A., Oliinyk, O. S., & Verkhusha, V. V. (2017, June). How to Increase Brightness of Near-Infrared Fluorescent Proteins in Mammalian Cells. *Cell Chemical Biology*, *24*(6), 758-766.e3.

Shimomura, O., Johnson, F. H., & Saiga, Y. (1962). Extraction, Purification and Properties of Aequorin, a Bioluminescent Protein from the Luminous Hydromedusan, Aequorea. *Journal of Cellular and Comparative Physiology*, *59*(3), 223–239.

Shinomiya, K., Huang, G., Lu, Z., Parag, T., Xu, C. S., Aniceto, R., ... Meinertzhagen, I. A. (2019, January). Comparisons between the ON- and OFF-edge motion pathways in the *Drosophila* brain. *eLife*, *8*, e40025.

Shinomiya, K., Karuppudurai, T., Lin, T.-Y., Lu, Z., Lee, C.-H., & Meinertzhagen, I. A. (2014, May). Candidate neural substrates for off-edge motion detection in *Drosophila*. *Current biology: CB*, *24*(10), 1062–1070.

Sine, S. M., & Engel, A. G. (2006, March). Recent advances in Cys-loop receptor structure and function. *Nature*, *440*(7083), 448–455.

Skerrett, I. M., & Williams, J. B. (2017). A structural and functional comparison of gap junction channels composed of connexins and innexins. *Developmental Neurobiology*, *77*(5), 522–547.

Smendziuk, C. M., Messenberg, A., Vogl, A. W., & Tanentzapf, G. (2015, August). Bi-directional gap junction-mediated soma-germline communication is essential for spermatogenesis. *Development*, *142*(15), 2598–2609.

Smith, L. A., Wang, X., Peixoto, A. A., Neumann, E. K., Hall, L. M., & Hall, J. C. (1996, December). A *Drosophila* Calcium Channel *A*1 Subunit Gene Maps to a Genetic Locus Associated with Behavioral and Visual Defects. *The Journal of Neuroscience*, *16*(24), 7868–7879.

Sobolevsky, A. I. (2015, January). Structure and gating of tetrameric glutamate receptors. *The Journal of Physiology*, *593*(Pt 1), 29–38.

Spéder, P., & Brand, A. H. (2014, August). Gap Junction Proteins in the Blood-Brain Barrier Control Nutrient-Dependent Reactivation of *Drosophila* Neural Stem Cells. *Developmental Cell*, *30*(3), 309–321.

Spradling, A. C., & Rubin, G. M. (1982, October). Transposition of Cloned P Elements into *Drosophila* Germ Line Chromosomes. *Science*, *218*(4570), 341–347.

Stevens, N. M. (1908). A study of the germ cells of certain diptera, with reference to the heterochromosomes and the phenomena of synapsis. *Journal of Experimental Zoology*, *5*(3), 359–374.

Strausfeld, N. J. (1971, September). The organization of the insect visual system (Light microscopy). *Zeitschrift für Zellforschung und Mikroskopische Anatomie*, *121*(3), 377–441.

Su, H., & O'Dowd, D. K. (2003, October). Fast Synaptic Currents in *Drosophila* Mushroom Body Kenyon Cells Are Mediated by α-Bungarotoxin-Sensitive Nicotinic Acetylcholine Receptors and Picrotoxin-Sensitive GABA Receptors. *Journal of Neuroscience*, *23*(27), 9246–9253.

Suver, M. P., Huda, A., Iwasaki, N., Safarik, S., & Dickinson, M. H. (2016, November). An Array of Descending Visual Interneurons Encoding Self-Motion in *Drosophila*. *The Journal of Neuroscience*, *36*(46), 11768–11780.

Suzuki, D. T., Grigliatti, T., & Williamson, R. (1971, May). Temperature-Sensitive Mutations in *Drosophila Melanogaster*, VII. A Mutation (parats) Causing Reversible Adult Paralysis. *Proceedings of the National Academy of Sciences*, *68*(5), 890–893.

Suzuki, Y., Schenk, J. E., Tan, H., & Gaudry, Q. (2020, March). A population of interneurons signals changes in the basal concentration of serotonin and mediates gain control in the *Drosophila* antennal lobe. *Current biology : CB*, *30*(6), 1110-1118.e4.

Sweeney, S. T., Broadie, K., Keane, J., Niemann, H., & O'Kane, C. J. (1995, February). Targeted expression of tetanus toxin light chain in *Drosophila* specifically eliminates synaptic transmission and causes behavioral defects. *Neuron*, *14*(2), 341–351.

Takemura, S.-y., Bharioke, A., Lu, Z., Nern, A., Vitaladevuni, S., Rivlin, P. K., ... Chklovskii, D. B. (2013, August). A visual motion detection circuit suggested by Drosophila connectomics. *Nature*, *500*(7461), 175–181.

Takemura, S.-y., Karuppudurai, T., Ting, C.-Y., Lu, Z., Lee, C.-H., & Meinertzhagen, I. A. (2011, December). Cholinergic Circuits Integrate Neighboring Visual Signals in a *Drosophila* Motion Detection Pathway. *Current Biology*, *21*(24), 2077–2084.

Takemura, S.-Y., Lu, Z., & Meinertzhagen, I. A. (2008). Synaptic circuits of the *Drosophila* optic lobe: The input terminals to the medulla. *Journal of Comparative Neurology*, *509*(5), 493–513.

ya Takemura, S., Nern, A., Chklovskii, D. B., Scheffer, L. K., Rubin, G. M., & Meinertzhagen, I. A. (2017, April). The comprehensive connectome of a neural substrate for 'ON' motion detection in *Drosophila*. *eLife*, *6*, e24394.

Tanouye, M. A., Ferrus, A., & Fujita, S. C. (1981, October). Abnormal action potentials associated with the Shaker complex locus of *Drosophila*. *Proceedings of the National Academy of Sciences*, *78*(10), 6548–6552.

Tchumatchenko, T., & Clopath, C. (2014, November). Oscillations emerging from noise-driven steady state in networks with electrical synapses and subthreshold resonance. *Nature Communications*, *5*(1), 5512.

Terlau, H., & Stühmer, W. (1998, September). Structure and Function of Voltage-Gated Ion Channels. *Naturwissenschaften*, *85*(9), 437–444.

Tseng-Crank, J., Pollock, J. A., Hayashi, I., & Tanouye, M. A. (1991, January). Expression of ion Channel Genes in *Drosophila*. *Journal of Neurogenetics*, *7*(4), 229–239.

Tsien, R. Y. (1998, July). THE GREEN FLUORESCENT PROTEIN. *Annual Review of Biochemistry*, *67*(Volume 67, 1998), 509–544.

Tsunoda, S., & Salkoff, L. (1995, March). Genetic analysis of *Drosophila* neurons: Shal, Shaw, and Shab encode most embryonic potassium currents. *The Journal of Neuroscience: The Official Journal of the Society for Neuroscience*, *15*(3 Pt 1), 1741–1754.

Unger, V. M., Kumar, N. M., Gilula, N. B., & Yeager, M. (1999, February). Three-Dimensional Structure of a Recombinant Gap Junction Membrane Channel. *Science*, *283*(5405), 1176–1180.

Venken, K. J. T., Schulze, K. L., Haelterman, N. A., Pan, H., He, Y., Evans-Holm, M., ... Bellen, H. J. (2011, September). MiMIC: A highly versatile transposon insertion resource for engineering *Drosophila Melanogaster* genes. *Nature Methods*, *8*(9), 737–743.

Viswanathan, S., Williams, M. E., Bloss, E. B., Stasevich, T. J., Speer, C. M., Nern, A., ... Looger, L. L. (2015, June). High-performance probes for light and electron microscopy. *Nature methods*, *12*(6), 568–576.

Waddell, J., Kim, J., Alger, B. E., & McCarthy, M. M. (2011). The depolarizing action of GABA in cultured hippocampal neurons is not due to the absence of ketone bodies. *PloS One*, *6*(8), e23020.

Waddell, S. (2013, June). Reinforcement signalling in *Drosophila*; dopamine does it all after all. *Current Opinion in Neurobiology*, *23*(3), 324–329.

Wardill, T. J., List, O., Li, X., Dongre, S., McCulloch, M., Ting, C.-Y., ... Juusola, M. (2012, May). Multiple Spectral Inputs Improve Motion Discrimination in the *Drosophila* Visual System. *Science*, *336*(6083), 925–931.

Waterhouse, A., Bertoni, M., Bienert, S., Studer, G., Tauriello, G., Gumienny, R., ... Schwede, T. (2018, July). SWISS-MODEL: Homology modelling of protein structures and complexes. *Nucleic Acids Research*, *46*(Web Server issue), W296-W303.

Weaver, L. N., Ma, T., & Drummond-Barbosa, D. (2020, September). Analysis of Gal4 Expression Patterns in Adult *Drosophila* Females. *G3: Genes/Genomes/Genetics*, *10*(11), 4147–4158.

Wertz, A., Borst, A., & Haag, J. (2008, March). Nonlinear Integration of Binocular Optic Flow by DNOVS2, A Descending Neuron of the Fly. *The Journal of Neuroscience*, *28*(12), 3131–3140.

Wheeler, D. A., Kulkarni, S. J., Gailey, D. A., & Hall, J. C. (1990). "Spectral analysis of courtship songs in behavioral mutants of Drosophila melanogaster": Erratum. *Behavior Genetics*, *20*(2), 339–339.

White, D., de Sousa Abreu, R. P., Blake, A., Murphy, J., Showell, S., Kitamoto, T., & Lawal, H. O. (2020, July). Deficits in the vesicular acetylcholine transporter alter lifespan and behavior in adult *Drosophila Melanogaster*. *Neurochemistry international*, *137*, 104744.

Willems, J., de Jong, A. P. H., Scheefhals, N., Mertens, E., Catsburg, L. A. E., Poorthuis, R. B., ... MacGillavry, H. D. (2020, April). ORANGE: A CRISPR/Cas9-based genome editing toolbox for epitope tagging of endogenous proteins in neurons. *PLOS Biology*, *18*(4), e3000665.

Wilson, R. I., Turner, G. C., & Laurent, G. (2004, January). Transformation of Olfactory Representations in the *Drosophila* Antennal Lobe. *Science*, *303*(5656), 366–370.

Wolken, J. J., Capenos, J., & Turano, A. (1957, May). Photoreceptor Structures. *The Journal of Biophysical and Biochemical Cytology*, *3*(3), 441–448.

Wu, C.-F., Ganetzky, B., Haugland, F. N., & Liu, A.-X. (1983, June). Potassium Currents in *Drosophila*: Different Components Affected by Mutations of Two Genes. *Science*, *220*(4601), 1076–1078.

Wu, C.-L., Xia, S., Fu, T.-F., Wang, H., Chen, Y.-H., Leong, D., ... Tully, T. (2007, December). Specific requirement of NMDA receptors for long-term memory consolidation in Drosophila ellipsoid body. *Nature Neuroscience*, *10*(12), 1578–1586.

Wu, M. N., Joiner, W. J., Dean, T., Yue, Z., Smith, C. J., Chen, D., ... Koh, K. (2010, January). SLEEPLESS, a Ly-6/neurotoxin family member, regulates the levels, localization and activity of Shaker. *Nature Neuroscience*, *13*(1), 69–75.

Xia, R.-Y., Li, M.-Q., Wu, Y.-S., Qi, Y.-X., Ye, G.-Y., & Huang, J. (2016). A new family of insect muscarinic acetylcholine receptors. *Insect Molecular Biology*, *25*(4), 362–369.

Yamagata, N., Ichinose, T., Aso, Y., Plaçais, P.-Y., Friedrich, A. B., Sima, R. J., ... Tanimoto, H. (2015, January). Distinct dopamine neurons mediate reward signals for short- and long-term memories. *Proceedings of the National Academy of Sciences of the United States of America*, *112*(2), 578–583.

Yamaguchi, S., Wolf, R., Desplan, C., & Heisenberg, M. (2008, March). Motion vision is independent of color in *Drosophila*. *Proceedings of the National Academy of Sciences of the United States of America*, *105*(12), 4910–4915.

Yamamoto, S., Jaiswal, M., Charng, W.-L., Gambin, T., Karaca, E., Mirzaa, G., ... Bellen, H. J. (2014, September). A *Drosophila* Genetic Resource of Mutants to Study Mechanisms Underlying Human Genetic Diseases. *Cell*, *159*(1), 200–214.

Yang, H. H., & St-Pierre, F. (2016, September). Genetically Encoded Voltage Indicators: Opportunities and Challenges. *The Journal of Neuroscience*, *36*(39), 9977–9989.

Yuan, Q., Joiner, W. J., & Sehgal, A. (2006, June). A sleep-promoting role for the *Drosophila* serotonin receptor 1A. *Current biology: CB*, *16*(11), 1051–1062.

Yuan, Q., Lin, F., Zheng, X., & Sehgal, A. (2005, July). Serotonin modulates circadian entrainment in *Drosophila*. *Neuron*, *47*(1), 115–127.

Zhang, S. L., Yue, Z., Arnold, D. M., Artiushin, G., & Sehgal, A. (2018, March). A Circadian Clock in the Blood-Brain Barrier Regulates Xenobiotic Efflux. *Cell*, *173*(1), 130-139.e10.

Zhang, W., Koehler, K. F., Zhang, P., & Cook, J. M. (1995, January). Development of a comprehensive pharmacophore model for the benzodiazepine receptor. *Drug design and discovery*, *12*(3), 193–248.

Zheng, Y., Hirschberg, B., Yuan, J., Wang, A. P., Hunt, D. C., Ludmerer, S. W., ... Cully, D. F. (2002, January). Identification of Two Novel *Drosophila Melanogaster* Histamine-gated Chloride Channel Subunits Expressed in the Eye*. *Journal of Biological Chemistry*, *277*(3), 2000–2005.

Zheng, Z., Lauritzen, J. S., Perlman, E., Robinson, C. G., Nichols, M., Milkie, D., ... Bock, D. D. (2018, July). A Complete Electron Microscopy Volume of the Brain of Adult *Drosophila Melanogaster*. *Cell*, *174*(3), 730-743.e22.

Zhu, Y., Nern, A., Zipursky, S. L., & Frye, M. A. (2009, April). Peripheral Visual Circuits Functionally Segregate Motion and Phototaxis Behaviors in the Fly. *Current Biology*, *19*(7), 613–619.

Acknowledgments

First and foremost, I would like to express my deepest gratitude to Axel, without whom this thesis would not have been possible. A heartfelt thank you for your enthusiasm, curiosity, and, above all, your trust in me. The inception of this thesis marked the beginning of a journey into the molecular realm, one that the lab had dabbled in, but not yet fully explored. I am profoundly grateful for the opportunity you gave me to lead this deep dive into the subcellular mechanisms of motion detection.

As with any journey, there are many people I would like to thank. Thank you, Sandra, for being my co-conspirator and friend. I have learned many valuable lessons from you, but honestly, this thesis would not exist without me embracing your "done is better than perfect" attitude. As cheesy as it sounds, teamwork truly makes the dream work, and that holds true for our scientific collaboration—one I am very grateful for. What is a PhD without colleagues to ask your burning scientific questions? A particular thank you to Georg, Lukas, Tabea, Jesus, Maria, and Aicha for your scientific insights and your willingness and excitement to share your knowledge. Thank you to Wolfgang for many cloning experiments, which represent the bulk of the work at the beginning of this thesis. Thank you, Michi, for your discretion and superb fly care—really, the best a fly can ask for. Thank you, Romina, for all your help with organising and the admin side of things. Of course, thank you to the entire Borst lab!

No thesis is complete without the support of a community outside of the lab, and in this respect, I feel incredibly blessed. There are too many people to thank, and you all know who you are—thank you! I like to joke that a quarter of this thesis is the work of Francis, but really, it's no joke. Thank you for caring for me and especially waiting while I "wash my brains." There are no words to describe my gratitude for your presence in my life and on this journey—danke! Thank you to my family; though I know you all wish I would just "get a real job," I thank you for loving me and letting me do this anyway.

Curriculum Vitae

Personal Information

- **Nationality:** Guyanese
- **Languages:** English (native), German (intermediate)
- **Programming languages:** Python (intermediate), R (intermediate), LaTeX (intermediate)

Education

- **2019-present:** Doctoral Researcher, Max-Planck-Institute for Biological Intelligence, Germany
  Supervisor: Alexander Borst
- **2015-2018:** Master of Science, Biology
  Ludwig-Maximilians Universität Munich, Germany
- **2007-2012:** Bachelor of Science, Honours Biology
  McMaster University, Hamilton, Canada

Conferences & Meetings

- **2022:** Poster presentation at Society for Neuroscience Conference "SfN" (San Diego, USA)
- **2021:** Oral presentation at CanFly Conference (Online)
- **2021:** Poster presentation at NeuroFly Conference (Online)
- **2021:** Oral presentation at Interact Conference (Munich, Germany)
- **2019:** Poster presentation at Wire-Up (Munich, Germany)

Publications

- Ammer, G., Vieira, R. M., Fendl, S., & Borst, A. (2022). Anatomical distribution and functional roles of electrical synapses in *Drosophila*. *Current Biology: CB*, S0960-9822(22)00435-3.
  https://doi.org/10.1016/j.cub.2022.03.040

- Fendl, S.,* Vieira, R. M.,* & Borst, A. (2020). Conditional protein tagging methods reveal highly specific subcellular distribution of ion channels in motion-sensing neurons. *eLife* 9, e62953.
  https://doi.org/10.7554/eLife.62953 (*Equal contribution)